Tailoring of epoxy material properties

PROEFSCHRIFT

ter verkrijging van de graad van doctor
aan de Technische Universiteit Delft,
op gezag van de Rector Magnificus Prof. ir. K.C.A.M. Luyben,
voorzitter van het College voor Promoties,
in het openbaar te verdedigen
op dinsdag 14 december 2010 om 12:00 uur
door

John Suman NAKKA

Master of Technology in Polymer Technology, Cochin University, India
Master of Science in Organic Chemistry, Andhra University, India

geboren te Visakhapatnam, Andhrapradesh, India

Dit proefschrift is goedgekeurd door de promotor:

Prof. dr. ir. L.J. Ernst

Copromotor: Dr. ir. K.M.B. Jansen

Samenstelling Promotiecommissie:

Rector Magnificus	voorzitter
Prof. dr. ir. L.J. Ernst	Technische Universiteit Delft, promotor
Dr. ir. K.M.B. Jansen	Technische Universiteit Delft, copromotor
Prof. dr. ir. R. Akkerman	Technische Universiteit Twente
Prof. dr. G. de With	Technische Universiteit Eindhoven
Prof. dr. S.J. Picken	Technische Universiteit Delft
Prof. dr. T. J. Dingemans	Technische Universiteit Delft
Dr. A. Mavinkurve	NXP Semiconductors, external advisor

ISBN/EAN: 978-94-91104-03-9

Copyright © 2010 by J.S. Nakka

All rights reserved. No part of the material protected by this copyright notice may be reproduced or utilized in any form or by any means, electronic or mechanical, including photocopying, recording or by any information storage and retrieval system, without the prior permission of the author.

Author email: tony_suman@yahoo.com

Printed by spec’s Ipskamp Drukkers

Summary

This research work is aimed to understand the effect of resin chemistry on the physical properties (e.g. moduli, viscoelasticity, moisture uptake, coefficient of thermal expansion) of cured aromatic epoxy-amine thermoset resins. This understanding will result into a good first approximation of the final properties. As a consequence in future it will be possible to design a resin with a well defined set of material properties.

Although this research work cannot be generalized to all kinds of polymeric materials, it gives the knowledge to understand and predict the properties within the class of polymeric materials being under consideration.

Motivation

Look at the bottles of commercially available resins and hardeners and you will find that they are specified with the properties such as equivalent weight, functionality (f) and purity. The properties specified on the bottles of the same kind of resins and hardeners are not always the same. It is mainly because of batch-to-batch variations during the production of the resins and hardeners. Also initial properties such as the mixing ratio and the initial conversion can vary due to the processing schedule in the production unit. Small changes in these initial properties can lead to large changes in the final physical properties of the cured resin. For example if the average functionality ($\overline{f}$) of the reacting mixture is changed from 2 to 2.1 the final reacted product will change from thermoplastic to thermoset. So, the motivation behind this research is to understand the effect of batch-to-batch variation in the initial properties (i.e., average functionality, mixing ratio, cure schedule) of a resin-hardener mixture on the final properties of their cured products.

The materials that are used for high-tech applications such as in aerospace and electronic industry must satisfy stringent specifications regarding dimensions and high temperature behavior. Usually, the materials used in the high-tech applications contain epoxy as adhesive layer or as matrix material. Hence any change in the initial epoxy composition immediately affects the end properties of these materials. Batch-to-batch variations can easily occur in the suppliers' production process. An additional advantage of the present study on the effect of resin chemistry on the physical properties is that a good base for future molecular dynamics simulations on epoxy materials is obtained.

Aim

The aim of the present study is to understand the effect of the initial resin composition on the final properties of their cured products. This understanding will result in a good estimate of the final properties of polymeric materials and thus can help to save time by rightly choosing the initial components without the need of a full experimental characterization. If a good understanding of the relation between the resin chemistry and final properties is known it will be possible to tailor the properties to the customers' demands.

SAMENVATTING (Summary in Dutch)

Het voorliggend onderzoek beoogt inzicht te geven in het effect van de chemische samenstelling van aromatische epoxy-amine harsen op de fysische eigenschappen (zoals modulus, viscoelasticiteit, vochtopname en thermische uitzettingscoefficient) van het volledig uitgeharde product. Dit inzicht zal leiden tot een goede eerste benadering van de uiteindelijke eigenschappen. Als gevolg daarvan zal het in de toekomst mogelijk worden om een hars met een specifieke set van eigenschappen te ontwerpen.
Hoewel dit onderzoek niet kan worden veralgemeniseerd tot alle polymere materialen, verschaft het de kennis om de eigenschappen te begrijpen en te kunnen voorspellen voor de beschouwde deelgroep van polymeren.

Motivatie

Op de verpakkingen van commercieel beschikbare kunstharsen en verharders worden eigenschappen gespecificeerd zoals equivalent gewicht, functionaliteit (*f*) en zuiverheid. De eigenschappen die gespecificeerd zijn op verpakkingen van dezelfde soort kunstharsen en verharders zijn echter niet altijd gelijk. Dat komt voornamelijk doordat de eigenschappen bij de productie van harsen en verharders van batch tot batch kunnen verschillen. Ook initiële eigenschappen zoals de mengverhouding en de beginconversie kunnen variëren als gevolg van het productieschema in de productiefaciliteit. Kleine wijzigingen in deze initiële eigenschappen kunnen leiden tot grote veranderingen in de uiteindelijke eigenschappen van de uitgeharde hars. Bijvoorbeeld, indien de gemiddelde functionaliteit ($\bar{f}$) van het reagerende mengsel verandert van 2 naar 2.1, dan zal het eindprodukt veranderen van thermoplast in thermoharder. Derhalve is de motivatie van dit onderzoek het begrijpen van het effect van batch tot batch variaties in de initiële eigenschappen (bijv. gemiddelde functionaliteit, mengverhouding, uithardingsschema) van de kunsthars-verharder mix op de viscoelastiche eigenschappen van het uitgeharde product.
De materialen die gebruikt worden voor high-tech toepassingen zoals in de luchtvaart- en de elektronische industrie moeten aan stringente specificaties voldoen met betrekking tot afmetingen en hoge temperatuur gedrag. Materialen die worden gebruikt in high-tech toepassingen bevatten gewoonlijk epoxy als lijmlaag of als matrix materiaal. Vandaar dat iedere verandering in de initiële epoxy samenstelling onmiddelijk leidt tot variatie in de uiteindelijke fysische eigenschappen van deze materialen. Batch tot batch variaties kunnen eenvoudig optreden tijdens het productieproces van de leverancier. Een

bijkomend voordeel van de huidige studie naar het effect van de harschemie op de fysische eigenschappen is dat dit een goede basis vormt voor toekomstige moleculaire dynamica simulaties aan epoxy materialen.

Doel

Het doel van het huidige onderzoek is inzicht te krijgen in het effect van de initiële samenstelling van de kunsthars op de eigenschappen van het uitgeharde product. Dit inzicht zal leiden tot a goede schatting van de uiteindelijke eigenschappen van polymere materialen en kan zodoende helpen om tijd te winnen bij de materiaalselectie omdat nu het aantal tijdrovende materiaal karakterisaties gereduceerd kan worden.
Indien een goed begrip van de relatie tussen de harschemie en de eindeigenschappen voorhanden is, dan wordt het mogelijk om in de toekomst epoxy-amine harsen op maat van de eindgebruiker te ontwerpen.

Table of Contents

3. Glass transition temperature (T_g)

4. Viscoelasticity

5. Physical Properties

Symbols and Abbreviation

T_g	Glass transition temperature [°C]
T_g^l	T_g of linear polymer [°C]
$T_{g\infty}$	T_g of partly reacted polymer [°C]
$T_g^{\tan\delta}$	Measured T_g using 1 Hz data from Dynamic Mechanical Analyzer (*DMA*) [°C]
$T_g^{V\&H}$	T_g determined using Van Krevelen and Hoftyzer approach [°C]
T_g^{Ben}	T_g determined using DiBenedetto's approach [°C]
$T_g^{B\&E}$	T_g determined using Bank and Ellis approach [°C]
T_{ref}	Reference temperature [°C]
τ	Relaxation time [s]
τ_0	Relaxation time Constant [s]
a_T	Shift factor
ω	Radial frequency [rad/s]
CS	Cure schedule
ρ	Density (g/cm^3)
f_E	Functionality of epoxy
f_A	Functionality of amine
CL	Chain length
r	Mixing ratio
p	Conversion
F	Flexibility parameter (mol/g)
v_C	Crosslink density (mol/m^3)
v_C^{Bel}	Crosslink density (in mol/m^3) calculated using Bellenger
v_C^{Scan}	Crosslink density (in mol/m^3) calculated using Scanlan
$v_C^{M\&M}$	Crosslink density (in mol/m^3) calculated using Miller and Macosko Theory
$v_C^{L\&C}$	Crosslink density (in mol/m^3) calculated using Lesser and Crawford approach
$X_C^{\text{L\&C}}$	Molar Crosslink density calculated using Lesser and Crawford approach
E'	Storage Modulus [MPa]
Tan δ	Damping
E_g	Glassy Modulus [MPa]

E_r	Rubbery Modulus [MPa]
$M_e^{\ eq}$	Epoxide equivalent weight [g/eq]
Φ_{fA}	Mol fraction of amine hydrogen's provided by f-th functional Amine
M_w^E	Molecular weight of Epoxy [g/mol]
M_w^A	Molecular weight of Amine [g/mol]
$\bar{M}_w$	Average Molecular weight of linear/crosslinked network [g/mol]
M_C	Average molecular weight between crosslinks
f_E	Functionality of Epoxy
f_A	Functionality of Amine
$\bar{f}$	Average functionality
CTE	Coefficient of thermal expansion [K^{-1}]
α_g	Coefficient of thermal expansion in the glassy region [K^{-1}]
α_r	Coefficient of thermal expansion in the rubbery region [K^{-1}]
$PWHH$	Peak width at half height of the tan δ curve [°C]
V^{Meas}	Measured specific volume [cm^3/g]
V_W	Calculated specific vander Waals volume [cm^3/g]
CME	Coefficient of moisture expansion
ε_M	Percentage moisture expansion
M_S	The weight percentage of moisture absorbed in the sample
V_M	The volume of the moisture absorbed sample [cm^3]
V_D	The volume of the dry sample [cm^3]
m_m	Weight of the moisture absorbed sample [g]
m_d	Weight of the dry sample [g]
ρ_M	The density of the moisture absorbed sample [g/cm^3]
ρ_D	The density of the dry sample [g/cm^3]

CHAPTER – I

Introduction

Chapter 1

Introduction

1.1. Introduction to Epoxy materials

Epoxy resins are widely used matrix materials in polymer composites for low temperature as well as for high temperature applications (from -50 °C to +120 °C) and have gained wide acceptance in many applications. They are extensively used in many applications such as coatings, adhesives, laminates and matrices for composite materials and structural components due to low shrinkage on curing. In general, epoxies are known for their excellent adhesion, chemical and heat resistance, good-to-excellent mechanical properties and very good electrical insulating property. Epoxy coatings are also widely used as primers to improve the adhesion of automotive and marine paints especially on metal surfaces where corrosion resistance is important. The high performance epoxy adhesives are used in the construction of aircrafts, automobiles, bicycles, boats, skis, snow boards and other applications where high strength bonds are required. Thermosetting epoxy resin systems are also becoming increasingly important in packaging of integrated circuits. The molding compounds used in electronic applications are typically based upon silica-filled epoxy-amine systems. A typical epoxy monomer which is commercially available is the bisphenol A epoxy monomer i.e., Bisphenol A diglycidyl ether (BADGE) and its chemical structure is shown by *Figure 1.1*.

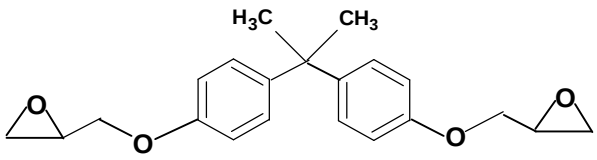

Figure.1.1. The chemical structure of Bisphenol epoxy monomeric resin.

Epoxy resin contains chemically reactive epoxide (or oxirane) groups as shown

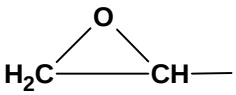

Epoxy resins are commercially available either as crystalline/amorphous solid or in liquid state. When heated to the melting temperature the epoxy resin turns into a clear homogeneous low viscous liquid and starts to flow. The epoxy resin contains an epoxide group which is a highly strained three membered ring ether and hence can easily undergo

a chemical reaction (scientifically termed as "curing") with a hardener or in some cases can react itself to form a hardened material (usually termed as cured resin).

Hardener

Hardener (or "curing agent") is a chemical compound which can react with the resin via a chemical reaction. Hardener is commercially available as second component in two component epoxy glues. Hardener is mixed with the resin in order to harden the resin. They are commercially available either as solid (crystalline/amorphous), liquid or also in some cases gaseous state. Some of the examples of hardeners are amines, imines, phenolics, anhydrides [Ellis, 1993].

Hardening (or Curing) process

The process of hardening of resins is conventionally termed as "Curing". The basic mechanism behind hardening or curing of resins is a chemical reaction occurring between the resin and the hardener. In some cases reaction hardening can occur due to the reaction of the resin and reacted product which is called *homopolymerisation*.

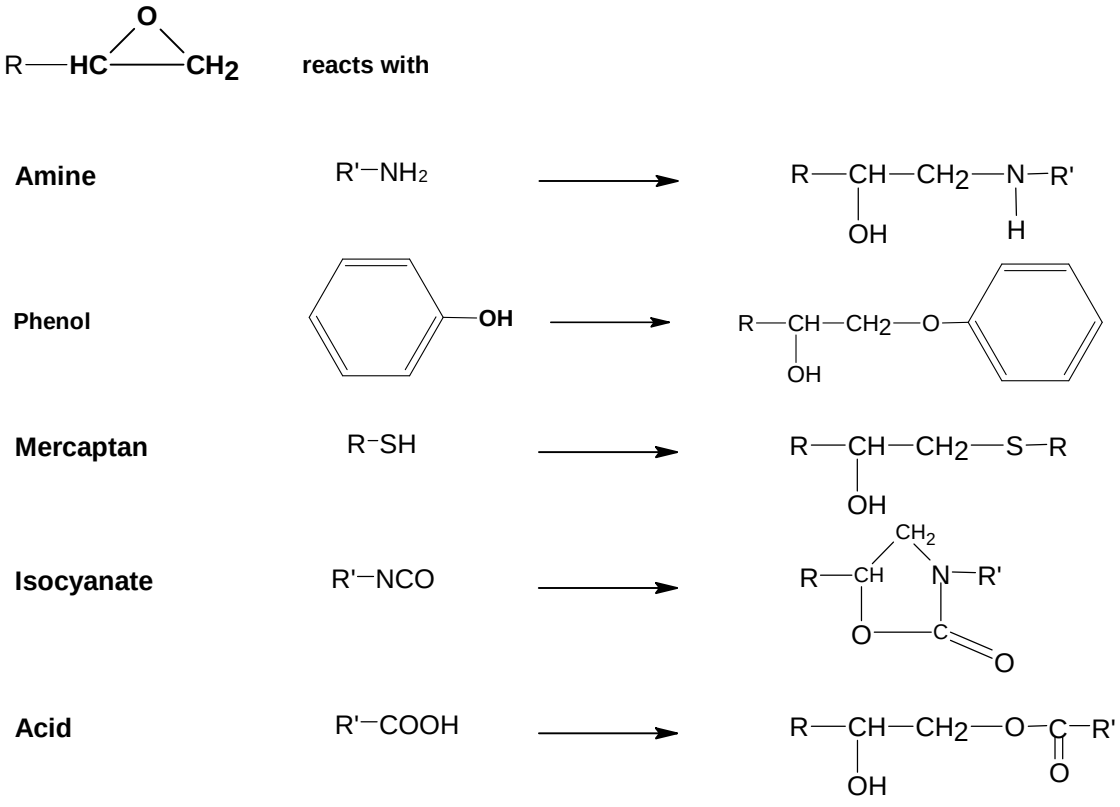

Figure.1.2. Addition reactions of the epoxy group with different reacting groups of hardener.

The special interest in epoxy resins is due to the very simple chemistry, namely the opening of the epoxide ring by an addition reaction with hardener and is shown in *Figure 1.2*. The reaction between epoxy and hardener can be carried out by a simple stepwise addition reaction where no volatiles are evolved. Hence their cured product is free of void-forming volatiles. Volatiles are gases which are formed during the reaction between the resin and hardener. Volatiles can be formed due to the evaporation of the solvent in case that the reaction of the resin and hardener is conducted in solvent medium. Also byproducts such as water can be formed due to the reaction of resin and hardener in condensation polymerization [*Figure 1.3*].

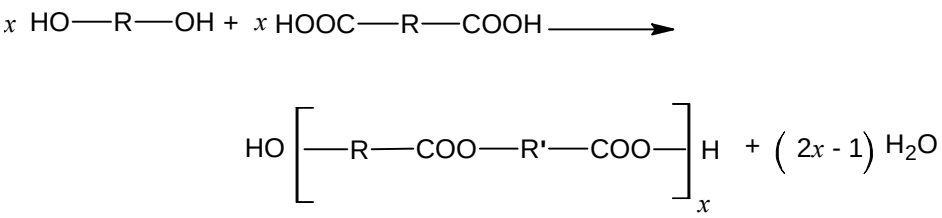

Figure.1.3. Condensation reaction between two polyfunctional molecules leading to the formation of a polyfunctional molecule with the elimination of water molecules.

The reaction of epoxy and hardener can be done in the absence of solvent. Also, the reacted product of epoxy and hardener is free from volatile solvents like water and therefore has a great advantage in processing these materials.

Although a range of chemical agents as shown in *Figure 1.2* can be used to cure epoxy resins, the most important curing reactions occur with amines. A wide range of epoxy resins, amines are commercially available in the market which contain homologous series of aliphatic to aromatic units with varying functionalities. Also the chemistry and range of commercial epoxies and amine hardeners allow the cured epoxies to produce a broad range of properties. Amine-cured epoxies are among the most commonly used matrix materials in engineering applications of reinforced polymeric matrix composites, in part due to their excellent engineering performance and ease of processing prior to cure. Other advantages of amine-cured epoxies are high modulus, excellent chemical and corrosion resistance, thermal stability, high rigidity, dimensional stability.

Depending on the epoxy and amine functionality i.e., *f*, the curing process of epoxy and amine can lead to the formation of two different kinds of polymers: *Thermoplastic* and *Thermoset.*

1.2. Thermoplastic polymers

Thermoplastic is formed when resin containing difunctional reactive groups are mixed *stoichiometrically* or *non-stoichiometrically* with difunctional reactive groups of hardener and cured. *Stoichiometry* is the amount to hardener(or curing agent) to be added to the resin such that the number of the reacting groups of resin and hardener are equal. *Figure 1.4* shows the thermoplastic material formed after the reaction of the difunctional epoxy and difunctional amine that are mixed stoichiometrically.

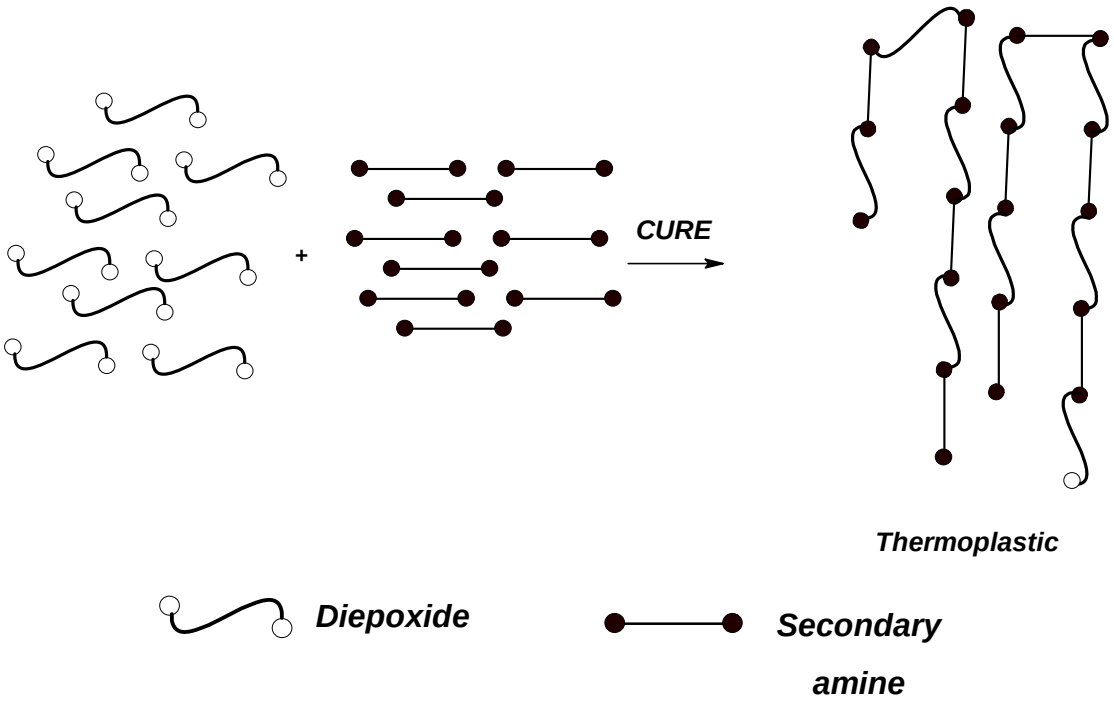

Figure.1.4. Cure reaction between difunctional epoxy and secondary amine leading to the formation of thermoplastic material containing linear chains.

The transformation of liquid resin into thermoplastic material occurs in one step and can be represented as:

Difunctional reactants $\xrightarrow{\textbf{\textit{Cure}}}$ ***Linear chains***

Thermoplastics are materials which flow on further heating. i.e., when a thermoplastic material is heated to a certain temperature (the melting temperature) the material melts and starts to flow and as the temperature is cooled below its melting temperature it regains its initial thermoplastic state. This is mainly because the linear chains that are formed due to the reaction are not interconnected and can slide past each other without restriction as shown in *Figure 1.4*. One of the important characteristics of thermoplastic

materials to dissolve in organic solvents is also due to the absence of intermolecular bonds. Typical thermoplastics are polyethylene, polypropylene, polystyrene and poly (vinyl chloride).

1.3. Thermoset polymers

Thermosets are polymeric materials which form a three dimensional network during the curing process. The formation of three dimensional networks happens only when there is at least one of the components (either epoxy or hardener) with functionality higher than two. During the formation of thermoset material, the curing resin changes from a viscous liquid of low stiffness in its virgin state to a solid of high stiffness in its fully cured state.

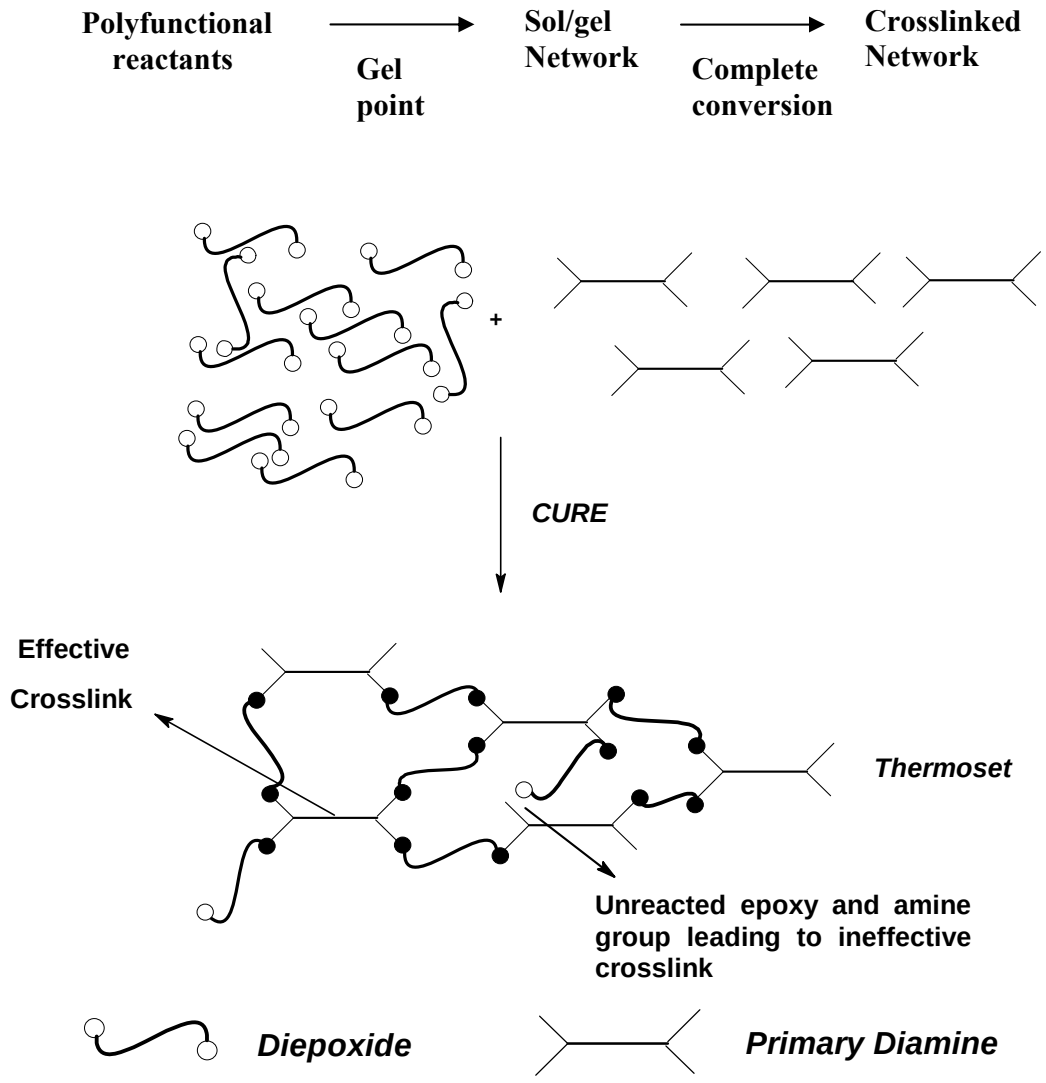

Figure.1.5. Cure reaction between difunctional epoxy and primary diamine leading to the network formation in a thermoset material.

Thermosets are materials which cannot be reprocessed on further heating. This is mainly because of the crosslinked network structure within the material which restricts larger deformation and flow. An example of network formation for a difunctional epoxy and tetra functional amine is shown in *Figure 1.5*. The cured sample containing a crosslinked network structure hinders the molecular chains to slide past each other. Also because of the crosslinked network the material cannot dissolve in a solvent. Instead, the solvent will cause a swelling of the thermoset network. Swelling of thermosets in solvent is a physical process in which the solvent molecules are physically bound with the network structure. Indeed, the ability of a thermoset network to swell in a solvent is exploited by researchers [Nicolas and Liliane (2003)] in determining experimentally the number of elastically effective crosslinks in the thermoset network. The number of elastically effective crosslinks was termed as "crosslink density" and is symbolized with the term v_C [see *Section 1.8.2*].

Figure 1.5 shows the cure reaction between a non-stiochiometric mixture of difunctional epoxy ($f_E=2$) and primary diamine ($f_A=4$) leading to a network containing both the elastically effective crosslinks and ineffective crosslinks. Thermosetting polymers are widely used as adhesives or packaging materials in the electronic industry and as matrix materials for advanced composites. Typical examples of thermosetting polymers are phenolic and urea-formaldehyde resins, unsaturated polyesters, and epoxy resins.

1.4. Typical failure problems in polymeric materials

Although, epoxies are versatile materials for many applications, there are two major problems which these materials encounter during production: *residual stresses* and *moisture uptake*.

i. Residual stresses: In production, the liquid epoxy resin cures and gradually transforms from a very low viscous liquid state to a highly viscous state and finally turns into a solid viscoelastic material with relatively high glassy modulus. These materials whose properties change with time and temperature are known as viscoelastic materials and will be discussed in more details in *Section 1.5*. Apart from the changes occurring in the state (liquid to solid) the curing resin also undergoes shrinkage during cure. This is termed as "cure shrinkage". Most reactive adhesives, such as epoxies, with no formation of by-products during cure experience some shrinkage because their solid polymerized mass occupies less volume than the reactants. This cure shrinkage is one of the causes for residual stresses. A second cause is the cooling stress induced during the cooling to room temperature after the curing step. Due to the mismatch in *CTE* of the resin and a second

material (substrate, filler) the two materials shrink (with a different rate) and thus introduce residual stresses. A good knowledge of the build up of the residual stress is very important especially when these materials are used in the important applications that are mentioned below.

a. In high precision applications, thin fragile optical components (like interference gratings) which are glued with epoxy resin on a rigid frame will experience shrinkage, induced stresses which may eventually destroy the fragile component by crack formation.

b. Also the fiber-reinforced composites are frequently cured in an autoclave, in which a combination of external pressure and vacuum is applied in order to obtain a high quality composite part. Chemical shrinkage during cure and thermal mismatch between fibers an matrix during cooling can induce residual stresses or cause defects in micro-cracks, delamination and warpage.

c. Thermomechanical reliability of electronic packages and assemblies is one of the major concerns in the electronic industry. Epoxy novolacs are typically employed to provide a densely crosslinked protective layer for encapsulating microelectronic devices. However, the trend towards miniaturization and consequently a continuing decrease in the scale of integrated circuits (IC) and on the other hand the increasing number of interconnect layers lead to increase in reliability problems. In addition, the need for lead-free solders requires a higher reflow temperature (up to 260 °C) which results in problems like package cracking, delamination and poor performance in humidity testing. It is reported that that 65% of the failure in microelectronics are due to thermo-mechanical related failures [Zhang et al., (2006)].

ii. Moisture Uptake: Epoxies are often used in many structural applications. For example fiber reinforced epoxy composites have emerged as attractive construction material for new constructions and also for the strengthening of existing buildings, bridges, pipelines etc. As structural materials, epoxies are always subjected to severe atmospheric conditions such as humidity, U.V. rays, heat etc. One of the major concerns of epoxies as structural material is its moisture uptake. Epoxy thermosets are known to absorb up to about 4-5% moisture. Moisture acts as a plasticizer and reduces the glass transition temperature of the resin which has a dramatic effect on their viscoelastic properties as well as on their maximum service temperature. A plasticizer is a low viscous substance which decreases the internal friction within the crosslinked network.

The *physical properties* of solid viscoelastic materials which are produced depend on the chemistry of the resin mixture and also on the cure profile i.e., pressure, temperature and time. Hence in order to prevent the defects such as warpage and fracture which are caused

due to residual stresses the principal requirement is to have a good understanding of the evolving viscoelastic properties of the curing resin as well as the cure profile. Secondly, in order to be able to predict the failure due to residual stresses and also due to moisture absorption the need for full characterization of polymeric epoxy material is inevitable. Full characterization includes the curing kinetics, cure shrinkage of the reacting resin, viscoelastic data, coefficient of thermal expansion (*CTE)* and coefficient of moisture absorption *(CME)* of the cured resin. The full set of material data is important especially for product designers which use this data as input parameters in finite element simulations using Finite element software in order to be able to predict the failure of these materials due to warpage, delaminations and cracking.

1.5. Stress relaxation in viscoelastic materials

When an instantaneous strain is applied to an ideal elastic solid rod a finite and constant stress will be recorded. For a linear viscoelastic solid subjected to a nominally instantaneous strain will result in an instantaneous stress that subsequently will decay with time (*Figure 1.6*). This behavior is referred to as stress relaxation. The characteristic of this stress relaxation time is referred as the relaxation time (τ). For linear polymers at high temperatures the stress may eventually decay to zero.

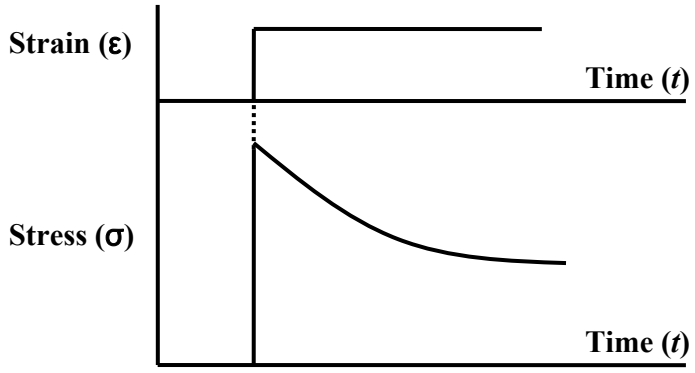

Figure.1.6. Stress relaxation of a viscoelastic material.

Making the assumption of linear viscoelastic behavior we can define the stress relaxation modulus *E(t)* as

$$E(t) = \sigma(t) / \varepsilon \qquad \textbf{(1.1)}$$

If *E(t)* is measured over a number of decades of time, and is plotted against *log t*, it exhibits a curve of the form as shown in *Figure 1.7*. From *Figure 1.7* it can be observed

that at very short times *E(t)* is in glassy region, while at very long times *E(t)* is in rubbery region. The region in between the glassy and rubbery region is the viscoelastic transition region. In the glassy region as well as the rubbery region the polymeric material is elastic i.e., *E(t)* is independent of time. In the viscoelastic region, *E(t)* is dependant on the time.

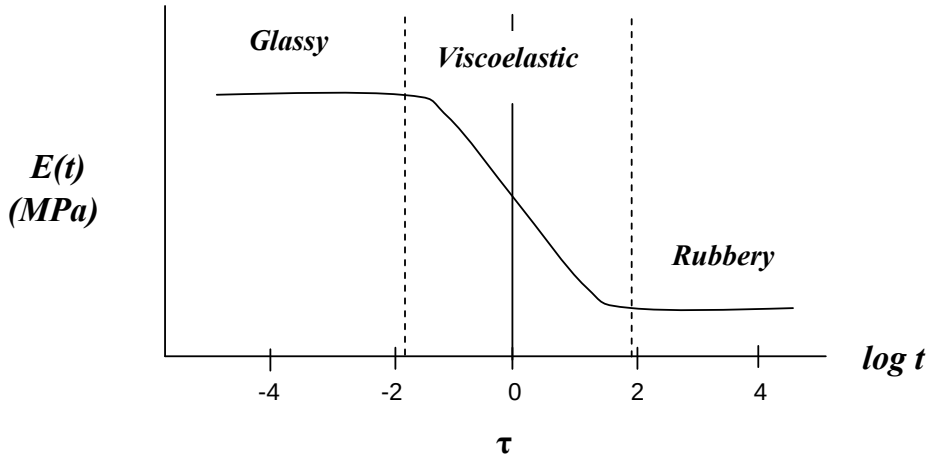

Figure.1.7. The stress relaxation modulus E(t) as a function of time (t) for a viscoelastic material.; τ is the characteristic of relaxation time

1.6. Viscoelasticity

The behavior of materials is usually discussed in terms of two particular types of ideal material: the elastic solid and the viscous liquid. The elastic solid has a definite shape and is deformed by external forces into a new equilibrium shape. On removal of the external forces the elastic solid reverts back to its original form. The elastic solid stores all the energy that it obtains from the external forces during the deformation. This energy is available to restore the original shape when the forces are removed. By contrast a viscous liquid has no definite shape and flows irreversibly under the action of external forces. Polymers can display both elastic solid and viscous liquid properties depending on the temperature and experimentally chosen time-scale. This form of response which combines both liquid-like and solid-like features is termed “Viscoelasticity”. The term “Viscoelastic” pertains to those substances which exhibit both viscous and elastic properties. Thermoplastics and thermosets are viscoelastic materials and their mechanical properties change with time and temperature. For polymeric materials the resistance against deformation (the modulus) is time and temperature dependent.

In *Section 1.5* the stress relaxation of viscoelastic material is discussed with respect to time only. The characterization of the polymeric material for studying the viscoelastic response takes much more time. By raising the temperature, viscoelastic processes are accelerated. This is used to bring the – at ambient temperature – long-term viscoelastic effects within experimental reach.

A well known characterization technique for understanding the effects of both time and temperature on the stress relaxation of polymeric material is by conducting dynamic measurements using a Dynamic Mechanical Analyzer (*DMA*). In this experimental method the polymer specimen is subjected to an alternating strain and simultaneously the stress is measured. For linear viscoelastic behavior, when equilibrium is reached, the stress and strain will both vary sinusoidally, but the stress lags behind the strain. A typical viscoelastic curve (*Figure.1.8*) shows the storage modulus response which is the measure of the sample's resistance to being deformed under multi-frequency Stress/Strain load with the increase in temperature.

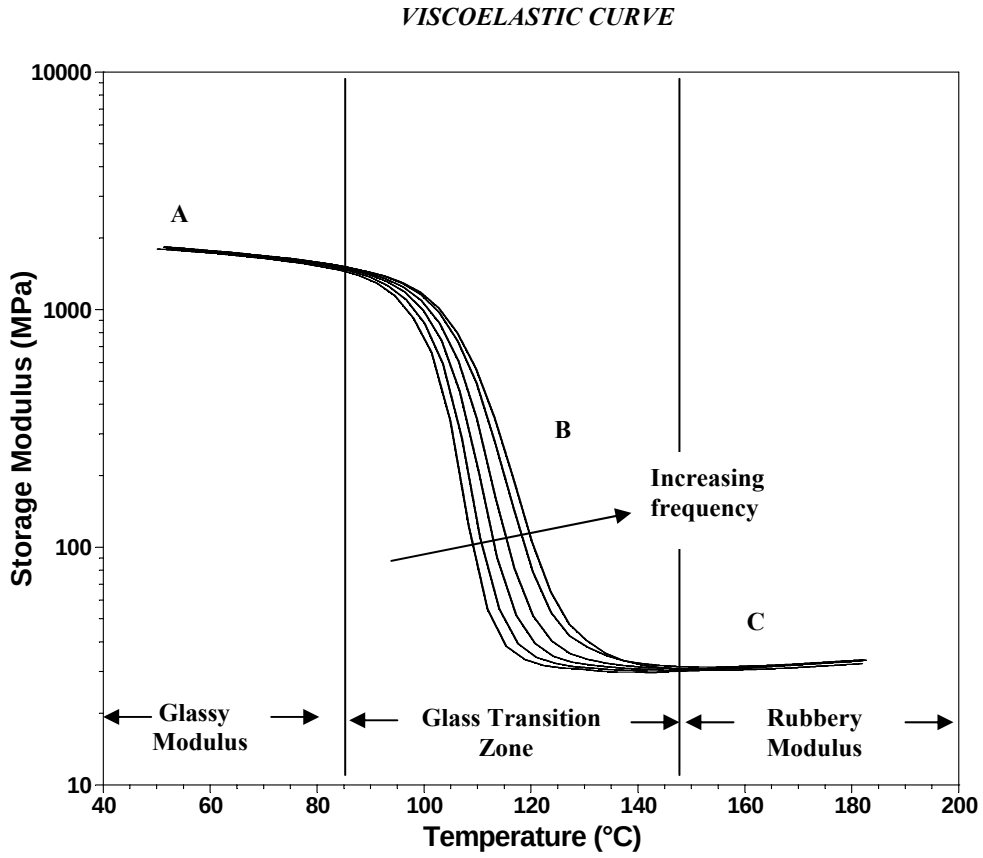

Figure.1.8. *Plot of storage modulus E'(ω) versus temperature. Each line corresponds to the modulus response with respect to temperature for different frequencies.*

The definition and the details of the storage modulus can be seen in *Section 2.8* of *Chapter II.* The viscoelastic curve as shown in *Figure 1.8* can be divided into three distinct regions (labeled A, B, C).

A. Glassy region:

In this region the material has the highest modulus and is largely independent of frequency and temperature. From *Figure.1.8* it can be seen that in the glassy region the modulus remains constant for all applied frequencies and appears as a plateau conventionally termed as the Glassy plateau or glassy state. The glassy plateau/state occurs due to the immobility of the molecular chains within the polymer network. The reason for the occurrence of immobility is due to the close packing of molecular chains which hinders the slippage of these chains. Hence the immobility of the molecular chains in the glassy state reflects only limited local molecular motions such as torsional oscillations, various configurational rearrangements of side chains, and rotations of terminal groups of side chains. Therefore in the glassy state, large-scale molecular motion does not take place.

B. Glass transition zone:

The storage modulus drops in this zone and is frequency dependent. The drop in the storage modulus is due to the large scale molecular motion of the polymeric chains until it reaches the equilibrium rubbery modulus. The drop in the modulus in this zone depends on the internal friction between the molecular chains.

C. Rubbery region:

In this region the material exhibits its lowest storage modulus and is again largely independent of the applied frequency i.e., purely elastic. The modulus remains constant and appears as a plateau region and hence is termed as the Rubbery plateau or state. In this state the molecular chains are free from random coiling and hindrances and can slip past each other and are only restricted by the crosslinks in the network. Thermoplastic materials do not show a rubbery modulus but start to flow above the glass transition (or above the melting point).

1.7. Factors affecting viscoelasticity

The viscoelastic curve changes its shape and position if material parameters like the molecular weight between crosslinks or the amount of aromatic groups are changed. This change in shape can in principle be described with independent parameters: The values of

the rubbery and glassy plateau and the position and width of the glass transition. Secondary effects, like the change of the glassy and rubbery modulus with temperature are then not taken into account. In literature many systematic studies are reported in which the changes in the viscoelastic behavior are mostly related to functionality (*f*), mixing ratio (*r)* and crosslink density (ν_C).

Many efforts have been focused on the development of relationships between the viscoelastic properties and specific characteristics of polymers, such as the molecular weight, molecular weight distribution, and degree of branching [Bidstrup and Macosko, 1990]. The effects of the properties such as functionality, molecular weight, conversion on the viscoelastic curve was discussed earlier by Crawford and Lesser, (1998), Ellis (1993), Bell (1970), Vladimirov and Oleinik, (1980 & 1988), Vakil and Martin, (1992) and many other researchers. White and Mather (1992) investigated the effect of cure on the viscoelastic properties by using ultrasonic methods, while dielectric techniques were employed to characterize the curing polymers [Simpson and Bidstrup, 1995] by relating the ionic mobility to the dynamic viscosity. Suzuki (1977) presented relaxation data for epoxies cured according to various cycles. In the study by Kim and Hahn (1989), the growth in the elastic modulus of thermoset resins is reported to have a linear relationship with the degree of cure in the region of liquid-solid transformation. Simon et al. (2000) researched on the cure-dependent storage modulus for a rubber toughened epoxy resin and also has given a general methodology to model the time-temperature-conversion effects of the viscoelastic response of thermosets. Mason (1964) extended the time-cure superposition to a more general concept of time-cure-temperature superposition and used the methodology to predict the viscoelastic properties of an epoxy resin having a high ultimate glass-transition temperature at any stage of the complex cure cycles. While the experimental data in all the above-cited papers are limited to the post-gelation region, O'Brien et al. (2001) revealed the complete mechanism that drives the development of material properties during the cure by presenting a series of experiments on unreacted or partially reacted liquid resins, as well as on post-gelled resins. The authors used inter-relationships between the viscoelastic properties obtained by both dynamic and static experiments, depending on the handling state of the resin systems, to evaluate one mechanical characteristic from another one.

The effect of stoichiometric ratio of epoxy resins and curing agents in order to control the degree of crosslinking was studied by many researchers. Kenyon and Nielsen (1969) found that the dynamic mechanical α-relaxation peak temperature reached a maximum at stoichiometry. The mechanism of mechanical relaxation, which is observed between 50°

and 90 °C in epoxide resins cured with aromatic and alicyclic diamines, has been investigated by comparing dynamic mechanical properties and chemical structures of these networks. This relaxation is denoted as the α-relaxation. The ultimate tensile strength was also found to reach a maximum at stoichiometry by some researchers [Mostovoy and Ripling, 1966], while others [Bell, 1970] reported that the ultimate strength was insensitive to the stoichiometric ratio. To sum up, no clear conclusion can be drawn from the reports in the literature on the effect of crosslinking upon the characterization on properties of epoxy resins. It can be believed that changing the stoichiometric ratio would inevitably alter the chemical composition of the materials. The change in the properties of thermosetting epoxy resin systems such as resin-hardener stoichiometry, resin and hardener molecular weight distributions and hardener chemistry are known to affect both the curing kinetics and the microstructure of the final product.
In summary the viscoelastic curve is largely affected by properties such as

i. Functionality (f)
ii. Mixing ratio
iii. Molecular weight between crosslinks (M_c)
iv. Aliphatic and aromatic nature of monomers
v. Backbone and dangling ends
vi. Percentage conversion

of the reacting systems. It turned out that the above mentioned properties are directly related to the crosslink density (ν_C). Some of the effects of the above mentioned properties on the viscoelastic curve are discussed below.

1.7.1. The Glassy State

The glassy state is independent of the molecular weight between crosslinks (M_c) and crosslink functionality *(f)* [Crawford and Lesser, 1998]. The glassy modulus increased with the increase in the percentage of conversion [Babayevsky and Gilham, (1973)]. The glassy state is governed by the cohesive energy density which is proportional to the density $\rho(t)$.Therefore a slight decrease in the glassy modulus with increasing temperature is observed within the glassy region (from *Figure 1.8*).

1.7.2. Effect on Glass transition temperature

The glass-transition temperature (T_g) is a measure of the mobility of the molecular chains in the polymer network. The glass transition is the reversible change in a polymer from a

hard glassy state to a rubbery state. The temperature at which the glass transition occurs is the glass transition temperature. The definition of T_g is defined in literature in many ways and is discussed in *Section 3.2* of *Chapter III*. The T_g has been found to increase with the degree of crosslinks [Fox & Loshaek (1955), Drum (1956), Martin & Mandelkern (1959), Heinze (1962)] and chain rigidity of the polymer network [Halary, 2000]. In fact, this observation has provided a means to estimate the glass-transition temperature by measuring the crosslinking [Fox & Losheak (1955), Martin & Mandelkern (1959), Heinze et al(1962)]. The important definitions and predictions of the glass transition temperature by Fox and Losheak, Nielsen, Dibenedetto and others are discussed in *Chapter III*. It is worth noting that the parameters such as chain flexibility and crosslink density cannot be completely decoupled: indeed, the sensitivity of T_g to the crosslinks increases with increasing chain rigidity, as revealed by Halary (1989). With the increase in percentage conversion of the reacting groups the glass transition temperature increases.

The influence of factors such as chemical structure, molecular weight, crosslinking and plasticizers in the glass transition of polymers can be related to the changes that they provoke on the free volume fraction, which reaches a critical value at the glass transition temperature. The factors affecting the glass transition can be classified into two types: (i) molecular factors i.e., those related to the chemical structure of the polymer chain, and (ii) external or controllable factors.

1.7.2.i. Factors related to the chemical structure

The factors related to the chemical structure than can effect the glass transition can be subdivided into: *a. Main chain factors* and *b. Side group factors*

a. Main chain factors

The chemical structure has a determining influence on the flexibility of the chain. For example, polymers such as polyethylene, $(\text{-CH}_2\text{-CH}_2\text{-})_n$, and polyoxyethylene $(\text{-CH}_2\text{-CH}_2\text{-O-})_n$, have relatively flexible chains as a result of the ease of rotation around their chain bonds. They have low values of T_g. The incorporation into the main chain of units that hinder rotation and consequently increase the rigidity of the chain clearly causes a large increase in T_g. For example, the incorporation of a p-phenylene ring (Ph) into the monomeric unit of polyethylene gives poly (p-xylene), which has a T_g of about 200 °C higher than that of PE (see *Table 1.1)*.

Repeating unit	***T_g (°C)***
-CH_2-CH_2-	-120
-CH_2-CH_2-O-	-67
-CH_2-Ph-CH_2-	80

Table.1.1. Values of T_g for various polymers.

b. Side group factors

In vinyl polymers, (-CH_2-CHR-) $_m$, the nature of the side group R has a pronounced effect on T_g as a result of restrictions on the rotation of the macromolecule. Large, inflexible, and bulky side groups cause an increase in rigidity, while flexible side groups have not a marked effect.

Side group R	***T_g (°C)***	***Polymer Name***
-CH_3	*-23*	*Polypropylene*
-Ph	*100*	*Polystyrene*
-Cl	*81*	*Polyvinyl chloride*
-OH	*85*	*Polyvinyl alcohol*
-CN	*97*	*Polyacrylonitrile*
-O-CH_2-CH_2-CH_2-CH_3	*-32*	-
-O-CH_2-CH-$(CH_3)_2$	*-1*	-
-O-C-$(CH_3)_3$	*83*	-

Table.1.2. Values of T_g for various polymers (-CH_2-CHR-)$_m$

Table 1.2 presents the values of T_g for several polymers of the general formula (-CH_2-CHR-)$_m$. The last three examples show how the flexibility of the molecule varies according to the degree of compactness of the different isomers of the butyl radical, leading in the case of poly (vinyl *tert* butyl ether) to a considerable increase in T_g.

The T_g for n-alkyl ethers of the general formula (-CH_2-CH-(OR')-)$_n$ where R' represents an n-alkyl group, are given in *Table 1.3*.

Polymer	***R'***	***T_g (°C) at 1 Hz***
Poly(vinyl methyl ether)	CH_3	-10
Poly(vinyl ethyl ether)	CH_2CH_3	-17
Poly(vinyl n-propyl ether)	$CH_2CH_2CH_3$	-27
Poly(vinyl n-butyl ether)	$CH_2CH_2CH_2CH_3$	-32

Table.1.3. Values of T_g for various polymers having the general formula (-CH_2-CH-(OR')-)$_n$.

Lower values of T_g are observed as the length of R' increase. The rise in the length of R' is associated with an increase in free volume at a given temperature. The larger flexible side groups cause less effective packing and thus increase the free volume. Molecular movements then start at a lower temperature which is seen as a decrease in the T_g in *Table 1.3*.

1.7.2.ii. External or controllable factors

Samples of external factors are rate of measurement, additives and fillers, thermal history, pressure, oxidation, atmosphere. Their effects on the glass transition temperature (T_g) are discussed in *Section 3.3* of *Chapter III*.

1.7.2.iii. Width of transition zone

The width of the glass transition zone in the temperature domain has been used as an indicator of heterogeneity [Barbeau, et al., (1999), Pascault et al. (2002)]. Near the glass transition the smaller and flexible groups or chain segments start to move first and are then followed by the larger and more inflexible segments. If segments with variable degree of flexibility are present in a single network, the network is called heterogeneous. Such networks show a broad glass transition region. It is already observed that heterogeneous networks showed broadening of the tan δ curve with the appearance of a shoulder peak and in some cases two tan δ peaks were shown. The definition and the details of tan δ can be seen in *Section 2.8* of *Chapter II*. For example, in photo cured polyurethane-acrylate networks, two tan δ peaks corresponding to distinct phases, separated by about 40-100 K are observed depending on the composition and cure conditions [Barbeau et al., 1999]. More importantly the width of the tan δ curve increased with the increase in heterogeneity. Whereas the homogeneous network shows a single tan δ peak [refer to *Section 2.8, Chapter II*]. Further a lower tan δ peak width is found in comparison to the peak width of the heterogeneous network.

The tan δ peak of a phenol-formaldehyde resin was found to be broadened and shifted to higher temperatures with higher crosslinking density. The transition width in the frequency domain has been quantified by past researchers by applying the KWW equation [*Equation 5.4, Chapter* 5] to the E' master curves and is given by the shape parameter β. Lower values of β indicate an increase in the width of the transition. While the studies by Kannurpatti et al. (1997 & 1998), Young et al. (1998) show that the breadth parameter β typically decreases with increased conversion.

1.7.3. Effect on Rubbery Modulus

In the rubbery region the material is very flexible, capable of being stretched to several times to original dimensions without breaking. The rubbery modulus of the network is dependent on the molecular weight between crosslink (M_c) and the crosslink functionality of the reacting mixtures. The effect of crosslink functionality on the rubbery modulus of a network has been addressed by the front factor, A in rubbery elasticity theory. The rubbery modulus of the networks could be described by the theory of phantom networks in which the crosslinks are free to fluctuate. With the increase in the functionality *(f)* and with the percentage of conversion the crosslink density and rubbery modulus increases.

1.8. Prediction of crosslink density [v_C] using different approaches

The crosslink density (v_C) can be determined from the experimental data i.e., using the rubbery modulus (E_r) from the viscoelastic curve and applying the theory of rubber elasticity which is discussed below.

1.8.1. Rubber elasticity

The polymer networks in the rubbery state are unique in their ability to reversibly deform to several times their size. The enormous deformability of networks arises from the entropic elasticity of the polymer chains that make up the network. Early researchers showed that the forces in a rubbery network are entropic in nature. The force applied to deform a network consists of two contributions. The first contribution is the energetic term that is the change of internal energy with sample length. The second contribution is the entropic tem that is the product of temperature and the change of entropy with sample length. In typical crystalline solids, such as metals, the energetic contribution dominates the force because the internal energy increases when the crystalline lattice spacings are distorted from their equilibrium positions. In rubbers, the entropic contribution to the force is more important than the energetic one. In the 'ideal networks' there is no energetic contribution to elasticity. So, the contribution of the energetic term from the change of internal energy with sample length becomes zero.

According to the theory of rubber elasticity [Flory, 1953&1979], the crosslink density (v_C) is defined as the number of moles of elastically effective network chains per unit volume of the sample [see *Equation 1.2*].

$$E_r = 3A\nu_c^{Meas}RT \qquad \textbf{(1.2)}$$

where A is the front factor often assumed to be unity, R=8.314 *J/mol/K*, T is the absolute temperature in K and ν_C^{Meas} is the measured crosslink density in mol/cm^3.

1.8.2. Flory-Rehner

Another experimental method to measure the crosslink density (v_C) is to determine the volume increase of polymer by swelling in a good solvent [Nicolas and Liliane (2003)]. The measurement of the crosslink density by swelling studies is based on the Flory-Rehner approach [Equation 1.3]

$$\nu_c^{FR} = \frac{\ln(1-V_2) + \Omega V_2^2 + V_2}{V_1\left(\frac{2}{f_{Cr}}V_2 - V_2^{1/3}\right)_1} \qquad \textbf{(1.3)}$$

$$V_2 = V_{extr} / V_{swollen}$$

where,

v_C^{FR}	-	*Concentration in effective elastic chains given by the Flory-Rehner relationship.*
V_2	-	*Fraction of polymer in the swollen network*
Ω	-	*Flory interaction parameter*
f_{Cr}	-	*Functionality of the crosslinker or hardener*
V_1	-	*Volume of solvent molecule*
V_{extr}	-	*Volumes of the dry extracted networks*
$V_{swollen}$	-	*Volumes of the swollen sample*

In the past, several researchers have tried to estimate the crosslink density on the basis of the initial composition. The two simplest approaches proposed by Bellenger and Scanlan are discussed below.

1.8.3. Bellenger

The dependency of T_g on the molecular structure of the monomers was studied by Bellenger (1987) and his coworkers. They focused on epoxy-amine networks because these networks are formed without side reactions. This is the case for a large number of systems for which it has been shown that T_g is a maximum when epoxide and amine are in stoichiometric ratio [Galy (1985) and Gupta (1985)]. In this case a "repeating unit" is defined whose composition reflects the epoxide/amine functionality and that contains the least integral number of groups. The least intergral number of groups indicates the stoichiometry. For example, 4 moles of trifunctional reactant can react with 3 moles of

tetra functional reactant to form ideal network. Such a "repeating unit" of molar weight M_{rep} contains N crosslinks. The crosslink density is therefore

$$\tilde{\nu}_C^{Bel} = N / M_{rep} \qquad \textbf{(1.4)}$$

Equation 1.4 gives the prediction of the maximum possible crosslink density without considering defects such as dangling ends, loops or incomplete conversion. Furthermore, this equation can only be used for formulations with a single epoxy and amine functionality.

The term crosslink density ($\tilde{\nu}_C^{Bel}$) is called as 'concentration of effective strands' and is expressed as the number of moles on a per gram basis rather than a per cm^3 basis. The difference in the units for the crosslink density (ν_C) which is determined experimentally from the rubbery modulus (E_r) and theoretically estimated by Bellenger is based on the definition of elastically effective crosslinks. The definition of a chain as 'elastically effective' goes back to Flory's (1953) original assumptions of a network. Flory's assumption is only applicable to the calculation of crosslink density of the network formed by the 100% reaction of stoichiometric mixtures and the effect of side reactions is neglected. *Equation 1.4* can be converted to the more common expression of crosslink density as the number of crosslinks per unit volume by multiplying with the density (ρ) then

$$\nu_C^{Bel} = \frac{\rho N}{M_{rep}} \qquad \textbf{(1.5)}$$

The *Equation 1.5* is not only applicable to epoxy-amine systems but also to other systems which form an ideal network without side reactions. Consider a simple reaction containing only two reactants:

$$1A_3 + 1B_3 \rightarrow Idealnetwork$$

Let A_3 be pure isocyanate trimer of hexamethylene diisocyante of molecular weight 504 and B_3 be an oligoester triol of molecular weight 1173 and the experimental density (ρ) of the reacted product is 1.13 g/cm^3. Hence the molar weight (M_{rep}) of the network formed after the reaction is 1×390+1×1173=1677 g. The crosslink density can be calculated by applying *Equation 1.5* as follows

$$\nu_C^{Bel} = \frac{\rho N}{M_{rep}} = \frac{1.13 \times 3}{1677} = 2.02 \times 10^{-3} mol/cm^3 = 2020 mol/m^3$$

1.8.4. Scanlan

Scanlan [1960] proposed a theory to calculate the crosslink density for mixtures of reactants having various functionalities.

$$\nu_C^{Scan} = \frac{3}{2}C_3 + \frac{4}{2}C_4 + \frac{5}{2}C_5 + ... = \sum_{f=3}^{\infty}\frac{f}{2}C_f \qquad \textbf{(1.6)}$$

where, f = the functionality of various reactants, and C_f = the concentration of reactant of functionality, expressed as moles per cubic centimeter of final film. The Equation 1.6 is applicable to stoichiometric as well as to non-stoichiometric mixtures which have undergone 100% conversion and is not applicable to partly cured systems. For the illustration of the use of Equation 1.6 let us consider the same reaction

$1A_3 + 1B_3$

in which the triol is partially replaced by an equimolar mixture of diol of molecular weight 782, triol (the same molecular weight 1173), and tetraol (molecular weight 1564) such that a constant equivalent weight of 391 g/Eq exists for all three hydroxyl functional reactants. The crosslinker, A3, is again pure isocyanate trimer of hexamethylene diisocyante of molecular weight 504. The new balanced reaction is

$3A_3 + 1B_2 + 1B_3 + 1B_4 \rightarrow Idealnetwork$

The weight of the network formed is 3×504+1×782+1×1173+1×1564= 5031 g. If the experimental density is again 1.13 g/cm^3 then the volume of the network is 5031/1.13= 4452 cm^3. Thus, the C_f values from left to right of the above showed reaction are 3/4452, 1/4452, 1/4452 and 1/4452 mol/cm^3. The diol reacts to form a linear chain and therefore does not contribute in the formation of the effective crosslink. Hence, inserting three of these C_f values into *Equation 1.6* (the diol value is not considered) gives the crosslink density as follows.

$$\nu_C^{Scan} = \frac{3}{2}\times\frac{3}{4452} + \frac{3}{2}\times\frac{1}{4452} + \frac{4}{2}\times\frac{1}{4452} = 1.80\times10^{-3}\, mol/cm^3$$

1.8.5. Miller and Macosko (M&M)

In 1979, Miller and Macosko (M&M) proposed a new equation for calculating the crosslink density of the networks formed from the reaction of stoichiometric as well as non-stoichiometric mixtures. The M&M equation is based on a statistical analysis of all possible ways that the monomer units can react. The M&M equation can be used to calculate the crosslink density for fully as well as partially reacted systems and is

discussed below. The Miller and Macosko theory is quite general and gives quantitative predictions for M_n, M_w, crosslink density (v_C), dangling ends, etc. and also includes effects like incomplete reaction in stoichiometric as well as non-stoichiometric mixtures. Miller and Macosko restated Flory's ideal network assumption for the calculation of the crosslink density as follows.

1. All functional groups of the same type are equally reactive;
2. All groups react independently of one another;
3. No intra molecular reactions occur in finite species.

Miller and Macosko [1976, 1978, 1980 & 1988] clarified the term 'elastically effective' by taking two situations as shown by *Figure 1.9 a & b.*

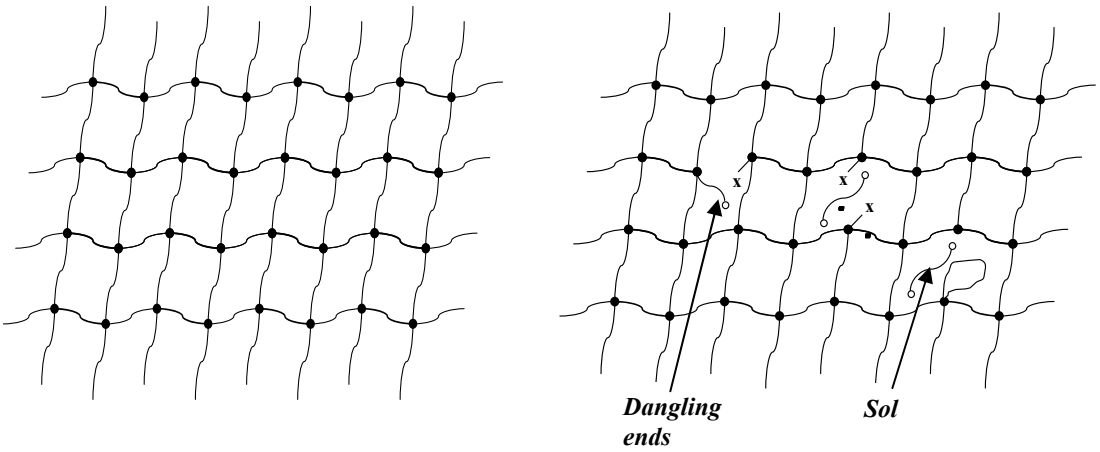

a. *b.*

Figure.1.9. a. Ideal network formed after cure of di-functional epoxy and tetra functional amine in which the conversion is complete (p=1).
b. Non-Ideal network containing dangling ends and sol in the cured product of difunctional epoxy and tetra functional amine in which the conversion is incomplete (p<1).

Figure 1.9 a. shows the homogeneous "Ideal" network also called "closed" network resulting from a single-step polymerization mechanism of a stoichiometric mixture of monomers, reacted to full conversion. In this case all network chains have reacted on both ends, and each end of all chains is attached to the network at different junction points. *Figure 1.9 b*. shows a homogeneous "nonideal" e.g. "open" network, obtained from the same chemistry as the previous one. These networks contain dangling chains and sol as a result of incomplete cure, non-stoichiometric composition, or presence of mono

functional monomers. In this case the network contains some chains that are not elastically effective. Some chains have both ends reacted on the same junction points: these are 'loops'. Some chains have reacted on one end but not on the other; these are called 'dangling ends'. Some chains have not reacted on either end and remain unattached to the network; these are called the 'sol' fraction (or) 'soluble' fraction. Loops, dangling ends and sol contribute to the volume of the sample, but they do not count as elastically effective chains. Therefore, according to the definition, the network in *Figure 1.9 b* has a lower crosslink density than the network of *Figure 1.9 a*.

1.8.6. Calculation of the Average functionality ($\bar{f}$) and Stoichiometric ratio

Let us consider an arbitrary mixture of polydisperse monomers A_i with f_i functional groups and monomers B_j with g_j functional groups. The number of average functionalities then becomes

$$\bar{f}_{n,A} = \frac{\sum n_{Ai0} f_i}{\sum n_{Ai0}}, \qquad \bar{g}_{n,B} = \frac{\sum n_{Bj0} g_j}{\sum n_{Bj0}} \tag{1.7}$$

in which n_{Ai0} and n_{Bj0} denote the initial number of moles of A_i and B_j monomers, respectively. The mole fractions of crosslinkable A and B groups are indicated by a_i and b_j and are calculated using *Equation 1.8*.

$$a_i = \frac{n_{Ai0} f_i}{\sum n_{Ai0} f_i}, \qquad b_j = \frac{n_{Bj0} g_j}{\sum n_{Bj0} g_j} \tag{1.8}$$

The stoichiometric ratio is defined as the initial ratio of all available A groups to those of all B groups

$$r_A = \frac{\text{initial no. A groups}}{\text{initial no. B groups}} = \frac{\sum n_{Ai0} f_i}{\sum n_{Bj0} g_j} \tag{1.9}$$

For equal numbers of A and B groups this ratio equals unity. Consider now the case that there are more B groups available (r_A<1) and that the A groups have reacted to extent p_A (defined as the number of reacted A groups divided by the initial number of A groups). Since the number of reacted B groups equals that of the reacted A groups the conversion of B, denoted as p_B, can then be expressed as

$$p_B = \frac{\text{no.reacted B groups}}{\text{initial no. B groups}} = \frac{\text{no.reacted A groups}}{\text{initial no. B groups}} = p_A r_A \qquad \textbf{(1.10)}$$

1.8.7. Miller and Macosko crosslink density ($v_C^{M\&M}$)

The crosslink density ($V_c^{M\&M}$), which is a function of conversion (p_A), mixing ratio (r_A) and functionality (f_i) can be calculated from the Miller and Macosko theory [Macosko & Miller, (1976)], and is given by the relation

$$\nu_C^{M\&M} = \frac{\sum_{m=3}^{f_k} \frac{m-2}{2} \sum_{f_i=m}^{f_k} n_{Ai0} P_{m,f_i}(x)}{V} \qquad \textbf{(1.11)}$$

where n_{Ai0} is the molar concentration of A_{f} , V is the network volume related to the molecular mass of the network (M_n) and density (ρ) as shown in *Equation 1.12.*

$$V = \frac{M_n}{\rho} \qquad \textbf{(1.12)}$$

and $P_{m, fi}(x)$ is the probability that an A_f monomer has become an effective crosslink of degree m, given by the relation

$$P_{m,f_i}(x) = \binom{f_i}{m} x^{f_i - m} (1 - x)^m \qquad \textbf{(1.13)}$$

Here x stands for the probability that a randomly picked A_f group is connected to a finite chain. This quantity follows by solving

$$p_A \sum b_{gj} \left[1 - r_A p_A (1 - \sum a_i x^{f_i - 1})\right]^{g_j - 1} - x - p_A + 1 = 0 \qquad \textbf{(1.14)}$$

where $0<x<1$. A numerical solution for x is readily obtained with mathematical tools like Mat Lab. For the system of a difunctional epoxy with a mixture of 2, 3 and 4 functional amine ($B_2+A_2+A_3+A_4$), a closed form solution exists:

$$x = \frac{\sqrt{a_3^2 - a_4(3a_4 + 2a_3 + 4a_2 - \frac{4}{r_A p_A})} - a_3}{2a_4} - \frac{1}{2} \qquad \textbf{(1.15)}$$

An example to calculate the crosslink density using Miller Macosko's theory formula for the reacting system $1A_3 + 1B_3 \rightarrow$ *Ideal network* at the conversion (p) of $p=1$ is shown below.

For the above mentioned system there is only one value of functionality (f) ($f=3$) for A_3 and only one value of functionality g ($g=3$) for B_3 and the stoichiometric balance ($r=1$). For this system, *Equation 1.14* reduces to

$$x^4[(2/p)-2]x^2-(1/p^3)x+1-(2/p)+(1/p^3)=0 \qquad \textbf{(1.16)}$$

The value of x for a selected value of p at 0.9 can be calculated by substituting these values in *Equation 1.16* and the determined value of x is 0. From *Equation 1.13*, the probability that the reactants A and B have reacted is $P_{3,f_i}(x) = P_{3,g_i}(x) = 1$. Since, A_3 and B_3 molecules that have reacted only once or twice do not contribute to the crosslink density, the total moles of chain ends bound at junction points is: $3P_{3,f_i}(x) + 3P_{3,g_i}(x) = 3(1) + 3(1) = 6$ moles. Since there are 6 moles of bound chain ends, the number of moles of elastically effective chains is 6/2=3, and the crosslink density ($v_C^{M\&M}$) = 3/ (volume at conversion (p) =1) =3/1484=2.02×10^{-3} *mol/cm*^{3}. It is also possible to calculate the crosslink density at different conversion (p) levels. The crosslink density value determined using Miller and Macosko, Scalan and Bellenger indeed are the same. Moreover, Miller and Macosko's [1976, 1978, 1980] approach has many other great advantages such as determining the crosslink density of the network at different conversion levels for stoichiometric as well as non-stoichiometic mixtures, gel point, average molecular weight, substituent effect, etc.

1.9. Conversion (p)

The conversion (p) is defined as the fraction of the functional groups that has reacted at time (t). The conversion can be determined using different methods e.g. Differential scanning calorimetry (*DSC*), Fourier transformation infrared spectroscopy (*FTIR*), Dielectric spectroscopy, Nuclear Magnetic resonance spectroscopy (*NMR*), etc. Two of these techniques *DSC, FTIR* are discussed in *Section 2.9 & 2.10* in *Chapter II.*

1.10. Objective

In this research study a systematic approach of understanding the effect of initial properties (otherwise called "compositional properties") of resin-hardener mixture on the final properties of their cured product is done by selecting four model systems based on

their changes that are listed below and are cured in order to obtain full conversion of reacting groups.

1. Aliphatic amine functionality
2. Aromatic epoxy functionality
3. Chain length
4. Pendant chain length

It is observed that the changes in the initial properties change the final properties (or "*physical properties*"). The properties exhibited by the cured resin under any external factors such as force, temperature, humidity, etc. are called *physical properties*. Examples of physical properties are modulus, T_g, coefficient of thermal expansion (*CTE*), humidity uptake, etc. Moreover the physical properties are dependent on the network properties of the cured resin. The properties of the network structure such as crosslink density, free volume, polarity etc which control the physical properties of the cured resin are called *network properties*.

Hence in order to be able to predict the physical properties of cured resins the network properties have to be determined. Furthermore, the network properties can be varied by changing the initial properties of the resin chemistry which are defined as *compositional properties*. Examples of compositional properties are functionality, mixing ratio, aliphatic or aromatic nature, etc. Hence it can be concluded that the final physical properties of the cured resin can be well controlled by changing the compositional properties of the reacting resin-hardener mixture. So, in order to relate all the different properties discussed above, a systematic procedure has been adapted and is discussed below. A schematic view of the relation between resin chemistry and final properties is shown in *Figure 1.10*.

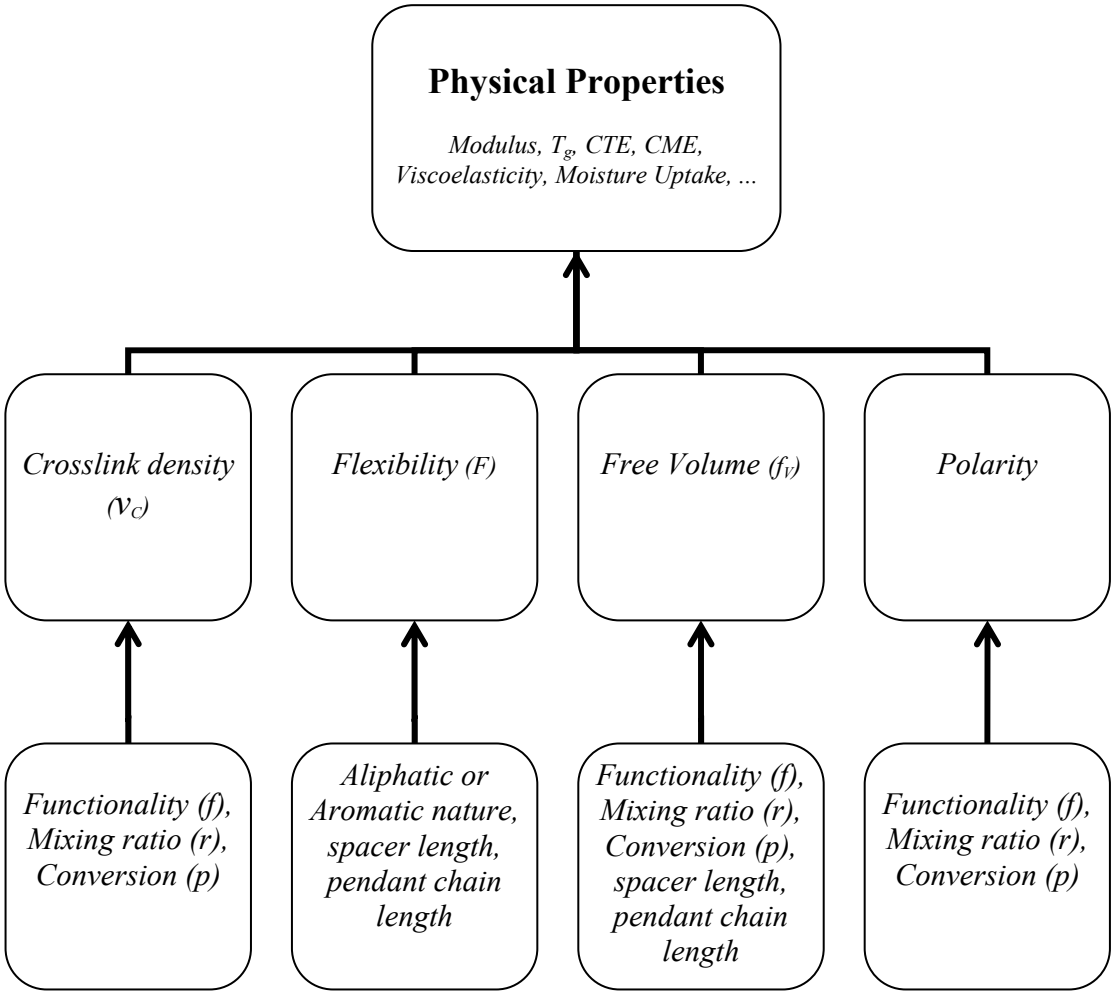

Figure.1.10. Schematic picture showing the dependency of the physical properties of the cured resin on various properties at different levels of the reacting resin-hardener composition.

1.11. Outline of the thesis

Initially in *Chapter II* four series of epoxy model systems are selected and the *compositional properties* i.e., functionality (*f*), mixing ratio (*r*), conversion (*p*) are varied. The variation of compositional properties would therefore lead to a change in the *network properties* of the cured sample. These *network properties* are then calculated using well-known equations as discussed in *Chapter I*. In *Chapter IV* & *V* the physical property T_g and the viscoelasticity of the cured product is predicted based on the *network properties*. In *Chapter VI* the other *physical properties* such as coefficient of thermal expansion (*CTE*), coefficient of moisture expansion (*CME*), density, etc. are related to the network properties using a mathematical model.

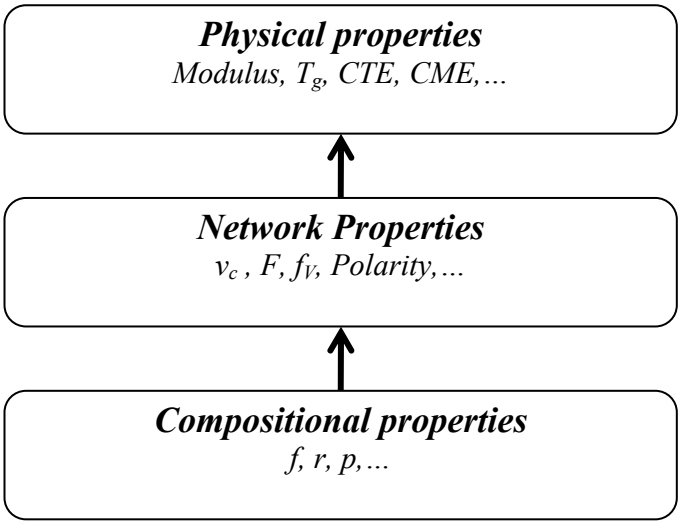

Figure.1.11. Schematic picture showing the order of the interdependency of the physical Properties on compositional properties.

In order to simplify the approach adapted for relating the initial resin chemistry and final physical properties a schematic view is presented with respect to the definitions of *physical*, *network* and *compositional* properties and is shown in *Figure 1.11.*

CHAPTER – II

Experimental

Chapter 2

Experimental

2.1. Introduction

The importance of the *compositional properties* on the *physical properties* especially on the viscoelasticity of the cured resin was discussed in *Chapter 1*. In this *Chapter* the selection of model systems consisting of series of epoxy and amine combinations is presented. The different types of aromatic epoxies and aliphatic amines are taken and their *compositional properties* are varied. The chosen systems are cured in order to be able to study the *physical properties*. In Section 2.2 the initial properties of the starting materials i.e., epoxies and amines are discussed. The cure mechanism between the epoxy and amine is shown in Section 2.2. From the starting materials the selection of four model systems is done. The four model systems and their importance are shown in Sections 2.4 & 2.5. The procedure for the sample preparation for the four model systems and the cure schedules used in the sample preparation is shown in Sections 2.6 & 2.7. Further in Sections 2.8, 2.9, 2.10, 2.11 & 2.12 the *compositional properties* and the *physical properties* of the prepared samples are determined using the Density setup, *DMA* (Dynamic Mechanical Analyzer), *DSC* (Differential Scanning Calorimetry), *FTIR* (Fourier Transform Infrared Spectroscopy) and *TMA* (Thermo Mechanical Analyzer).

2.2. Initial properties of starting materials

Resin	***Structure*** ***Name , Purity, M.P***	***f***	***M_w*** ***(g/mol)***	***ρ*** ***(g/cm^3)***
Epoxy	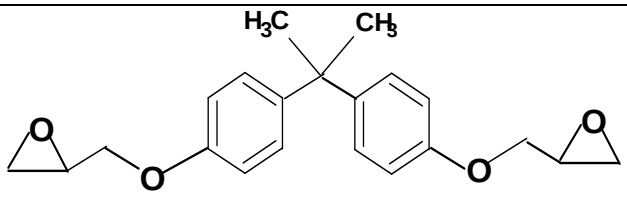 ***BADGE,*** *99%, 40 °C*	$f_E=2$	340.41	1.16
	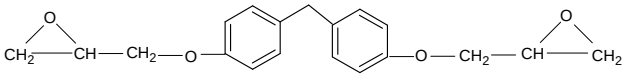 ***BFDGE,*** *98%[t], 46 °C*	$f_E=2$	312.37	1.19
	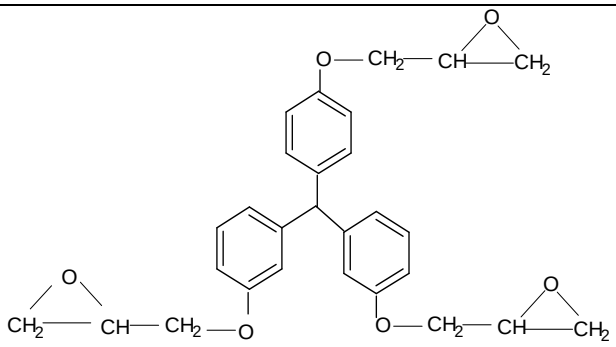 ***TMTE,*** *98%[t], 49 °C*	$f_E=3$	460.53	1.25^t
	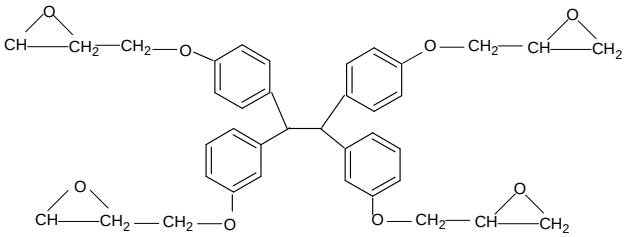 ***TPGE,*** *95%[t], 80 °C*	$f_E=4$	622.7	-

Table.2.1. Initial properties of virgin epoxy resin.

Curing agent/ Hardener	***Structure Name , Purity, M.P/B.P***	***f***	***M_w (g/mol)***	***ρ (g/cm^3)***
Amines	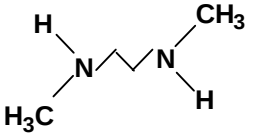 ***DMEDA,*** *99%, 119 °C* *B.P*	$f_A = 2$	88.15	0.819
	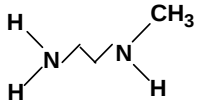 ***MEDA,*** *95%, 115 °C* *B.P*	$f_A = 3$	74.13	0.850
	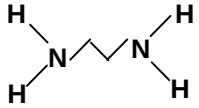 ***EDA,*** *99%, 117 °C* *B.P*	$f_A = 4$	60	0.897
	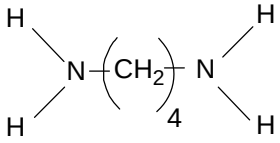 ***BMDA,*** *99%, 25 °C* *M.P*	$f_A = 4$	88.15	0.874
	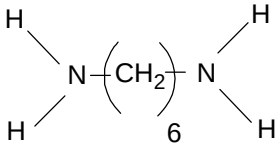 ***HMDA,*** *99%,* *40 °C* *M.P*	$f_A = 4$	116.21	0.799
	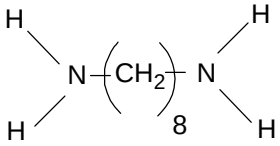 ***OMDA,*** *98%, 51 °C* *M.P*	$f_A = 4$	144.26	0.827
	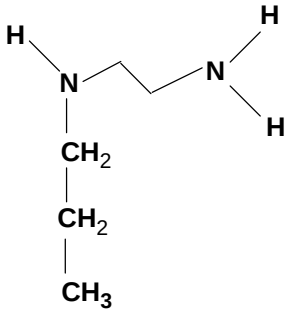 ***NPDA,*** *97%, 148 °C* *B.P*	$f_A = 3$	102	0.829

	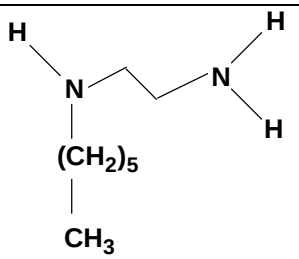 ***NHDA,*** *97%, 102°C* $^{B.P}$	$f_A = 3$	144.26	0.832

Table.2.2. Initial properties of virgin amine curing agent.

where,

f	-	*Functionality*
M.P	-	*Melting point*
B.P	-	*Boiling point*
M_w	-	*Molecular weight*
T	-	*Tentative value*
ρ	-	*Density*

Note: The selected epoxies and amines that are shown in Table 2.1 and 2.2 are commercially available chemicals and are used without further purification.

Chemical Names

BADGE	*Bisphenol A digylcidyl ether*
BFDGE	*Bisphenol F diglycidyl ether*
TMTE	*Tris (4-hydroxyphenyl) methane triglycidyl ether*
TPGE	*Tetra phenyloethane glycidyl ether*
DMEDA	*N, N'-Dimethylethylene diamine*
MEDA	*N-Methylethylene diamine*
EDA	*1, 2-Diamino Ethane*
BMDA	*1, 4-Diamino Butane*
HMDA	*1, 6-Diamino Hexane*
OMDA	*1, 8-Diamino Octane*
NPDA	*N-Propylethylene diamine*
NHDA	*N-Hexylethylene diamine*
TPGE	*Tetraphenyloethane glycidyl ether*

2.3. Cure Mechanism

The cure reaction between epoxy and amine is due to a step-wise addition reaction and the curing mechanism is shown as follows.

Reactions

a.

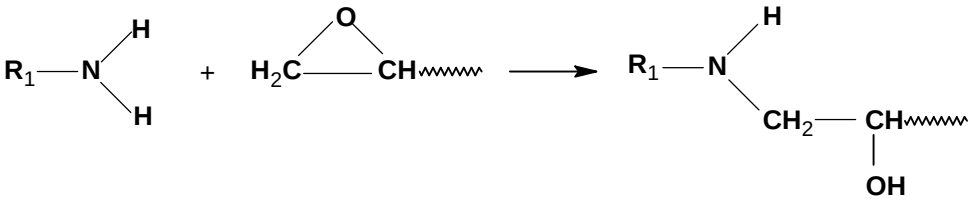

b.

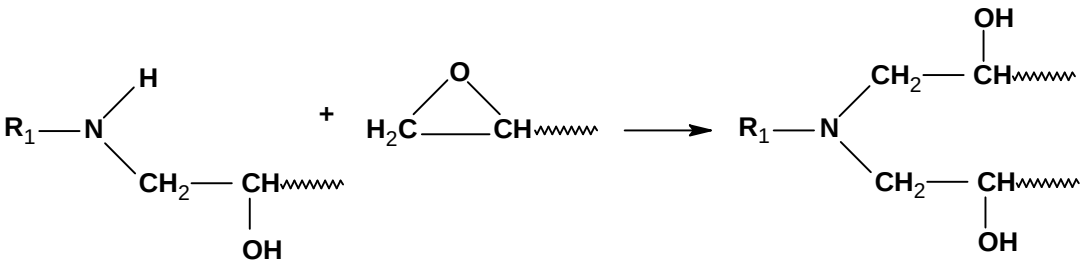

c.

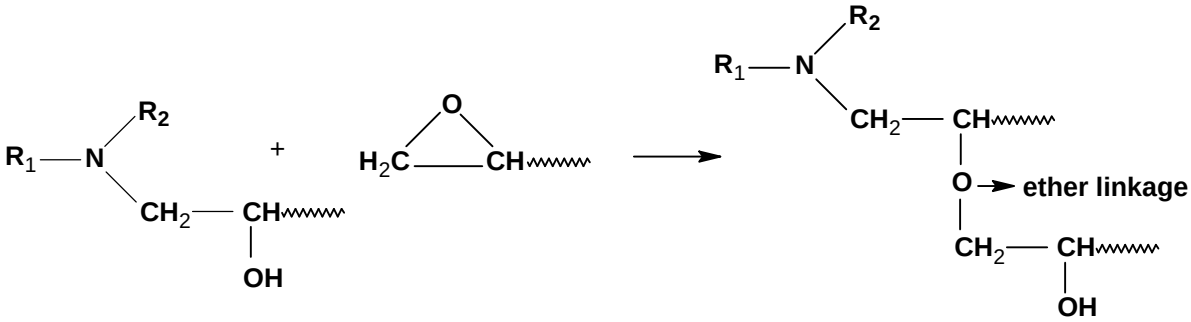

Figure.2.1. a. Epoxide ring-opening reaction with primary amine b. Epoxide ring-opening reaction with secondary amine, c. Etherification reaction between hydroxyl group of reacted epoxy and unreacted epoxy groups (usually occurs at temperatures above 100 °C) (or) homo polymerization of epoxy.

All the starting materials as specified in *Table 2.1 & 2.2* are selected and are divided into four model systems which are shown in *Table 2.4*.

2.4. Importance of the selection of MODEL Systems

2.4.1. MODEL I – Effect of the Aliphatic Amine functionality

To understand the effect of varying the aliphatic amine functionality on the epoxy-amine cured network, Bisphenol A diglycidyl ether (*DER 332*) which is an aromatic epoxy resin of constant functionality (f_E = 2) is selected and is cured with aliphatic amine (or acyclic amine) where the functionality is varied (f_A = 2, 3, 4).

2.4.2. MODEL II – Effect of the Aromatic Epoxy functionality

To understand the effect of varying the aromatic epoxy functionality on the epoxy-amine cured network three aromatic epoxy resins (*BFDGE*, *TMTE, TPGE*) which vary in their functionality (f_E = 2, 3, 4) are selected and are cured with an aliphatic amine having a constant functionality (f_A =2).

2.4.3. MODEL III – Effect of the Chain Length in the network structure

To understand the effect of chain length in the cured epoxy-amine network structure an aromatic epoxy (*DER 332*) of constant functionality (f_E = 2) is taken and is cured with homologous series of aliphatic amines having a constant functionality (f_A = 4). The 'chain length' is otherwise termed as 'spacer length' which is defined as the number of non-reacting groups (*CL*=2, 4, 6, 8) in between the reactive end groups of amine.

2.4.4. MODEL IV – Effect of the Pendant Chain length in the network structure

To understand the effect of Pendant chain length in the cured epoxy-amine network structure an aromatic epoxy (*DER 332*) of functionality (f_E = 2) is taken and is cured with aliphatic amines of constant functionality (f_A = 3) but varying in their side group or pendant chain length (*P = 1, 3, 6*).

	Constant Parameters	***Variable Parameters***
Model I	*Aromatic & Acyclic nature*	f_A, *r, CS*
Model II	*Acyclic nature*	*Aromaticity, r,* f_E, *CS*
Model III	*Functionality, Aromatic and Acyclic nature*	*Chain length*
Model IV	*Functionality, Aromatic and Acyclic nature*	*Substituent Chain length*

Table.2.3. Table showing the selection of Model systems based on constant and variable parameters.

r - *Mixing ratio*
f - *Functionality*
CS - *Cure Schedule*

The simplification of the importance of the Model System is shown in *Table. 2.3*

2.5. Model systems and their chemical structures

All the starting materials as specified in *Table 2.1 & 2.2* are selected and are divided into four model systems which are shown in *Table* 2.4.

Model System	***Chemical Structure of Resin***	***Chemical Structure of hardener***
I	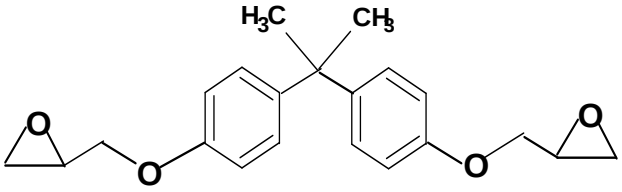	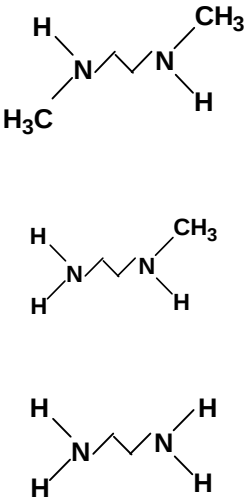
II	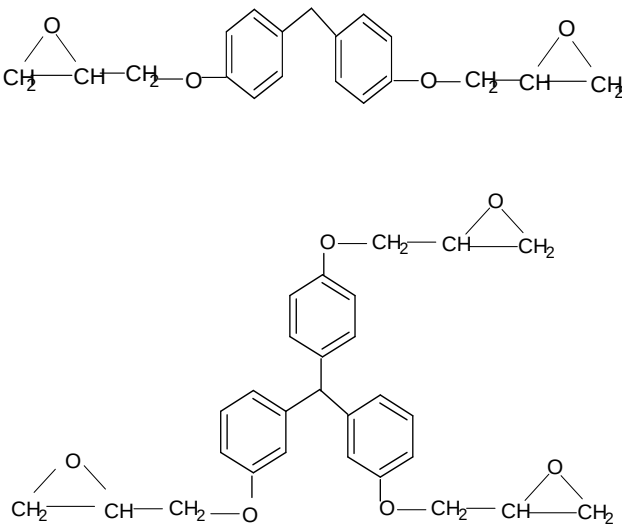	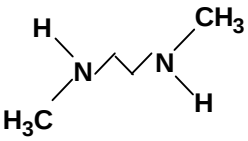

	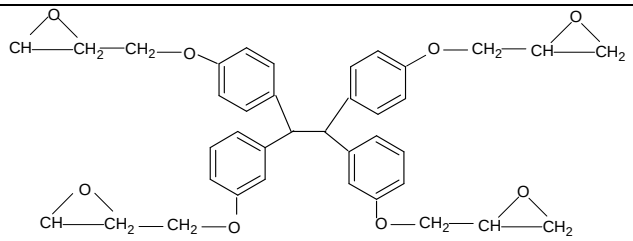	
III	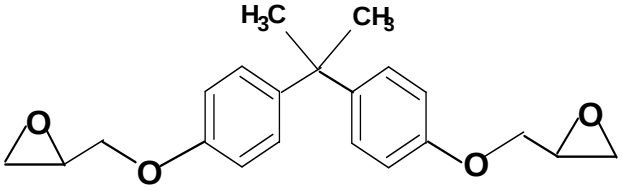	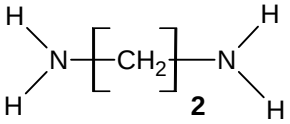 **2** 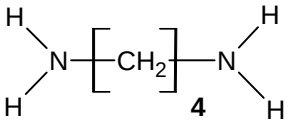 **4** 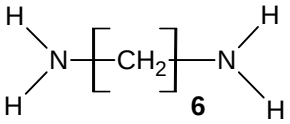 **6** 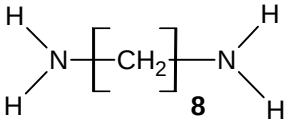 **8**
IV	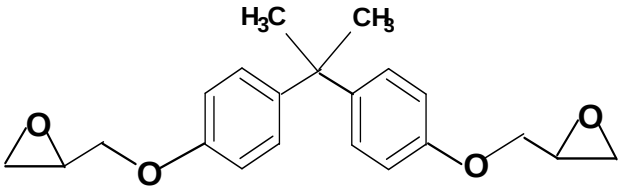	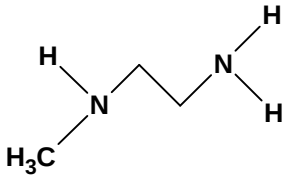 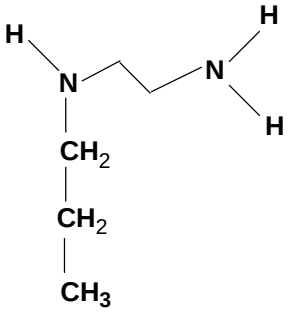

		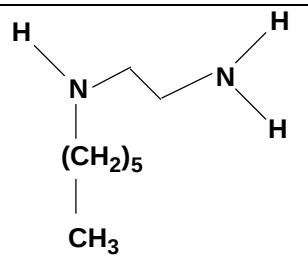

Table.2.4. Table showing selection of resin and curing agents for Model Systems.

2.6. Sample preparation

The sample preparation for *DMA* studies is done by resin casting in an aluminum mold. The aluminum mould consists of an aluminum insert with gaps of dimension 6.0 x 1.5 x 3 mm and is fastened in between two aluminum plates into which the premixed resin is poured and cured at different curing schedules. High temperature mirror glaze wax, (Meguiar's Inc., Irvine, U.S.A) is used as mould releasing agent. Firstly, a known amount of epoxy resin is taken in a beaker. Since pure epoxy partly crystallizes at room temperature they are heated at 80 °C for half an hour so that the epoxy crystals melt and also the absorbed moisture is removed. To this a stoichiometric amount of amines is added and mixed thoroughly. The prepared mixture is then cast in the aluminium mould. Then they are cured and post-cured at different temperatures to obtain full conversion of the epoxy. Cured samples of stoichiometrically mixed amines and epoxy are prepared with different mixing ratios and cure schedules. For all formulations containing different mixing ratios the curing is done initially at 80 °C for 3 hours and 100 °C for 1 hour and then post cured.

Table 2.5 shows the different stoichiometric mixing ratios and post curing temperatures. Preliminary measurements showed a too high post cure temperature for the lower functionality resins resulted in the undesired etherification reaction shown in *Figure 2.1.c*. Therefore in order to avoid etherification all the mixtures were post cured at not more than 150 °C for 4 hours. But for the samples *E4, P3* and *P6* in model IV (*Table 2.5*) the curing was performed at more than 150 °C because the conversion did not reach 100% when it was cured at 150°C. The cure schedules of all the samples are shown in *Table 2.5*. The samples *P3* and *P6* cured at 200 °C showed 99% and 96% conversion as determined using *FTIR* and are discussed in *Section 3.9.4* of *Chapter III*. The sample *E4* when cured at *200 °C* for 8 hours showed a rubber modulus of *15 MPa*. Whereas the sample *E3* cured at 150 °C for 2 hours showed *22*

MPa in the *DMA* studies. This cannot be the case since the *E4* which is formed by the reaction of four functional *TPGE* epoxy and a difunctional *DMEDA* amine is expected to have a higher rubbery modulus than the sample *E3* which is formed by the reaction of the trifunctional *TMTE* epoxy and a difunctional *DMEDA* amine. In the case of an ideal network formation for the sample *E4* the predicted Miller and Macosko crosslink density ($\nu_c^{M\&M}$) for *E4* shows 3000 mol/m^3. Applying *Equation 10* to calculate the rubber modulus (E_r) from $\nu_c^{M\&M}$ (i.e., 3000 mol/m^3) gives the value of 40 *MPa*. Increasing the curing schedule to 250 °C for 3 hours for the *E4* sample showed traces of dark brown (an indication of degradation) on the surface of the sample. The sample was then polished and the *DMA* characterization of the sample showed that the rubbery modulus rises from 15 MPa to 80 *MPa*. The new rubbery modulus value (i.e., 80 *MPa*) is twice the predicted rubbery modulus value. The unexpected increase in the value of the rubbery modulus can only happen in case that the reacting system undergoes side reactions such as homopolymerization [refer *Section 2.3, Chapter II*]. From the above discussion it is obvious that a higher curing schedule such as 250 °C for 3 hours does not favor the formation of ideal networks. Also, increase of the curing time at lower temperature (200 °C) does not lead to the formation of a fully reacted system (or ideal network). The situation occurs mainly due to steric hindrance, where the bulky aromatic groups hinder the reaction of epoxy groups with the amine. The starting material i.e., *TPGE* epoxy resin has a melting point of 80 °C and the mixing of *DMEDA* with *TPGE* at 100 °C has a very low gel time (about 10 seconds) which makes the *E4* system very difficult to follow using *FTIR*. Alternatively, the mixing of the *DMEDA* with *TPGE* can be performed in a low boiling point solvent and further the solvent could be removed by evaporation in vacuum prior to the start of the cure studies in *FTIR*. But the above mentioned procedure would result in erroneous conversion values if the solvent is still present in the reacting mixture. Hence, further characterization such as density, CTE, moisture absorption, etc. is not performed on the sample *E4*.

2.7. General representation of Model systems

Model Number	*Code*	*Cure Schedule*	*epoxy/amine functionality*	*Density (ρ) (g/cm^3)*
I	*A2*	*100_4H*	2/4	1.16
	A3	*150_4H*	2/3	1.191
	A4	*150_4H*	2/4	1.21
II	*E2*	*100_4H*	2/2	1.207
	E2.5	*120_2H*	2.5/2	1.212
	E3	*150_2H*	3/2	1.217
	E4	*200_8H*	4/2	-
III	*CL2*	*150_4H*	2/4	1.21
	CL4	*150_4H*	2/4	1.189
	CL6	*150_4H*	2/4	1.180
	CL8	*150_4H*	2/4	1.164
IV	*P1*	*150_4H*	2/3	1.191
	P3	*200_2H*	2/3	1.175
	P6	*200_4H*	2/3	1.152

Table.2.5. Model system numbers, Code, Cure schedule, epoxy/amine functionality, density.

2.8. Density

The densities of the cured resins are measured using the Archimedes principle which states that the volume is proportional to the difference in weight between a dry and submerged sample. *Figure 2.2* shows the experimental set-up used for the determination of the density.

The experimental set up consists of a weighing balance and glass beaker filled with silicone oil (Type: M100, Dow Corning). The sample weight is determined both in air and in oil. The density is calculated as follows

$$Density(\rho) = \frac{\rho_{\text{oil}} \text{ x } Sample_{\text{dry}}}{Sample_{\text{dry}} - Sample_{wet}} \qquad \textbf{(2.1)}$$

ρ_{oil} is the density of silicone oil (0.957 g/cm^3), $Sample_{dry}$ is the weight in grams of the sample in air and $Sample_{wet}$ is the weight in grams of the sample in silicone oil. The test procedure was calibrated with polystyrene and polycarbonate samples of known density.

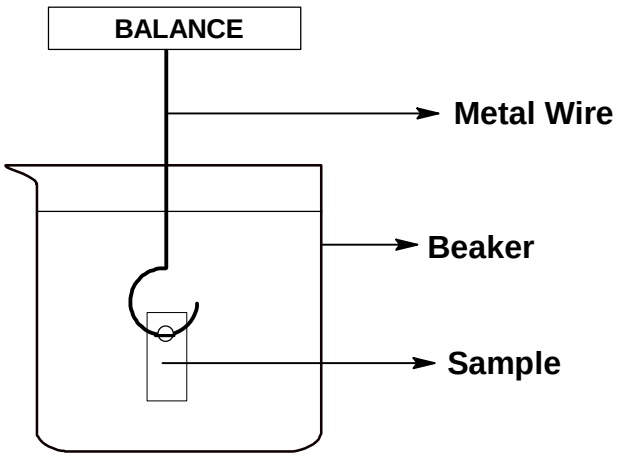

Figure.2.2. Figure showing a polymeric sample placed in a beaker containing silicone oil with the support of a metal wire.

2.9. Dynamic Mechanical Analysis (*DMA*):

As discussed earlier in *Chapter 1,* polymers are viscoelastic materials i.e., their properties change with time and temperature. *DMA* is a well known technique that is used to study the time (frequency) and temperature effects of polymers. Moreover, *DMA* gives much information such as modulus, damping (tan δ), glass transition (T_g), phase morphology, chemical aging, etc.

Instrument Model

The model name of the instrument used for the characterization of the cured resin is *TA-Instruments Q800* (Dynamic Mechanical Analyzer).

Principle

During dynamic testing, an oscillatory (sinusoidal) strain is applied to the polymeric material and the resulting stress response developed in the polymeric material is measured. From analyzing the stress response the (frequency dependent) storage modulus and the so-called loss factor are obtained.

Mode of Testing

The viscoelastic response of the polymeric material can be studied by conducting the dynamic test in different test modes. Some examples of test modes are dual cantilever, compression, tensile and shear. A typical tensile mode is shown by *Figure 2.3.* Here the polymeric sample is clamped in between a fixed clamp (on the top) and a movable

clamp (below). In this set up a sinusoidal strain is applied on the sample using the movable clamp.

Typical Sample geometry:

Length (L) = 5 to 30 mm, Width (W) = Up to 6.5 mm, Thickness (t) = Up to 2 mm.

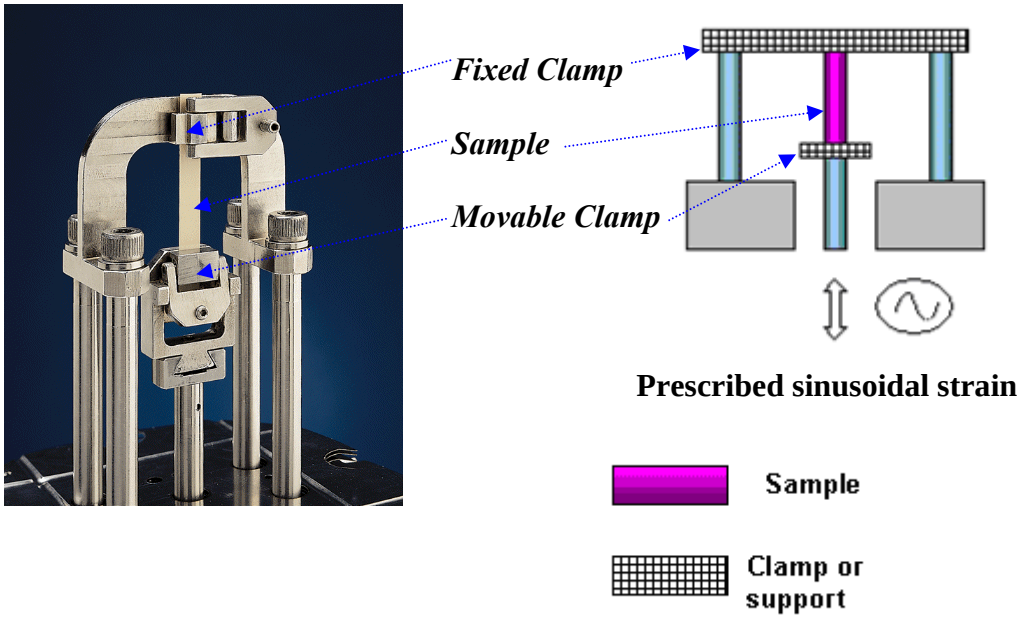

Figure.2.3. Figure showing a polymeric sample clamped in tensile mode in a Dynamic Mechanical Analyzer (DMA). A two-dimensional front view of the tensile mode is shown towards the right.

Procedure

The thermo-mechanical (or viscoelastic) characterization of the cured samples as indicated in *Table 2.5* was done by preparing rectangular sample bars having typical dimensions as indicated above. The cured samples are mounted in the *DMA* in tensile mode as shown in *Figure 2.3* and then multi-frequency strain sweeps (0.3-60 Hz) with simultaneously increase in temperature [heating rate of 1 °C min^{-1}] were applied.

The Dynamic mechanical test is used to measure the response of a material to a sinusoidal or periodic strain. When a periodic strain is applied to a perfectly elastic material the stress response will be in phase with the applied strain. Whereas viscous liquids show a stress response that is 90^0 out of phase to the applied periodic stress. Unlike elastic materials and viscous liquids, polymers show a combination of both types of behavior which is termed as "viscoelastic" behavior. The stress and strain

curves therefore lag in time which is called "Showing a phase lag (δ)" and is shown in *Figure 2.4*.

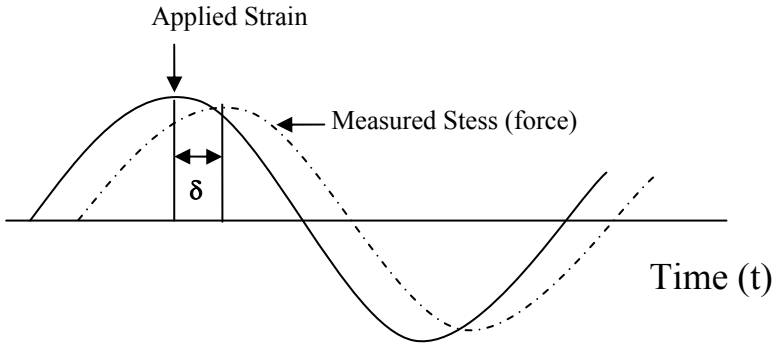

Figure.2.4. The stress response of polymeric material to an applied strain is shown by phase lag (δ).

Since the stress and strain are generally not in phase, two quantities can be determined: a modulus and a phase angle or a damping (tan δ) term and is discussed below.

When a periodic deformation,

$$\varepsilon = \varepsilon_0 . \sin \omega t \qquad \textbf{(2.2)}$$

is imposed upon purely elastic material, the stress will be periodic according to

$$\sigma = \sigma_0 . \sin \omega t \qquad \textbf{(2.3)}$$

With viscoelastic materials, however, a phase shift occurs:

$$\sigma = \sigma_0 . \sin\left(\omega t + \delta\right) \qquad \textbf{(2.4)}$$

This can be understood as follows: For an ideal spring $\delta = 0$*;* for a pure liquid:

$$\sigma = \eta . \left(d\varepsilon / dt\right) = \eta . \varepsilon_0 . \omega . \cos \omega t = \sigma_0 . \sin\left(\omega t + \frac{\pi}{2}\right) \qquad \textbf{(2.5)}$$

then $\delta = \frac{\pi}{2}$;

the stress lags behind the strain over a quarter of a period. For a viscoelastic material δ is in between these extremes: $0 < \delta < \frac{\pi}{2}$.

The *Equation* for σ can be worked our further:

$$\sigma = \sigma_0.\sin(\omega t + \delta) = \sigma_0.[\sin\omega t.\cos\delta + \cos\omega t.\sin\delta] =$$

$$= (\sigma_0.\cos\delta).\sin\omega t + (\sigma_0.\sin\delta).\cos\omega t$$

This *Equation* shows the existence of *two components of the stress*; the first once is in-phase with the deformation, with amplitude $\sigma_0.\cos\delta$, the second one has a phase difference of 90^0, with amplitude $\sigma_0.\sin\delta$.

We can also define two moduli σ/ε;

$$E'(in-phase) = (\sigma_0/\varepsilon_0).\cos\delta \qquad \textbf{(2.6)}$$

$$E''(90^0\, out-phase) = (\sigma_0/\varepsilon_0).\sin\delta \qquad \textbf{(2.7)}$$

and the stress can be written as:

$$\sigma = \varepsilon_0.(E'.\sin\omega t + E''.\cos\omega t) \qquad \textbf{(2.8)}$$

where E' and E'' are referred to as the storage modulus and loss modulus. While,

$$Tan\delta = E''/E' \qquad \textbf{(2.9)}$$

Dynamic mechanical results are generally given in terms of complex moduli or compliances. The complex moduli are defined by

$$E^* = E' + iE'' \qquad \textbf{(2.10)}$$

where E^* is the complex tensile modulus. The storage modulus (E') is the real part of this modulus. The Loss modulus (E'') is the imaginary part of the modulus and $i = \sqrt{-1}$. E'' is the energy dissipation term.

2.9.1. Storage Modulus (E')

The elastic part of the modulus is the storage modulus (*E'*). *E'* is defined as the stress in phase with the strain divided by the strain and is shown by *Equation 2.10.* It measures the energy stored and recovered per cycle of the applied oscillatory force. The plot of storage modulus versus temperature is shown in *Figure 2.5*.

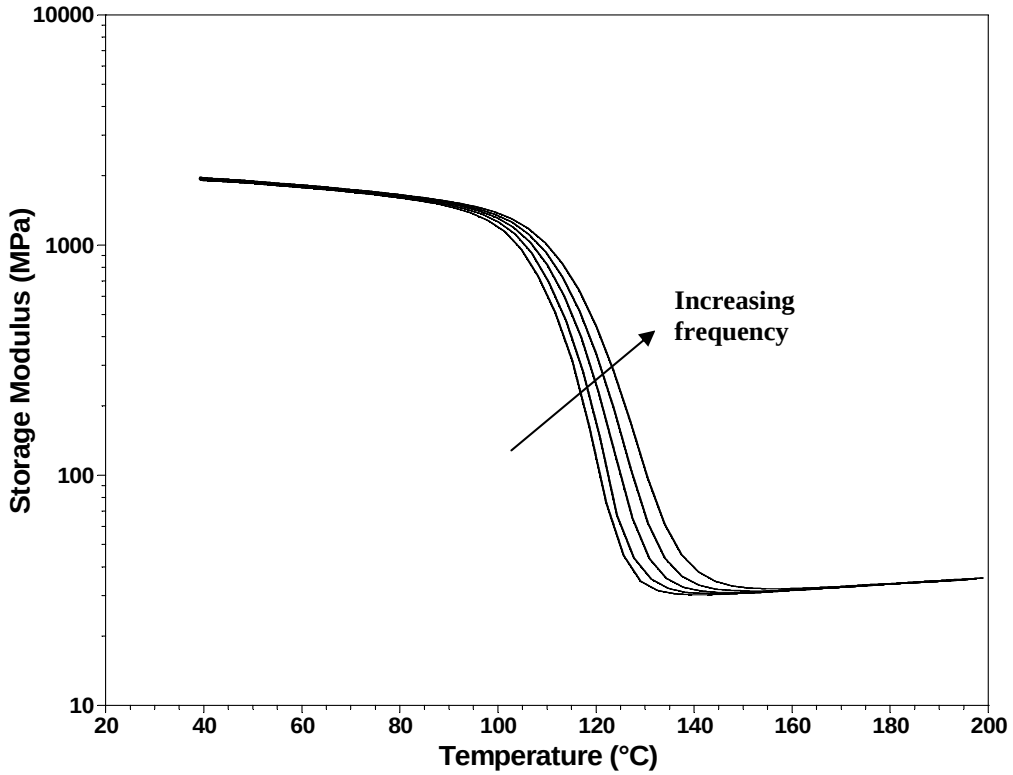

Figure.2.5. Storage modulus (E') versus Temperature.

The storage modulus response of a polymeric material can be subdivided into three regions (glassy, glass transition and rubbery) and can be described similar to *Figure 1.8* in *Chapter I.* More importantly form *Figure 2.5* it can be understood that the response of the elastic component i.e., the storage modulus of a thermoset polymer drops above a certain temperature (i.e., glass transition temperature) and reaches a plateau i.e., the rubbery plateau. A thermoplastic polymer will flow on heating (see *Section 1.2* in *Chapter I*) and therefore drop of the elastic component goes to zero.

2.9.2. Loss Modulus (E'')

E'' denotes the viscous part, and is the measure for the energy dissipated into heat per period of vibration; it is called "*Loss Modulus*". The *Loss modulus* is defined as the stress 90^0 out of phase with the strain divided by the strain and is given by *Equation*

2.10. A typical plot of the loss modulus versus temperature is shown by *Figure 2.6*. It can be observed from *Figure 2.6* that at temperatures further below T_g the modulus (E'') is shown as a plateau. Moreover in the glassy region, the values of E'' are lower than E' *values (Figure 2.5).* This is because in the glassy region the polymeric material tends to exhibit more of elastic behavior and so the value of E'' is lower than *E'*, whereas in the glass transition zone region, the increasing contribution of the viscous component increases the loss modulus value until it reaches a maximum. After reaching the peak maximum the E'' drops due the increase in entropy and remains as a plateau in the rubbery region.

The changes in the behavior of the loss modulus with temperature in *Figure 2.6* can be better explained on the molecular scale. In the glassy region, the coiled state of the molecular chains hinders the molecular mobility. So, when a mechanical stress is applied on the polymer sample the entropy of the molecular chains is slightly affected and tends to regain its original state once the mechanical stress is removed and thereby shows elastic response. Whereas, in the glass transition zone, the molecular motion of the polymer chains is initiated and also the polymer sample gets softened. Therefore in the glass transition zone the relaxation of polymer chains occurs and increases the free volume [*refer Section 5.2*]. Due to the increase in the free volume the uncoiling of the molecular chains (i.e., entropy decreases) occurs. The process of uncoiling of the molecular chains is shown as viscous response. Moreover, the viscous response remains until the molecular chains reach their fully extended state.

After reaching the fully extended state the free volume decreases and in consequence the viscous flow becomes more and more difficult due to increase in the friction between the polymer chains. The peak maximum of the loss modulus is the maximum friction between the molecular chains. After reaching the peak maximum, the loss modulus drops until the polymeric material reaches the rubbery region. Finally in the rubbery region, the polymeric material turns into a viscous fluid and therefore the freedom of the molecular chain mobility increases. The increase in the mobility of the molecular chains induces molecular coiling (i.e., entropy increases) due to which the polymeric material exhibits elastic response in the rubbery region. The elastic response is observed as a plateau in *Figure 2.6.*

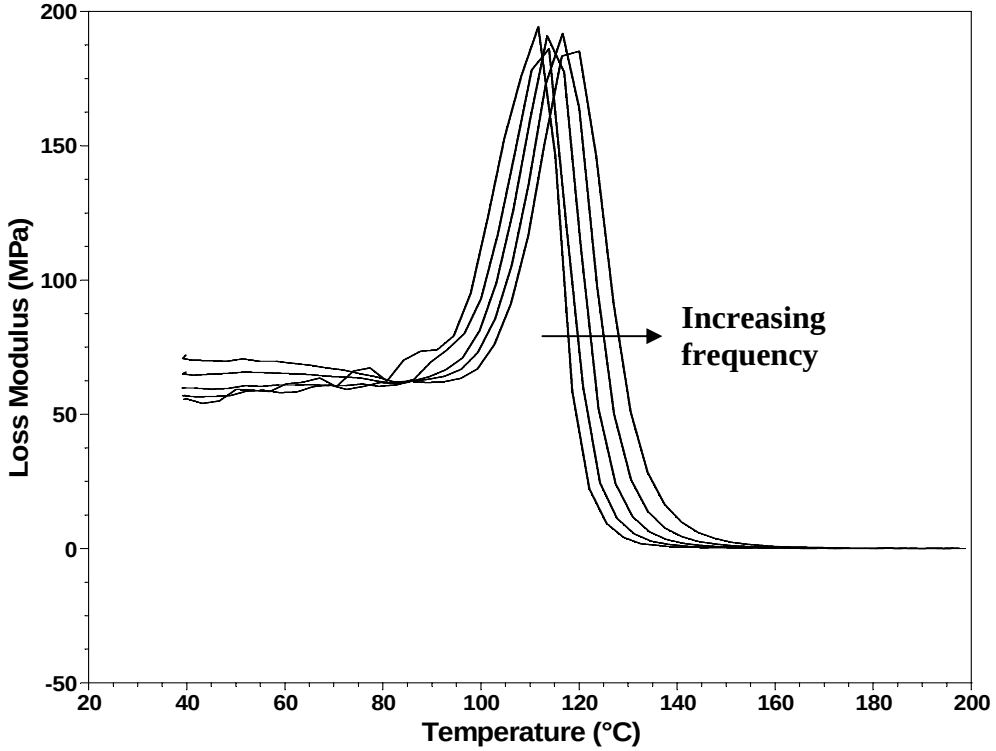

Figure.2.6. Loss modulus (E″) versus Temperature.

*2.9.3. Damping (*Tan *δ)*

Tan δ, a damping term, is a measure of the ratio of energy dissipated as heat to the maximum energy stored in the material during one cycle of oscillation. Tan δ is indicative of molecular motion processes and is called the *loss tangent* or *dissipation factor*. The damping term tan δ is shown by *Equation 2.9,* where E'' is the energy dissipated in taking the sample through a stress cycle and E' is the energy stored in the sample when the strain is a maximum [Billmeyer, 1984]. Hence the internal friction is measured as tan δ or loss tangent from dynamic experiments. A typical tan δ curve with respect to temperature is shown by *Figure 2.7*. Tan δ is extremely sensitive to all kinds of transitions, relaxation processes, structural heterogeneities, and the morphology of multiphase systems such has crystalline polymers, polyblends, and filled or composite materials. More importantly the temperature at the peak maximum of the tan δ curve for 1 Hz frequency determines the glass transition temperature (T_g) according to Nielsen, 1994. The glass transition temperature that is determined from the 1 Hz tan δ curve using *DMA* is denoted by $T_g^{\tan\delta}$ in this thesis. The glass transition temperature can also be determined using different methods. A detailed study on the determination and prediction of the glass transition temperature using different

methods is discussed in *Chapter III*. The glass transition corresponds to the onset of liquid like motion of much longer segments of molecules. This motion requires more free volume than the short-range excursions of atoms in the glassy state. The rise in the relative free volume with increasing temperature above T_g leads to the higher observed volume expansion coefficient in this region.

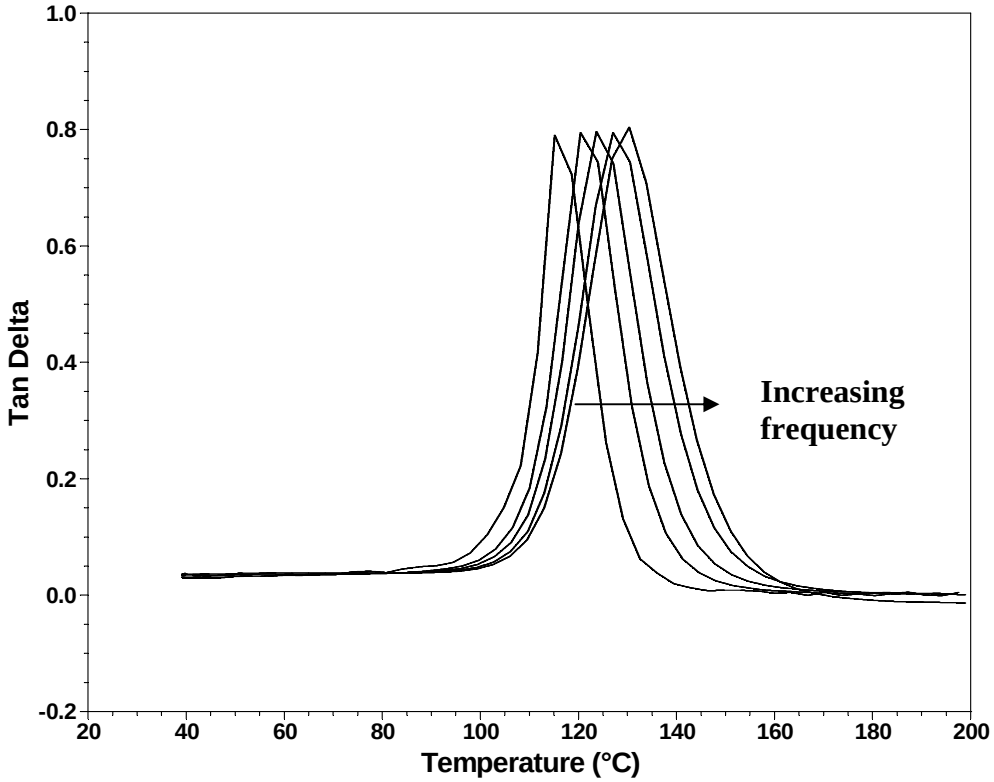

Figure.2.7. Tan δ *versus Temperature*

2.10. Differential Scanning Calorimetry (*DSC*)

DSC is a common technique used to obtain the quantitative and qualitative information of the polymers. It can be used to measure a number of characteristic properties such as melting temperature, glass transition temperature (T_g), crystallization temperature, oxidation etc. Also *DSC* can be used to follow the cure kinetics of the reacting resin and hardener. The *DSC* analyses of the cure kinetics of thermoset resins, such as epoxies, have been discussed in a number of studies and various models are available to quantify the kinetics of reaction as a function of time and temperature [Gonis et al., (1997), Baselga et al., (2003), White and Hann, (1992), Catalani et al., (2005), Simon et al., (2005)].

Principle

DSC is a thermo-analytical technique in which the difference in the amount of heat required to increase the temperature of the polymer sample pan and reference pan are measured as a function of temperature as shown in *Figure 2.8*. Both the sample and reference pans are maintained at nearly the same temperature throughout the experiment. The difference in the heat flow between the sample pan and the empty pan (or reference) is measured as the heat content.

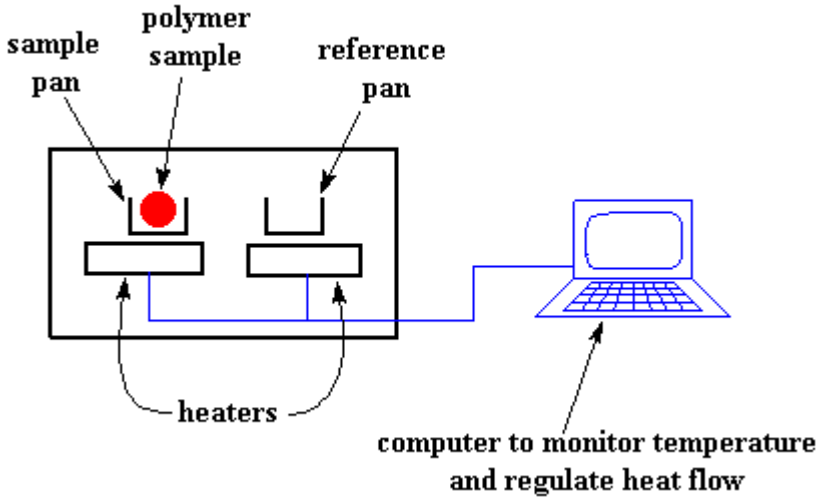

Figure.2.8. Differential scanning calorimetry (DSC) instrument set up

Procedure

The percentage conversion of reacting resin can be determined using *DSC* by placing a sample of between 5 to 10 mg into a sealed aluminum crucible into the *DSC* oven and performing a dynamic temperature scan from -50 ^{0}C to 300 °C at a rate of 10 °C /min under a constant flow of nitrogen gas. A typical exothermic reaction peak is shown by *Figure 2.9*.

Initially, the heat content of the resin-hardener mixture is measured by finding the peak area underneath the exothermic curve and is called the total heat content of the reaction. If a partly reacted sample is subjected to a *DSC* scan a lower amount of heat is released. This amount of heat is called the residual heat of reaction. Commonly it is assumed that the residual heat of reaction decreases linearly with conversion. Therefore the conversion (p) from *DSC* can be determined using *Equation 2.11*.

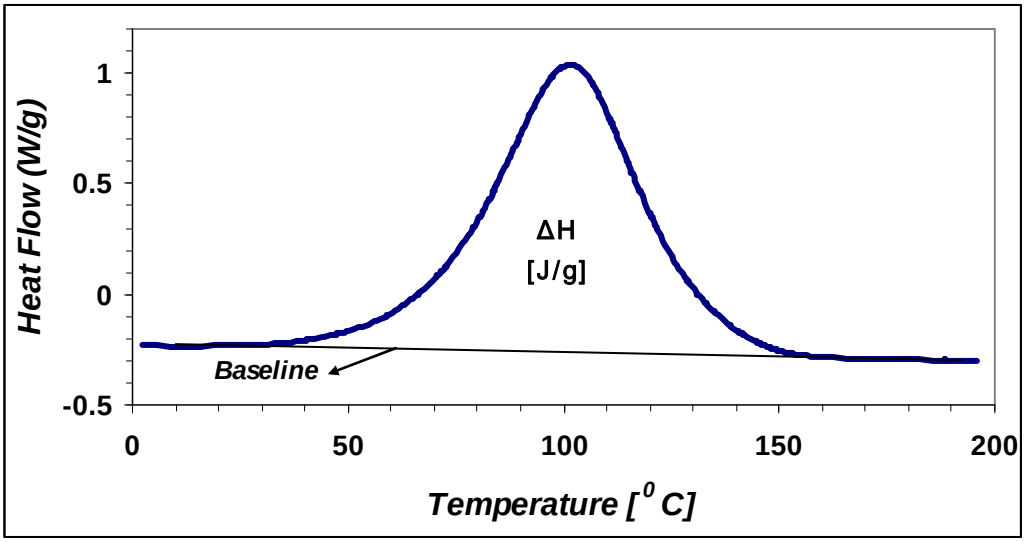

Figure.2.9. Plot of Heat flow (W/g) versus temperature. ΔH is the total area under the peak curve and above baseline (__).

$$p = 1 - \left(\frac{\Delta H_{residual}}{\Delta H_{total}} \right) \qquad (2.11)$$

where,

$\Delta H_{residual}$ - Heat content at time *t*,

ΔH_{total} - Total heat content

p - Conversion.

The conversion determined using *DSC* is based on the heat flow evolved during the reaction and so the technique cannot be used to differentiate between the heat flow due to the main reaction and an unexpected side reaction and therefore a better technique like the Fourier transform infrared (*FTIR*) spectroscopy was used by many researchers [Morgan and Mones, (1987), Bellenger et al., (1987), Wang and Gillham, (1990), Stevens, (1981), Stevens, G.C., (1981)].

2.11. Fourier Transform Infrared Spectroscopy (*FTIR*)

Fourier transform infrared spectroscopy is a measurement technique for collecting infrared (IR) spectra (or spectrum) of organic materials in the infrared spectrometer. The infrared spectrometer measures the wavelength and the intensity of the absorbed infrared light by the sample. Since each chemical bond within the sample absorbs infrared light at a certain wavelength, the infrared spectroscopy technique is used for the identification of different kinds of organic material. In the *FTIR* technique, the IR

light is guided through the interferometer before passing through the sample in *FTIR* technique. Performing a mathematical Fourier transform on the measured signal (or "interferogram") in the interferometer gives the *FTIR* spectra. The versatility of the *FTIR* technique is due to the following advantages which are discussed below.

Advantages

i. *Percentage of conversion of each reacting group can be followed independently.*
ii. *Online determination of the percentage conversion during IR scan.*
iii. *Time saving (i.e., takes few seconds for collecting spectrum).*
iv. *Non-destructive.*
v. *Improved sensitivity in comparison to the conventional spectrometer.*

Although *FTIR* has many advantages there are some disadvantages as discussed below.

Disadvantages

i. *The percentage conversion above 95% is difficult to measure since the vanishing peaks cannot be distinguished from background noise* [Ellis, (1993)].
ii. *Overlapping peaks are difficult to integrate.*
iii. *The spectrum obtained is sensitive to the surface uniformity of the sample especially if the state of the solid or gelled.*

Procedure

The following steps shown below describes the procedure that is used in order to be able to get a spectrum in the *FTIR* spectrometer

i. *The source emits infrared radiation across the frequencies of interest.*
ii. *The infrared beam leaves the source and is deflected by a mirror, the mirror directs the beam into the interferometer where the spectral encoding takes place.*
iii. *The infrared beam exits the interferometer and is deflected by a couple of mirrors before it reaches the detector. The detector produces an electrical signal in response to the encoded radiation striking it.*
iv. *A* ***background interferogram*** *is generated by recording the amount of radiation reaching the detector over time.*
v. *The sample is placed in the path of the encoded infrared beam. The frequencies of infrared radiation that are absorbed and the strength of the absorptions determine the* ***samples spectrum***.

Absorbance

Absorbance can be determined using the Beer-Lambert law. The Beer-Lambert law relates the amount of light transmitted through a sample to the thickness of the

sample. The *absorbance (A)* of a solution or solid sample is directly proportional to the thickness and the concentration of the sample, as follows:

$$A = \varepsilon cb \qquad \textbf{(2.12)}$$

where,

ε - *Molar absorptivity,*
c - *Concentration of the sample solution*
b - *Path length*

Let I_0 and I are the intensities of light entering and transmitted through the sample.

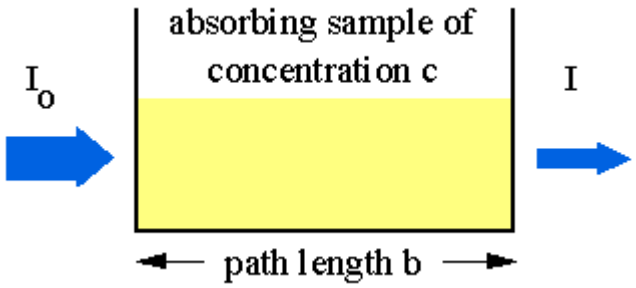

Figure.2.10. Figure showing light of intensity (I_0) passing through a sample.

The absorbance (A) can be defined using *Equation 2.13*.

$$A = \log I_0 - \log I = \log(I_0 / I) \qquad \textbf{(2.13)}$$

Absorbance is therefore dimensionless. Transmittance is defined as the relative intensity:

$$T = (I / I_0) \qquad \textbf{(2.14)}$$

The *FTIR* spectra of the sample can be obtained in two regions: mid-IR region (*4000-400 cm^{-1} or 30-2.5 μm*) and near –IR region (*14000-4000 cm^{-1} or 2.5-0.8 μm*). The spectrum obtained in mid-IR is due to the fundamental vibrations and associated rotational-vibrational structure. The absorptions observed in the near-IR region are overtones or combinations of the fundamental stretching bands which occur in the 3000-1700 cm^{-1} region. *Tables 2.6 & 2.7* shows the IR values of different groups in the near and mid- -IR [Stuart, 2004; Mijovic et al., 1995; Varley et al., 1995; Bakker et al., 1993; Billaud et al., 2002; John and Geroge., 1992].

Near-IR bands:

Functional Group	Wave number (cm^{-1})
Terminal epoxide combination	4518
Secondary amine N-H overtone	6683
Hydroxyl group overtone	6993
Aromatic ring C-H combination	5967
Epoxide C-H	4522[a], 5881 [b], 6070 [b]
Primary amine N-H	4522 [a], 5072 [a]
Primary and secondary amine N-H	6577-6692 [b]
Hydroxyl O-H	4903 [a], 6990 [b]
Aromatic C-H	4619 [a], 4682 [a], 5992 [b]

Table.2.6. The absorbance peak wave number of different chemical groups in near-infrared region.

[a]Combination band
[b]Overtone band

Mid-IR bands:

Functional Group	Wave number (cm^{-1})
Epoxide	916
Epoxide ring Stretching	1240
C-H (aromatic) CH_3-C Isopropylidene	1183
Phenyl Band (aromatic ether)	1034
C-H Str (aromatic)	1510
C-H Str (aliphatic)	2855
-NH_2 Anti Sym	3338
-NH	3389-3330
Harmonic –NH_2	3210
Benzene ring	3038, 1514
C-N-C	13955, 1377
C-N	1289, 1275
Broad and associated OH Stretching	3400
Sharp and unassociated –OH Stretching	3600
C=C	1607
-NHR, -OH (Secondary amine and Hydroxyl)	3500-3300

Table.2.7. The absorbance peak wave number of different chemical groups in mid-infrared region.

Instrument Model

The model name of the instrument used for spectral analysis of the cured resin is *Thermo Electron Nicolet 6700*. The IR spectra of a sample can be obtained in different methods depending on the state (solid, liquid and gas) of the sample and the sampling mode. Although several sampling techniques do exist, two well known sampling modes are *i. Transmission mode* and *ii. Attenuated total reflection (ATR) mode.*

Transmission mode

Transmission mode is the simplest mode in which the polymeric sample is kept in the path of the infrared light as shown in the *Figure 2.11* and the spectrum is obtained in *FTIR*. In this mode, the thickness as well as the transparency of the sample is very important since the part of the infrared ray beam has to pass through the sample and reach the detector in order to obtain a spectrum. For solid samples, the spectrum can be obtained by keeping a thin transparent film in the path of the infrared light. Whereas for the liquid samples, a medium is required such that the liquid sample can be coated on the medium to obtain a spectrum. Some of the commonly used mediums are KBr pellet, NaCl, Quartz crystals, etc. The selection of the medium depends on the wavelength of the spectrum to be observed. For example, a KBr pellet is a good medium to get a spectrum in the mid-infrared region whereas a quartz crystal is used for the near-infrared region. Also liquid samples can be poured into cuvettes made out of polystyrene (PS), polymethyl methacrylate (PMMA), quartz, etc. in order to be able to get a spectrum. During the curing process, the liquid resin changes into a solid sample with the raise in temperature and hence to follow the cure reaction with *FTIR* is difficult due to the following reasons.

i In the case of a cure reaction at higher temperatures (>100 °C), the cuvettes such as PMMA, PS cannot be used. This is mainly because the refractive index of the cuvette changes as the temperature nears the softening temperature (T_m). Alternatively, quartz cuvettes which have a higher melting temperature (T_m>800 °C) can be used. The commercially available quartz cuvettes are expensive and also after the cure reaction in the cuvvette the cured resin (solid) sticks to the walls of the cuvette. The removal of the solid resin from the walls of the cuvette is practically impossible without creating cracks on the surface of the quartz crystal inside the

cuvette. Therefore the quartz cuvvettes have to be disposed after the curing reaction. Due to the above mentioned problems, the usage of the quartz cuvvettes is not recommended.

ii Commercially available transmission mode set up for studying the cure reaction with the increase in temperature are very expensive.

Hence a new transmission set up containing four heating elements that can heat up to 175 °C is designed and fabricated. The disposable quartz wafers are used to study the cure reaction in the near infrared region. In order to follow the cure reaction using the new set up following procedure is adapted.

i. Initially the back ground spectrum of the quartz wafer is taken.

ii. A drop (about 0.5 mg) of epoxy resin-hardener mixture is placed in between two quartz wafers and then pressed such that the drop spreads equally in between the two surfaces of the wafer. The quartz wafer containing the resin drop is then placed in the new transmission mode set up and spectrum is taken.

The spectrum for the resin drop is obtained after undergoing the baseline correction using the background spectrum of the quartz wafer. The baseline correction is the process to correct a sloping, curving, shifted or otherwise undesirable baseline of a spectrum, so that the baseline appears flat and near zero absorbance units (or 100% transmittance). A baseline consists of those portions of a spectrum where there are no significant absorptions are observed. The details of the new set up are discussed below.

New Transmission mode set up:

The newly build up transmission accessory contains two aluminum plates which can be fastened along with an aluminum spacer as shown in *Figure 2.11*.

Each aluminum plate contains two heating elements above and below the transmission window. The heating elements are connected to a temperature controller through the heating element wires. One of the aluminum plates contains a thermocouple wire which is placed internally and close to the transmission window in order to find the temperature of the heating element. The thermo couple which is placed internally is called the internal thermocouple. The transmission set up is initially calibrated with quartz glass to find the heating rate. The two quartz glass

wafers are fastened with a thermo couple and placed in the transmission window. The thermocouple that is placed in between the quartz wafers is called the external thermocouple. Calibration experiments are conducted to ensure that the temperature reading of the internal and external thermocouple has close readings. Solids, liquids and gels can be used for characterization in this mode provided the sample is transparent with sufficiently small thickness for the IR light to pass through the sample.

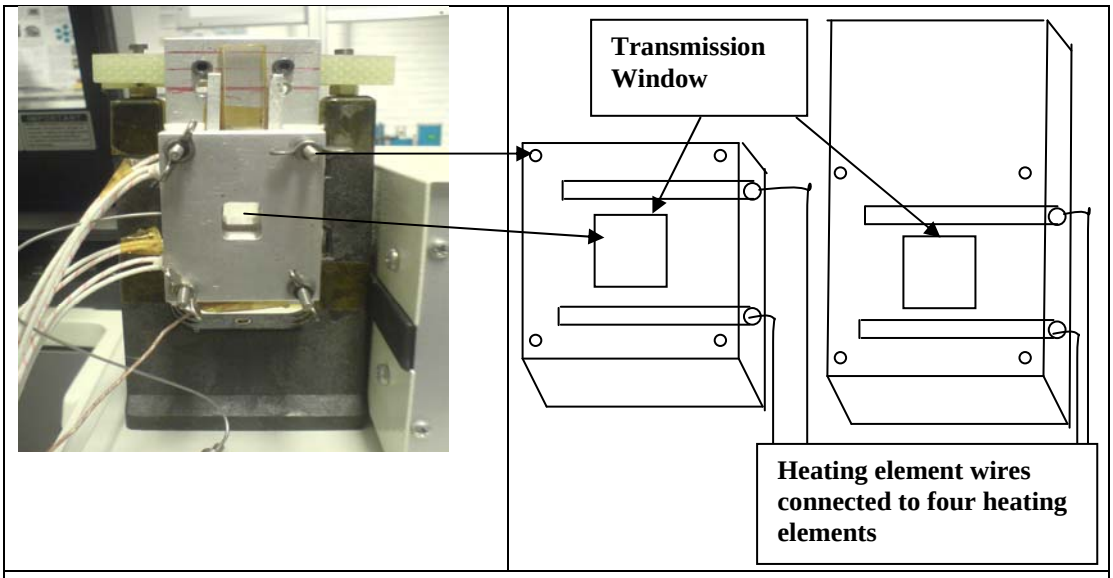

Figure.2.11. Transmission mode accessory set up for Near-IR studies

Sample Specifications:

Aluminum plates: *Plate 1: 200 mm X 100 mm X 10 mm* *Plate 2: 120 mm X 100 mm X 10 mm*	*Quartz plate: 20 mm X 5 mm X 0.3 mm*
Heating elements: 45mm X 6 mm	*Transmission window: 20 mm X 10 mm*

In order to test the reliability of the transmission mode set up the initial mixture of *E3* from Model III is placed on the quartz wafer and cured according to the following cure schedule.

i. 40 °C for 2 hours

ii. 60 °C for 2 hours

The spectrum of the reacting mixture is taken at regular intervals of time i.e., every 300 s and is shown in *Figure 2.12.* It can be seen that with the increase in time and temperature the epoxy peak area at 4528 cm^{-1} decreases and also amine N-H peak around 5000 cm^{-1} decreases. Where as the OH band around 4800 cm^{-1} increases. This clearly shows that the curing kinetics can be followed with the new transmission set-up in *FTIR*.

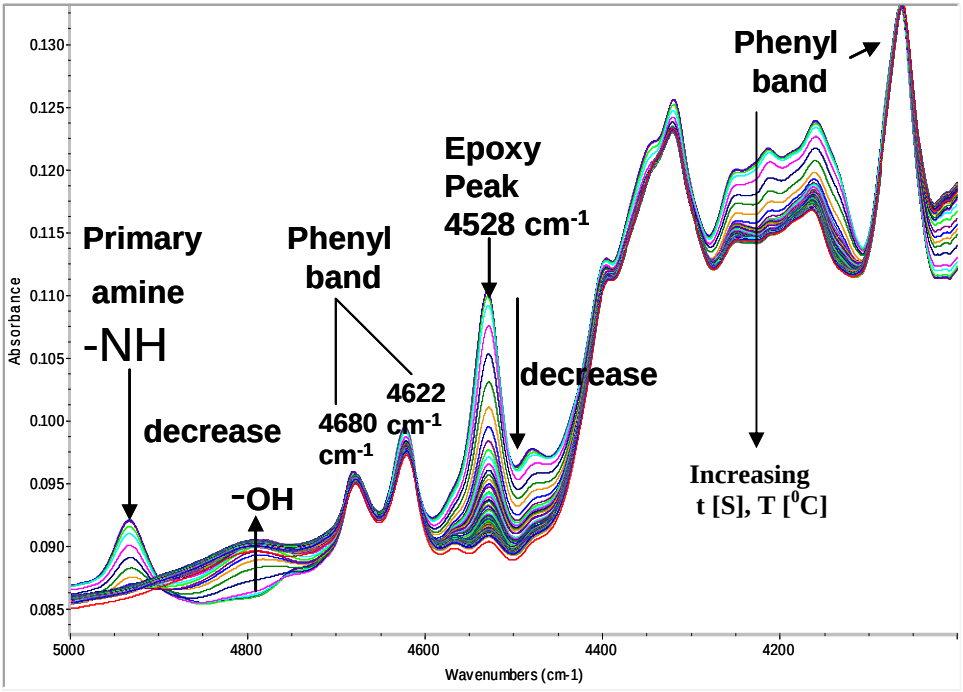

Figure.2.12. Cure kinetics spectrum of the reacting epoxy-amine system model II (E3) obtained in the Transmission mode set up for Near-IR studies.

Conversion

FTIR can be used for analyzing the cure reactions of epoxy resins [Morgan and Mones, (1987), Bellenger et al., (1987), Wang and Gillham, (1990), Stevens, (1981), Stevens, (1981), George et al., (1991), St. John and George, (1992)]. Each chemical group (reacting or non-reacting) of the resin-hardener mixture in *FTIR* shows a characteristic absorbance peak at a certain wavelength. Hence during the curing process the absorbance peak area of the reacting group decreases whereas the peak area of the non-reacting group does not change. Since the peak area of the non-reacting groups does not change and hence can be considered as internal reference peak. Hence the conversion (p) of the reacting groups can be determined in two methods as shown by *Equations 2.15 & 2.16.*

Method (i):

$$Conversion(p) = 1 - \frac{A_t}{A_0} \qquad \textbf{(2.15)}$$

where, A_t = Area of the absorbance peak of the reacting group at time (t)

A_0 = Area of the absorbance peak of the reacting group at time ($t=0$)

The disadvantage of *Equation 2.15* is that the absorbance also varies with the sample thickness. Therefore in practice, the decrease in peak area is first normalized to the peak area of a non-changing reference peak. The latter equation will be used throughout this thesis to determine the conversion based on the *FTIR* measurement.

Method (ii):

$$Conversion(p) = 1 - \frac{A_t / A_t^{ref}}{A_0 / A_t^{ref}} \qquad \textbf{(2.16)}$$

where,

$R_g(0)$ = The ratio of peak area of a reacting group to reference peak area at time ($t=0$),

$R_g(t)$ = The ratio of peak area of a reacting group to reference peak area at time (t),

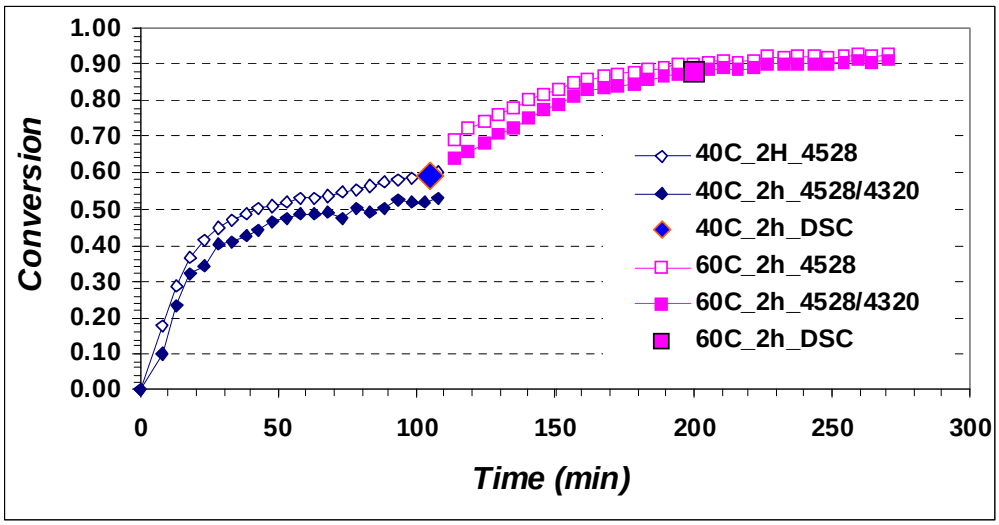

Figure.2.13. The unfilled, filled symbol corresponds to the conversion of epoxy determined using Method (i) and Method (ii). A filled symbol with larger size corresponds to the conversion determined by DSC.

Further, the conversion of epoxy was determined alternatively using either *Method i* or *Method ii* as described in *Section 1.7, Chapter 1* and is compared to the results of *DSC*. The comparison is shown by *Figure 2.13*.

For the *method 2* the reference being selected was the combination bands of aliphatic methyl groups at 4320 cm^{-1}. It can be seen from *Figure 2.13* that results of *FTIR* are in good agreement with those from *DSC*.

i Attenuated total reflection (ATR)

The Attenuated total reflection mode is used especially if the thickness of the material to be characterized in transmission mode is large and also if the material is opaque and does not allow for infrared light to pass through it.

The basic mechanism behind this mode is that the infrared light is passed through an infrared transmitting ZnSe crystal with a high refractive index, allowing the radiation to reflect within the *ATR* crystal several times as shown by *Figure 2.14* before it reaches the detector. As discussed earlier the transmission mode using the quartz wafer can only be used to follow the cure reaction in near infrared region. So, in order to follow the cure reaction of the selected model systems in mid infrared region, the *ATR* containing ZnSe is used.

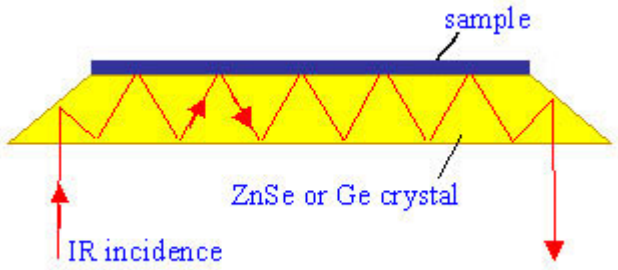

Figure.2.14. Schematic of a polymeric sample on crystal (ZnSe) in ATR mode.

Sample State

Solids, liquids and gels can be used irrespective of the thickness

2.12. Coefficient of thermal expansion (α_L)

When the temperature of a substance is changed the energy that is stored in the intermolecular bonds between the atoms changes. With the increase in the stored energy the length of the molecular bonds also increases. As a result, solids typically

expand in response to heating and contract on cooling; this dimensional response to temperature change is expressed by its coefficient of thermal expansion (*CTE*). The coefficient of linear thermal expansion, α_L and the glass transition temperature (T_g) [Gupta and Brahatheeswaran, 1991] can be determined using a thermo-mechanical analyzer (*TMA*) and is shown by the *Equations 2.17 & 2.18*.

$$\alpha_L = (1/L_0)(\Delta L/\Delta T) \qquad \textbf{(2.17)}$$

where $\Delta L/\Delta T$ is the slope of the dimensional change - temperature curve and L_0 is the initial length of the solid sample.

$$f_{V(SB)} = (\alpha_r - \alpha_g)T_g^{TMA} \qquad \textbf{(2.18)}$$

Here, α_g, α_r *and* T_g^{TMA} represent the *CTE* in the glassy region, the *CTE* in the rubbery region and the glass transition temperature determined using *TMA*.

Procedure

A rectangular flat sample containing a silica spacer above and below is placed on the support within the furnace as shown in *Figure 2.15*. The thermal expansion of the silica spacer is very low in comparison to that of the sample and therefore the thermal expansion of the silica spacer could be neglected. The silica spacer that is placed above and below the sample is to ensure that any load applied on the silica spacer can distribute the load uniformly through out the sample. A flat tipped probe which is used for sensing the length change is placed on the sample. A small static force is applied and the sample is subjected to a temperature program. The probe movements can record the sample expansion or contraction. The length changes of the sample are measured by a sensitive position transducer which is a linear variable displacement transducer (LVDT) which is connected to the probe. The probe and the support are made from a material such as quartz glass, which has a low reproducible, and accurately known coefficient of thermal expansion, and also has low thermal conductivity, which helps to isolate the sensitive transducer from the changing temperatures in the furnace. A thermocouple placed near the sample indicates its temperature. The chamber inside the furnace is filled with inert gas (nitrogen) to prevent oxidation and also to assist the heat transfer to the sample. A load of 0.1 N is

applied using a force motor on the sample which has the typical dimensions of 5-10 mm in height and width. Other parameters include the temperature ramp from room temperature to 180 °C with a heating rate of 10 °C per minute. Initially, the sample is subjected to a heat scan in order to remove the thermal ageing. In the second scan, the measurement of the dimensional changes with temperature is done and a typical plot of the dimensional changes with increase in temperature can be seen form *Figure 2.16*. The slope of the dimensional change with temperature is the measure of the coefficient of thermal expansion (α_L).

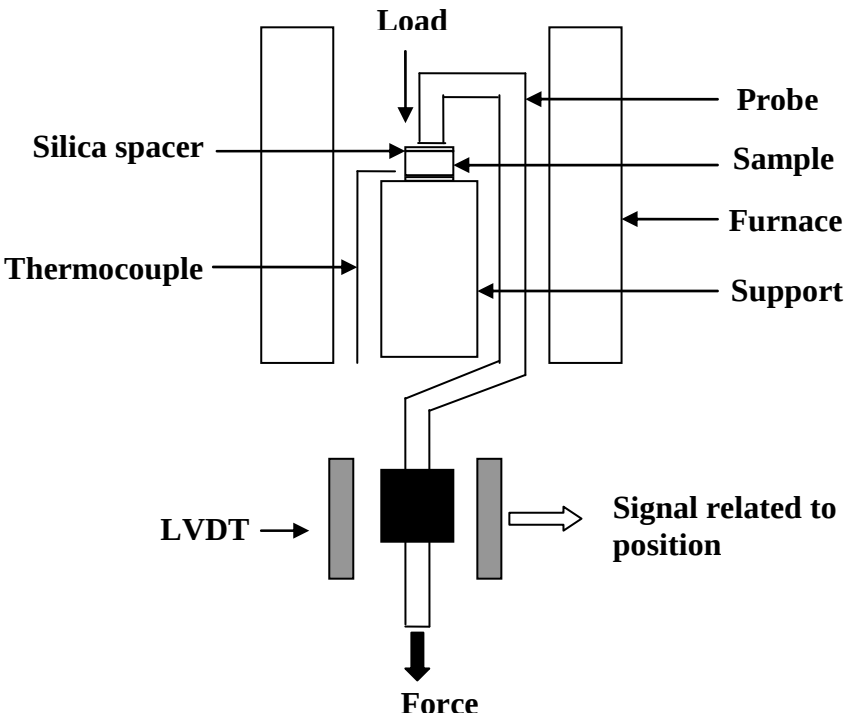

Figure.2.15. Compression mode set inside the furnace of the Thermo-mechanical analyzer (TMA).

Figure 2.16 shows a typical plot of the dimensional change with respect to temperature for a polymeric sample in the thermo mechanical analyzer (*TMA*) in the second heat scan. *Figure 2.16* shows that the dimensional change of the polymeric sample increases with increasing temperature. Moreover two distinct linear regions are observed below and above the glass transition temperature (T_g). T_g is the point intersection of the lines drawn through the two regions. The T_g determined using *TMA* is denoted by T_g^{TMA} in this thesis. It is compared with the $T_g^{\tan \delta}$ in *Table 3.2* of *Chapter III*.

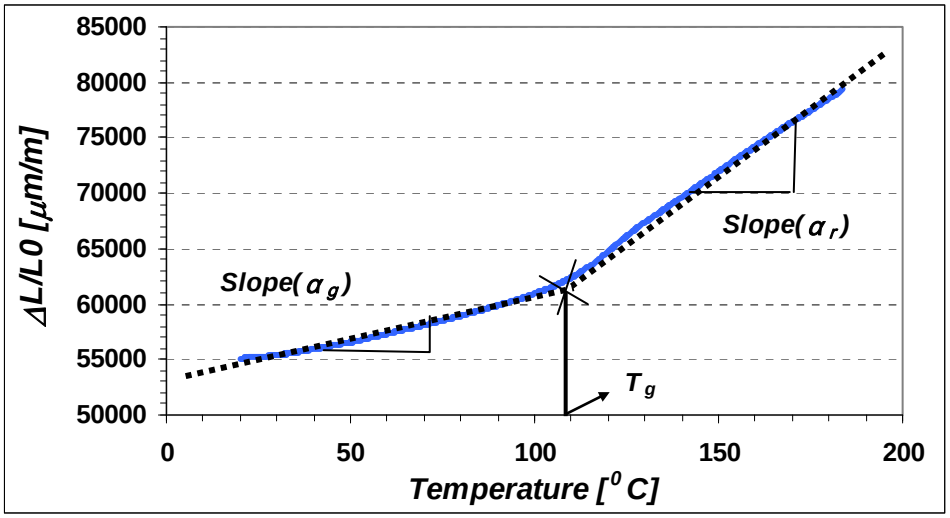

Figure.2.16. Dimensional change ($\Delta L/L_0$) versus Temperature of a polymeric material. The slope below and above T_g gives the coefficient of linear thermal expansion in the glassy and rubbery regions.

The slopes of the two linear lines below and above T_g in *Figure 2.16* are the measures of the thermal expansion coefficients in the glassy state (α_g) and the rubbery state (α_r).

CHAPTER – III

Glass Transition Temperature

Chapter 3

Glass Transition Temperature

3.1. Introduction

The glass transition temperature (T_g) marks the change from glassy to rubbery behavior in the viscoelastic curve as depicted in the *Figure 1.6* in *Chapter I*. This remarkable behavior, the change from the glassy to the rubbery state is a characteristic property of polymeric materials. Since the change from the glassy to the rubbery state occurs with respect to a certain temperature range, the definition of T_g becomes complicated. But it is quite obvious that T_g cannot be defined with a single point in the transition zone in *Figure 1.6* in *Chapter I*. Moreover, the determination of T_g of the polymeric sample also depends on the method and sensitivity of the instrument, which will be discussed in *Section 3.3* of this *Chapter*. Although it is complicated to define T_g from the above discussed observations, it is universally accepted that T_g is related to the mobility of the molecular chains within the polymeric sample. Based on the molecular mobility of polymeric chains, many definitions of T_g exist in the literature and will be discussed later in *Section 3.2* of this *Chapter*.

Importance of understanding T_g

Understanding the glass transition temperature (T_g) of polymers is very important for various reasons.

First and most obvious is that T_g determines the upper bound for the usage temperature of the polymer. For instance, if the T_g of the polymer is greater than or equal to 100 °C then the polymer is in the glassy state with relatively high stiffness (usually 2-3 GPa). Therefore polymer with a T_g more than 100 °C can be used in applications where the polymer should withstand a high temperature (~100 °C) and also should have high stiffness.

Other reasons for understanding the T_g is the influence of T_g on the chemorheology as well as the residual stresses of a thermoset [Masaki shimbo et al., (1985) & Halley and Mackey, (1996)].

Mechanical properties show profound changes in the region of the glass transition. For example, the elastic modulus may decrease by a factor of over 1000 times as the

temperature is raised through the glass transition region in unfilled polymers. Many other physical properties change rapidly with temperature in the glass transition region. These properties include coefficients of thermal expansion, heat capacity, refractive index, mechanical damping, nuclear magnetic and electron spin resonance behavior, electrical properties, tensile strength and ultimate elongation in thermosets.

In addition to its practical importance, T_g has important theoretical implications for the understanding of the molecular origin to polymer mechanical behavior and plays a central role in establishing the frame work, mentioned above, which relates the properties of different polymers to each other.

Furthermore, a predictive model is needed for the determination of T_g such that the tailoring of the viscoelastic properties in thermosets could be achieved.

3.2. Literature definition of T_g

According to Bellenger (1984), the glass transition temperature (T_g) is defined as the temperature at which the forces holding the distinct components of a polymeric material together are overcome, so that these components become able to undergo large-scale viscous flow, limited mainly by the inherent resistance of each component to such flow.

Stutz and his coworkers [Stutz et al., (1990)] correctly point out that T_g has been experimentally shown to be a short–range phenomenon, so it should not matter whether a crosslink is elastically effective or not, since this definition of a crosslink would involve a long-range effect.

Boyer (1963) has suggested that the glass transition is associated with a coordinated segmental motion of 10-20 of the chain backbone atoms, a rather local phenomenon.

According to Gibbs and DiMarzio (1958), the glass transition temperature is viewed as a thermodynamic transition and thus is a long-range phenomenon comprising the whole sample, and therefore it does matter whether a crosslink is elastically effective. The short-range nature of T_g observed experimentally is due to the finite time scale of the experiments.

When a polymer is heated up to T_g, it acquires enough thermal energy to be able to overcome two types of resistance to the large-scale motions of its components:

1. The *cohesive forces* holding different components together consist of polar and Van der Waals forces between different molecules and molecular segments which is not

specific for polymers but also for other materials like ice and glass. The relevant components for the glass transition in amorphous polymers are chain segments. The cohesive forces can be quantified in terms of properties such as cohesive energy density. The increase in the polarity increases the cohesive forces i.e., cohesive energy density contributes to the increase of the T_g. Thus as an example in the series polypropylene (T_g=-10 °C), poly(vinylchloride) (T_g=85 °C) and polyacrylonitrile (T_g=101 °C) the size of the side groups is about the same, but the polarity increases. The effect of cohesive energy density or the strength of intermolecular forces is further illustrated by the series poly (methyl acrylate) (T_g=3 °C), poly (acrylic acid) (T_g=106 °C) and poly (zinc acrylate) (T_g>400 °C). In this series strong hydrogen bonds in poly(acrylic acid) greatly increase the intermolecular forces over those found in the methyl ester polymer. The intermolecular forces are increased more in the zinc compound by even stronger ionic bonds, which have many of the characteristics of crosslinks.

2. Due to *Internal friction* between the individual components (i.e., chain segments in polymers) which resists the viscous flow. Resistance to the viscous flow of polymer chain segments is related to the topological and geometrical arrangements of their atoms. This is especially expressed by the somewhat universal concept of chain stiffness. The glass transition occurs when there is enough freedom of motion for chain segments of up to several "statistical" (Kuhn) segments in length to be able to execute cooperative motions [Bershtein et al., 1985]. As a general rule the length of the Kuhn segments increases with increasing chain stiffness. Main-chain aliphatic groups, ether linkages, and dimethylsiloxane groups build flexibility into a polymer and lower the T_g; the effect of the length of aliphatic side groups is illustrated in *Section 1.7* in *Chapter I*. On the other hand, large or rigid groups such as substituted aromatic structures and pendant tertiary butyl groups raise the glass transition temperature. The effect of decreasing molecular flexibility by the substitution of bulky side groups onto a polymer chain is illustrated by the series polyethylene (T_g= 40 °C), polypropylene (T_g= -10 °C), Polystyrene (T_g= 100 °C) and poly (2, 6-dichlorostyrene) (T_g= 167 °C). However, it is the flexibility of the group, not its size that is the determining factor of T_g. Thus increasing the size of an aliphatic group can actually lower the glass transition temperature.

The "intrachain" effect of the stiffness of individual chain segments is generally somewhat more important than the "interchain" effect of the cohesive (attractive) forces between different chains in determining the value of T_g.

The effects of chain stiffness and of cohesive forces on the value of T_g are different from each other. For example, a pendant hydroxyl group has relatively little effect on the chain stiffness, but can increase the cohesive forces very significantly by hydrogen bonding. On the other hand, the chain stiffness and interchain cohesive forces are not completely independent of each other. Many interrelationships exist between the structural features increasing chain stiffness and the structural features increasing interchain cohesion. For example, phenyl rings are much more rigid than cyclohexyl rings, and therefore result in a larger chain stiffness. Phenyl rings are also denser than cyclohexyl rings, and result in much higher cohesive energy densities. Based on the considerations summarized above, it is not surprising that most theories of the glass transition depend on the chain stiffness and/or the cohesive forces. The same statement can be also made for all empirical correlations for T_g, which either explicitly or implicitly attempt to account for the effects of chain stiffness and cohesive forces.

3.3. Measurement of T_g

The glass transition temperature can be detected in a variety of experiments, which can be roughly classified into those dealing with dimensional changes of the polymer, and those measuring the nature and extent of molecular motion.

Perhaps the most common way of measuring T_g is by means of the thermal expansion coefficients undergoing marked changes at T_g using *TMA* (*Section 2.10, Chapter II*) and therefore can be defined as the temperature at which the thermal expansion coefficient undergoes a step change at heating and cooling rates of 1 °C /min. Similarly, a Pressure-Volume-Temperature (*PVT*) set up which measures the volumetric expansion coefficients can also be used to measure T_g.

Experiments that are sensitive to the onset of molecular motion in polymer chains may be used to detect the glass transition. Such methods include the measurement of internal friction, dielectric loss in polar polymers and nuclear magnetic resonance (NMR) spectroscopy.

Other methods include heat capacity (C_p) measurements, refractive index, stiffness and hardness.

Figure 3.1 shows the experimental data obtained from the characterization of polymers using different instruments and the method that can be used to determine the T_g of the polymer.

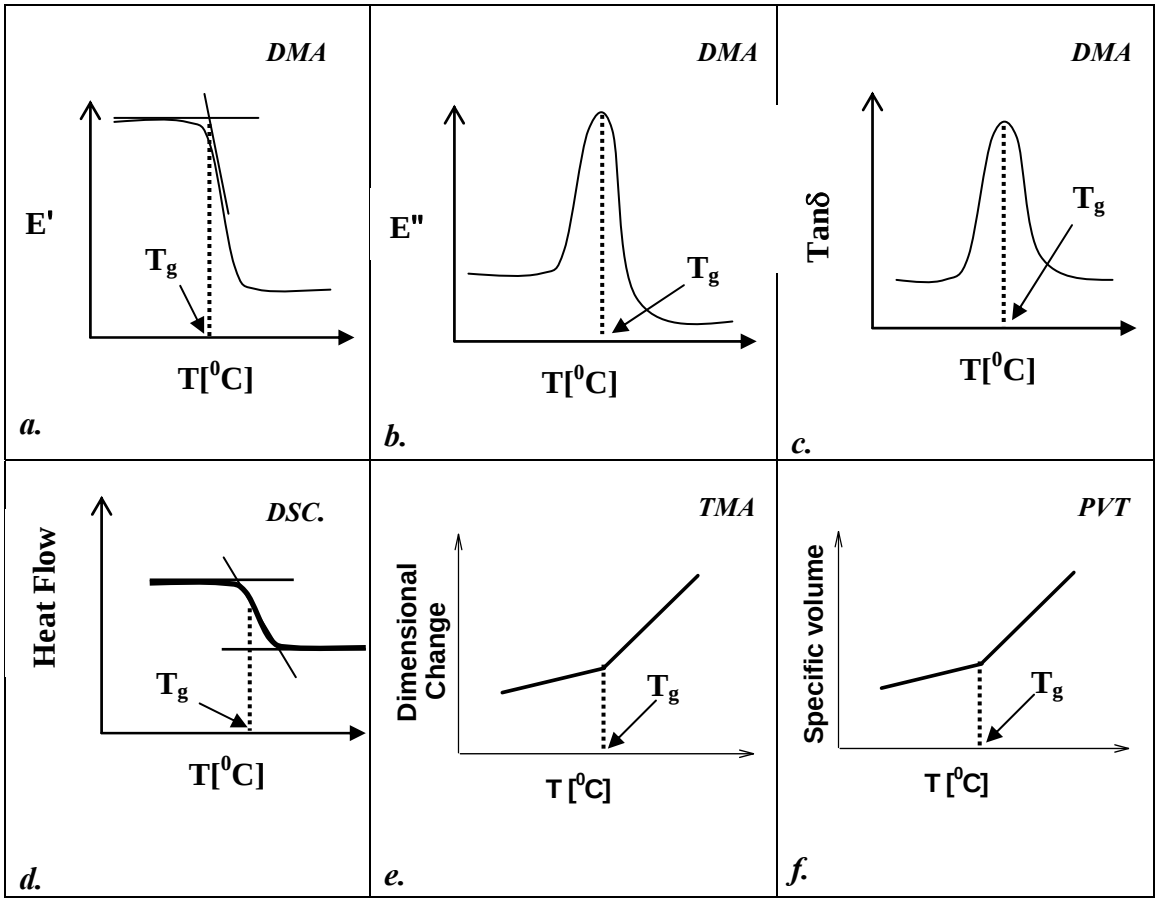

Figure 3.1. T_g determined using different experimental techniques [shown at the top right hand corner in each box]. T_g is the temperature (a) At the drop in storage modulus (E') for 1 Hz frequency (b) Peak maximum of the loss modulus (E'') curve for 1 Hz frequency (c) Peak maximum of the tan *δ curve for 1 Hz frequency d. mid-point of the drop in the heat flow (e,f) Point of intersection of linear regions.*

The T_g determined using different experimental techniques yield different T_g values and can vary up to 20%. Also the T_g determined from the data obtained from the same instrument can also vary. For example, *Figure 3.1 a, b, c* shows three ways of determining the T_g from the *1 Hz* data of storage modulus (*E'*), loss modulus (*E''*), tan δ obtained from the characterization of the polymer in *DMA*.

An excellent review article by Lee (1983 & 1989) provides detailed quantitative critical assessments, and extensive lists of the original references, for some of the best–known empirical correlations for T_g.

Rate of measurement. The glass transition temperature is generally measured by experiments that correspond to a time scale of seconds or minutes. If the experiments are done more rapidly, so that the time scale is shortened, the apparent T_g value is shifted. Thus as generally measured, T_g is not a true constant but shifts with the time scale of the experiment or observation. For example in ultrasonic's scanning technique a very high frequency scale of 10^6 Hz is applied. While a ramp of 10° C /min is normally used for the *DSC*, the *TMA* and quasi-stationary for *PVT*.

Apart from the rate and method of measurement, there are other e*xternal factors* by which the measured T_g is affected. These are discussed below.

i. *Structural and compositional factors.* The most fundamental of these are the chain stiffness and the interchain cohesive forces.
ii. *Crosslinking* is another structural factor which can affect T_g. T_g increases with increasing crossling denisty (ν_C) [Ogata,1993]
iii. *Average molecular weight* of the polymer chains. T_g increases asymptotically, with increasing average molecular weight, to its limiting values for the "high polymer" at infinite average chain molecular weight [Nielsen , 1994].
iv. The presence of *additive, fillers, unreacted residual monomers and/or impurities*, whether deliberately included in the formulation of a resin, or left over as undesirable by-products of the synthesis. For example, plasticizers of low molecular weight generally decrease T_g [Couchman, (1983), Sears and Darby, (1982)].
v. *Thermal history.* Either the annealing or the physical ageing of test specimens at elevated temperatures below T_g usually results in an increase of T_g. For example, this effect has been studied [Neki and Geil, 1973] in detail for bisphenol-A polycarbonate.
vi. *Thermal, thermo-oxidative and/or photochemical degradation.* The onset of rapid degradation sometimes occurs in the temperature range of the glass transition, obscuring the distinction between the glass transition and degradation. For example, T_g values of 700 K or above, reported in the literature for some polymers with very stiff chains, are often not true T_g values, since degradation and softening take place simultaneously and inextricable.
vii. The *pressure* also affects the value of T_g. Most measurements of T_g are performed under normal atmospheric pressure, so that the effect of pressure is very seldom

considered in any detail in correlations for T_g. For example, T_g went from (a) 100 °C at atmospheric pressure to 182 °C at 200 *MPa* pressure for poly styrene, (b) 103 °C at atmospheric pressure to 121 °C at 100 *MPa* for Poly (methyl methacrylate) [Aharoni, 1998].

The glass transition varies from -143 °C for poly (diethyl siloxane) rubber up to above 300 °C or above the decomposition temperature for highly crosslinked phenol-formaldehyde resins and polyelectrolytes.

The explicit nature of the glass transition is not clear, and many theories, some conflicting, have been proposed. It represents an interrupted approach to a hypothetical thermodynamic state of zero configurational entropy and close-ordered segmental packing. This state cannot be reached because the molecular motions that permit rearrangement to better packing and lower entropy become exponentially slower with decreasing temperature. Although the theoretical nature of the glass transition is subject to debate, the practical importance of T_g cannot be disputed.

3.4. Predictions for T_g

3.4.1. Principle of Molar Additive Contribution

Several authors have proposed correlations between the chemical structure and the glass transition temperature of polymers [Hayes (1961), Barton and Lee (1968), Lee (1970)]. Their methods are usually based on the assumption that the structural groups in the repeating units provide weighed additive contributions to the T_g.

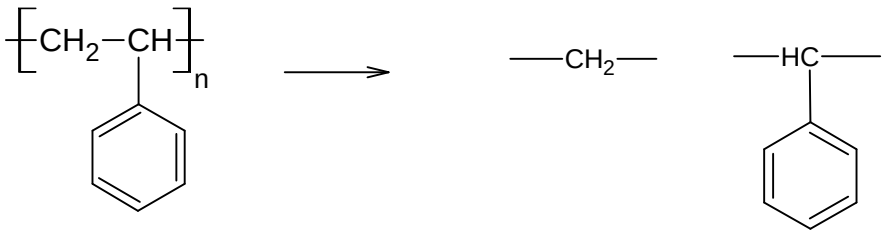

Figure 3.2. The separation of polystyrene into individual structural groups.

As an example, *Figure 4.2* shows how polystyrene polymer can be separated into structural groups.

In the case of ideal additivity the contribution of a given group is independent of the nature of adjacent groups. Although this ideal case is seldom encountered in practice,

additivity can often be approximated by a proper choice of structural groups. The general form of the correlations for T_g is

$$T_g \sum_i s_i = \sum_i s_i T_{gi} \qquad \textbf{(3.1)}$$

where T_{gi} is the specific contribution to T_g of a structural group, and s_i is a weight factor attributed to a given structural group.

Hayes (1961) assumed $\Sigma_i\ s_i T_{gi}$ to be identical with the molar cohesive energy and derived from this a number of rules for calculating the individual s_i-values. Barton and Lee (1968) suggested that s_i is identical with the weight or mol fraction of structural groups and calculated values of the characteristic constant T_{gi} for the groups involved. In a more recent article Lee (1970) compared four methods of counting s_i for a small selected group of polymers. A good correlation could be obtained by assuming that the T_{gi}-value of a given structural group was dependent on the nature of adjacent groups. However, this leads to a very large number of T_{gi}-values. The correlation obtained with independent T_{gi}-values was far less good.

3.4.2. Van Krevelen and Hoftyzer Approach

Van Krevelen and Hoftyzer (1975) have shown that in applying *Equation. 3.1* the use of weight fractions for s_i instead of numbers of chain atoms offer some advantages. Also for reasons of uniformity with the other additive quantities, it was decided to introduce the following additive quantity:

$$Y_g = \sum_i Y_{gi} = T_g.M \qquad \textbf{(3.2)}$$

where Y_g is the molar glass transition function (*K.g/mol*), T_g is the glass transition temperature and M is the molecular weight of the repeating unit and ΣY_{gi} is the sum of the individual group contributions. So,

$$T_g = \frac{Y_g}{M} = \frac{\sum_i Y_{gi}}{M} \qquad \textbf{(3.3)}$$

Table 3.1 shows the individual group contribution values used in the calculated T_g of the selected four model systems.

Group	***Y_{gi} (K.g/mol)***	***Group***	***Y_{gi}***
—O—	4000	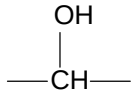	13000
—CH_2—	2700		3200
CH_3—	3000	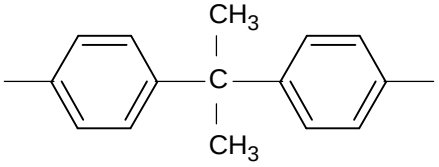	87000
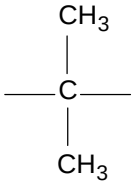	8500 [f] 15000 [s]	—N—	7000 [f] 14000 [s]

Table.3.1. Showing Y_{gi} values used for the calculation of T_g using the molar additivity principle [Van Krevelen, 1976].

[a] Sterically free

[s] Sterically hindered

The prediction of T_g using the principle of molar additive contribution was previously done by van Van Krevelen and Hoftyzer (1976) for linear polymers only. The role of crosslinking was not discussed in their work. The principle of molar additive contribution can be extended to a crosslinked network by considering that the crosslinking site is sterically hindered and hence the value of a molar glass transition function (*K.g/mol*) of a sterically hindered group is taken and calculated. As an example the calculation of the T_g for the crosslinked network of the sample *(A4)* is shown below. *Example:*

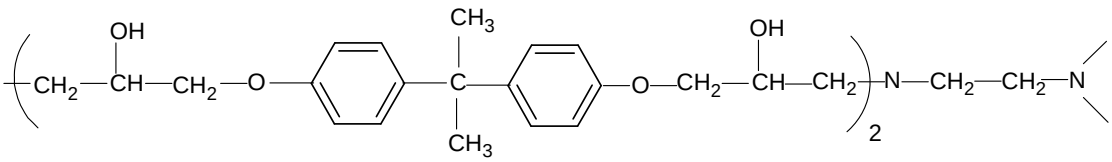

Figure 3.3. The structure of the crosslinked network for the sample (A4).

$Y_g = 87000 + 4\times 2700 + 2 \times 13000 + 2 \times 4000 + 0.5(2 \times 2700 + 2 \times 14000) = 148500$

$M_w^{\ Network} = 340.41+0.5*60=370.41$

$T_g^{\ VH} = 148500 \div 370.41 = 401\ \text{K} = 128\ ^\circ\text{C}$

Here $M_w^{\ Network}$ is the molecular weight of the network and the T_g value is obtained using the Van Krevelen and Hoftyzer approach and is denoted as $T_g^{\ VH}$.

In order to understand the effect of crosslink density on the glass transition temperature of curing resins many equations are determined and some of them are discussed below.

It is well known that for linear polymers various physical approaches in order to predict the glass transition via., free volume, entropy, cohesive energy, etc., resulted in a wide variety of relationships between structure and glass transition temperature (T_g) [Van Krevelen and Hoftyzer, (1976)]. An even more complicated situation exists in the case of network polymers for which the contribution of crosslinks i.e., crosslink density on the T_g was studied by many researchers. Here important empirical relations were derived. These are discussed below.

3.4.3. Lee and Hartmann Approach

Lee and Hartmann studied an extensive series of epoxide-amine systems [Lee and *Hartmann*, 1983 & 1984] using the *Equation*s *3.4 & 3.5*.

$$MT_g^{\ -1} = \sum M_i T_{gi}^{\ -1} \qquad \textbf{(3.4)}$$

$$M \ln T_g = \sum M_i \ln T_{gi} \qquad \textbf{(3.5)}$$

3.5. T_g and crosslink density (ν_C)

The introduction of a crosslink will not only restrict the segmental mobility of the polymeric chains but also decrease the free volume (i.e., the unoccupied volume in which the polymeric chains are not present). The restricted mobility of the polymeric chains accompanied by the decrease in the free volume will cause an increase in the glass transition temperature (T_g). According to Fox and Loshaek and others, it is assumed that in crosslinked polymers the T_g is a function of the crosslink density (ν_C). Among the numerous theoretical and empirical relations reported in literature most involve linear dependences [Fox and Loshaek (1955), Kanig (1967)]. Exponential

[DiMarzio (1964), Nielsen (1969)] or logarithmic relationships (shibayama, 1975) can also be found.

3.5.1. Fox and Loshaek Approach

Simple free volume considerations lead to a linear equation of the type

$$T_g = T_{gl} + K_{FL}\nu_C \qquad \textbf{(3.6)}$$

where T_{gl} is the glass transition temperature of the corresponding linear polymer, ν_C is the crosslink density and K_{FL} is a Fox and Loshaek constant. The validity of the relationship [*Equation 3.6*] was verified for polyurethanes and poly (styrene/divinyl benzene) networks. However, in the latter case, K_{FL} was found to depend on the functionality of the crosslinking reactants. For the materials under study, K_{FL} varies from almost 50-60 *K kg mol*$^{-1}$ for DGEBA-aromatic diamine systems to 6-10 *K kg mol*$^{-1}$ for completely aliphatic DGEBD-DA2 (Aromatic epoxy (f_E = *2*) cured with aliphatic amine (f_a = 4) and DGEE-DETA (Aliphatic diepoxy cured with aliphatic amine) systems. A physical basis of this relationship is the hypothesis that at T_g, the excess free volume of the linear polymer is proportional to the crosslink density in the network. Hence *Equation 3.6* cannot be applied to systems of high crosslink density such as polyesters, at least because of the "copolymer effect" [Cook, 1978]. In this case free volume or more general considerations [Bank and Ellis, (1982)] would lead to *Equation 3.7.*

$$T_g = \sum \frac{x_i T_{gi}}{x_i} \qquad \textbf{(3.7)}$$

where x_i is a parameter characterizing the network composition (segments, chain ends and the repeating unit), and T_{gi} is a component value characterizing the contribution of the *i*th species to T_g. *Equation 3.7* can be applied to epoxies.

3.5.2. Dimarzio's Approach

From considerations of configurational entropy, DiMarzio (1964) obtained:

$$\frac{T_g - T_{gl}}{T_{gl}} = \frac{K_{DM} F \nu_C}{1 - K_{DM} F \nu_C} \qquad \textbf{(3.8)}$$

The above *Equation* can be rewritten as

$$T_g^{DiM} = \frac{T_{gl}}{1 - K_{DM} F (\nu_C^{M\&M} / \rho)} \qquad \textbf{(3.9)}$$

where,

T_{gl}, = T_g of uncrosslinked or linear polymer,
K_{DM} = Constant
F = Flexibility parameter
ρ = Density (g/m^3)
$\nu_C^{M\&M}$ = Crosslink determined using Macosko and Miller in *mol/m^3* [*Equation 1.14, Chapter 1*]

In the case of polyesters having an aliphatic skeleton, Cook finds that $K_{DM}F$ is nearly constant (*0.12-0.16 kg mol^{-1}*) [Cook, 1978]. However, for the epoxies under study, $K_{DM}F$ varies from 0.02 to 0.12 *kg mol^{-1}* and increases more or less regularly with the aromatic content, or with the stiffness of segments as hypothesized by DiMarzio (1964). According to DiMarzio's (1964) hypothesis, the value of $(T\text{-}T_{gl}) / \nu_C T_g$ is proportional to F, K_{DM} being a universal constant equal to 2.91.

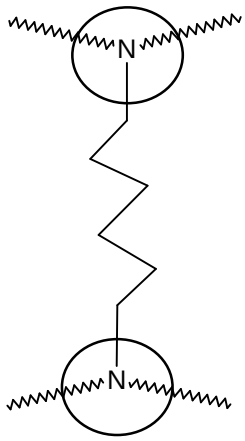

Figure 3.4. Crosslinked network containing trifunctional crosslink unit.

In order to apply *Equation 3.9* to epoxies the flexibility parameter F has to be determined. The following points are to be considered:

a. In the case that the ideal network formation due to the reaction epoxy and amine hardener, the trifunctional crosslink reactant (i.e., amine nitrogen atoms) is taken into consideration (*Figure 3.4*) and the influence of the bridge structure cannot be ignored.

For instance, $K_{DM}F$ is about 110 $g\ mol^{-1}$ for DGEBA- Diamino diphenyl methane (DDM) system and 70 $g\ mol^{-1}$ for DGEBA- 1, 12-diamino dodecane (DA_{12}).

b. It can be observed that $K_{DM}F$ is nearly constant in a series whose members differ only by the number of repeating units. To take into account this result, the simplest mode of calculation of F would be

$$F = \frac{1}{n}\left(\sum F_n\right) \qquad \textbf{(3.10)}$$

where, ΣF_n is the sum of the linear segments attached to the crosslinks**.**

For example, if $n=3$, then F can be determined using *Equation 3.10* as shown as follows

$$\Rightarrow F = \frac{1}{3}\left(F_1 + F_2 + F_3\right) = \frac{1}{3}\left(\frac{m_1}{\gamma_1} + \frac{m_2}{\gamma_2} + \frac{m_3}{\gamma_3}\right)$$

where, m is the molar mass of the segment which contains γ rotatable bonds in its skeleton.

1. In certain cases many types of crosslink reactants coexist. It can be proposed that

$$F = \frac{\sum N_i F_i}{\sum N_i} \qquad \textbf{(3.11)}$$

where N_i is the number of crosslink reactants of type i (whose flexibility parameter is F_i) in the "monomer unit" of the network.

2. The method of counting flexible bonds carries some ambiguity, even in the case of crosslinked homopolymer [Cook, (1978), DiMarzio, (1964)]. It can be proposed to take into account all the skeleton bonds except aromatic ones.

Example:

The glass transition temperature predicted using DiMarzio's approach [eq.3.9] for sample *(A4)* is shown below

T_{gl} = 331,	T_g [K] is the T_g of linear or uncrosslinked polymer [See *Table* 3.2],
M_1=M_2= 342,	Molecular weight of reacted epoxy (*g/mol*),

M_3= 28;	Molecular weight between crosslinks in the reacted amine (*g/mol*),
γ_1= 12, γ_2=3,	Number of Skeletol aliphatic bonds in reacted epoxy and amine,
F_1=M1/γ_1=28.5;	Flexibility of the epoxy unit, in this case $F_1 = F_2$
F_3= M_3/γ_3=9.33,	Flexibility of the amine unit
$F_{(Total)}$= (F_1+F_2+F_3)/3= 22.11	Total flexibility (*g/mol*)
K_{DM} = 2.91,	
$v_C^{M\&M}$ = *3270*	Crosslink density (*mol/m*^{3})
ρ=*1.21* ×10^6	*Density (g/m*^{3}*)*

Applying DiMarzio's approach [Eq.3.9]

T_g^{DiM} = 331/ [1 – 2.91×22.11×(3270/*1.21* ×10^6)]= 401 K (= 128 °C)

T T_g^{DiM} value of 128 is obtained using Dimarzio's approach [*Equation 4.9*] for the sample *(A4)* is in agreement to the T_g^{VH} value obtained using Van Krevelen and Hoftyzer (which is also 128 °C).

3.6. Effect of reacting groups and crosslinks on T_g

Stutz et al., (1990) developed a generalized approach using the prevailing basic concepts; that is to start with the backbone glass transition temperature as a reference and then to independently characterize the influence of remaining reactant groups and crosslinks.

3.6.1. Influence of Remaining reactant Groups on the Glass Temperature

In the general case of crosslinked polymers it is not reasonable to characterize the influence of remaining reactant groups by the molecular weight as with linear polymers, because the molecular weight is only defined up to the gel point. Thus, it would seem more suitable to use the remaining reactant group concentration for characterization. Assuming that the reactive groups of a polymer have different properties than the chain-repeating units, the relative change of the glass transition temperature for a polymer with respect to its ideal backbone glass temperature T_g^{∞} should be proportional to an elementary increment γ and the concentration of reactive groups, thus

$$\frac{T_g - T_g^{\infty}}{T_g} = -\gamma c_0 (1-p) = -\frac{\gamma f}{M_{mon}}(1-p) \qquad \textbf{(3.12)}$$

where f is the functionality of the reacting group per monomer unit, M_{mon} is the molecular weight of the monomer and p the remaining reactant group conversion. Rearrangement leads to

$$T_g = T_g^{\infty} - K_1(1-p) \qquad \textbf{(3.13)}$$

with

$$K_1 = \frac{\gamma f T_g^{\infty}}{M_{mon}} \qquad \textbf{(3.14)}$$

where, K_1 is a constant specific for each polymer. Thus *Equation 3.13* characterizes the influence of reactant groups of a polymer on its glass transition temperature, independent of the functionality of the system. With crosslinking systems, it predicts a linear relation between glass transition temperature and reactive groups at low conversion, where the influence of the reacting group is still negligible.

3.6.2. The influence of Crosslinks on the T_g

DiBenedetto Approach

DiBenedetto, as cited by Nielsen (1969), characterized the influence of crosslinks on the glass transition temperature by

$$\frac{T_g - T_g^l}{T_g^l} = \frac{\left[\frac{E_x}{E_m} - \frac{F_x}{F_m}\right] X_C}{1-(1-F_x/F_m)X_C} \qquad \textbf{(3.15)}$$

where $T_g^{\,l}$ is the glass temperature of the uncrosslinked polymer as a reference and E_x/E_m is the ratio of the lattice energies of crosslinked and uncrosslinked monomer units. F_x/F_m is their mobility ratio of the glass temperature. The *Equation 3.15* was derived by DiBenedetto (1987) based on multidimensional lattice representations and refined statistical mechanical approaches for understanding the thermodynamic behavior of polymers. DiBenedetto defined the lattice energy of a polymer in terms of reduced molecular parameters i.e., properties of the repeating units. For most polymers it is expected that the mobility of a crosslinked unit at the glass temperature is essentially zero, thus *Equation 3.15* simplifies to

$$\frac{T_g - T_g^l}{T_g^l} = K\frac{X_C}{1 - X_C} \qquad \textbf{(3.16)}$$

where K is a constant which was estimated by DiBenedetto to be 1.2 for styrene/divinylbenzene copolymers, and X_C is the crosslink density expressed as the mol fraction of monomer units present at crosslinks at any stage of the reaction. The glass transition temperature of the uncrosslinked reference polymer T_g^l has generally been interpreted as the backbone glass transition temperature T_g^∞. However, this is an approximation valid only when the number of the remaining reactant groups is small and constant. In the general case discussed here, the uncrosslinked reference polymer is the one with its particular number of remaining reactant groups at any stage of the reaction. Therefore, the reference glass transition temperature changes with the degree of cure. So, T_g in *Equation 3.13* can be replaced by T_g^l and is shown by *Equation 3.17*.

$$T_g^l = T_g^\infty - K(1 - p) \qquad \textbf{(3.17)}$$

Here, T_g^l is the glass temperature of the linear reference polymer at conversion p. Finally, substituting T_g^l [from *Equation* 3.17] in DiBenedetto's *Equation* [*Equation 3.16*] yields:

$$T_g = [T_g^\infty - K_1(1 - p)]\left[1 + K_2\frac{X_C}{1 - X_C}\right] \qquad \textbf{(3.18)}$$

where T_g^∞ again is the true backbone glass transition temperature, K_1 is a constant characterizing the influence of remaining reactant groups on the glass transition temperature, and K_2 is another constant characterizing the influence of the crosslinks. X_C is the crosslink density.

Experimental results on the Glass Transition Temperature of Polymers

Several special cases can be derived from the general *Equation 3.18*. In the case of linear polymers $v_C=0$ and *Equation 3.18* reduces to *Equation 3.13*, which transforms to the Flory-Fox equation on replacement (1-p) by $1/M_n$. For post synthesis crosslinking of high-molecular-weight polymers, (*1-p*) is zero, so that

$$T_g^{DiB} = T_g^l \left[1 + K_2 \frac{X_C}{1 - X_C} \right] \qquad \textbf{(3.19)}$$

Equation 3.19 reduces to the Fox-Loshaek equation for low-crosslink densities. Moreover, the crosslink density (X_C) is a function of the conversion (p) and can be obtained using *Equation 3.20.*

$$X_C = a_i \sum_3^f \left(\frac{i}{2} - 1 \right) X_i \qquad \textbf{(3.20)}$$

where X_i is the fraction of the curing agent present at functionality *i (i=0, 1, 2…f)* and a_i is the mol fraction of the curing agent in the initial monomer mixture.

Note: In the definition of crosslink density by the DiBenedetto approach Eq. 3.20 has no units since all the terms in the Equation are in terms of fractions only.

3.7. T_g and average Molecular weight between crosslink's (M_c):

The dependency of M_c on T_g is well described by two models, one based on the concept of network free volume while the other model is based on the principle of corresponding states. The linear behavior between $T_{g\alpha}$ (i.e., T_g of the reacting system) and $1/M_c$ was first described by Fox and Loshaek, (1955). Banks and Ellis, (1982) proposed a linear relationship based on the addition and redistribution of the network free volume. In this model, $T_{g\alpha}$ is described by the following *Equation 3.21*

$$T_{g\alpha} = T_g^l + \frac{\varsigma}{M_C} \qquad \textbf{(3.21)}$$

Here, T_g^l is the glass transition temperature of the linear polymer backbone at infinite molecular weight. The above model proposes that the T_g of a polymer network i.e., $T_{g\alpha}$ is a result of two factors: T_g of the linear polymer backbone at infinite molecular weight (T_g^l) and the increase in $T_{g\alpha}$ is due to crosslinking. T_g^l is affected by the type of curing agent which changes the linear polymer backbone stiffness. In the second term the factor ζ is proportional to the molecular weight of the unreacted resin and to the ratio of the incremental free volume contributions from the resin and curing agent [Vakil and Martin, 1992] and is given by *Equation 3.22*.

$$\varsigma = \frac{\gamma_2}{\gamma_1}\frac{M_R}{2}T_{g,2} \qquad \textbf{(3.22)}$$

The type of curing agent has a smaller effect on ζ which represents the entropic contribution for the addition of crosslinks. In terms of the network free volume theory, tetrafunctional crosslinks would have less incremental free volume than trifunctional crosslinks. In this, γ_i is equal to dX_i/dT, X_i is volume contribution from species i, and subscripts 1 and 2 refer to the linear polymer and the curing agent respectively. γ_2/γ_1 then characterizes the relative rates of increase X_2 and X_1 with temperature. M_R is the molecular weight of the repeating unit in the linear polymer. $T_{g,2}$ is the glass transition temperature of a hypothetical network formed by the end-linking of the curing agent molecules. Lesser and Crawford, (1997&1998), calculated the average molecular weight between crosslinks (M_C), the average crosslink functionality (f_C) for the networks formed by the reaction of the reacting mixtures containing different functionalities and is shown by *Equation 3.23* and *3.24*. Alternatively, the crosslink density (in *mol/m*^{3}) can also be determined from M_C using the Lesser and Crawford approach which is denoted as $v_C^{L\&C}$ and is shown by *Equation 3.26*. Moreover, Lesser and Crawford predicted T_g using DiBenedetto's approach [*Eq. 3.19*] [denoted as T_g^{DiB}] by calculating X_C using *Equation 3.28 (*termed as $X_C^{L\&C}$*)*. The term X_C which was earlier mentioned as 'crosslink density' by DiBenedetto is termed as 'molar crosslink density' by Lesser and Crawford. The results of the predicted T_g i.e., T_g^{DiB} are shown in *Table 3.2* and the calculated values of $v_C^{L\&C}$ and $X_C^{L\&C}$ are shown in *Table3.3*.

Note: The term crosslink density (v_C) is expressed in mol/m^3 *whereas the term molar crosslink density (X_C) has no units.*

3.7.1. Calculation of M_C: (Applicable to full conversion only)

The molecular weight between crosslinks (M_C) can be calculated as follows:

$$M_C = \frac{2\left(M_e^{eq} + \sum_{f=2}^{\infty}\frac{M_W^A}{f_A}\Phi_{fA}\right)}{\sum_{f=3}^{\infty}\Phi_{fA}} \qquad \textbf{(3.23)}$$

where,

$$M_e^{eq} = \frac{M_W^E}{f_E} \qquad \textbf{(3.24)}$$

M_W^E = *Molecular weight of epoxy*
f_E = *Functionality of epoxy*
M_e^{eq} = *Epoxide equivalent weight of the resin*
Φ_{fA} = *Mol fraction of amine hydrogens provided by f-th functional amine*
f_A = *Functionality of amine*
f_C = *Average functionality*
M_w^A = *Molecular weight of amine*

The overall average functionality f_c is given as follows:

$$f_C = \frac{\sum_{f=3}^{\infty} \Phi_{fA}}{\sum_{f=3}^{\infty} \frac{\Phi_{fA}}{f_A}} \qquad \textbf{(3.25)}$$

Example:

The calculation of the average functionality for sample (A4) in Model I is shown as follows.

When, $\Phi_{fA} = 1$; $M_W^E = 340$; $f_E = 2$; $M_e^{eq} = 340/2 = 170$; $M_w^A = 60$,
Applying *Equation 3.22* ⇒ $M_c = 2(170 + (60/4)*1)/1 = 370$ g/mol (=0.37 kg/mol);
For tetrafunctional amine: $\Phi_{fA} = 1$; $f_A = 4$
Applying *Equation 3.23* ⇒ $f_c = 1 \div (1/4) = 4$;

3.7.2. Calculation of Crosslink density ($v_C^{L\&C}$): (Applicable to full conversion only)

$$\nu_C^{L\&C} = \frac{2(f_c - 2) \times \rho}{f_C \times M_C} \qquad \textbf{(3.26)}$$

where, M_C = Molecular weight between crosslinks (*g/mol*)
ρ = Density *(g/m^3)*
f_C = Average functionality

The determination of the crosslink density for the sample A4 is illustrated below.
When $f_C = 4$, $M_C = 370$ (g/mol), $\rho = 1.21 \times 10^6$ g/m^3

Applying *quation 3.25* $\Rightarrow v_C^{L\&C} = 2\times (4\text{-}2) \times 1.21\times 10^6 / (4\times 370) = 3270\ mol/m^3$

The crosslink density value determined using Crawford's approach is in good agreement with that of Bellenger and Miller & Macosko.

3.7.3. Calculation of Molar crosslink density ($X_C^{L\&C}$)

$$X_m = \frac{\sum_{f=3}^{\infty} \frac{\Phi_f}{f}}{\left(\frac{1}{2} + \sum_{f=2}^{\infty} \frac{\Phi_f}{f}\right)} \qquad \textbf{(3.27)}$$

Since the crosslink density depends on the crosslink functionality the inclusion of crosslink functionality into *Equation 3.27* becomes

$$X_C^{L\&C} = \left(\frac{f_C}{2} - 1\right) X_m \qquad \textbf{(3.28)}$$

The determination of the molar crosslink density ($X_C^{L\&C}$) for the sample A4 is illustrated below.

When the functionality of amine (f_A)= 4, Φ_f=1,

Applying *Equation 3.27* $\Rightarrow X_m = 0.25 / (0.5+0.25) = 0.25/0.75 = 0.333$

For sample *A4* the average functionality (f_C)= 4, *[see Equation 3.25]*

Applying *Equation 3.28* $\Rightarrow X_C^{L\&C} = [(4/2) - 1]\times 0.333 = 0.333$

3.8. Experimental

In the present section, a selection of experimental results is presented in *Table 3.2* and compared with the predictions using different approaches. As mentioned earlier, T_g can be measured using different experimental techniques and so the value of the T_g can vary. Therefore, only three definitions for the measured T_g are considered in this thesis and are mentioned below.

The temperature at the peak maximum for the tan δ *curve* for 1 Hz data obtained from the dynamic Mechanical Analysis *(DMA)* and is denoted by $T_g^{\tan\delta}$

The temperature at the peak maximum for the loss modulus *(E″)* curve for 1Hz data obtained from *DMA* and is denoted by $T_g^{E''}$

The temperature at the point of intersection of the bilinearly fit applied to the dimensional change of the sample with increasing temperature in Thermal Mechanical Analysis *(TMA)* and is denoted by T_g^{TMA}

Model No.	***Sample Code***	***T_g [°C]***							
		Measured			***Predicted***				
		$T_g^{\tan\delta}$	$T_g^{E''}$	T_g^{TMA}	T_g^{l}	$T_g^{V\&H}$	T_g^{DiM}	T_g^{DiB}	$T_g^{B\&E}$
						Eq.3.7	***Eq.3.9***	***Eq.3.16***	***Eq.3.21***
I	*A2*	*93*	*75*	*78*	*90*[a]	*94*	*89*	*89*	*89*
	A3	*121*	*112*	*116*	*72*[#]	*116*	*116*	*116*	*118*
	A4	*135*	*118*	*120*	*58*[#]	*128*	*128*	*140*	*145*
II	*E2*	*64*	*53*	*54*	*65*[#]	*65*	*65*	*65*	*65*
	E2.5	*90*	*91*	*74*	*73*[#]	*93*	*93*	*92*	*96*
	E3	*117*	*105*	*110*	*82*[#]	*121*	*121*	*127*	*127*
III	*C2*	*135*	*118*	*120*	*58*[#]	*128*	*128*	*140*	*145*
	C4	*128*	*121*	*117*	*53*[#]	*121*	*121*	*133*	*136*
	C6	*119*	*110*	*109*	*49*[#]	*114*	*114*	*128*	*129*
	C8	*108*	*105*	*100*	*45*[#]	*107*	*107*	*123*	*123*
IV	*P1*	*121*	*112*	*116*	*72*[#]	*116*	*116*	*116*	*118*
	P3	*98*	*91*	*82*	*59*[#]	*107*	*103*	*101*	*103*
	P6	*82*	*74*	*67*	*45*[#]	*95*	*80*	*85*	*86*

Table.3.2. The measured and predicted T_g's for all the samples of the selected four model systems.

The three definitions for the measured T_g as well as the predictions for the T_g and crosslink density (ν_C) of all the samples in the four model systems (except for sample *E4* in *Model II*) are tabulated and are shown by *Tables 3.2 &3.3*.

From *Table 3.2* it can be observed that the measured T_g value obtained from tan δ [i.e., $T_g^{\tan\delta}$] is higher in comparison to the T_g values obtained from the loss modulus ($T_g^{E''}$) and those obtained from the thermal expansion was T_g^{TMA} whereas the values of $T_g^{E'}$ and T_g^{TMA} are close. From the discussion above it can be understood that the value

of T_g can vary depending on the definition of T_g. Moreover, the predicted glass transition temperatures from different approaches as shown in *Table 3.2* are close to the values of the $T_g^{\tan\delta}$.

Mod. No.	***Sam Cod.***	***Crosslink density (v_C)*** *[mol/m^3]*				***F*** *[g/mol]*	***f_C***	***M_c*** *[kg/mol]*	***$X_C^{L\&C}$***
		Measured	***Predicted***						
		v_C^{Meas}	***$v_C^{M\&M}$***	***v_C^{Bel}***	***$v_C^{L\&C}$***				
		Eq. 1.2	***Eq. 1.11***	***Eq. 1.5***	***Eq. 3.25***	***Eq. 3.11***	***Eq. 3.24***	***Eq. 3.22***	***Eq. 3.22***
I	*A2*	*1104*	*0*	*0*	*0*	*23.92*	*2*	*-*	*-*
	A3	*1861*	*2039*	*2039*	*2039*	*22.83*	*3*	*0.39*	*0.22*
	A4	*3135*	*3270*	*3270*	*3270*	*22.11*	*4*	*0.37*	*0.33*
II	*E2*	*195*	*0*	*0*	*0*	*22.75*	*2*	*-*	*-*
	E2.5	*1163*	*1024*	*1024*	*1260*	*21.54*	*2.5*	*0.40*	*0.11*
	E3	*2262*	*2030*	*2057*	*2194*	*20.33*	*3*	*0.39*	*0.22*
III	*C2*	*3135*	*3270*	*3270*	*3270*	*22.11*	*4*	*0.37*	*0.33*
	C4	*3048*	*3097*	*3097*	*3097*	*22.73*	*4*	*0.38*	*0.33*
	C6	*2931*	*2966*	*2966*	*2966*	*23.00*	*4*	*0.4*	*0.33*
	C8	*2822*	*2827*	*2827*	*2827*	*23.15*	*4*	*0.41*	*0.33*
IV	*P1*	*1861*	*2039*	*2039*	*2039*	*22.83*	*3*	*0.39*	*0.22*
	P3	*1561*	*1767*[f]	*1920*	*1920*	*26.57*	*3*	*0.41*	*0.22*
	P6	*1004*	*1095*[f]	*1762*	*1762*	*32.17*	*3*	*0.44*	*0.22*

Table.3.3. The samples of the four model systems with their measured & predicted crosslink densities, Flexibility parameter (F), Average functionality (f_C), Molecular weight between crosslinks (M_C), molar crosslink density ($X_C^{L\&C}$).

Mod. No. - *Model Number*

Sam Cod. - *Sample Code*

T_g^{DiM} - *T_g determined using DiMarzio approach*

$T_g^{V\&H}$ - *T_g determined using molar additive contribution (Van Krevelen & Hoftyzer)*

T_g^{DiB} - *T_g determined using DiBenedetto's approach*

$T_g^{B\&E}$ - *T_g determined using Bank and Ellis's approach*

f	-	*Calculations based on % conversion determined using FTIR*
v_C^{Meas}	-	*Crosslink density calculated from rubbery modulus using theory of rubber elasticity*
$v_C^{M\&M}$	-	*Crosslink density calculated using Miller and Macosko's Theory*
v_C^{Bel}	-	*Crosslink density calculated using Bellenger's approach*
$v_C^{L\&C}$	-	*Crosslink density calculated using Lesser and Crawford's approach*
#	-	*Calculated by fitting the values of $T_g^{V\&H}$, K_{DM}, F values to DiMarzio's equation*

[a] *The T_g^l value obtained from the previous experimental work [Nakka, 2008] is the intercept value of the linear fit applied to the T_g data versus increasing average functionality.*

Note: The values of Mc and $X_C^{L\&C}$ for samples A2 and E2 does not exist as Equation 3.23 and 3.28 is only applicable for model systems containing functionality (f) equal to 3, for at least one of the reactants.

The crosslink density (v_C) values determined using the approaches by Miller & Macosko, Bellenger, Lesser and Crawford give identical results for systems that are fully reacted (100% conversion). Whereas for the systems that show less that 100% conversion, the Bellenger and Lesser and Crawford's approaches cannot predict the crosslink density. Moreover, the Miller & Macosko approach has the advantage of calculating the crosslink density of the network at different conversion (p) levels. Therefore the v_C^{Bel} , $v_C^{L\&C}$ for *P3* and *P6* are higher than $v_C^{M\&M}$ (see *Table 3.3)* since v^{Bel} is the crosslink density determined using Bellenger's approach at 100% conversion.

As discussed earlier, the T_g for the polymeric sample can be determined using the 1 Hz viscoelastic data for *E',* tan δ *and E''* obtained from *DMA*. In the following Section the T_g obtained from the tan δ curve for 1 Hz data is analyzed for each model system separately. They are compared with their predictions.

3.9. Results and Discussion

3.9.1. MODEL I -Effect of Aliphatic Amine functionality

Bisphenol A diglycidyl (Aromatic epoxy) resin of constant functionality (f_E = 2) is selected and is initially mixed independently with three aliphatic amines which vary in their functionality (f_A = 2, 3, 4). Further, the different epoxy-amine mixtures are cured according to the cure schedule specified in *Table 2.5*. The mixing and curing is done to understand the effect of varying the aliphatic amine functionality in the epoxy-amine reacting mixture on the ultimate glass transition temperature (T_g) of the hardened (or fully cured) epoxy thermoset. The cured samples are then characterized for their viscoelastic behavior by applying sinusoidal multi frequency strains in the Dynamic Mechanical Analyzer (*DMA*) in tensile mode. The viscoelastic response at 1 Hz is analyzed for the determination of the glass transition temperature (T_g). *Figures 3.5 & 3.6* show the storage modulus (*E'*) and tan δ response of *Model I* cured samples with respect to temperature.

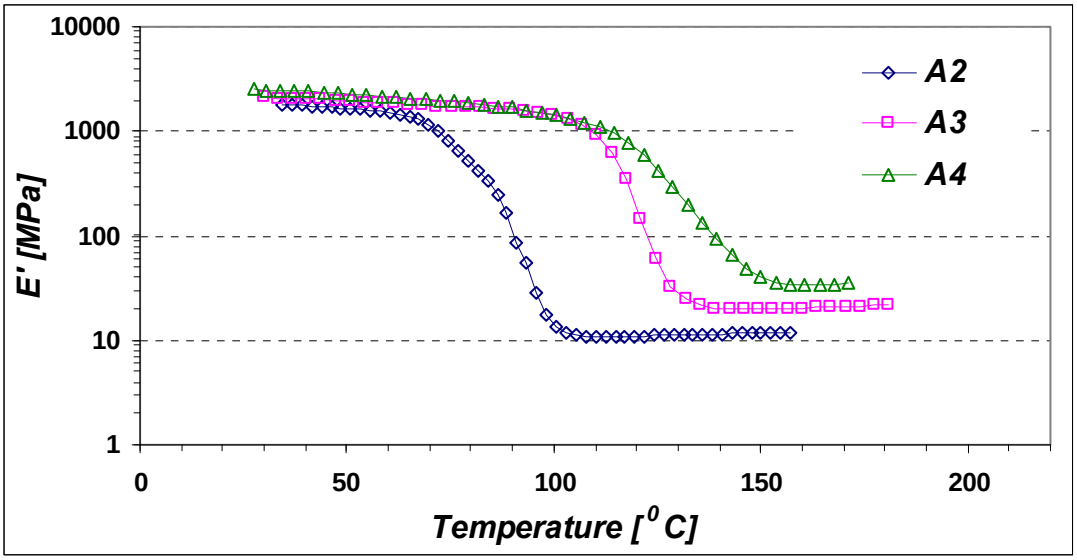

Figure 3.5. Storage Modulus (E') versus temperature at 1 Hz frequency of Model I samples.

As described earlier in *Chapter II* each individual viscoelastic curve shows three regions namely the glassy region, the glass transition region and the rubbery region. The moduli in the glassy and rubbery region are termed as glass modulus (E_g) and rubbery modulus (E_r) respectively [*Chapter 1; pp.1*]. From *Figure 3.5* it can be seen that the glassy modulus (E_g) is independent of the amine functionality. Whereas the

glass transition temperature ($T_g^{\tan\delta}$), rubbery modulus (E_r) increases with the increase in the amine functionality.

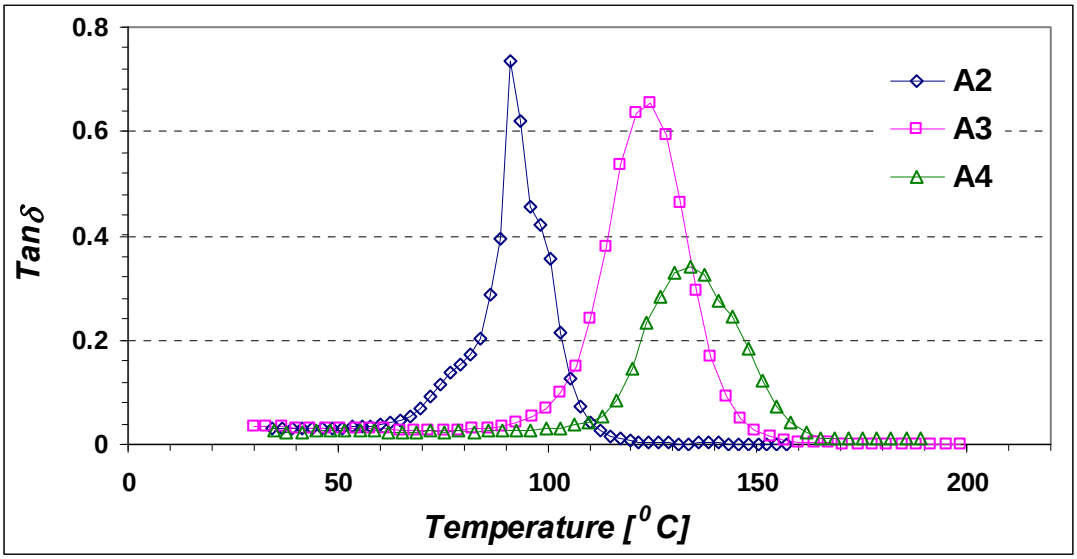

Figure 3.6. Tan δ *response versus temperature at 1 Hz frequency for Model I samples.*

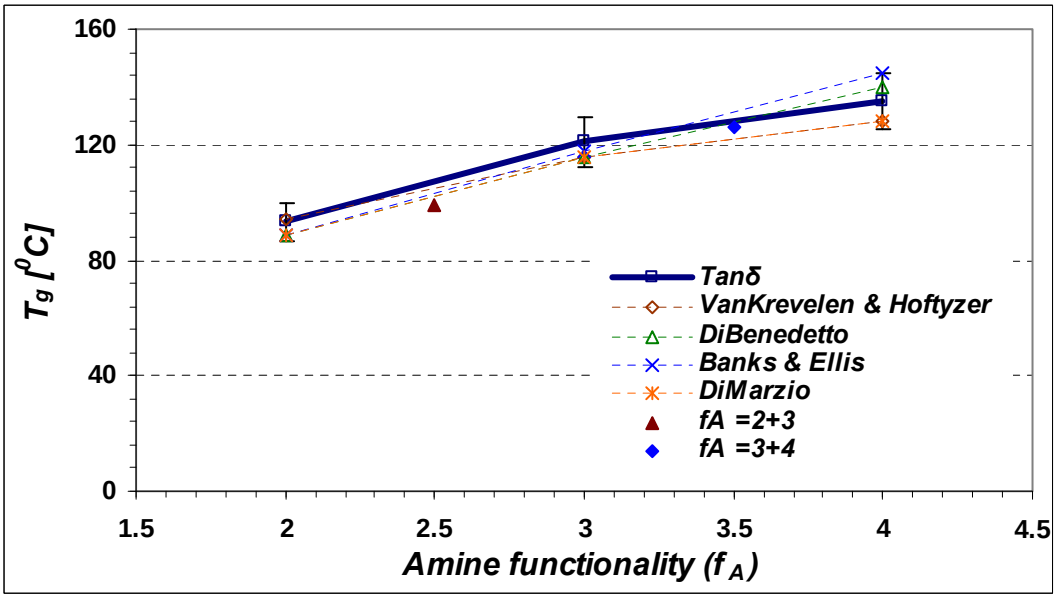

Figure 3.7. Measured $T_g^{\tan\delta}$ *and predicted* T_g *values versus amine functionality for Model I samples. The intermediate mixtures are shown by filled symbols.*

The glass transition temperature can also be predicted using several methods as described earlier in this *Chapter*. The results of measured $T_g^{\tan\delta}$ and the predicted T_g using different methods are shown in *Figure 3.7* for the epoxy systems in which the amine functionality was varied (*Model system I*). The thick line in *Figure 3.7*

corresponds to the measured $T_g^{\tan\delta}$. It can be observed that the $T_g^{\tan\delta}$ increases with the increase in the functionality of aliphatic amine curing agent or hardener in the epoxy-amine reacting mixture. Moreover, the measured T_g is predicted well by different approaches as can be observed by comparison with measurement values [Error Bar 7%]. Intermediate mixtures which are resin mixtures containing DER epoxy ($f_E=2$) and a mixture of amines ($f_A=2+3$, $f_A=3+4$) are also prepared. The average functionalities of these intermediate mixture are f_A =2.5, f_A =3.5 and their corresponding cure schedules are 100 °C for 4 hours and 150 °C for 3 hours. The $T_g^{\tan\delta}$'s of cured networks of the intermediate mixtures fall close to a linear trend and are shown as filled symbols in *Figure 3.7* [Nakka et al., 2008]. Since the T_g of the hypothetical linear polymer i.e., T_g^l and also the crosslink density values vary for the three samples (*A2, A3, A4*) three fit parameters are obtained. The linear regression data for Banks & Ellis [*eq.3.20*] and DiBenedetto's approach [*eq.3.16*] are shown in *Table 3.4*.

Sample name	*A2*	*A3*	*A4*
Functionality of amine (f_A)	*2*	*3*	*4*
ζ (Kg K/mol)	*0*	*18*	*32*
k (-)	*0*	*0.45*	*0.50*

Table.3.4. Sample names, functionality of amines and the fit parameters ζ, k used for the prediction of $T_g^{B\&E}$, T_g^{DiB} for the Model System I .

The fit parameters ζ and k increase with the increase in the functionality of amine in cured samples. The term ζ is related to the network free volume increment [see *eq.3.22*, *Section 3.7*] and so the tetrafunctional crosslinks would have less incremental free volume than trifunctional crosslinks [Lesser and Crawford, 1997]. The lower incremental free volume for tetrafunctional crosslinks leads to an increase in the T_g. And therefore the value of ζ for the tetrafunctional network is higher in comparison to trifunctional networks. The above reasoning is valid from the observed values of ζ shown in *Table 3.4*. Nielsen (1969) often-cited a value of a 39 *kg K/mol* for tetrafunctional networks but this is not always true and can vary. Moreover the value of the hypothetical T_g of the linear polymer, T_g^l, is usually taken as constant for the prediction of T_g within a series of similar kind of reacting mixtures. This is not always

true as the T_g^l can vary depending on the chain stiffness of the backbone chain and substituent groups. For example, the introduction of aliphatic nature on the backbone or in the substituent group can decrease the T_g of the uncrosslinked linear polymer. The value of DiBenedetto's constant k increased with the increase in the functionality of amine in the cured samples. The increasing trend is expected as the constant k value characterizes the influence of the crosslinks and so the trifunctional networks have a lower k value in comparison to tetrafunctional crosslinks [Stutz et., al (1990), Lesser and Crawford (1997&1998)].

3.9.2. MODEL II – Effect of Epoxy functionality

To understand the effect of varying the epoxy functionality in the epoxy-amine reacting mixture on the glass transition temperature (T_g) the Model II system is selected. The model system II contains three aromatic epoxy resins namely *BFDGE, TMTE* and *TPGE* (as shown in *Table 2.5)* which vary in their functionality (f_E= 2, 3, 4*)* and are cured independently with an aliphatic diamine *DMEDA* (f_A =*2*) according to cure schedules as shown in *Table 2.5*. The viscoelastic characterizations of the cured samples are done in *DMA.* The viscoelastic data i.e., storage modulus (*E'*) and tan δ for 1 Hz data is shown in the *Figures 3.8 & 3.9.* From *Figure 3.8* it can be seen that the glassy modulus (E_g) remains constant for *E2, E3, E4* whereas the rubbery modulus (E_r) increased from *E2* to *E3* and then decreased from *E3* to *E4*.

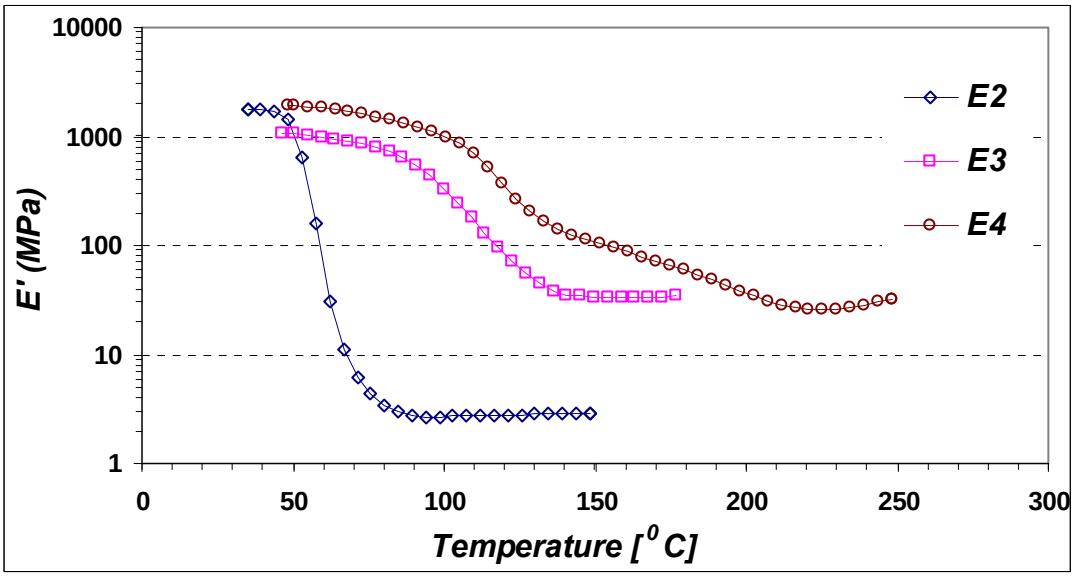

Figure 3.8. Storage Modulus (E') and tan δ *response versus temperature at 1 Hz frequency of Model II samples.*

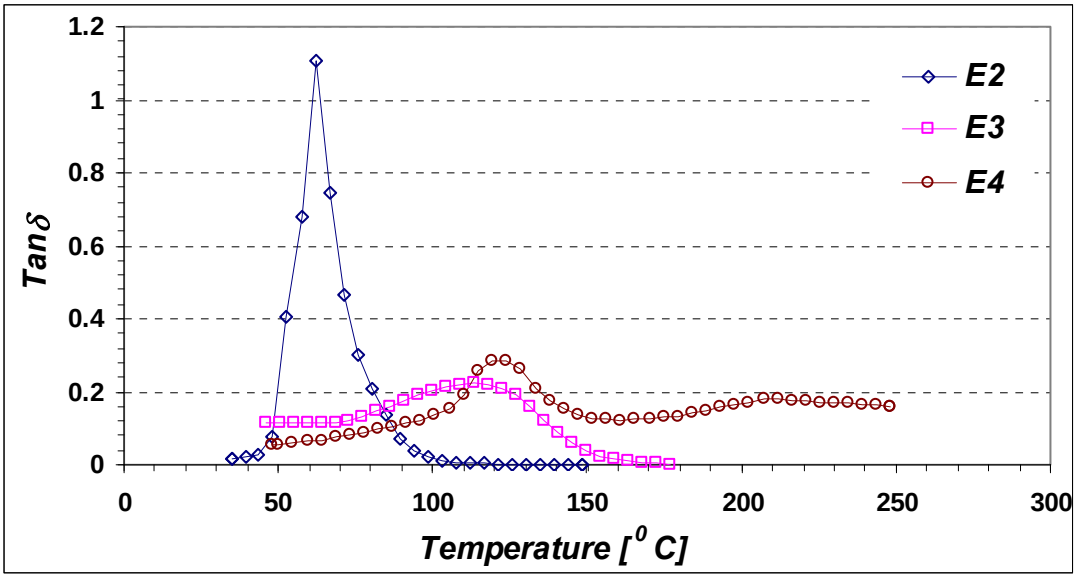

Figure 3.9. Storage Modulus (E') and tan *δ response versus temperature at 1 Hz frequency of Model II samples.*

Analysis of the Modulus in the rubbery region:

The 1 Hz data of the sample *E2* in the rubbery region shows a rubbery plateau above 100 °C with a rubbery modulus (E_r) *of 3 MPa*. Since the sample *E2* is formed due to the reaction between *BFDGE* (f_E= 2) and *DMEDA* (f_A =*2*) it is expected to contain uncrosslinked linear chains within the sample and hence should be thermoplastic in nature. It means that with the rise in temperature, the characteristic property of thermoplastics to melt at a certain temperature (called melting temperature) should lead to a drop in the modulus, which approaches zero ath higher temperatures. It can be observed from *Figure 3.8* that the sample *E2* clearly shows a rubbery plateau which indicates that the sample contains a small fraction of partly crosslinked network chains. This could be because of the reaction of hydroxyl groups (obtained from the reaction of epoxy-amine) with the remaining epoxy groups. This is also called homopolymerisation. So, in order to avoid the crosslinked network state within the sample *E2* a new mixture is made by mixing 0.5 wt % excess amine to the *BFDGE-DMEDA* stoichiometric mixture.

Similarly, 0.5wt % excess amine is added to the stoichiometric mixture of *TMTE-DMEDA*. Both mixtures are then cured according to the cure schedules specified in *Table.2.5* and are characterized in *DMA*. *Figure 3.10* shows the *E'* and tan *δ* data for 1 Hz frequency for both formulations.

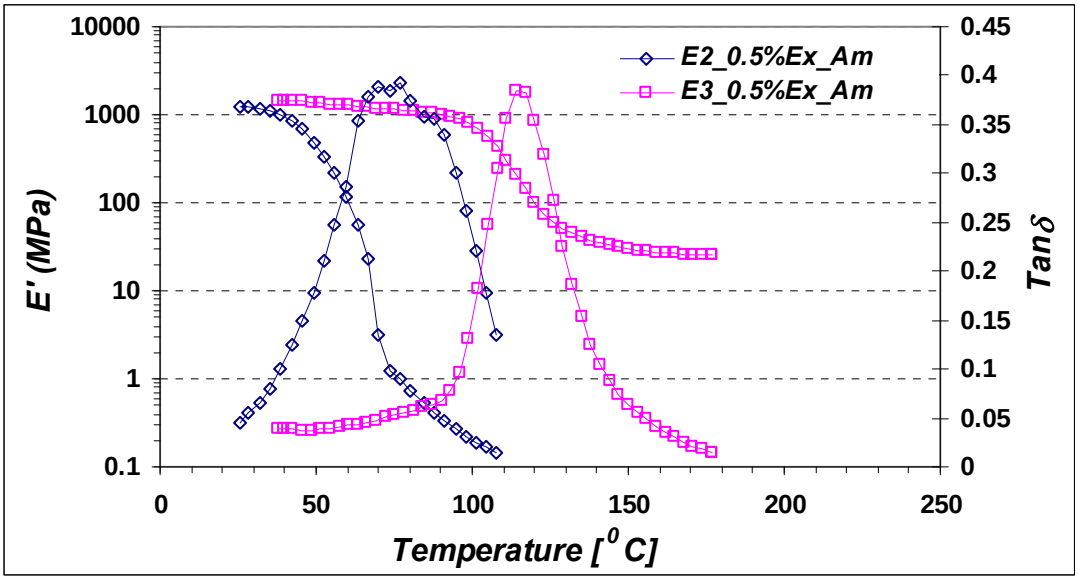

Figure 3.10. Storage Modulus (E') and tan *δ response versus temperature at 1 Hz data of the samples containing excess of amine.*

The 1 Hz data for the sample *E4* in its rubbery region shows that the modulus decreases with the increase in temperature (*Figure 3.8*) and does not have a clear rubbery plateau for the sample *E4*. This can be because of incomplete reaction between the epoxy and amine. Moreover the tan δ peak for the sample *E4* showed two tan δ peaks at 122 °C and 207 °C which occurs during the temperature scan. The second tan δ peak at 207 °C could be because of the reaction of the remaining epoxy groups. In order to assure that the sample *E4* is fully cured the sample *E4* is further cured at 250 °C for 30 minutes.

Figure 3.11 shows the viscoleastic data for *1 Hz* frequency for the sample *E4* cured at 250 °C for 30 minutes. It can be seen from *Figure.3.11* a single tan δ peak is observed. This indicates homogeneity and also the modulus in the rubbery region decreased with the increase in temperature. Also around 300 °C there is a sudden drop in the rubbery modulus which is an indication of degradation [Bicerano, 2002]. The temperature at the tan δ peak maximum for *1 Hz* frequency which is the glass transition temperature is found to be 109 °C. This is lower than the T_g (118 °C) of sample *E*. This means that the degradation leading to the decrease in the T_g as well as the reaction of the remaining epoxy units takes place at the same time. This is mainly due to the steric hindrance caused by the rigid aromatic structure within the *TPGE* epoxy resin in the *E4* sample. Since 100% conversion of epoxy groups for the sample *E4* is not possible and also the T_g determined for the sample *E4* cured at 250 °C for 3

hours does not contain an ideal network. So, the T_g data of *E4* cannot be taken for the analysis as it would lead to erroneous interpretation of T_g results. Hence the viscoelastic data for the sample *E4* is omitted for the analysis.

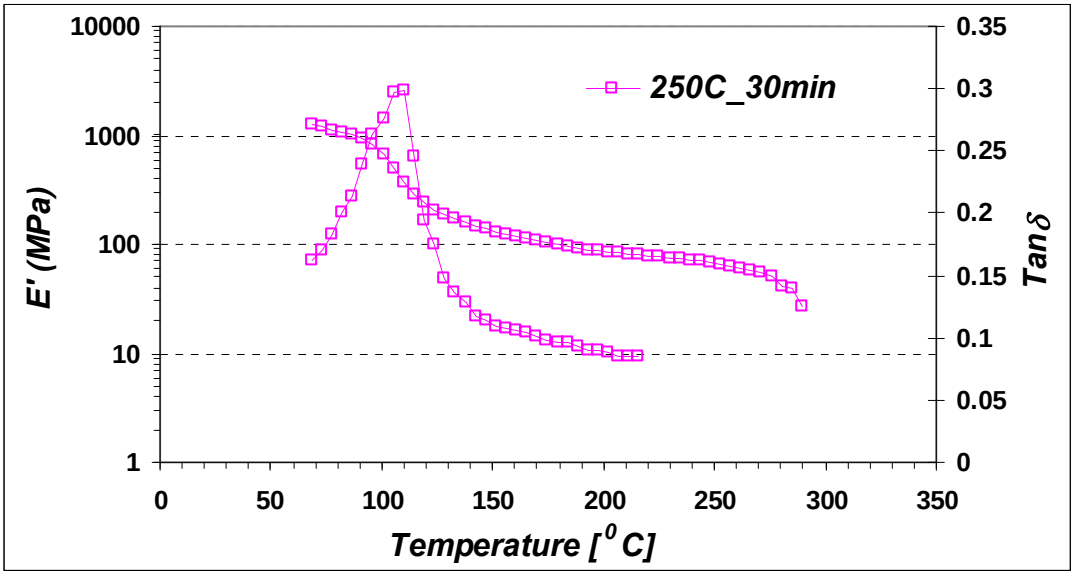

Figure 3.11. Storage Modulus (E') and tan *δ response versus temperature at 1 Hz frequency of the E4 sample cured at 250 °C for 3 hours.*

Therefore the $T_g^{\tan \delta}$ for the samples *E2_0.5%Ex_Am* and *E3_0.5%Ex_Am* in the model system II is used for the analysis of the T_g. Also an intermediate resin mixture is prepared by mixing *BFDGE* epoxy (f_E =2) and *TMTE* epoxy (f_E=3) in mol ratio (0.5:0.5) to attain the average functionality of 2.5 and then stoichiometrically mixed with aliphatic diamine *DMEDA* (f_A=2) and cured at 120 °C for 2 hours. The $T_g^{\tan \delta}$ and predicted T_g using different approaches are shown in *Figure 3.12*.

It can be observed from *Figure 3.12* that the $T_g^{\tan \delta}$ is in close agreement with the predictions (Error bar of 10%). Moreover the T_g prediction using DiMarzio's approach is closer to $T_g^{\tan \delta}$ in comparison to other approaches. The linear regression data for Banks & Ellis and DiBenedetto's approach are shown in *Table 3.5*.

From *Table 3.5* it can be observed that ζ increases with the increase in epoxy functionality which is rather expected since the trifunctional crosslinks in *E3* lead to a lower free volume in comparison to *E2.5* and *E2*. Since the sample *E2.5* is made from a mixture of *BFDGE* epoxy (f_E =2) and *TMTE* epoxy (f_E=3), it would have more incremental free volume due to a lower number of trifunctional networks in comparison to *E3*. And so the value of ζ is lower in comparison to *E3*. The

DiBenedetto's constant (*k)* for *E2.5* and *E3* is the same. This means that the value of *k* depends on the type of the crosslinked network (tri or tetra) formed rather than on the number of crosslinks (especially during the formation of ideal networks).

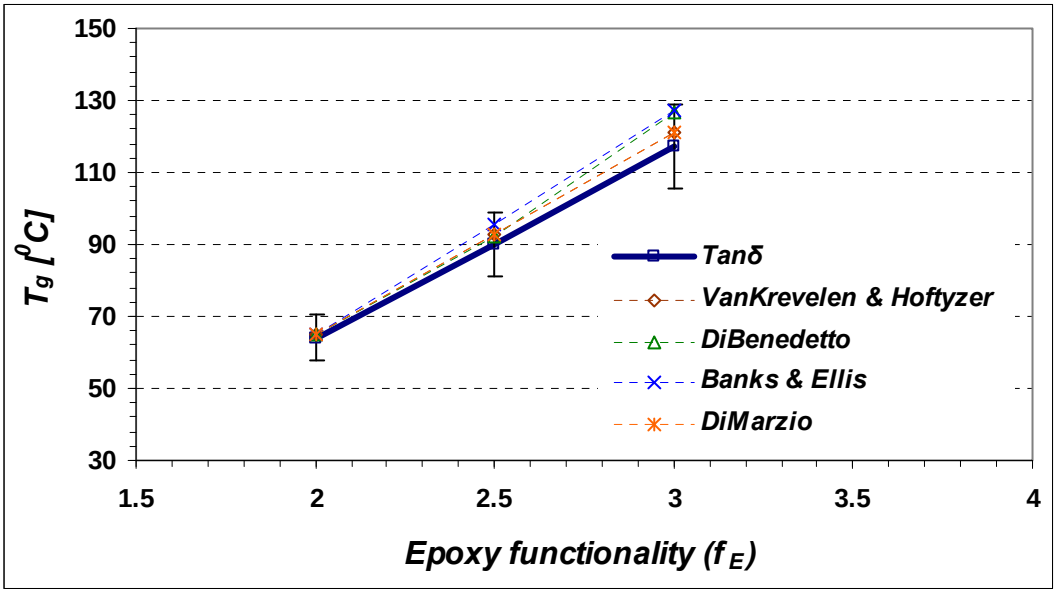

Figure 3.12. Measured T_g ($T_g^{\tan\delta}$) in comparison to predicted T_g's versus functionality (f) of epoxy resin.

Sample name	*E2*	*E2.5*	*E3*
Functionality of Epoxy (f_E)	*2*	*2.5*	*3*
ζ (Kg K/mol)	*0*	*9*	*18*
K(-)	*0*	*0.45*	*0.45*

Table.3.5. The sample names, functionality of amines and the fit parameters ζ, k used for the prediction of T_g using Banks & Ellis, DiBenedetto for Model II system.

3.9.3. MODEL III – The effect of the chain length in a network structure

To understand the effect of the chain length or spacer length in the network structure on the glass transition temperature (T_g) an aromatic epoxy (*BADGE*) was cured independently with homologous series of four aliphatic amines (*EDA, BMDA, HMDA, OMDA*) [*Table 3.6*] varying in their chain length and having a constant functionality (*f=4*).

AMINE	*Chemical Structure*	*Chain length*
EDA	$H_2N—CH_2—CH_2—NH_2$	2
BMDA	$H_2N—CH_2—CH_2—CH_2—CH_2—NH_2$	4
HMDA	$H_2N—CH_2—CH_2—CH_2—CH_2—CH_2—CH_2—NH_2$	6
OMDA	$H_2N—CH_2—CH_2—CH_2—CH_2—CH_2—CH_2—CH_2—CH_2—NH_2$	8

Table.3.6. Homologous series of amine hardener with increasing chain length

The increase in the chain length was denoted with the number of carbon atoms in the aliphatic amine i.e., *C2, C4, C6, C8*. The cure schedules for all the formulations are shown in the *Table 2.5* in *Chapter II*. The cured samples are characterized for their viscoelastic behavior using a Dynamic Mechanical Analyzer (*DMA*) in tensile mode. The viscoelastic response at 1 Hz frequency is analyzed for the determination of the glass transition temperature (T_g). The storage modulus (E') and tan δ data for 1Hz frequency is shown in *Figure 3.13 & 3.14*. From *Figure 3.13* it can be seen that the glassy modulus (E_g) and the rubbery modulus (E_r) remain constant.

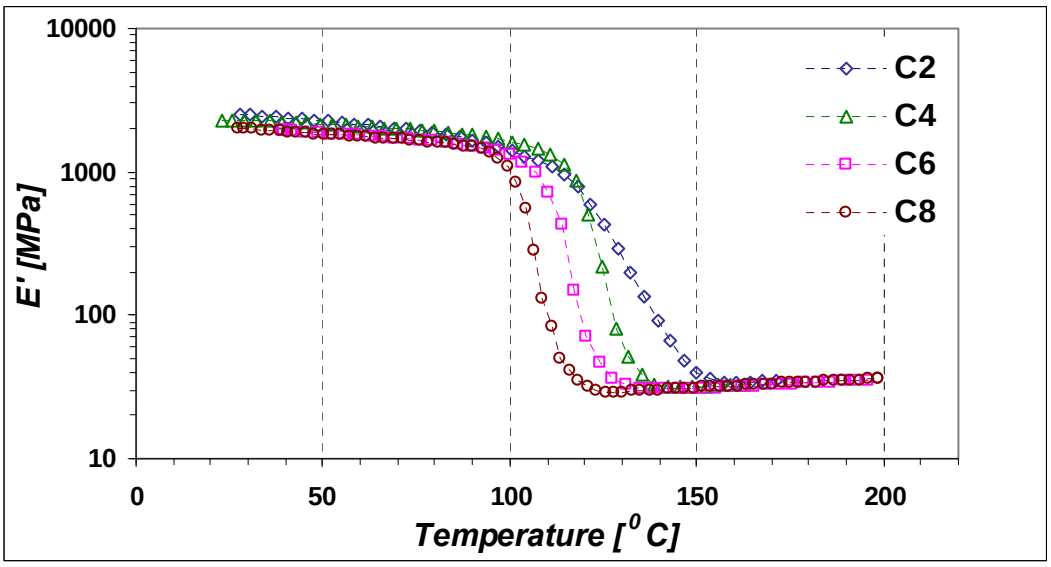

Figure 3.13. Storage Modulus (E') response versus temperature at 1 Hz frequency for the Model III system.

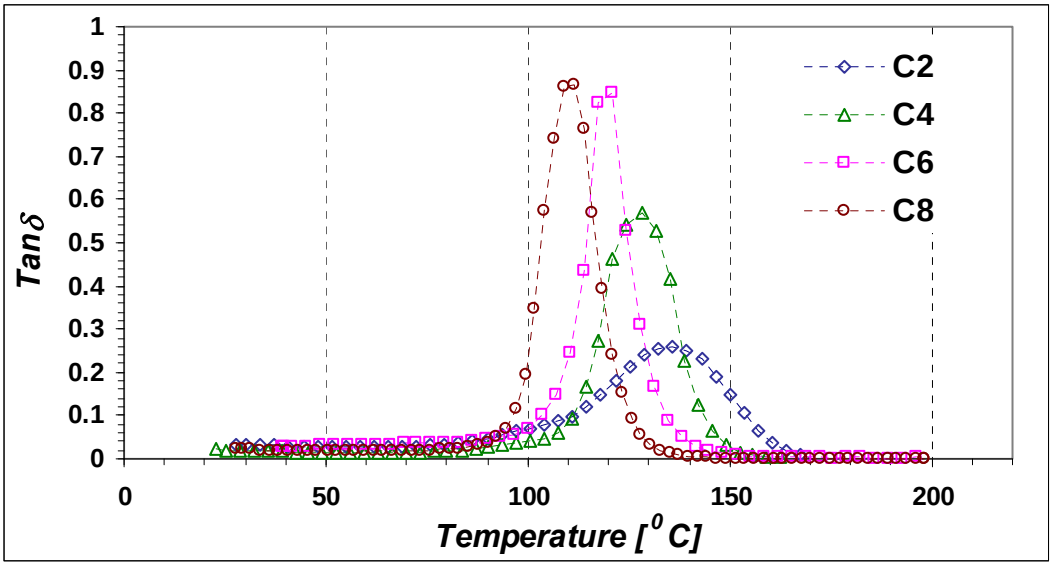

Figure 3.14. The tan *δ response versus temperature at 1 Hz frequency for Model III system.*

Figure 3.14 shows that the increase in chain length from *C2* to *C8* clearly shows three distinct changes on the tan δ curve i.e., increase in the height, decrease in the broadening, decrease in the glass transition temperature ($T_g^{\tan \delta}$). In the previous model systems it was observed that with the increase in the crosslink density (v_C^{Meas}) , both the E_r and T_g increased. For the Model III system it can be observed from *Table 3.3* that with a slight decrease in the ν_C from *C2* to *C8*, the rubbery modulus (E_r) remained constant, whereas the $T_g^{\tan \delta}$ decreased by about 30 °C .

The measured T_g ($T_g^{\tan \delta}$) further can be compared with the predicted T_g and is shown in *Figure 3.15*. From *Figure 3.15*, the measured as well as the predicted T_g decreased with the increase in chain length. This is only due to the increase in the chain length in the epoxy-amine crosslinked network. The increase in aliphatic chain length in the crosslinked network increases the flexibility in the network and hence the crosslinked network with the highest chain length (*C8*) in the Model III series is expected to have the highest flexibility. Moreover, since T_g is related to the mobility of the molecular chains and so with the increase in the flexibility of the molecular chains the Tg decreases. Hence with the increase of temperature the crosslinked network containing the highest flexibility shows the highest mobility and thereby should show the lowest $T_g^{\tan \delta}$. This is clearly evident from *Figure 3.15*. With the increase in chain length the $T_g^{\tan \delta}$ of the cured network decreases linearly (10% Error Bar).

Also *Figure 3.15* shows that the measured $T_g^{\tan\delta}$ and the predicted T_g by *DiMarzio* and *Van Krevelen & Hoftyzer* are in close agreement [Error of 10%]. The Banks & Ellis and the DiBenedetto approaches for the predictions of T_g deviate more than 10% from $T_g^{\tan\delta}$. The fit parameters for the prediction of T_g using Banks & Ellis and DiBenedetto's approach are shown in *Table 3.7*.

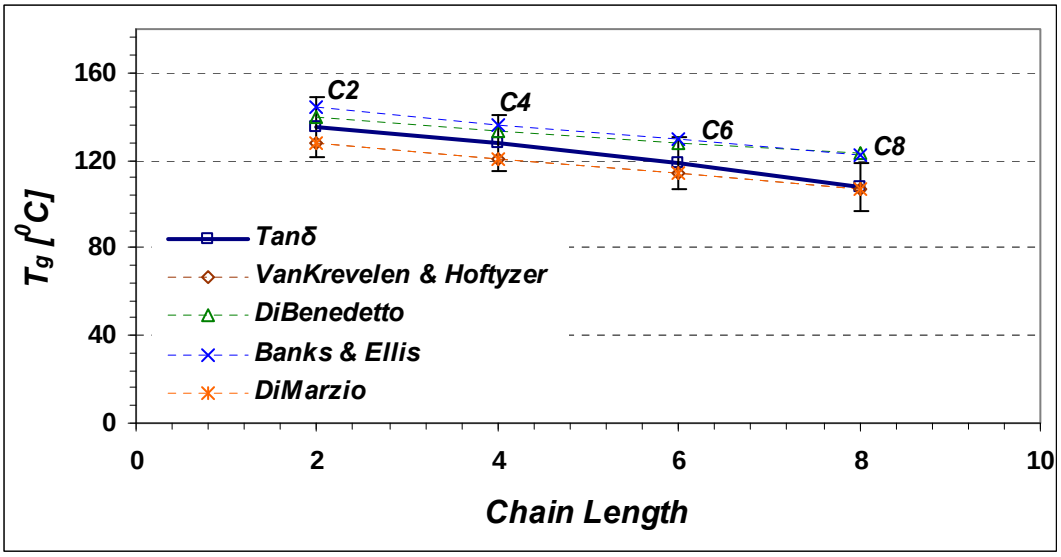

Figure 3.15. Measured $T_g^{\tan\delta}$ in comparison to predicted T_g's against the chain length.

Sample name	*C2*	*C4*	*C6*	*C8*
Chain length of aliphatic amine	*2*	*4*	*6*	*8*
ζ (Kg K/mol)	*32*			
k (-)	*0.50*			

Table.3.7. Model III system sample names, amine chain length and the fit parameters ζ and k are used for the prediction of $T_g^{B\&E}$, T_g^{DiB}.

From *Figure 3.15* it can be observed that a single fit parameter value of *ζ and k [see Table 3.7]* for the Banks & Ellis and DiBenedetto approaches is sufficient to predict the *T_g's for C2, C4, C6, C8.* Also the prediction values for T_g using the Banks & Ellis and the DiBenedetto approaches is higher in comparison to those of the DiMarzio and Van Krevelen & Hoftyzer approaches. This is mainly because all the samples in *Model IV* have tetrafunctional crosslinks but also increasing chain length between the

crosslinks. The effect of the increasing chain length is taken into account by the increasing weight contribution in the Van Krevelen & Hoftyzer approach. On the other hand the flexibility parameter (*F*) takes in to account the effect of increasing chain length in DiMarzio's approach.

3.9.4. MODEL IV –The effect of Pendant chain length

To understand the effect of pendant chain length in the cured epoxy-amine network structure on the glass transition temperature the Model IV system is selected. The Model IV system contains an aromatic epoxy (*BADGE*) of functionality ($f_E = 2$) which is cured independently with aliphatic amines *NPDA, NHDA, TPGE* of constant functionality ($f_A = 3$) but varies in their side group (or substituent) chain lengths (*SCL*= 1, 3, 6). The chemical structure of the reactants and the cure schedule is specified in the *Tables 2.3, 2.4 & 2.6* of *Chapter II.* The side chain present in the amine reactant in the epoxy-amine reaction mixture remains as pendant chain in the network structure of the reacted epoxy-amine product. The typical structure of network containing propyl pendant chains for the sample *P3* is shown in *Figure 3.16*.

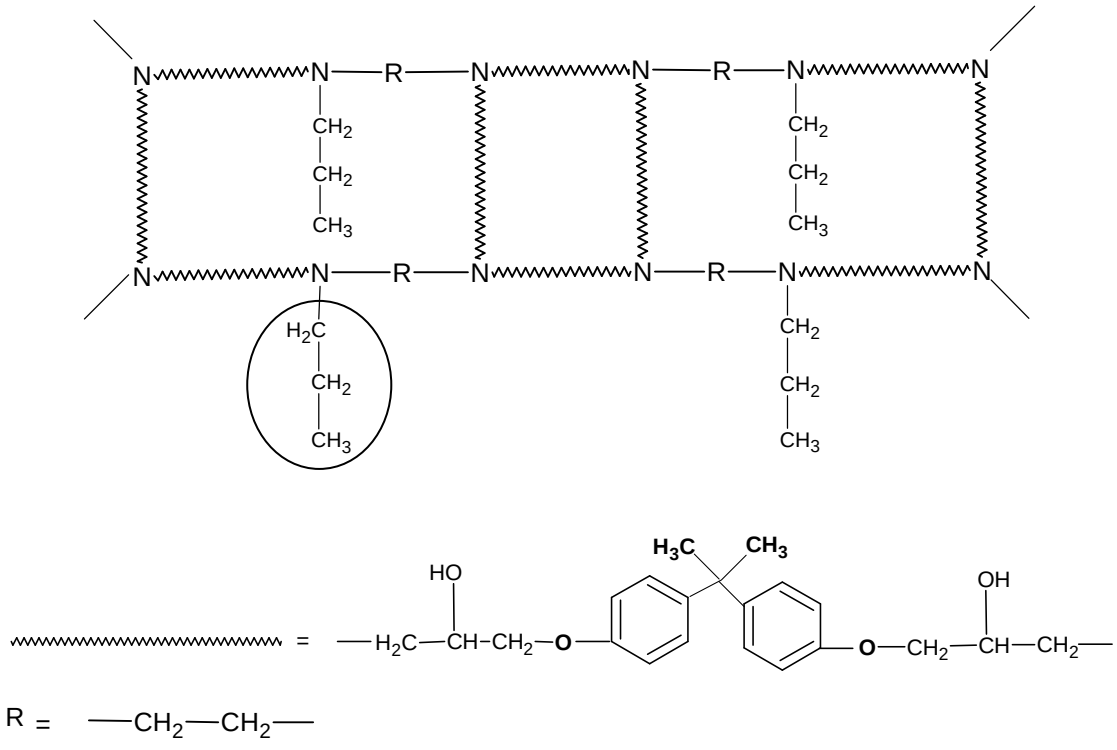

Figure 3.16. Network structure of sample P3 containing a propyl pendant group (indicated by the circle).

The viscoelastic responses at 1 Hz frequency for the samples *P1, P3 and P6* that are characterized in *DMA* are shown in *Figures 3.17 & 3.18*.

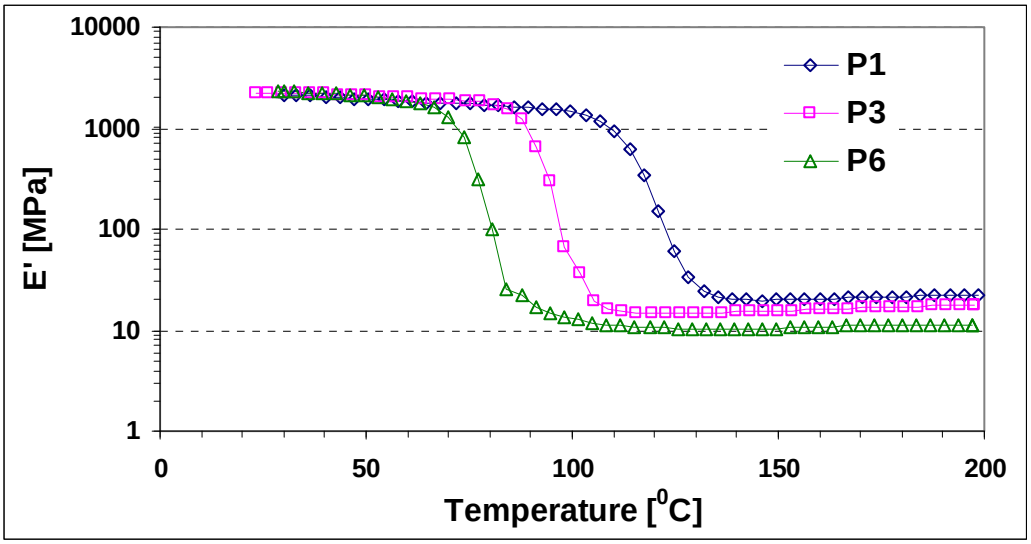

Figure 3.17. Storage Modulus (E') response versus temperature at 1 Hz frequency for the Model IV system.

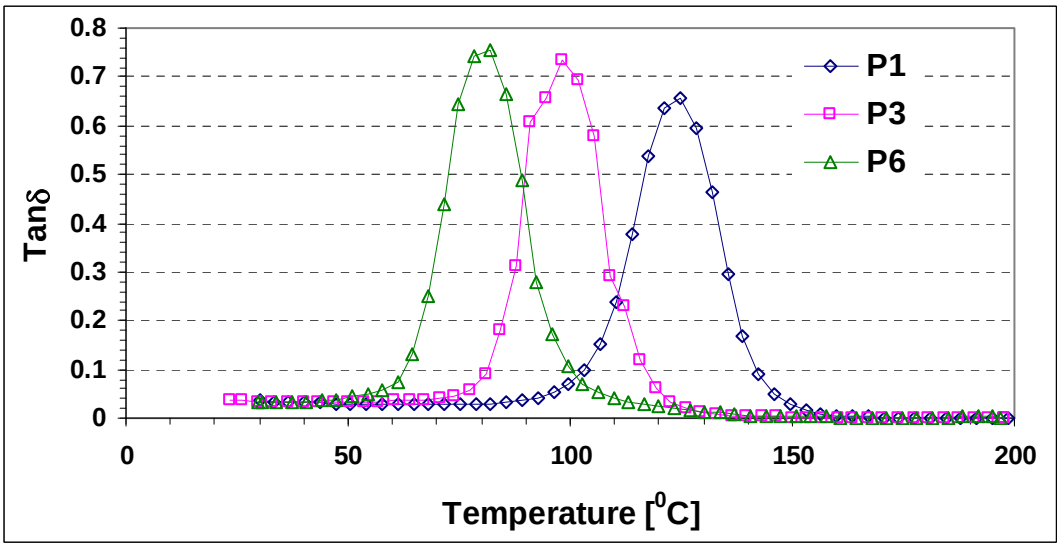

Figure 3.18. Tan *δ response versus temperature at 1 Hz frequency for the Model IV samples.*

It can be observed from *Figure 3.17* that the glassy modulus remains constant with the increase in the pendant chain length, whereas the rubbery modulus of *P1* and *P3* are close. The rubbery modulus of *P6* is less in comparison to *P1* and *P3*. This was not expected since the initial functionality of all the three amines in the initial epoxy-amine mixture is constant (i.e., $f_A = 3$) and so the network formed after curing with

BADGE epoxy ($f_E = 2$) should give a similar three dimensional network for the three samples *P1, P3 and P6*. So, it is expected that the rubbery modulus for the samples *P1, P3* and *P6* are equal. But there is a difference in the rubbery modulus for the three samples *P1, P3* and *P6.* This can be observed from *Figure 3.17.* Therefore *FTIR* studies are carried out to investigate the conversion of epoxy in the three samples.

FTIR Studies:

FTIR studies were conducted in the Mid-Infrared region in *ATR* (Attenuated Transmission Reflectance) mode for understanding the percentage conversion in the cured samples. Different kinds of peaks [see *Table 2.6*] due to bond stretching, bending, rocking, scissoring etc. can be obtained from the *FTIR* spectra in the Mid-IR region. The reacting epoxy-amine mixture and their reacted product can be followed with different peaks, but only the peaks of interest such as the reacting peaks i.e., epoxy group or oxirane ring, amine N-H stretching, reference peaks (aromatic ring, aliphatic C-H), peaks of reacted product (e.g. hydroxyl group) are considered for following the epoxy-amine reaction and also to determine the % of conversion.

***P1*:**

In the *Figure 3.19* the spectrum of pure epoxy (DER 332 or BADGE) and the sample *P1* is shown. For the pure BADGE resin it can be observed that the peak at 913 cm^{-1} pertains to the epoxy group or oxirane ring. Other characteristic peaks 2965 cm^{-1}, 1506 cm^{-1} and 1230 cm^{-1} are the methyl C-H stretching, aromatic C-H and aromatic C-O stretching, respectively [see *Table 2.6*]. The infrared spectrum of the sample (*P1)* in the Mid-infrared region is shown below the spectrum of BADGE in *Figure 3.19*.

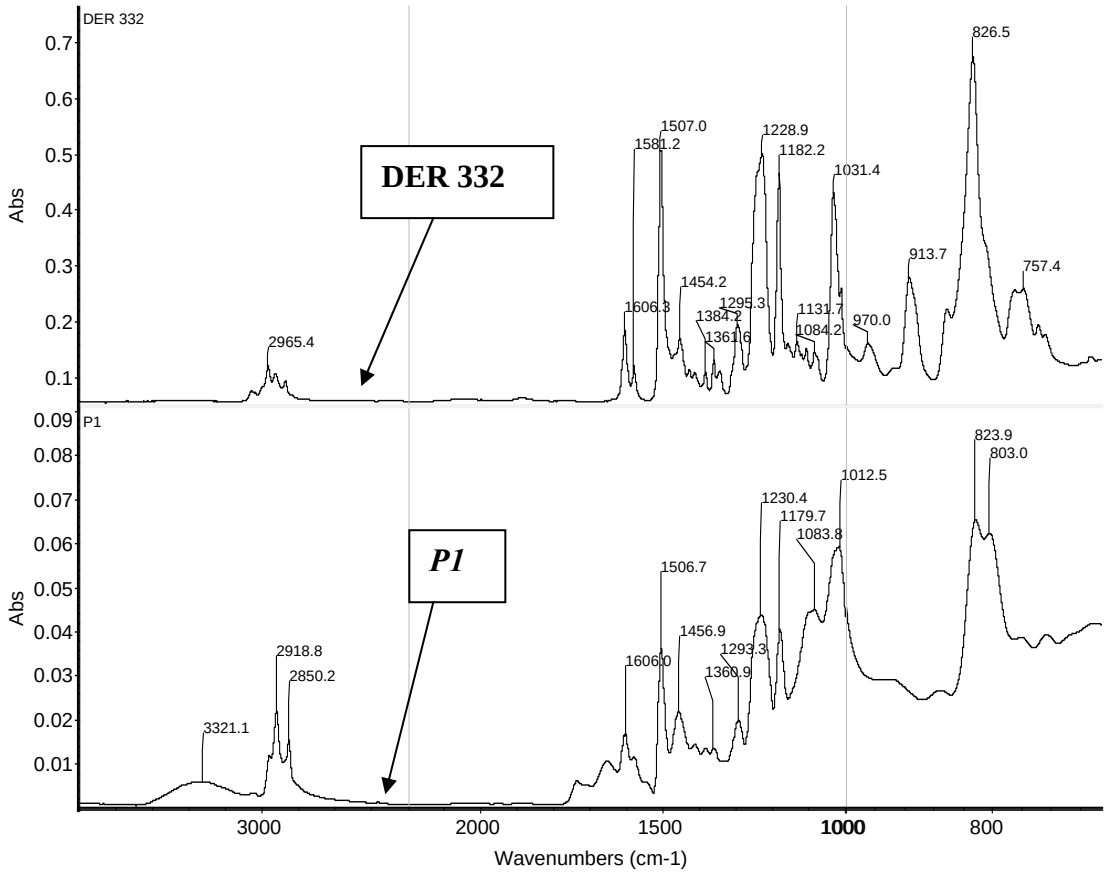

Figure 3.19. Mid-infrared spectrum for pure BADGE (DER 332) epoxy and sample P1 cured at 150 °C for 3 hours.

From *Figure 3.19* it can be observed that the epoxy peak at *913 cm^{-1}* for sample *P1* is absent. Broad stretching around *3321 cm^{-1}* indicates the formation of hydroxyl groups due to the reaction between epoxy (BADGE) and amine (MEDA). The absence of an epoxy peak at *913 cm^{-1}* for the sample *P1* indicates that the epoxy has fully reacted.

The infrared spectrum of the sample (*P3)* cured at *200 °C for 2h* in the Mid-Infrared region is in shown in *Figure 3.20*. From *Figure 3.20* it can be observed that in the region around *913 cm^{-1}* a distinct epoxy peak is not observed but a slight scatter is found. Since it is very difficult to find the peak area of the scattered region it can be concluded that the percentage conversion of epoxy groups is close to 100%. Hence for the calculation of the crosslink density for the *P3* sample using Miller Macosko's approach the percentage conversion of 99 is used.

P3:

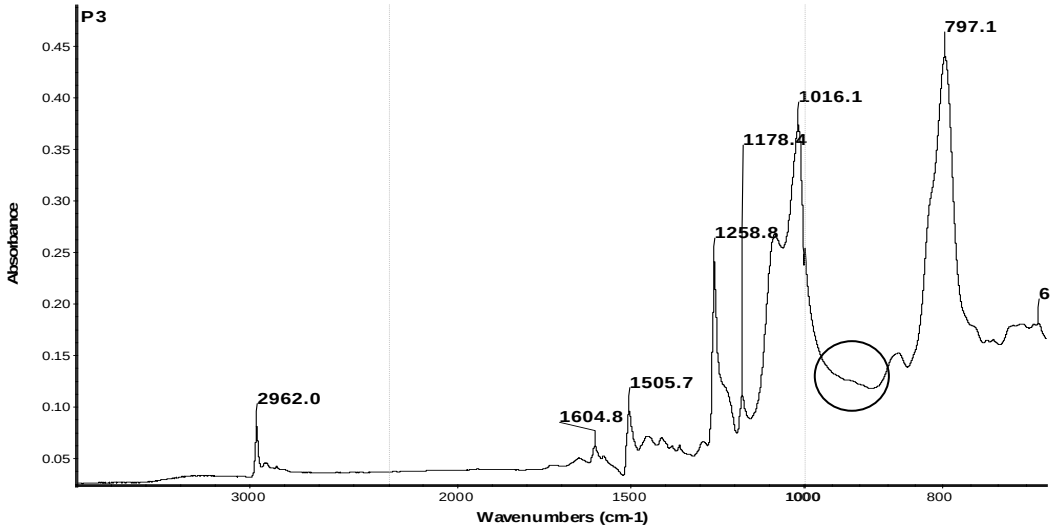

Figure 3.20. Mid infrared spectum of the sample P3 cured at 200 °C for 2 hours.

P6:

The spectrum of the initital resin mixture containing a stoichiometric mixture of BADGE epoxy and *N-Hexylethylene diamine (NHDA)* is shown in *Figure 3.21*. In *Figure 3.22* the spectra of the reacted mixtures of *P6* cured at *100 °C* for 2 hours followed by post curing at *200 °C* for 4 hours and *250 °C* for 3 hours is shown.

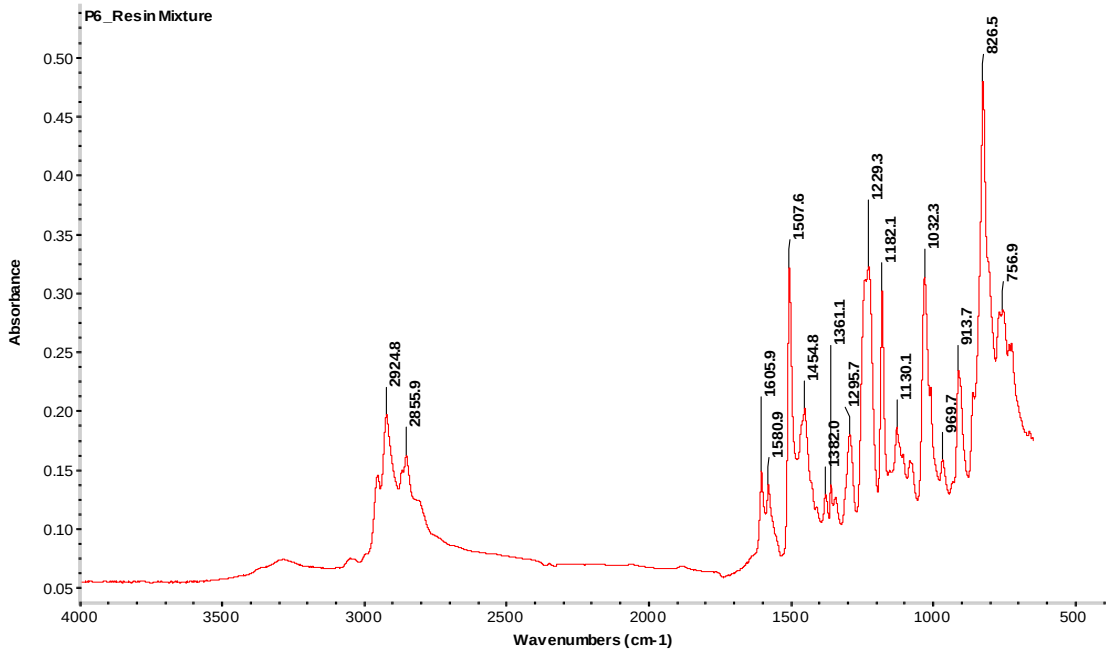

Figure 3.21. Mid infrared spectrum of initial resin mixture of P6 sample

Analysis:

P6 (Resin mixture)

- The presence of the peak at *913 cm^{-1}* indicates the presence of an oxirane ring.
- A stretching band between *3000-3500 cm^{-1}* and the peak at *719 cm^{-1}* indicate the presence of primary N-H amine
- The peak at *1607 cm^{-1}* indicates an aromatic ring
- The peak at *1229 cm^{-1}* indicates aromatic ether
- The presence of *1182 cm^{-1}* indicates C-N stretching.
- The peaks at *2924 cm^{-1}* and *2855 cm^{-1}* indicate a methyl group (CH_3) and methylene group (CH_2)

100°C _2h

- The absence of N-H stretching at *3335 cm^{-1}* indicates that the amine has reacted forming a hydroxy (–OH) group. The –OH group is shown as a broad stretching at *3300 cm^{-1}*
- The presence of the peak at *719 cm^{-1}* indicates that amine is still present
- The presence of the *1231 cm^{-1}* peak indicates aromatic ether
- Peaks at 1082 *cm^{-1}* and 1018 *cm^{-1}* indicate C-O-C bonds and C-O-H - this means that some percentage of the cyclic epoxy ring at 913 cm^{-1} is converted to C-O-H
- The peak at 913 *cm^{-1}* indicates that an epoxy ring is still present

200 °C _4h

- The absence of the *912 cm^{-1}* peak indicates that epoxy rings has undergone a reaction
- The increase in the area of the –OH stretching at *3500 cm^{-1}* indicates conversion of the remaining epoxy groups
- The absence of peaks at *3335 cm^{-1}, 719 cm^{-1}* (primary amine N-H) indicate that the amine has fully reacted
- The increase in Peak area of *1082 cm^{-1}* (C-O-C) contradicts that epoxide groups still remain unreacted. So, this may be due to C-OH (at 1000 - 1100 cm^{-1}), which is affecting the adjacent peak areas.

250 ^{0}_3h:

- The decrease in the peak area of the –OH stretching from 200_4h to 250_3h indicates removal of water.

The sudden decrease in absorption peak areas of the reacting and unreacting groups (such as reference peak) indicate that degradation occurred due to steric hindrances at 250_3H. (Note: The sample also looked black due to char formation).

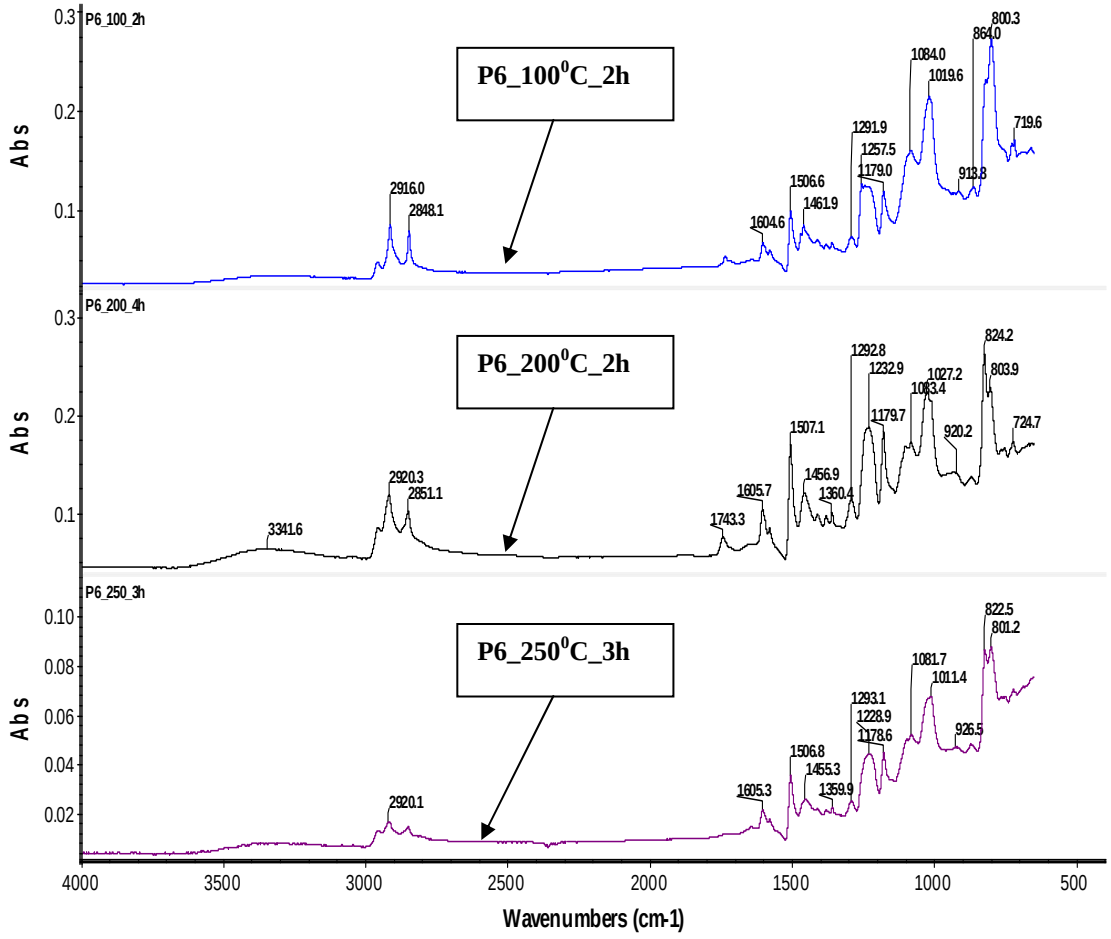

Figure 3.22. Plot of absorbance spectrum for P3 cured at 100 °C for 2h (above), at 200 °C for 2 h (middle) and at 250 °C for 3 h (below).

Determination of % Conversion

As discussed earlier in *Chapter II*, the % conversion can be determined either from the peak area of the reacting group only or the peak area of the reacting group with respect to the area of a reference peak [see *Section 2.10, Equation 1.18 &1.19*]. Since the determination of a normalized peak is a better approach, *Equation 1.19* is used. The peak area of epoxy with respect to the peak area of the reference peak i.e.,

aromatic C-H at *1506* cm^{-1} shows an epoxy percentage conversion of 85% for the sample *P6* which is cured at *100 °C* for 2 hours. For the sample *P6* cured at *200 °C* for 4 hours the % conversion of epoxy is 95%. From the *FTIR* results it can be concluded that the samples *P3* and *P6* show 99% and 95% conversion. These values are used in the calculation of crosslink density using the Miller and Macosko approach i.e., $v_C^{M\&M}$ and futher $v_C^{M\&M}$ is used in the prediction of T_g^{DiM} using *Equation 3.9.* Hence the $T_g^{\tan\delta}$ of both the samples *P3* (cured at *200 °C* for 2 hours) and *P6* (cured at *200 °C* for 4 hours) are analyzed and compared with the predicted T_g using different approaches and is shown below.

From *Figure 3.23* it can be observed that the predicted T_g values using the Banks & Ellis, DiBenedetto and DiMarzio approaches are in close agreement with $T_g^{\tan\delta}$. Whereas the T_g values predicted using the Van Krevelen and Hoftyzer appoach for the samples *P3* and *P6* are slightly over predicted. The over predicted T_g values for Van Krevelen and Hoftyzer's approach are because these predictions are based on the molar additive principle which cannot take into account the percentage of conversion. The fit parameters for the prediction of T_g using Banks & Ellis and DiBenedetto's approach are shown in *Table 3.8*.

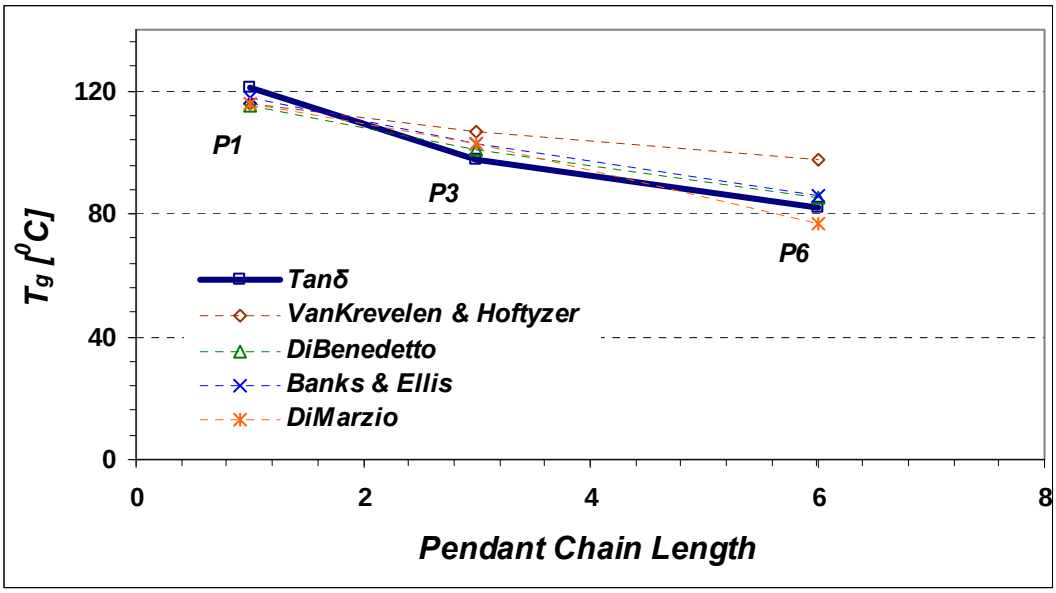

Figure 3.23. Measured T_g ($T_g^{\tan\delta}$) *in comparison to predicted* T_g*'s against the increase in pendant chain length.*

Sample name	*P1*	*P3*	*P6*
Pendant chain length	*1*	*3*	*6*
ζ (Kg K/mol)	*18*		
k (-)	*0.45*		

Table.3.8. Sample name, pendant chain length of amines and the fit parameters ζ and k used for the prediction of $T_g^{B\&E}$, T_g^{DiB} .

The measured T_g ($T_g^{\tan \delta}$) decreased with the increase in pendant chain length within the crosslinked network. The decrease in T_g from *P1* to *P6* is due to two factors

a. The flexibility of the pendant chains
b. The % of Conversion of epoxy

Flexibility of the pendant chain is mainly due to the increase in the aliphatic chain length from *P1* to *P6*. It was already observed from the Model III system that the introduction of flexibility decreases the T_g. Therefore for the Model IV system it is also expected to that T_g decreases with the increase in flexibility of the pendant chain. From *Figure 3.23 it* can be observed that the $T_g^{\tan \delta}$decreases with the increase in pendant chain length. But the observed decrease in $T_g^{\tan \delta}$ with the increase in the pendant chain length in *Figure 3.23 is* not only due to the flexibility but also due to the incomplete reaction between epoxy and amine in *P3* and *P6*. *FTIR* results showed that the % of conversion of the epoxy in samples *P3* and *P6* is 99% and 95%. Since incomplete reaction leads to formation of a crosslinked network containing a lower number of crosslink points and so the crosslink density decreases. Moreover the decrease in the crosslink density decreases the glass transition temperature (T_g) [*Ogata, 1993*]. From the above discussion it can be concluded that T_g decreases due to the increase in the flexibility and also due to an incomplete reaction of epoxy.

From *Figure 3.23 it* can be observed that the $T_g^{V\&H}$ is higher in comparison to the measured T_g and other predictions. This is because the $T_g^{V\&H}$ uses the principle of molar additivity which can only give a reliable prediction for 100% reaction. On the otherhand the T_g predictions using the approaches of Bank and Ellis, DiBenedetto or DiMarzio are in close agreement with $T_g^{\tan \delta}$. And the crosslinked densities for *P3* and *P6* are calculated by considering 99% and 96% epoxy conversion.

3.6. Overall Analysis

In order to compare the T_g*'s* of all the four model systems a fundamental or scaling parameter is a prerequisite. The analysis of the predicted T_g for all the four model systems showed that the crosslink density (v_C) is an important parameter which controls the T_g. On the other hand the flexibility parameter (F) is also an important parameter that has be taken into account while predicting T_g. The flexibility parameter (F) includes the contribution of chain stiffness between the crosslinks as proposed by DiMarzio. The parameter F is essentially an increasing function of the content of aromatic nuclei [Bellenger et al., 1987]. So, in order to predict the T_g's of the cured samples of all the four model systems, Dimarzio's approach [Eq. 3.9] is used. The predicted values of the T_g's (i.e., T_g^{DiM}) [see *Table 3.2*] for all the samples are plotted against the measured T_g ($T_g^{\tan \delta}$) and are shown in *Figure 3.24*.

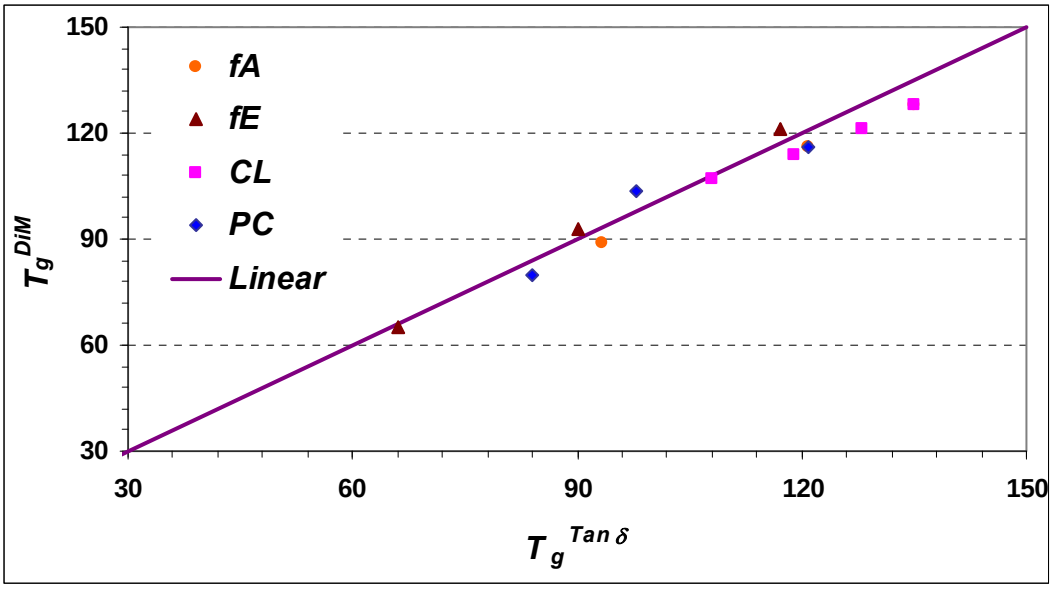

Figure 3.24. Predicted T_g (T_g^{DiM}) versus measured T_g ($T_g^{\tan \delta}$).

It can be seen from *Figure 3.24* that the T_g^{DiM} values are in close agreement with the $T_g^{\tan \delta}$ values. The slight deviation of the T_g^{DiM} values for the model III system from the line is because the T_g^{Dim} values are calculated based on the values of T_{gl} determined using molar addivity. The T_{gl} values determined using molar additivity are usually closer to the *DSC* results. Moreover, the T_g values based on differential scanning calorimetry (*DSC*) are usually always lower than the values obtained through *DMA*. Hence it can be concluded that the DiMarzio's approach results in a

good prediction of the T_g. More importantly DiMarzio's prediction uses two parameters being the crosslink density (ν_C) and the flexibility parameter (F). Hence it can be concluded that v_C and F are the two scaling parameters that should be used for the design of a polymeric material having a desired T_g.

3.7. Conclusions

Both the T_g and E_r can be rised by increasing the amine or epoxy functionality (Model system I & II). However, varying the amine chain length offers a way to independently change the T_g without effecting the crosslink density and the rubbery modulus (E_r). The typical range in which T_g can be varied is about 40 °C. A further reduction in T_g can also be obtained by adding aliphatic pendant chains *(Model IV*) since the pendant chains act as internal plasticizer within the crosslinked network. In that case it is accompanied with a small decrease in the rubbery modulus since the 100% of conversion of the reacting group is not possible.

CHAPTER – IV

Viscoelasticity

Chapter 4

Viscoelasticity

4.1. Introduction

In this chapter the analysis of the viscoelastic curve will be done for each of the four model systems individually. Further, in order to model the viscoelasticity the viscoelastic master curve is generated using the Frequency-Temperature-Superposition (*FTS*) principle (discussed in *Section 4.8*). In the subsections of the *Section 4.8* the generated viscoelastic mastercurve for each of the four model systems is analyzed. Finally in *Sections 4.10* the modeling of the generated viscoelastic master curve for the four model systems is discussed.

4.2. Analysis of the viscoelastic Curve

The viscoelastic response of a polymeric material, as illustrated in *Figure 1.7* in *Chapter I* is once again reproduced by *Figure 4.1*.

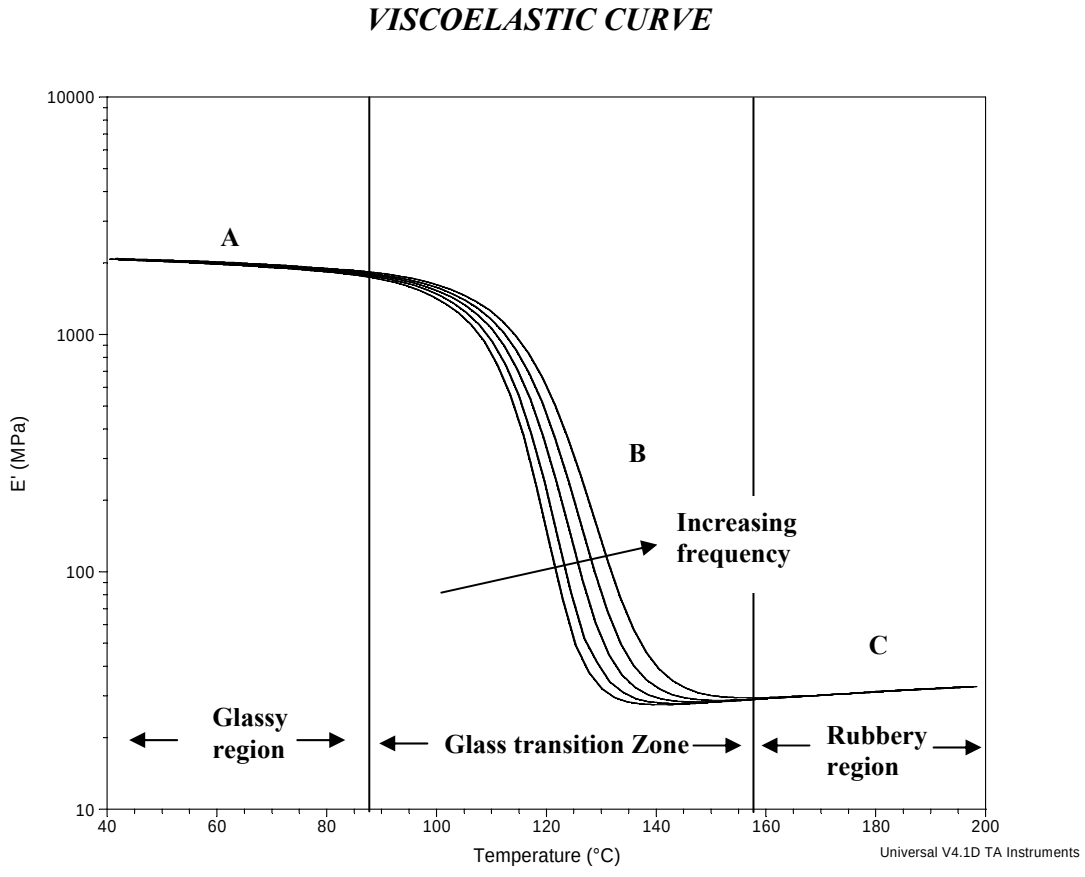

Figure 4.1. Plot of storage modulus (E') versus Temperature.

a. Glassy region

The region at which the modulus value is relatively high in comparison to the other regions of the viscoelastic curve is the glassy region and is indicated by A in *Figure 4.1*. The glassy region is observed as a plateau and is conventionally termed as the "Glassy Plateau". Moreover, the storage modulus in the glassy plateau is elastic for short term loading and thus found to be independent of the applied frequency. The modulus at any point on the glassy plateau is commonly termed as the glassy modulus (E_g). The glassy modulus has to be defined such that its value is identically obtained for all the selected model systems in *Chapter II* [*Table 2*] . One way of defining the glassy modulus is by taking the modulus value at a fixed temperature below the glass transition temperature (T_g), This fixed value has to be such that the modulus value is always in the glassy region.

b. Glass Transition Zone

The region between the glassy (A) and rubbery (C) region is the glass transition zone or region and is shown as B in *Figure. 4.1*. In the glass transition region the storage modulus is frequency dependent and drops by a few decades with increasing temperature as shown in *Figure 4.1*. The drop in the storage modulus depends on the degree of crosslinking. For a highly crosslinked system the drop in the storage modulus can be one decade whereas for lowly crosslinked systems the drop can be three or more decades. The decay from a higher modulus value to a lower one with respect to temperature in the glass transition zone is mainly dependent on the molecular chain rigidity and the crosslink density of the network [Halary, 1989]. The drop in the modulus in the glass transition zone is due to uncoiling of the polymeric chains and the process of uncoiling is termed as "relaxation". Relaxation is mainly dependent on the internal friction between the molecular chains within the sample. So, the influence of crosslinks or entanglements of the polymer chains increases the internal friction and thereby the time to relaxation (or relaxation time τ) increases. The tan δ (or damping) is a measure of the internal friction and hence tan δ is an important parameter that has to be analyzed. Damping is a sensitive indicator of all kinds of molecular motions that are going on in a material. Aside from the scientific interest in understanding the molecular motions that can occur, these motions are of great practical importance in determining the mechanical behavior of polymers. Tan δ is defined as the ratio of the loss modulus to the storage modulus and is given by

Equation 2.9 [Chapter 2]. Nielsen and Landel (1994) defined tan δ as a measure of the ratio of energy dissipated as heat to the maximum energy stored in the material and is also called *dissipation factor* or *loss tangent.* Moreover as discussed earlier in *Chapter IV,* the temperature at the peak maximum of the tan δ curve for 1 Hz can also be used to indicate the glass transition temperature (T_g) of the polymeric material.

c. Rubbery region

The region above the glass transition temperature in *Figure 4.1* is the rubbery region. In the rubbery region, the polymer material is rubbery in state and therefore exhibits elastic properties. The rubbery region appears as a plateau region and the plateau is commonly termed as the "Rubbery plateau". Further, the modulus in the rubbery region (or plateau) is independent of the frequency and is commonly termed as Rubbery modulus (E_r). The rubbery modulus is proportional to the absolute temperature according to the rubber elastic theory [see *Equation 4.1*]. Also the slope of the rubbery plateau remains constant as shown in *Figure 4.1*. Hence the definition of the rubbery modulus has to be defined for a systematic analysis of the rubbery modulus for the selected four model systems in *Chapter 2*. There can be many ways of defining the rubbery modulus out of which two possibilities are shown below

i) The rubbery modulus is the modulus at a fixed temperature above the glass transition temperature (T_g)

ii) The rubbery modulus is the minimum value of the modulus in the viscoelastic curve

But in some cases the transition region (B) as shown in *Figure 5.1* is very broad. For example in the highly crosslinked system [Nielsen, (1969), Ueberreiter and Kanig, (1950), Manson and Lange, (1996), Tobolsky et al., (1964)] the transition region is very broad. In highly crosslinked systems, the modulus value at fixed temperature [for example 10 °C] above $T_g^{\tan \delta}$ could be still in the glass transition zone. In such a case the definition (*i*) of the rubbery modulus as shown above is not well defined. The definition (*ii*) of the rubbery modulus in the above mentioned case is also not an ideal definition since the minimum modulus can be still in the glass transition zone. Hence for all the four model systems (*Table 2.4*) the rubbery modulus is defined as the minimum modulus in the rubbery plateau which is far from the transition zone.

4.3. Viscoelastic analysis of Model System I

The viscoelastic reponse of the cured sample for the Model I system in tensile mode in *DMA* is shown by *Figure 3.5* in *Chapter* III. The glassy and the rubbery modulus data of the Model I system is shown in *Figure 4.2*.

Glassy Modulus:

From *Figure 4.2* it can be see that the glassy modulus which is taken as the storage modulus at T_g*-60 °C* for the 1 Hz frequency is independent of the functionality of the amine. This is because in the glassy region, the large scale molecular chain motion in the network has ceased and only small scale motions shorter than typically the distance between the crosslinks can occur. Hence, the crosslink density and the factors which affect the crosslink density have no effect on the glassy modulus.

Rubbery Modulus:

From *Figure 4.2* it can be seen that the rubbery modulus increases with the increase in the functionality of amine. This is because in the rubbery region the molecular segments move over distances larger than the distance between the crosslinks. More crosslinks leads to more restriction of the large scale movements and thus a larger modulus. According to the theory of rubber elasticity, it is well know that the rubbery modulus (E_r) is directly proportional to the crosslink density as shown by *eq.4.1*

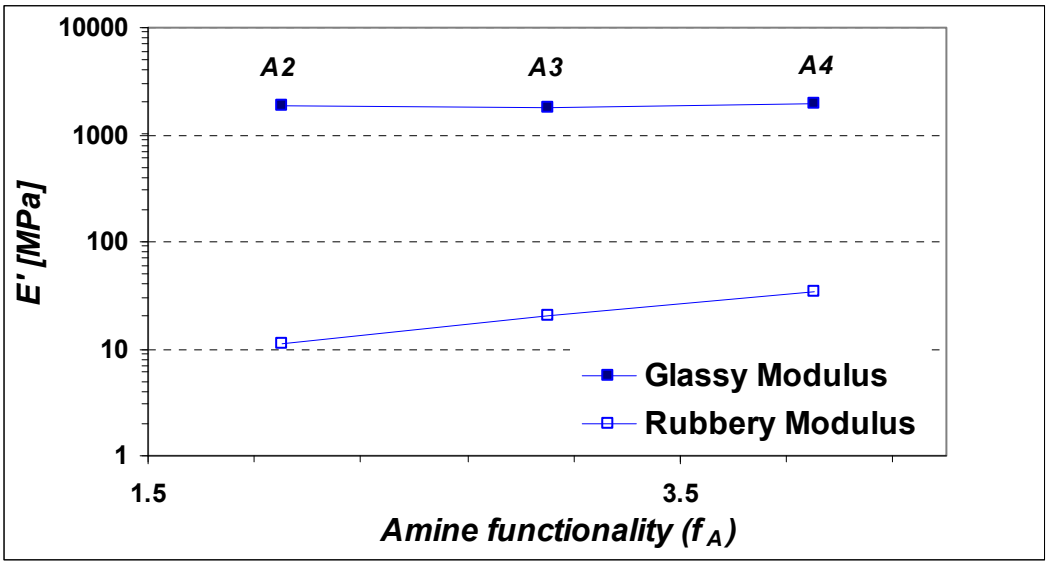

Figure 4.2. Glassy Modulus (E_g), Rubbery modulus (E_r) for the 1 Hz data with respect to the increase in functionality (f) of aliphatic amine curing agent.

$$E_r = 3A\nu_c^{Meas}RT \qquad \textbf{(4.1)}$$

where A is the front factor which is often dependent on the crosslink mobility and is assumed to be unity, R=8.314 J/mol/K, T is the absolute temperature in K and V_c^{Meas} is the measured crosslink density. From *Figure 4.3* it can be found that the measured crosslink density increases with the increase in the amine functionality (full lines with filled symbols). The crosslink density prediction using the M&M approach [see *Table 3.3*] show a good agreement with the measured crosslink density for amine functionality $f_A=3$ & $f_A=4$ but deviate for amine functionality $f_A=2$ as shown in *Figure 4.3* (the dashed line with open symbols). The deviation between the measured and predicted crosslink density values for the A2 sample is discussed below**.**

Discussion

The sample A2 is the cured product formed after reaction between the difunctional epoxy (*DER 332*) and a difunctional amine (*DMEDA*) according to the cure schedule as shown in *Table 2.4* in *Chapter II*. Since the functionality of both the *DER 332* and *DMEDA* is 2 and hence their reacted or cured product (i.e., sample A) is expected to contain only an uncrosslinked linear chain structure as shown in *Figure 4.5.a.* And so it should have a crosslink density value which is equal to zero. The above assumption of zero crosslink density is supported by the M&M theory since the substitution of f=2 in *Equation 2.10* leads to a zero crosslink density. So, according to the M&M theory the crosslinked network is only obtained if the functionality of one of the reacting systems is more than 2. Whereas a value of 1104 (mol/m^3) is observed for the measured crosslink density (ν_C^{Meas}) as the value is obtained from the rubbery modulus using *Equation 4.1*. Since the differences between the measured and the M&M crosslink density predictions are large, the purity was investigated for the reacting systems using Gas Chromatography & Mass Spectroscopy (GC&MS) and Nuclear Magnetic Resonance (NMR) Spectroscopy. The GC&MS and NMR results showed that the reacting systems are relatively pure. Hence it can be concluded that the rubbery modulus of 10 MPa for the sample A must be because of homopolymerisation [Matejka et al., 1994] of the epoxy shown by *Figure 2.1.c* in *Chapter II***.**

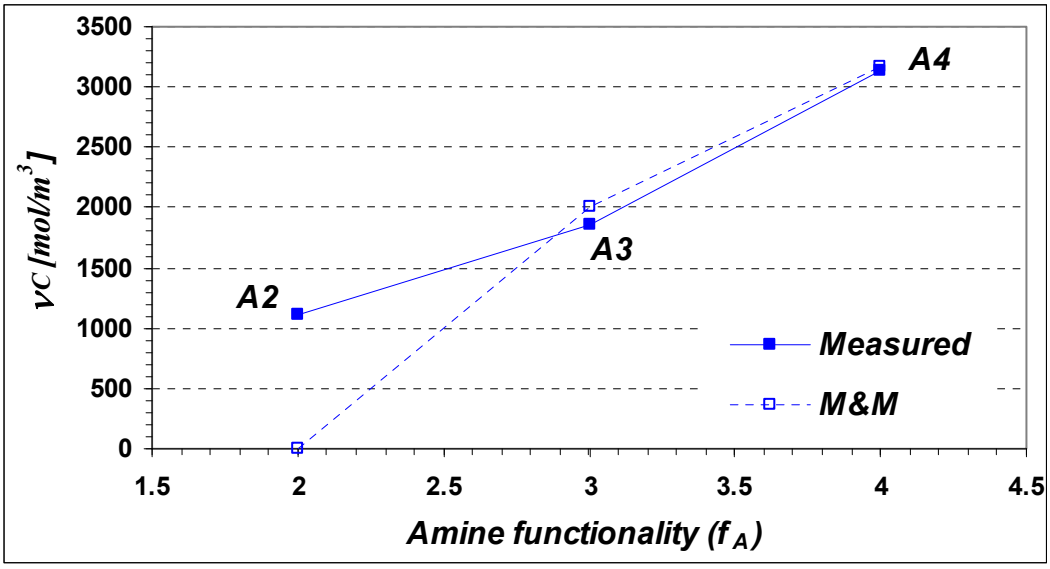

Figure 4.3. Crosslink density (mol/m^3) versus amine functionality (f_A). Full and dashed lines correspond to measured and predicted crosslink density. The deviation between predicted and measured values for the A2 system is attributed to epoxy homopolymerisation.

Tan δ *(Damping) Curve:*

The tan δ (*Damping*) curves for the three samples *A2, A3* and *A4* as shown in *Figure 4.4* are used for analysis.

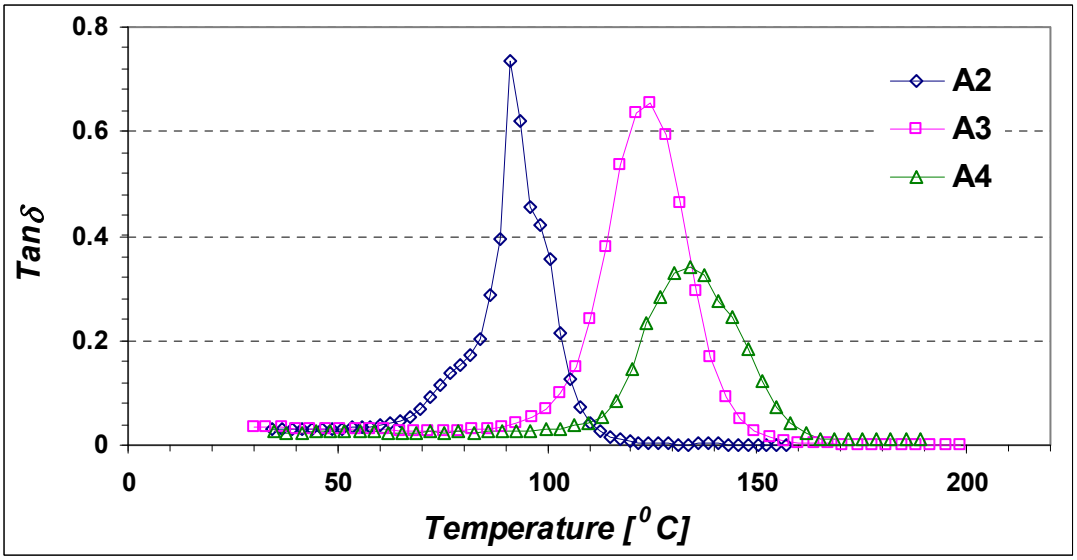

Figure 4.4. Tan δ peak for 1Hz frequency versus temperature.

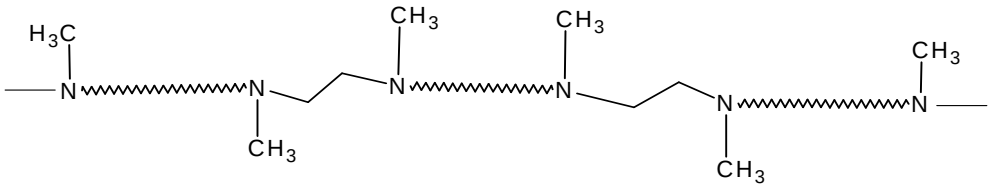

a.

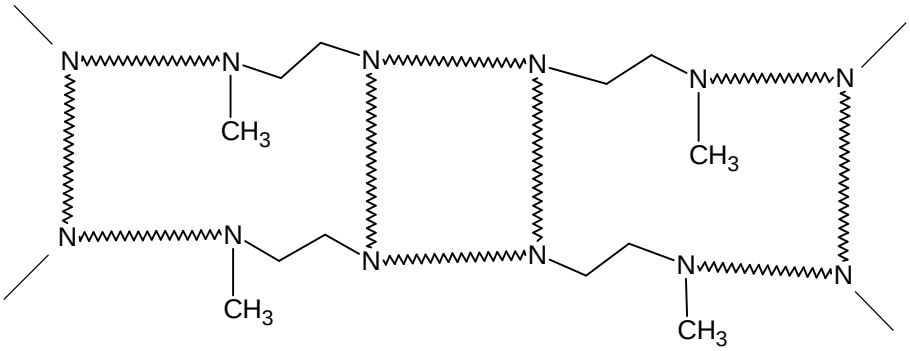

b.

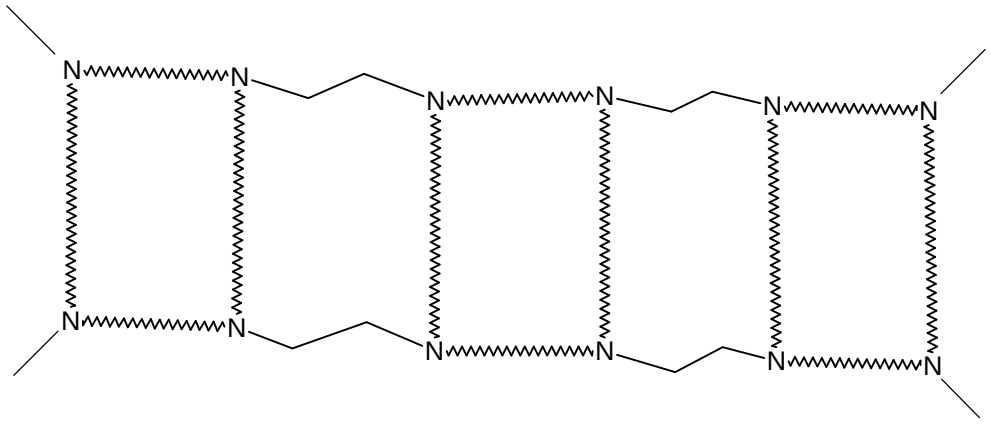

c.

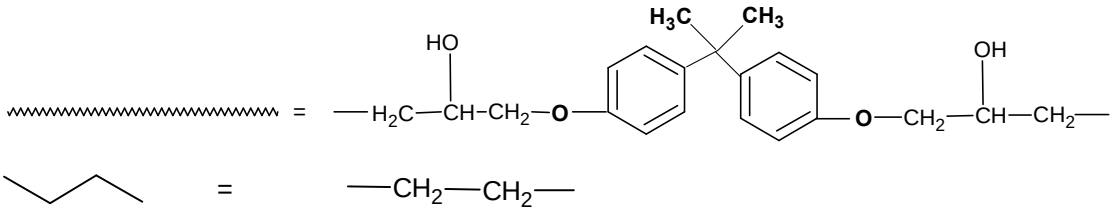

Figure 4.5. a. Structure of linear chain expected for A2 b. Example of network structure of sample A3 c. Example of network structure of sample A4.

From *Figure 4.4* it can be observed that with the increase in the amine functionality (from samples *A2* to *A4*) the height of the tan δ peak for 1 Hz frequency decreases. The tan δ *(*damping) peak for 1 Hz frequency is associated with the partial loosening of the polymer structure such that the groups and small chain segments can move near T_g and hence the height of the damping peak mainly depends on the stiffness of the network. It means that the higher the stiffness of the network, the lower will be the loosening of the polymer structure and thereby a lower tan δ peak will be shown. From *Figure 4.5.c* it can be observed that the sample *A4* has a network structure which has more crosslinking points in comparison to *A3* (*Figure 4.5.b*). The structure of *A2* does not contain linear chains similar to *Figure 4.5.a* since it is partly homopolymerised to form a three dimensional network structure and thus shows a rubbery plateau and has a rubbery modulus (E_r) of 10 MPa (*Chapter IV, Figure.*). From *Figure 4.2* it can be observed that the rubbery modulus of *A2* is lower than for *A3* and threfore it can be confirmed that the network structure of the sample *A2* has less crosslinking points in comparison to *A3***.**

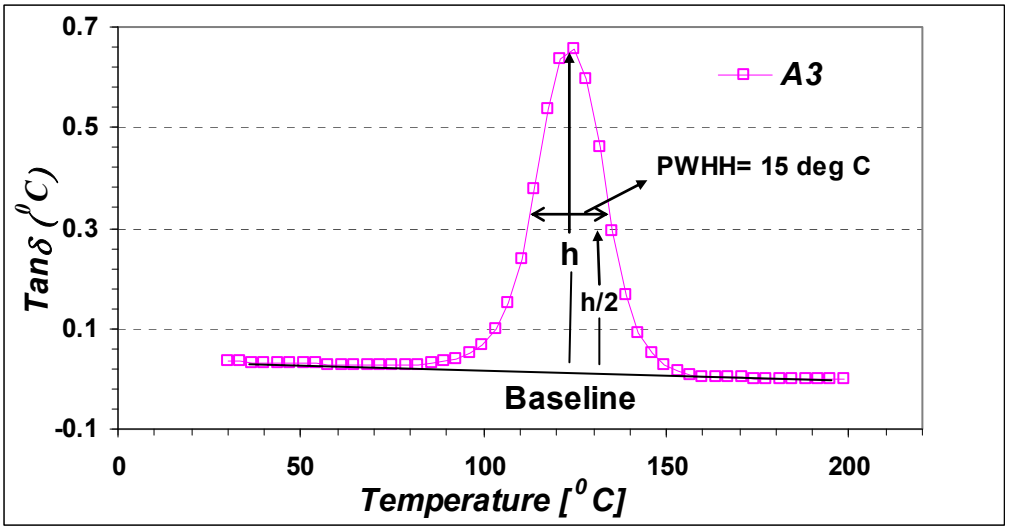

Figure 4.6. Plot of tan δ *versus Temperature for sample A3. The peak height is Indicated by h and the width at half height of* tan δ *curve is indicated by PWHH.*

From *Figure 4.6* it can be observed that the width of the tan δ curve broadens with the increase in the functionality of amine. For a systematic analysis of the broadness of the tan δ curve for the Model I samples the width of the tan δ curve at half height for 1 Hz is taken and is denoted as tan δ *(PWHH)[Peak width at half height]*. In order to determine the peak width at half height *(PWHH)* for the tan δ curve a baseline is

drawn connecting the initial rise and final drop of the tan δ curve and then a line is drawn from the centre of the base line towards the tan δ peak as shown in the *Figure 4.6*. The width at half height of the tan δ peak is the tan δ *(PWHH)*. Tan δ *(PWHH)* indicates the temperature increase which is needed for the crosslinked network to undergo the relaxation process**.**

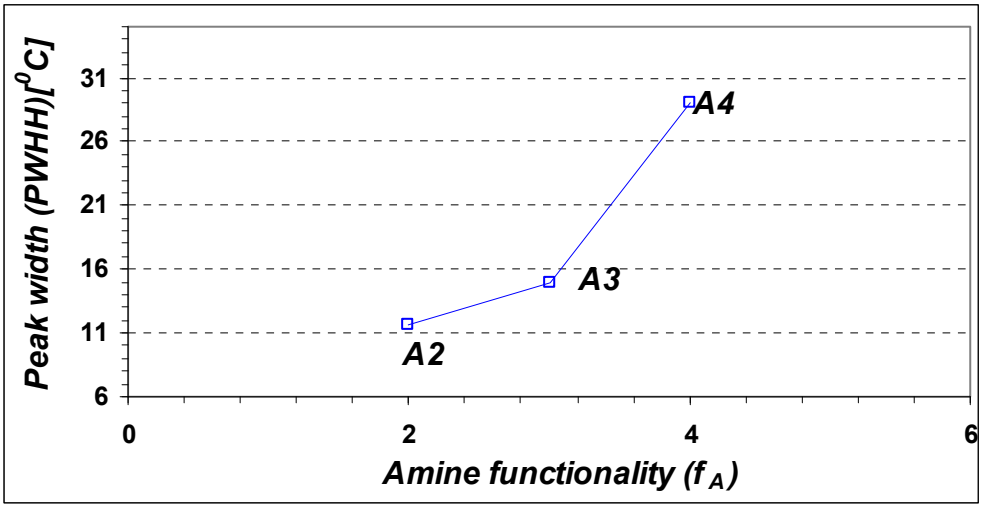

Figure 4.7. The peaks width of the tan δ *curve at its half height (PWHH) for 1 Hz frequency versus amine functionality.*

Figure 4.7 shows the increase in *PWHH* with the increase in amine functionality. This is mainly because of the fact that with the increase in the amine functionality in the reacting mixture, the increase in the crosslink density of the cured network occurs. On molecular scale, as the crosslink density increases the number of crosslinking points increases and therefore the network structure comes closer and thus shows a higher $T_g^{\tan \delta}$. After reaching $T_g^{\tan \delta}$, the free volume plays an important role on the molecular mobility. Since the crosslinked network containing a higher crosslink density will generate less free volume and so it takes more temperature to undergo the relaxation process i.e., to reach from the glassy state to rubbery state. So, in the Model I system the sample *A4* has the highest crosslink density and therefore it shows the maximum tan δ peak width at half height (*PWHH*). While, A2 has the lower crosslink density in comparison to A4 and A3 and hence has the least *PWHH***.**

4.4. Model System II: Epoxy functionality

The viscoelastic reponse of the cured samples for the Model II system in tensile mode was earlier shown in *Figure 3.10* in *Chapter* III. The glassy and the rubbery modulus data of the Model II system is shown in *Figure 4.8*.

Glassy Modulus:

From *Figure 4.8* it can be seen that the glass modulus which is taken as the modulus at T_g*-60 °C,* is independent of the functionality of the epoxy in the reaction mixture.

Rubbery Modulus:

Figure 4.8 shows that the rubbery modulus increases with the increase in the functionality of amine. This is because of the fact that as the functionality of the epoxy in the reaction mixture increases, the number of crosslinking points increase within the network structure or in other words the crosslink density (ν_C) increases.

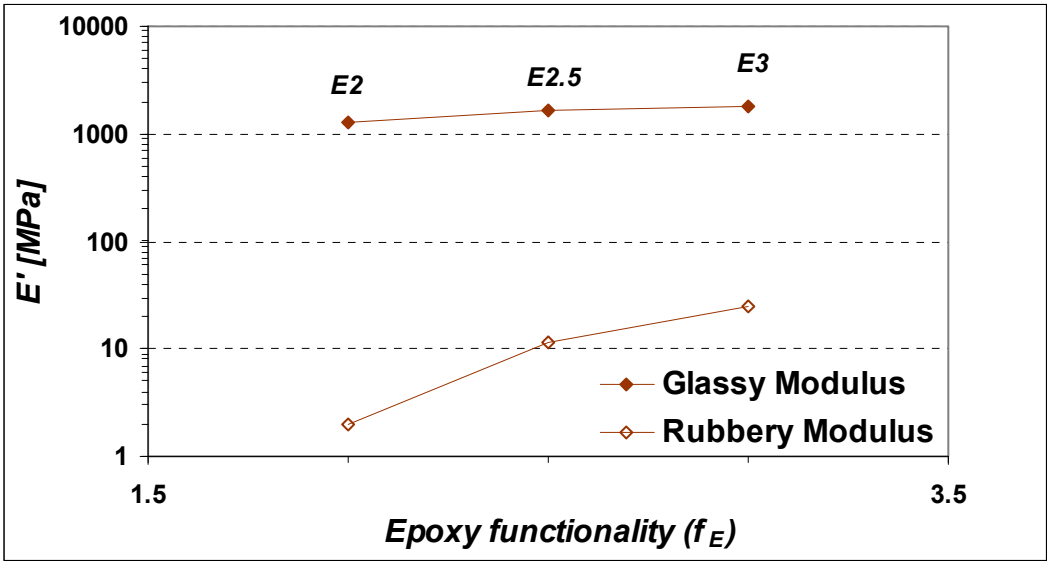

Figure 4.8. Glassy and rubbery modulus with respect to the increase in the functionality (f_E) of the aromatic epoxy.

The values of the measured and calculated crosslink density using the Miller and Macosko theory are shown in *Figure 4.9*. It can be seen from *Figure 4.9* that the measured crosslink density increases with the increase in the epoxy functionality. Also it can be seen that the crosslink density is quite well predicted using the Miller and Macosko approach.

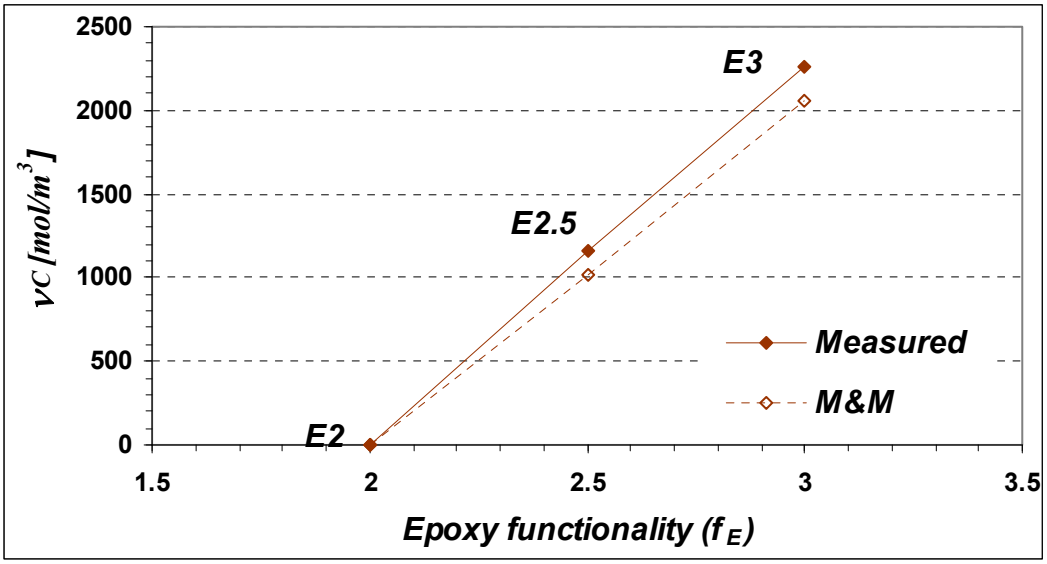

Figure 4.9. Crosslink density (mol/m^3) versus epoxy functionality.

Tan δ *(Damping) Curve:*

The tan δ (*Damping*) curves for the three samples *E2, E2.5* and *E3* of the Model II system is shown by *Figure 4.10*. From *Figure 4.10* it can be seen that the change in peak height as well as the width or broadness of the tan δ curve does not show a systematic trend with the increase in epoxy functionality. A decrease in the height and also a broadening of the tan δ curve from *E2.5* to *E3* is observed**.**

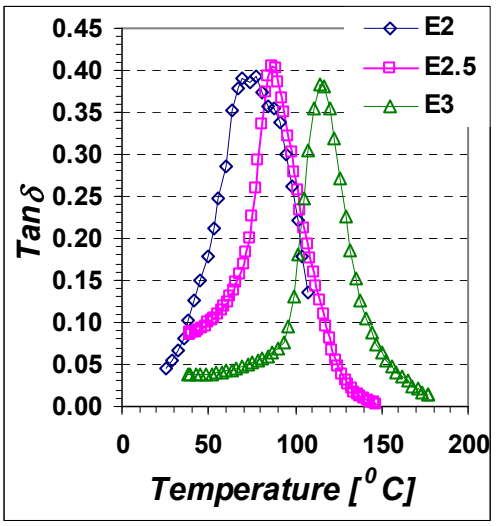

a.

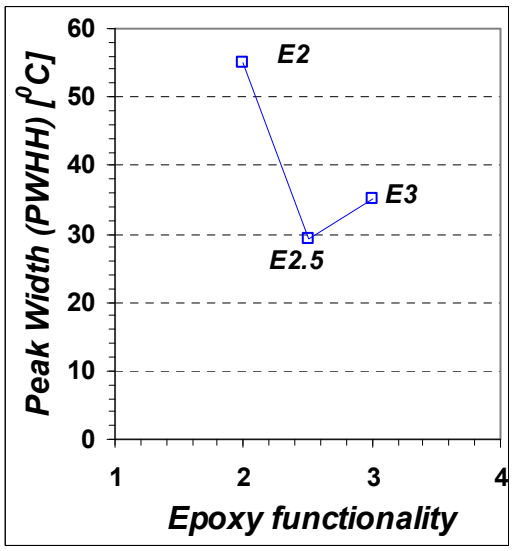

b.

Figure 4.10.

a. Tan δ *curve for 1 Hz frequency versus temperature.*

b. Tan δ *peak width at half height for1 Hz frequency versus epoxy functionality.*

The analysis of the height as well as the width of the tan δ curves of Model system II is discussed below**.**

Discussion

The sample *E2* which is a formed by BFDGE (*f=2*) and DMEDA (*f=2*) was shown in the *Table 2.4* in *Chapter II*. Due to the reaction of the difunctional reactants, the sample *E2* is expected to contain only linear chains and hence should be thermoplastic in nature. Further, from *Figure 4.10. a. the* damping data for *E2* above *110 °C* does not exist as the sample has melted during the *DMA* run. This confirms that the sample *E2* is thermoplastic in nature. Since the tan δ data above 110 °C of *E2* is absent a base line cannot be drawn for the determination of the height as well the width of the tan δ curve. In order to obtain at least an estimate we take that tan δ =0 line as the baseline and determine the PWHH to be about 55 °C. The extremely wide peak for the linear system suggests a broad distribution in the length of the linear chains. The smallest chains start to move already at room temperature whereas the longest ones only commence at above 100 °C. Since the tan δ peak height and the width of the sample *E2* cannot be determined, the tan δ *(PWHH)* data of *E2* cannot be compared with *E2.5* and *E3*. However, it can be observed from *Figures 4.10 a&b* that the $T_g^{\tan \delta}$ and the *PWHH* increase from *E2.5* and *E3.* This trend is expected since the crosslink density of *E3* is higher in comparison to *E2.5*.

4.5. Model System III: Effect of Chain (or) Spacer Length

The viscoelastic reponse of the cured samples for the Model III system in tensile mode is shown by *Figure 3.13*. The analysis of the glassy and rubbery modulus data of the Model III system is dicussed below**.**

Glassy Modulus:

From *Figure 4.10* it can be seen that the glassy modulus (modulus at T_g*-60 °C)* remains constant (or independent) of the increase in the chain length. This is because of the restriction of the motion of the molecular chains below the glass transition temperature.

Rubbery Modulus:

In contrast with the previous systems, for the model III system the E_r remains almost constant (a slight decrease form 35 to 30 unit can be observed), while at the same time

the T_g increases (see *Table 3.2*). This is useful for the tailoring of the viscoelastic properties of the cured resins, since this gives us a means of varying the T_g independent of the crosslink density.

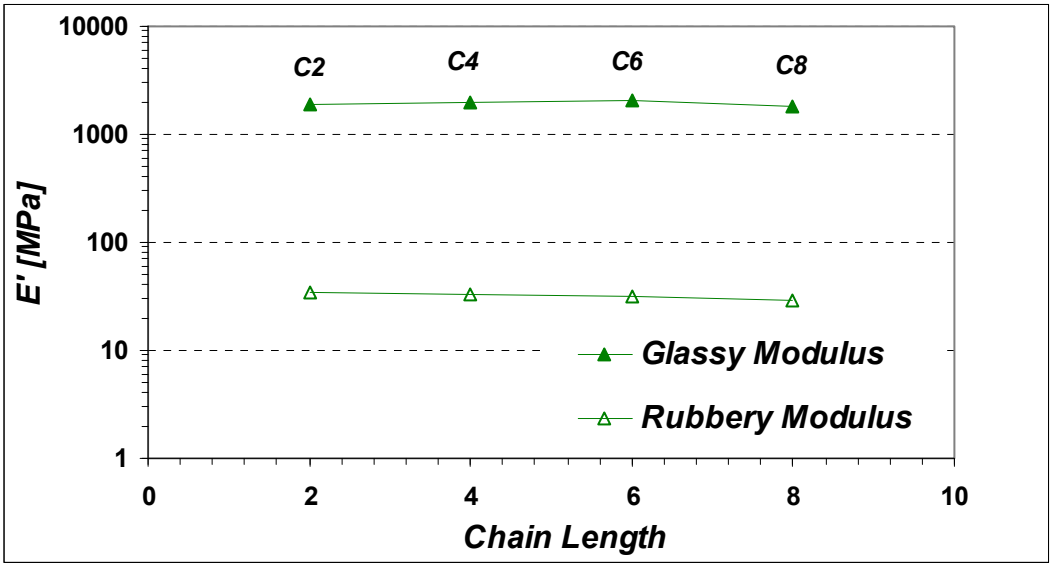

Figure 4.11. Glassy and rubbery modulus versus chain length of aliphatic curing agent.

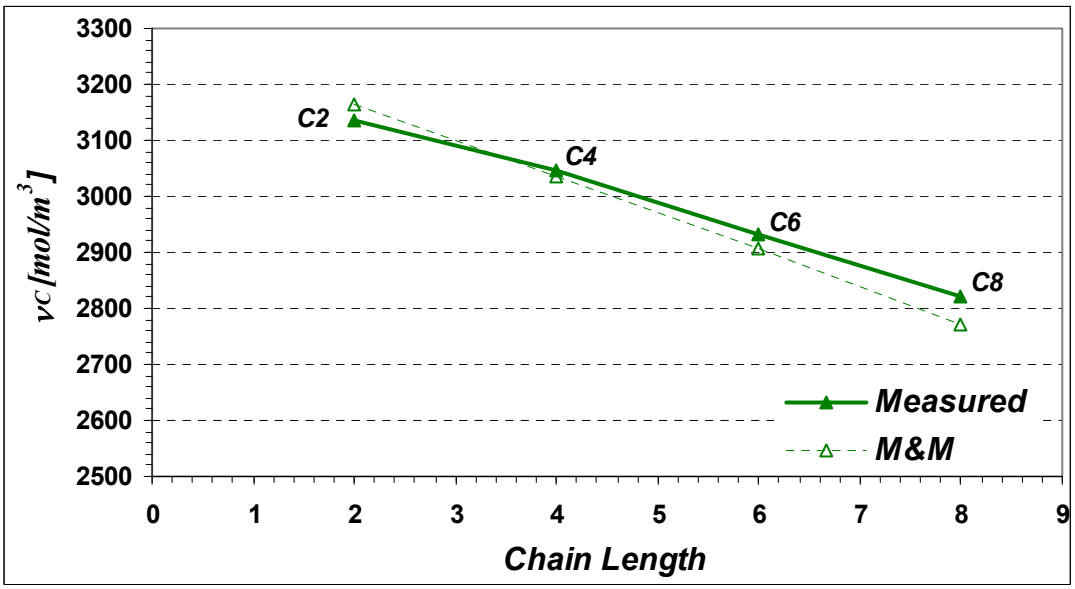

Figure 4.12. Crosslink density (mol/m^3) versus chain length of the amine.

Since the initial resin mixture of the Model III system contains DER epoxy of constant functionality ($f_E = 2$) and a homologous series of aliphatic amines with also a constant functionality ($f_A=4$), the network formed after curing should have a constant number of reacting sites. Hence the series of networks formed are expected to have

similar crosslink density values. A close inspection of the change in rubbery modulus shows that it slightly decreases with increasing chain length (from 35 MPa for *C2* to 30 MPa for *C8*). This was expected since with longer spacers the distance between the crosslinks increases and thus the E_r and v_C should decrease. *Figure 4.12* clearly shows that with the increase in chain length the crosslink density decreases slightly. Moreover the prediction of the crosslink density using the Miller and Macosko theory is in close agreement with the measured crosslink density as shown in *Figure 4.12*.

Tan *δ* *(Damping) Curve:*

The tan *δ* (*Damping*) curves for the samples C*2, C4, C6 and C8* of the Model III system are shown by *Figure 4.13a*. From this *Figure* it can be seen that the height of the damping peak increases from C2 to C8 and also the width of the tan *δ* curve decreases from C2 to C8.

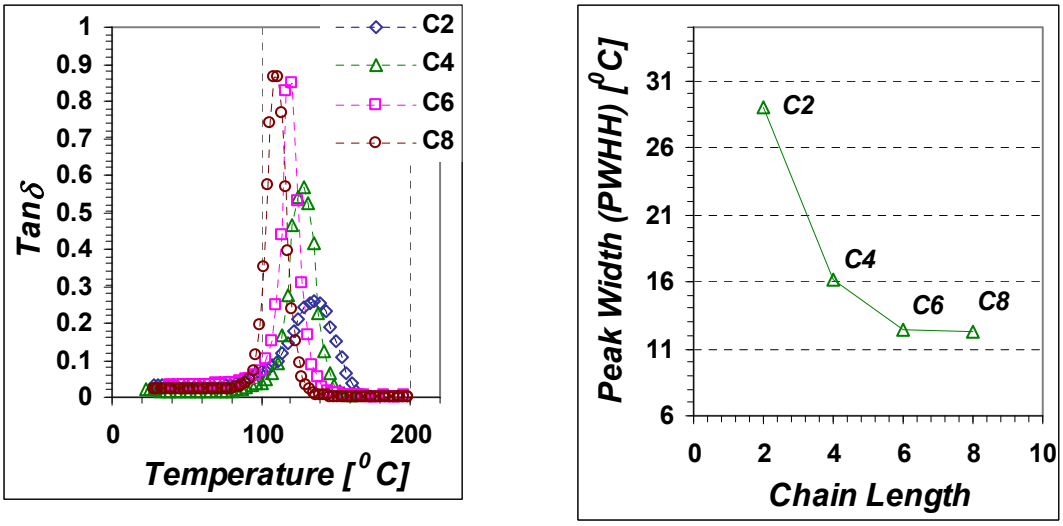

a. *b.*

Figure 4.13. *a.* Tan *δ peak for 1 Hz frequency versus temperature.*
b. The peak width of the tan *δ curve at its half height for 1 Hz frequency versus network chain length.*

Discussion:

The samples C*2, C4, C6 and C8* are from the cured products formed by the independent reaction of stoichiometric mixtures of DER 332 (*f=2*) epoxy with aliphatic amines *EDA, BMDA, HMDA and OMDA* having a constant functionality (*f=4*) (see *Table 2.1* of *Chapter II)*. As the four samples C*2, C4, C6 and C8* are

formed with an equal number of reacting groups. Therefore the network of all the samples should have an equal number of crosslinking sites or points. The equal number of crosslinking points should therefore result in similar network structures for the samples C*2, C4, C6 and C8.* This is illustrated in *Figure 4.14.*

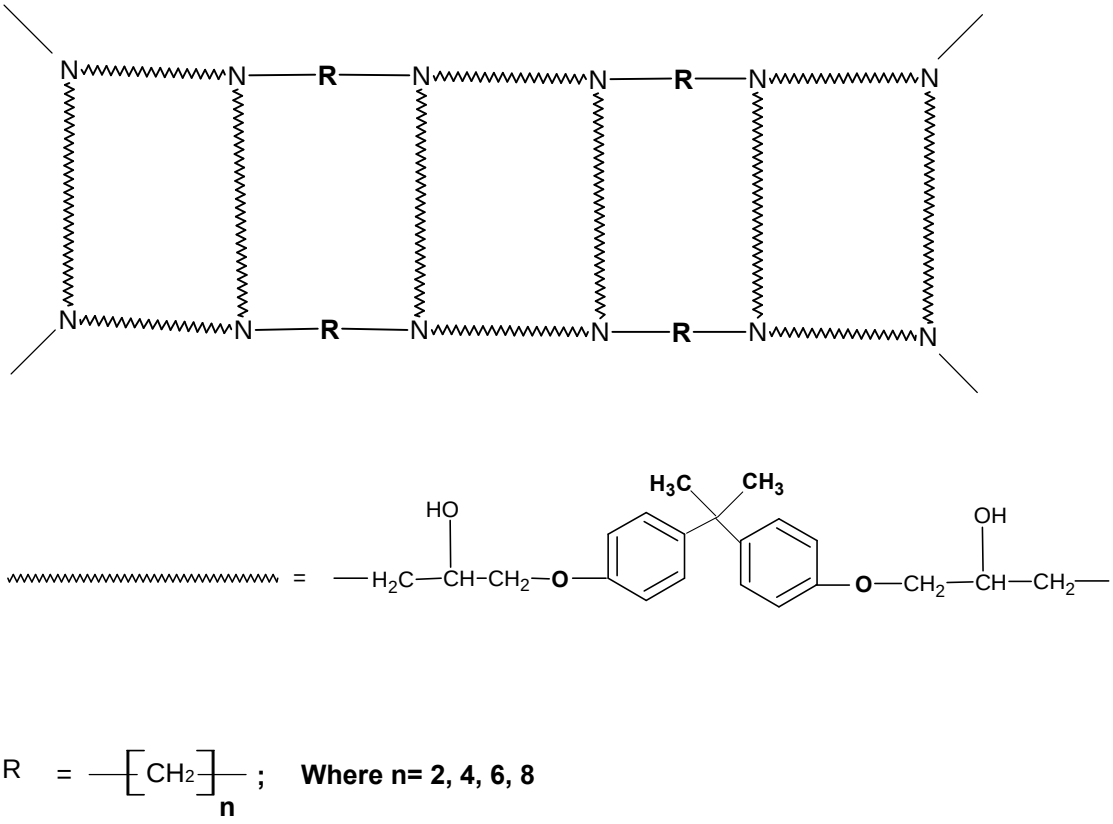

Figure 4.14. Generalized representation of the network structure. The n values for samples C2, C4, C6 and C8 are 2, 4, 6 and 8, respectively.

Although the samples C*2, C4, C6 and C8* have a similar network structure, the aliphatic chain length (indicated by *n* in *Figure 4.14*) of the amine unit increases from *C2* to *C8* making the network structure broader. The increase in the aliphatic chain length from *C2* to *C8* on the other hand increases the flexibility of the network structure. With the increase in the flexibility of the network the segmental mobility within the network increases and hence the network undergoes a transition faster with respect to time and temperature and reaches the equilibrium rubber modulus at a lower temperature. Consequently, the T_g decreases and also the *PWHH* decreases. Furthermore, *C8* has the highest spacer length and so there is less steric hindrance due

to more free volume. And soon after the start of the glass transition all segments will be able to move and only a small transition region is needed. On the other hand the segmental movements in sample *C2* are much restricted as it contains the least spacer length within the model system IV sample series. And therefore the transition in sample *C2* takes much longer with respect to time and temperature. Moreover, the steep decrease in *PWHH in Figure 4.13b* suggests that a spacer length of 3 to 4 methylene units is needed to overcome the interaction with the bulky aromatic groups in DER 332**.**

4.6. Model System IV: Pendant Chain Length

The viscoelastic reponse of the cured samples for the Model IV system in tensile mode is shown in *Figure 3.17*. The glassy and the rubbery modulus data of the samples *P1*, *P3* and *P6* of the Model IV system is shown in *Figure 4.15*.

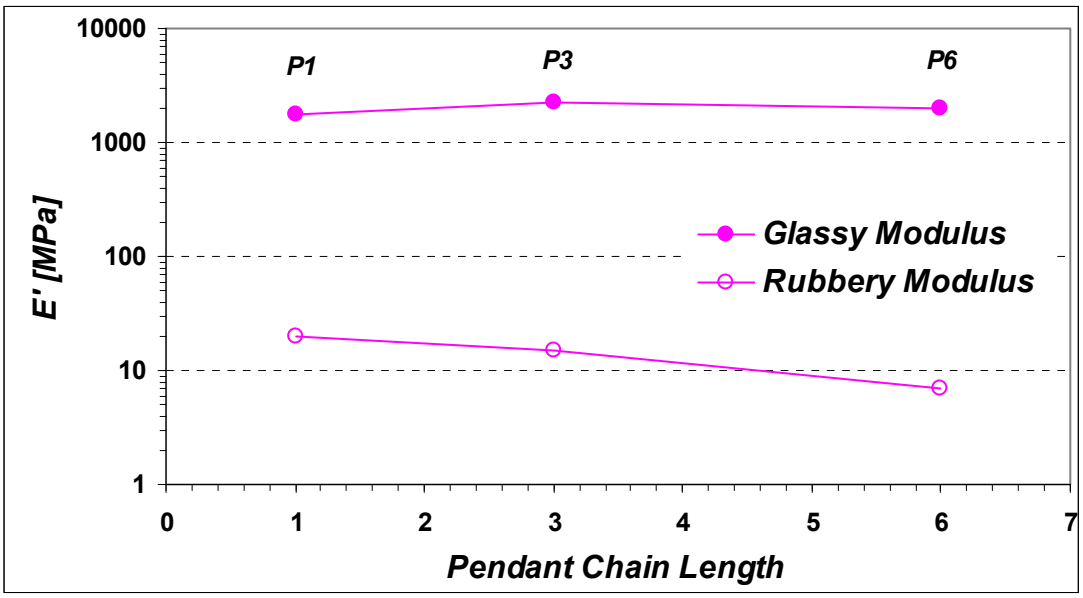

Figure 4.15. Glassy and rubbery modulus with respect to the increase of pendant chain length.

Glassy Modulus:

From *Figure 4.15* it can be seen that the glassy modulus (modulus at T_g*-60 °C)* remains constant, i.e. independent of the increase in chain length. It means that the introduction of pendant chains within the network structure does not have any affect on the glassy modulus. The restriction of molecular motion below T_g to transitions over a few atoms length (which is much smaller than the size of a pendant chain) is

the reason for the independency of the glass modulus for the samples *P1*, *P3* and *P6* as shown in *Figure 4.15*.

Rubbery Modulus:

From *Figure 4.15* it can be seen that the rubbery modulus decreases with the increase in the pendant chain length. This was not expected because the network formed after curing the stoichiometrically mixed epoxy and homologous series of amines in the *Model IV* sample series should have a constant number of reacting sites and hence the cured materials are expected to have identical crosslink density values. The explanation from the IR data (*Chapter III*) showed that the *P1* sample was fully cured (100% Conversion). Whereas, *FTIR* results of the samples *P3* cured at *200 °C for 2 hours* and *P6* cured at *200 °C* for *4* hours showed 99% and 96% conversion. Consequently, there are still epoxy groups remaining in the network of the cured samples. These will remain in the network structure as dangling ends (or) pendant groups similar to R' in *Figure 4.16*. The incomplete reaction of epoxy in the *P3* and *P6* samples should decrease the number of crosslinking sites from the ideal network formation as shown from *Figure 4.16*.

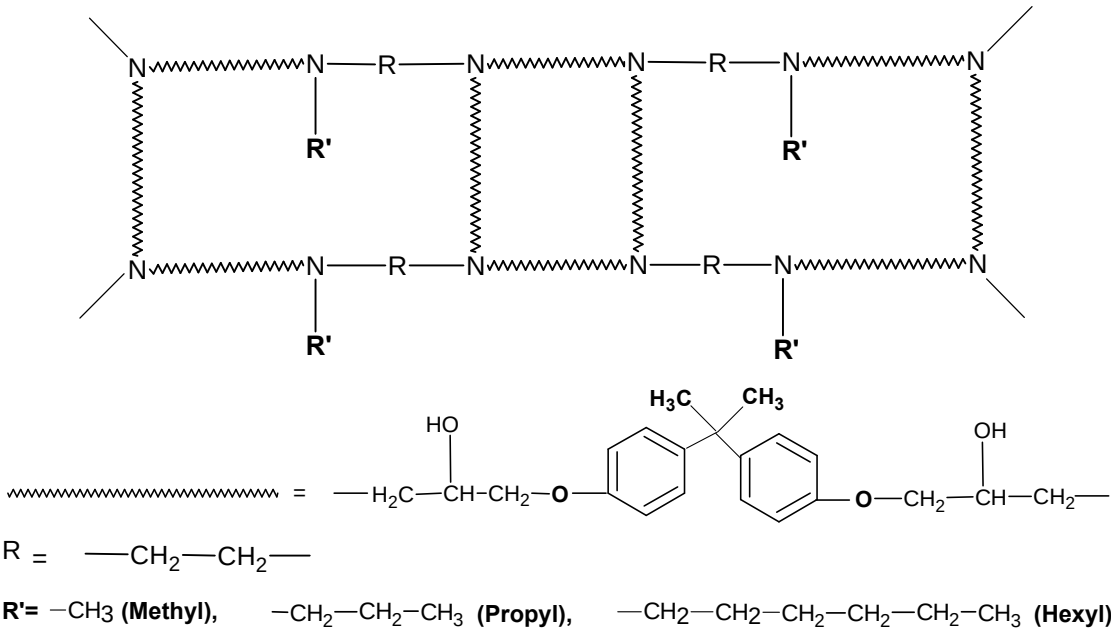

Figure 4.16. Generalized representation of the network structure. Where R' for P1, P3 and P6 are methyl, propyl, hexyl groups, respectively.

This incomplete conversion was taken into account while calculating the crosslink density using the M&M theory (see *Figure 4.17*). Therefore it can be observed from *Figure 4.17* that the decrease in the measured crosslink density (v_C^{Meas}) from P1 to P6 is predicted using the Miller and Macosko approach within an errror of 5%**.**

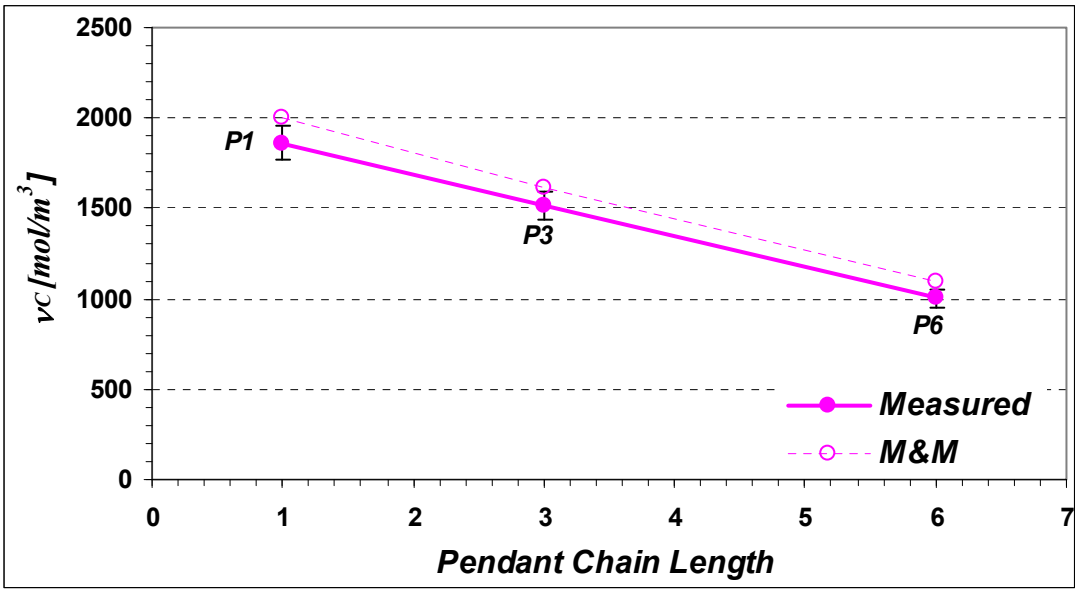

Figure 4.17. Crosslink density (mol/m^3) versus pendant chain length. Note that for P3 and P6 the conversions of 99% and 96% were found (based on FTIR data) for the calculation of $v_C^{M\&M}$.

Tan δ *(damping) Curve:*

The tan δ (*damping*) curves for the samples *P1, P3* and *P6* in the Model IV system are shown in *Figure 4.18.a*. The decrease in the $T_g^{\tan \delta}$ from P1 to P6 as shown in *Figure 4.18a* is due to the decrease in crosslink density. Also from *Figure 4.18 a*. it can be seen that the height as well as the broadness of the tan δ peak increases from *P1 to P6.* The peak height of the tan δ curve is related to the flexibility of the network and so in the series of the samples in the Model IV system the sample *P6* is expected to show a higher tan δ peak height in comparison to the samples *P3* and *P1*. The maximum tan δ peak in sample *P6* is mainly due to the highest aliphatic chain of the pendant group i.e., the hexyl group. Whereas the sample *P1* has the lowest aliphatic pendant chain length group i.e., the methyl group and therefore *P1* shows the least tan δ peak height in the Model IV sample series. The expected increase in the peak height of the tan δ curves from *P1* to *P6* is clearly observed from *Figure 4.18a*.

Moreover, above $T_g^{\tan \delta}$ the molecular mobility depends on the free volume. Therefore the sample *P6* has the least molecular mobility in comparison to *P3* and *P1* due to the highest pendant chain length group i.e., the hexyl group. The hexyl group occupies the portion of the free volume and hinders the mobility of the network. Therefore the sample P6 requires a larger temperature range to undergo the transition region i.e., from the glassy to the equilibrium rubbery state. Whereas, the propyl and methyl groups in the samples *P3* and *P1* show comparatively less hindrance. Therefore a lower temperature is needed to reach the equilibrium rubbery mdoulus. The *PWHH* is one way of defining the amount of temperature required to undergo the transition region. Hence the *PWHH* values for the samples *P1, P3* and *P6* in the Model IV sample series are expected to show an increasing trend. From *Figure 4.18b* it can be seen that the PWHH increased from *P1* to *P3* as expected, whereas the *PWHH* for the sample *P6* decreased. The unexpected decrease in the PWHH for the sample P6 in *Figure 4.18b* is mainly due to the lower % of conversion of epoxy groups (i.e., 95% Conversion)**.**

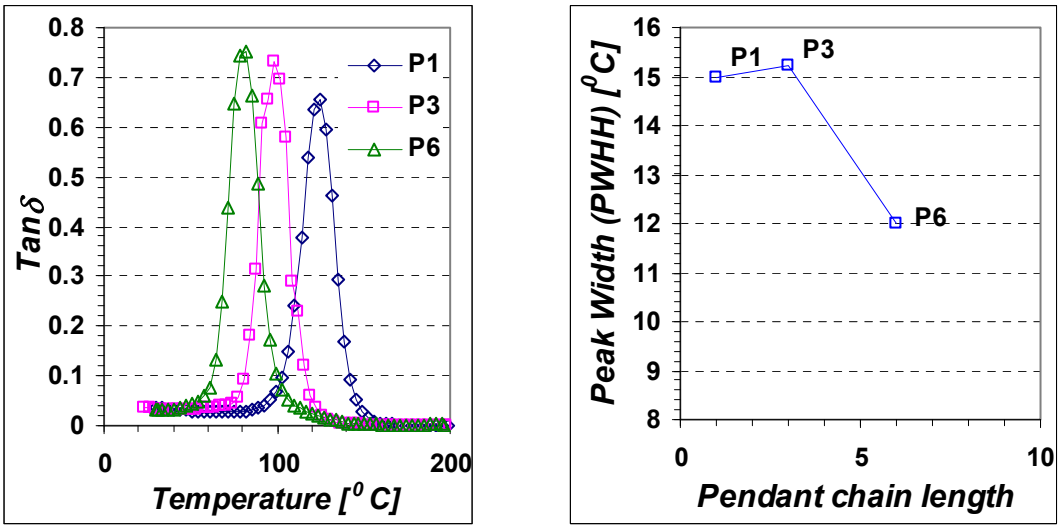

a. *b.*

Figure 4.18. *a.* Tan *δ peak for 1Hz frequency versus temperature.*
b. PWHH versus pendant chain length.

4.7. *PWHH* versus Crosslink density ($v_C^{M\&M}$)

One of the objectives of this work is to model the viscoelastic curves, and therefore it is necessary to describe the variation of the width of the glass transition. It is generally accepted that the primary, or most fundamental, motions responsible for the relaxation

are activated at the onset of the relaxation, while the peak breadth and height depend on the co-operativity or extent of motions [Nielsen, (1969), Ueberreiter and Kanig, (1950), Tobolsky et al., (1964)]. As the molecular motion in most of the cases is controlled by the crosslink density and therefore the *PWHH* of the tan δ is plotted against the crosslink density as shown by *Figure 4.19*. It can be seen from *Figure 4.19* that the *PWHH* increases with the increase in crosslink density ($\nu_C^{M\&M}$). Note: The *PWHH* of the sample *E2* is omitted (for details refer to *Section 4.2*). More importantly it can be concluded that the *PWHH* did not scale up with respect to the crosslink density**.**

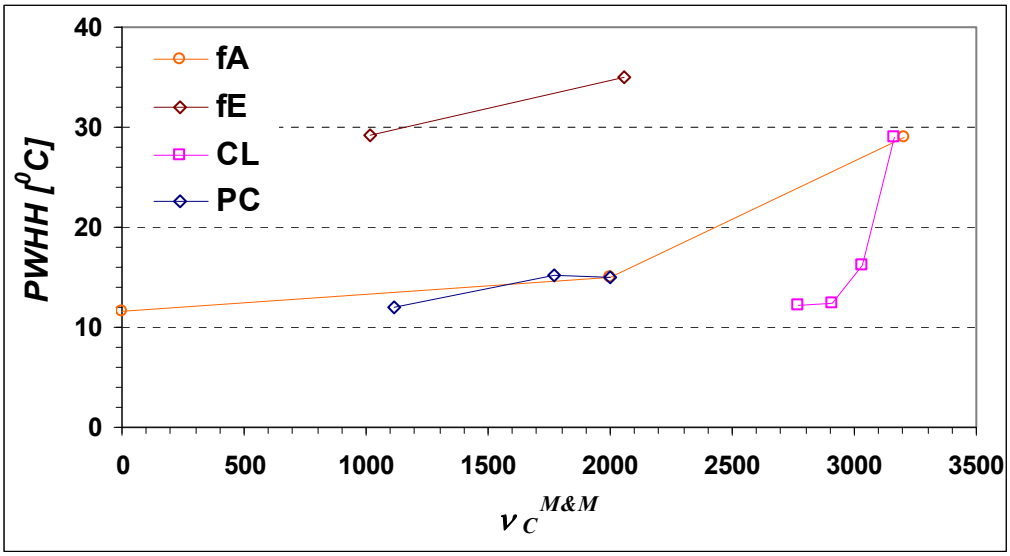

Figure 4.19. The peak width at half height of the tan δ *curve of all model systems versus the calculated crosslink density* ($\nu_C^{M\&M}$).

4.8. *PWHH* versus Flexibility (*F*)

Figure 4.20 shows the plot of *PWHH* versus the flexibility parameter (*F*) for the four model systems**.** It can be seen from *Figure 4.20* that the *PWHH* decreases linearly with the increase in the flexibility. The decreasing trend of PWHH in *Figure 4.20* shows that the co-operativity or extent of motions in the transition region is dependent on the flexibility (*F*). As the flexibility (*F*) indicates the concentration of the flexible bonds (aliphatic) in the network, it can be concluded that the increase in the concentration of the aliphatic chain length in the network causes the decrease in the PWHH. On the other hand the increase in the aromatic content in the network should increase the tan δ *(PWHH)*. The expected trend as discussed above is clearly observed

in the Model II system. The sample A3 which has the highest number of aromatic groups showed the least flexibility (*F*) and the highest tan δ *(PWHH)* out of the four model systems. Note: The *PWHH* decreased with respect to the increase in the free volume ($f_{V(D)}$) [see *Chapter V, Section*] but the *PWHH* did not scale up well. Moreover the PWHH shows a better scaling with respect to the flexibility as shown in *Figure 4.20*.

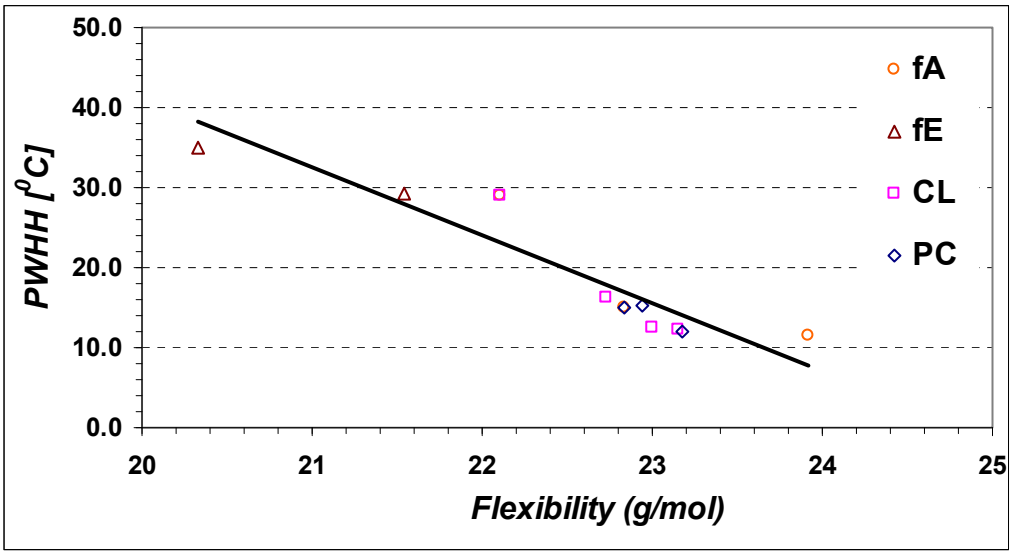

Figure 4.20. The peak width at half height of the tan δ *curve of all model systems with respect to Flexibility.*

4.9. Viscoelastic Master Curve

In *Chapter III* and *Chapter IV* the analysis of the modulus curves for all the four Model systems with respect to temperature for a single frequency was only discussed. Since, thermosets are polymeric materials whose properties vary with temperature as well as with time, the incorporation of time (or frequency) dependency on the viscoelasticity is very important. This can be done by constructing a Viscoelastic Master curve using the Time Temperature Superposition principle (TTS) which was first proposed by Boltzman [J.D.Ferry., 1980].

The aim of the present section is to develop a model in which both the temperature and the time (frequency) dependency of the storage modulus is captured. The challenge is to find a single model capable of describing the viscoelasticity of all synthesized systems. This will be done by approximating the shape of the viscoelastic curve with a parameterized function and studying the change in parameters in the

different experimental systems. First we will discuss fits to the separate systems, and then a generalised model is proposed which will be used to describe the master curves of all the systems.

The principle of time-temperature superposition is based on the observation that time-temperature and frequency-temperature effects in polymers are quite related. It implies that the mechanical response at short times (or high frequencies) is analogous to the response at low temperature, and vice versa. For example, increasing temperature will shift the same event (mechanical response) to shorter times, or increasing the frequency will shift the same event to lower temperatures. This principle is commonly used to determine viscoelastic properties beyond the range of frequencies covered by experimental measurements.

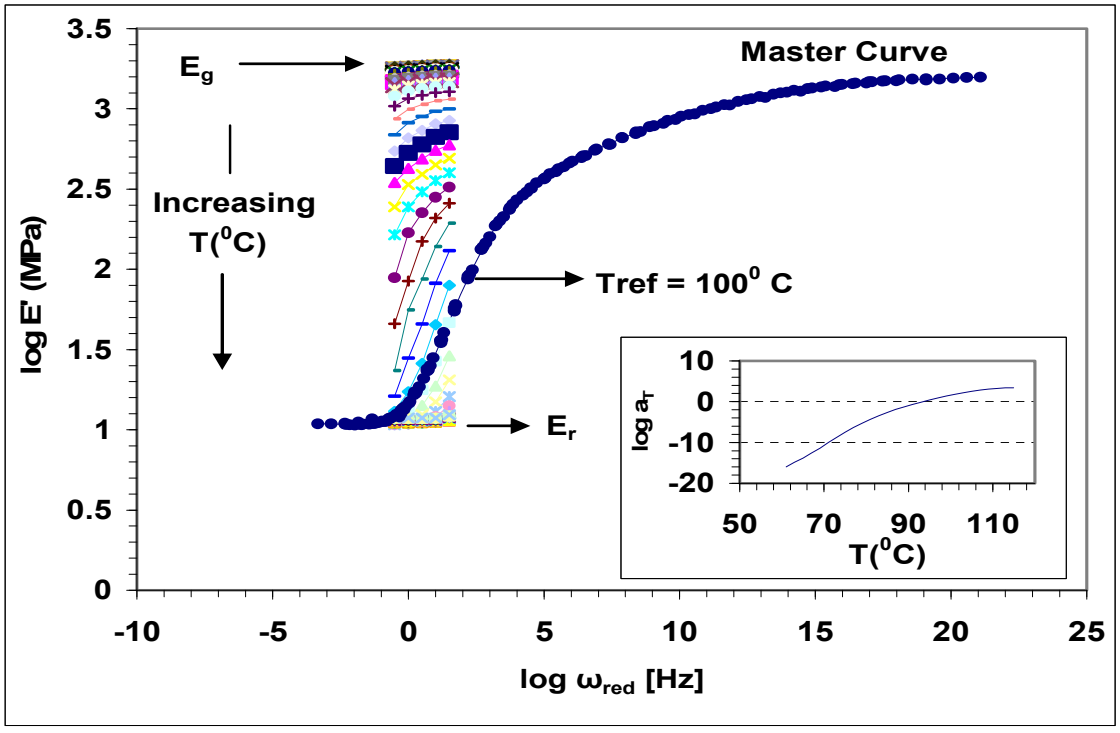

Figure 4.21. Plot of the Storage modulus (E') with respect to the reduced frequency (ω_{red}) for A2 of the Model I system. E_g, E_r and T_{ref} are the glassy modulus, rubbery modulus and the reference temperature. The symbol led lines (.-) are the modulus values of all frequencies at different temperatures. The master curve is shown by a full line (_). A plot of the shift factor (log a_T) versus temperature is shown as an insert.

In order to generate a viscoelastic master curve the obtained modulus data at different temperatures from the *DMA* experiment is plotted with respect to a frequency scale as shown in *Figure 4.21*. According to the Frequency Temperature Superposition (*FTS*) principle the modulus data can be shifted along the frequency axis towards a reference temperature to generate a so-called master curve (included in *Figure 4.21*). *Figure 4.21* shows the storage modulus master curve plotted against a reduced angular frequency (ω_{red}) for the sample *A2* which is obtained after shifting the modulus data on the frequency scale to a reference temperature (T_{ref} = 100 °C) [Fox & Flory, 1950]. here ω_{red} is given by

$$\omega_{red} = \frac{\omega}{a_T} \qquad (4.2)$$

with ω the angular frequency (*rad/s*) and a_T the shift factor. The corresponding shift factor is shown as an insert in *Figure 4.21*.

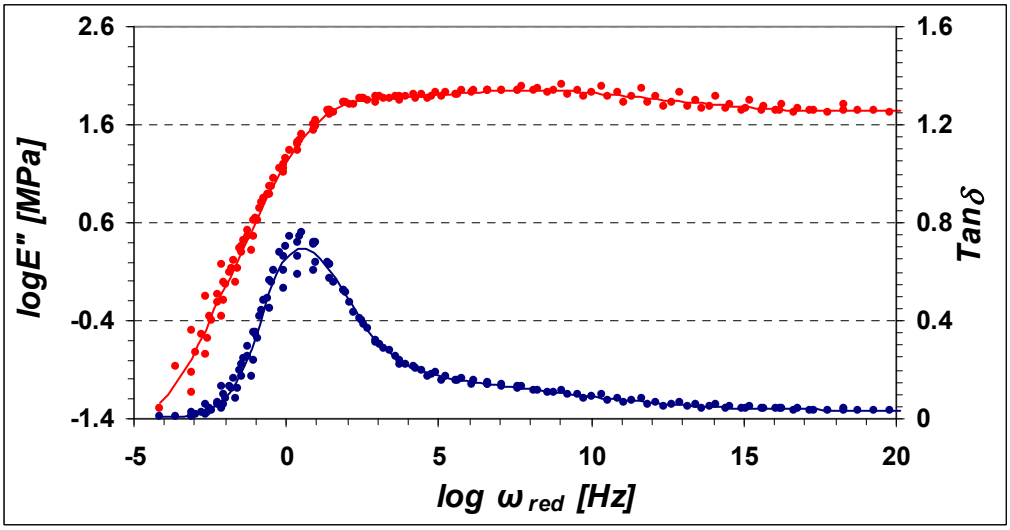

Figure 4.22. Plot of the Loss modulus (E") and tan *δ with respect to the reduced frequency (ω_{red}). The Master curve is shown by dots (.) and the full line (-) represents the average of the dotted points for A2. The primary axis is for the loss modulus and the secondary axis is for the* tan *δ data.*

From *Figure 4.21* it can be seen that the glassy modulus (E_g) is observed at higher frequency and the rubbery modulus is seen at lower frequency on the Master Curve. If the same shift factor is applied to *E"* (Loss modulus) and tan *δ* (Damping) data the master curves obtained are shown in *Figure 4.22*. It can be seen that this resulted in a

reasonable superposition of this data set as well. The *Figure 4.21* shows a better *FTS* for the storage modulus data, a unique storage modulus master curve is formed in comparison to loss and tan δ master curves as shown in *Figure 4.22.* So, for the cured samples of the four Model Systems the storage modulus (E') master curves and their corresponding shift factors are analyzed. Furthermore the master curves are modeled using a well-known fit function. This will be discussed in the *Section 4.10.*

4.9.1. Model System I

The storage modulus master curves for the increasing amine functionality and their corresponding shift factor curves are obtained by shifting the storage modulus data towards a reference temperature (T_{ref} =100 °C) using the frequency temperature superposition principle. They are shown in *Figure 4.23*.

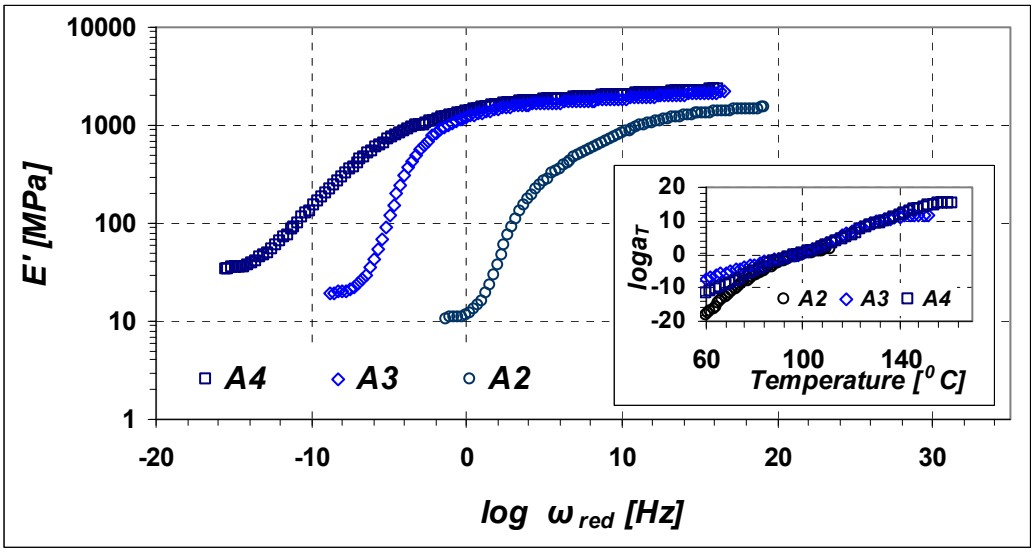

Figure 4.23. Master curves obtained at reference temperature T_{ref} = 100 °C using the frequency temperature superposition principle for the increasing amine functionality series i.e., A2, A3 and A4. The corresponding shift factors are shown as insert.

The T_g's of *A2, A3* and *A4* are *135 °C, 121 °C and 93 °C* respectively. An intermediate temperature of *100 °C* is selected as T_{ref} for generating the Master Curves. From *Figure 4.23* it can be observed that the glassy modulus (E_g) remains constant. The rubbery modulus (E_r) increases with the increase in amine functionality i.e., from *A2* to *A4*. The increase in rubbery modulus is due to the increase in the crosslink density. This was earlier discussed in the *Section 4.2*. More importantly the

viscoelastic transition region shifted to a lower frequency scale with the increase in amine functionality. Note that the glass transition shifts from about 10^{+6} to 10^{-6} from *A2* to *A4* with respect to reduced frequency. This means that there is a shift of 12 decades along the frequency axis. Furthermore from *Figure 4.23* it can be seen that with increasing amine functionality the slope of the mastercurve in the transition region clearly decreases. The slope (n) is indicated in *Table 4.2*. This results into a broader transition region. Also from *Figure 4.23* it can be seen that the shift factor ($log\ a_T$) curves increased to higher temperatures with the increase in amine functionality**.**

4.9.2. Model System II

The *Figure 4.24* shows the storage modulus master curves for the samples *E2, E2.5 and E3*. Their corresponding shift factor curves are obtained by shifting modulus data towards a reference temperature (T_{ref} *=100 °C)* using the frequency temperature superposition principle. The reason for the selection of T_{ref} *=100 °C* is because the sample *E2* melted above *100 °C*. Hence the modulus data above *100 °C is* scattered and the selection of a temperature above 100 °C as T_{ref} is not a good choice.

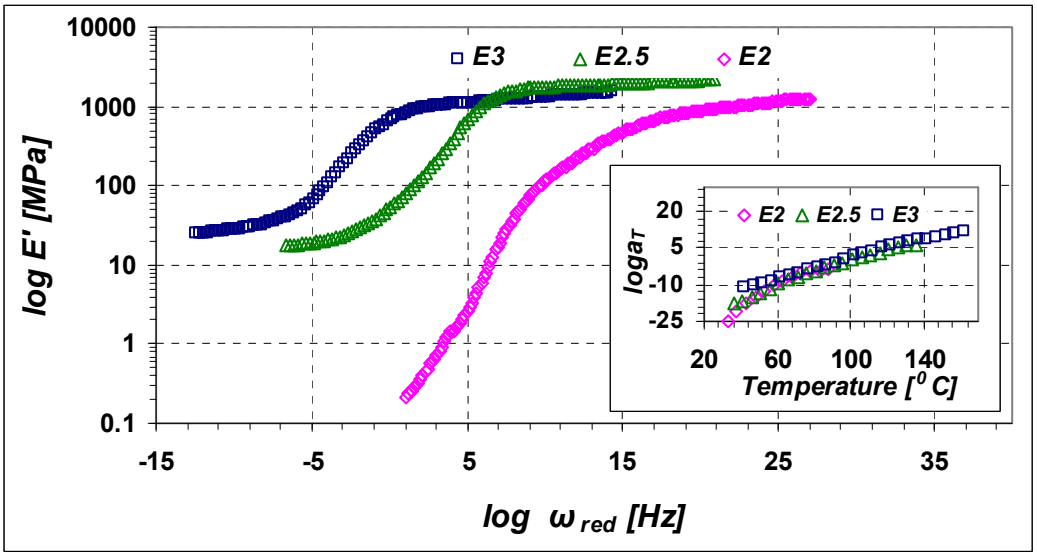

Figure 4.24. Master curves obtained at reference temperature (T_{ref} = 100 °C) using frequency temperature superposition principle for E2 and E3 versus the reduced frequency (ω_{red}).

From *Figure 4.24* it can be observed that the glassy modulus (E_g) of *E2, E2.5* and *E3* remains constant. The rubbery modulus of *E2* gradually decreases and goes to zero

and confirms that the rubbery plateau does not exist for *E2*. This is mainly because of the thermoplastic nature of the *E2* sample which melts during the *DMA* heat scan. Moreover the viscoelastic transition region has been shifted towards a lower frequency scale with the increase in epoxy functionality. The glass transition shifts from 10^{+9} to 10^{-3} with respect to the reduced frequency from *E2* to *E3*. This means that there is a shift of 12 decades along the frequency axis. Also from *Figure 4.24* we can see that the shift factor (*log* a_T) curves shift to higher temperatures with the increase in amine functionality. The slope of the master curves does not appear to change much for these series. Note: In contrast to the amine functionality series, here a four functionality series is not present.

4.9.3. Model System III

The *Figure 4.25* shows the master curves and their shift factor (at reference temperature, T_{ref}*=100 °C*) for the samples *C2, C4, C6, C8***.**

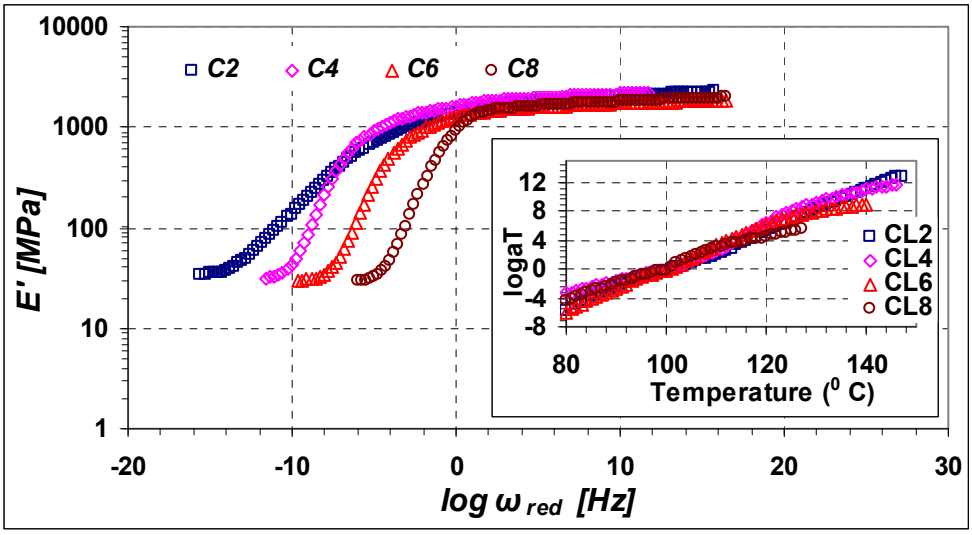

Figure 4.25. Master curves obtained at reference temperature T_{ref} *= 100 °C for C2, C4, C6 and C8 versus the reduced frequency* (ω_{red}).

From *Figure 4.2* it can be observed that the glassy modulus (E_g) and the rubbery modulus (E_r) are independent of the increase in chain length between the crosslinks. From *Figure 4.25* it can be observed that the master curve shifts about 6 decades from *C2* to *C8* with respect to the frequency scale. Also from *Figure 4.25* it can be observed that the shift factor curve shifts towards a lower temperature scale from *C2* to *C8*. The slope of the C2 curve is quite different form that of the *C4, C6, C8***.**

4.9.4. Model System IV

Figure 4.26 shows the viscoelastic master curves and their shift factor values that are obtained after applying the frequency-temperature superposition principle at a reference temperature T_{ref} =*100 °C* for the samples *P1* and *P3*. It can be seen from the *Figure 4.26* that the glassy modulus remains constant whereas the rubber modulus slightly increases as was discussed earlier in *Section 4.5*. From *Figure 4.26* it can be observed that the master curve shifted from 10^{-7} to 10^{+4} along the reduced frequency. This means that a shift of 11 decades is observed. This shift of 11 decades is mainly because of the increase in the pendant chain length which increases the flexibility of the network structure. Furthermore, the shift factor (*log* a_T) curves (see *Figure 4.26*) also shifted to lower temperatures with increasing pendant chain length i.e., from *P1* to *P6*. The slope of *P6* in the transition region is lower than the slope of *P1* & *P3***.**

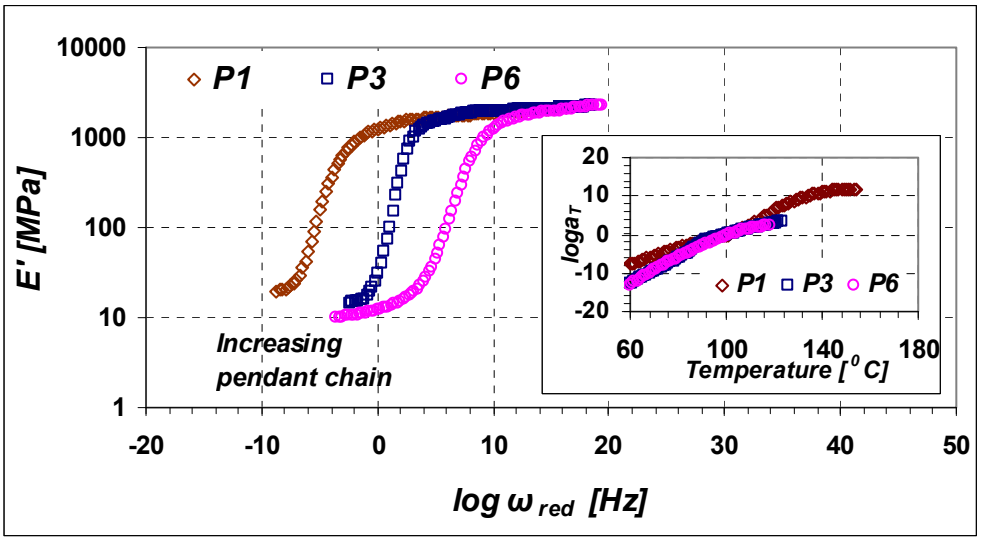

Figure 4.26. Master curves obtained for reference temperature T_{ref} = 100 °C for P1, P3 and P6 versus the reduced frequency (ω_{red}). The corresponding shift factor curves for P1, P3 and P6 are shown as insert.

4.10. Modeling the viscoelastic relaxation curve

In order to describe the measured relaxation function, simple analytical functions can be used [*Table 4.1*]. The advantage of the analytical function is that the large set of data points is then reduced to 4 to 5 shape parametes which can be compared more easily. Furthermore, if the variation of these parameters with respect to changes in chemistry is understood, it will be possible to generate an overall model for the

viscoelastic curves of all the amine-epoxy systems. A general form of the *Equation*s is shown below

$$E(t) = E_r + (E_g - E_r)\hat{Z}(t) \qquad \textbf{(4.3)}$$

Here $\hat{Z}(t)$ denotes the kernel function and E_r, E_g denote the rubbery and glassy limits.

Out of the analytical models proposed above, the best constitutive model is that one which can well describe the shape of the viscoelastic relaxation curve with the least number of parameters. Therefore, the selection of the Kohlrausch-Williams-Watts (KWW) (stretched exponential) expression, which has only one parameter χ in the kernel function, is taken as a fit function to describe the viscoelastic response of all our model systems. Initially, the KWW function is fitted to all the master curves and it is found that the KWW-fit function describes the shape changes of all master curves relatively well. So, the KWW-fit function (*Table 4.1, Eq.4.4*) is chosen in modeling the viscoelastic relaxation curve for all the model systems**.**

Model Name	Analytical Models	*Equation*
Kohlrausch-Williams-Watts (KWW):	$\hat{Z}(t) = \exp\left[-(t/\tau)^{\chi}\right]$	**(4.4)**
Cross Model:	$\hat{Z}(t) = \dfrac{1}{1+(t/\tau)^{\chi}}$	**(4.5)**
Kobeko:	$\hat{Z}(t) = \dfrac{1}{\left[1+(t/\tau)\right]^{p}}$	**(4.6)**
Havriliak Negami(or HN-fit):	$\hat{Z}(t) = \dfrac{1}{\left[1+(t/\tau)^{\chi}\right]^{p}}$	**(4.7)**

Table.4.1. Viscoelastic Models

Description of KWW-fit function:

The KWW-fit function is a simple analytical function which is used to describe the constructed (or) measured relaxation master curves. It contains five parameters, which are the glassy storage modulus (E_g) [MPa], the rubbery modulus (E_r) [MPa], the

reduced angular frequency (ω_{red}) [rad/s], the position of the transition region (τ_0) [s^{-1}] and the power law parameter χ, which represents the slope of the transition region.

4.11. A Systematic Approach to Model Viscoelastic Master Curves

Step I

In order to be able to predict the viscoelastic relaxation curve, firstly main features of all the master curves are fitted to the KWW-fit function [*eq. 4.4*] to capture the viscoelastic parameters i.e., E_g, E_r and χ.

$$E' = E_r + (E_g - E_r)\exp[-(\omega_{red}\tau_0)^{-\chi}] \qquad \textbf{(4.8)}$$

Step II

In order to compare the different experimental master curves it is necessary to use a common shift factor curve. A reference temperature (T_{ref}) is chosen to be T_0 and then the WLF (Williams-Landel-Ferry) fit parameters are determined.

$$\log a_T = \frac{-C_1^0(T - T_0)}{C_2^0 + (T - T_0)} \qquad \textbf{(4.9)}$$

The common shift factor parameters that are determined are C_1^0, C_2^0. It is well known that the relaxation time constant (τ_0) in *Equation.4.8* depends strongly on the temperature. For thermorheological simple materials this temperature dependency can be taken into account with the so called shift function $a_T\ (T, T_{ref}) = \tau_0(T)/\tau_0(T_{ref})$. Where τ_0 is determined by taking the reference temperature in the *Equation 4.10* as shown below

$$\tau_0 = \tau_{0g}\ a_T\left(T_0, T_g^{DiM}\right) \qquad \textbf{(4.10)}$$

Here T_g^{DiM} is dependent on the crosslink density as well as the flexibity of the network (refer to *Chapter III*).

Step III

The determined common shift factors C_1^0, C_2^0 are used for obtaining new master curves and can be called *Local fit* master Curves. Fitting the KWW-function to local

fit master curves generated different values of χ, E_g and E_r within each system. In order to be able to describe the relaxation curve of all the master curves within each model system a global model, which contains fixed values for the parameters χ and E_g has to be predicted. Note: The values of E_r and τ_0 are dependent on the crosslink density of the network and therefore can change. Finally, the predicted global master curves are generated using parameters χ, E_g, E_r and τ_0 and are subsequently compared with the experimental master curves.

The fit parameters determined by following *steps I & II* as mentioned in *Section 4.8* are shown in *Table 4.2*. Using these parameters and common shift factor parameters C_1^0=*18.3,* C_2^0= *79.9,* the experimental master curves are generated. Further, global master curves are generated using $\tau_g = 4.30\times10^{-4}$ and, E_g= *1700 MPa*, χ =*0.176* and common shift factor (or WLF parameters) C_1^0=*18.3,* C_2^0= *79.9*. The global master curves are then compared with experimental master curves and are discussed below. The *Figures 4.27, 4.29, 4.31 & 4.33* show the experimental master curves (symbols) for the Model systems I, II, III & IV. From *Figures 4.27, 4.29* it can be seen that the mastercurves shift towards a lower frequency scale with the increase in amine functionality. Also the rubbery modulus (E_r) and T_g^{DiM} of the Model system I increased with the amine functionality. The shift in master curves, E_r and T_g^{DiM} in the Model system I is controlled by the crosslink density. *Figure 4.31* shows that the master curves of Model system III shifted towards the higher frequency scale from *C2* to *C8*. For the Model system III the E_r remained constant whereas the T_g decreased with the increase in the flexibility from C2 to C8. The master curves (*Figure. 4.33*) of the Model system IV shifted towards higher frequency scale with the increase in the pendant chain length i.e., from *P1* to *P6*. Also in *Figure 4.33* it can be seen that E_r decreased with the crosslink density. The T_g decreased with the increase in the pendant chain length from *P1* to *P6*. Moreover the relaxation time constant (τ_0) increased with the increase in the predicted crosslink density ($\nu_c^{M\&M}$) for the four model systems (*Figure. 4.28, 4.30, 4.32* and *4.34*). The slope χ for Model I, II, IV did not show any systematic trend with respect to the crosslink density ($\nu_c^{M\&M}$). For the Model III the slope decreased with the increase in the $\nu_c^{M\&M}$. From the above discussion it can be understood that by changing the parameters i.e., crosslink density and the flexibility, the relaxation master curves also change. The changes in the relaxation master curves are predicted quite well using global master curves (full

lines) as shown in *Figures 4.27, 4.29, 4.31 & 4.33* and so it can be concluded that the KWW fit function describes the relaxation master curves reasonably well**.**

Model No.	E_r	E_g	τ_0 [s]	τ_g [s]	*X*
A2	10.8	1410	2.52E-03	0.060	0.197
A3	19.8	1690	6.02E+05	0.121	0.229
A4	31.7	1620	1.00E+14	0.119	0.125
E2	2.85	800	2.63E-06	1.98	0.20
E2.5	19	2020	0.0142	0.68	0.149
E3	25	1970	6.45E+03	0.81	0.197
C2	31.7	1620	1.00E+14	0.119	0.125
C4	32.6	1810	7.43E+08	0.071	0.237
C6	31.7	1560	1.51E+05	0.061	0.258
C6	31	1630	8.47E+01	0.081	0.305
P1	19.9	1660	6.09E+05	0.122	0.232
P3	15.6	1950	5.39E-02	0.142	0.328
P6	13	2080	5.78E-05	0.062	0.246

Table.4.2. The parameters E_r, E_g, τ_0, τ_g and χ fitted to the KWW Equation to generate experimental master curves.

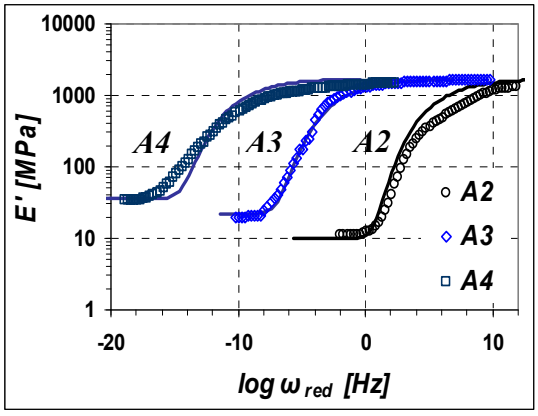

Figure 4.27. The experimental master curves (Symbols) at T_{ref}=100 °C in comparison to the globally fitted master curves (full lines) for Model system I.

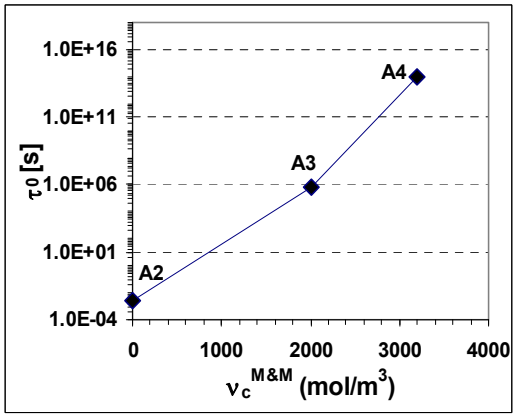

Figure 4.28. The relaxation time constant (τ_0) at T_{ref}=100 °C versus predicted crosslink density (ν_C) for Model system I.

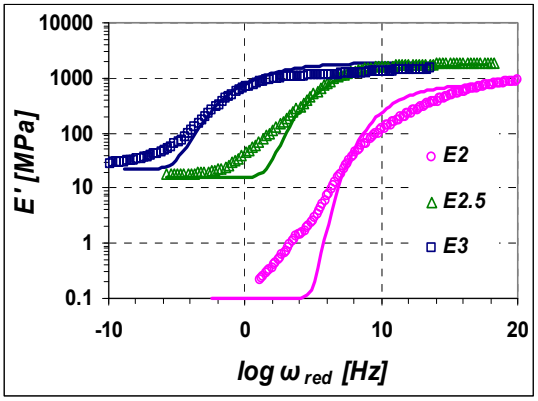

Figure 4.29. The experimental master curves (Symbols) at T_{ref}=100 °C in comparison to the globally fitted master curves (full lines) for Model system II.

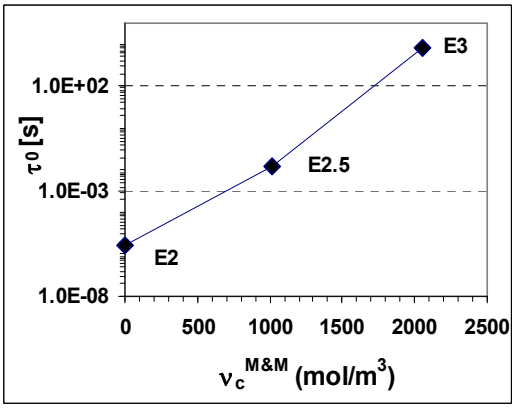

Figure 4.30. The relaxation time constant (τ_0) at T_{ref}=100 °C versus the predicted crosslink density (ν_C) for Model system II.

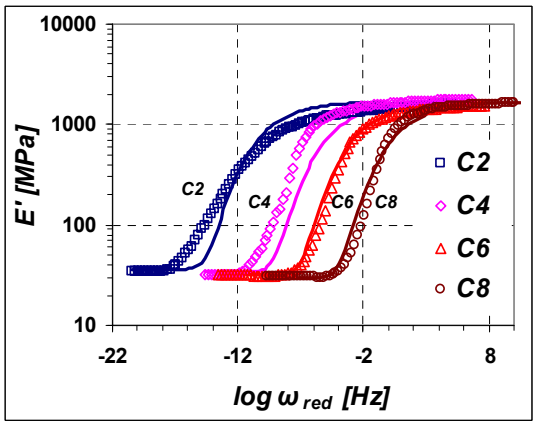

Figure 4.31. The experimental master curves (Symbols) at T_{ref}=100°C in comparison to the globally fitted master curves (full lines) for Model system III.

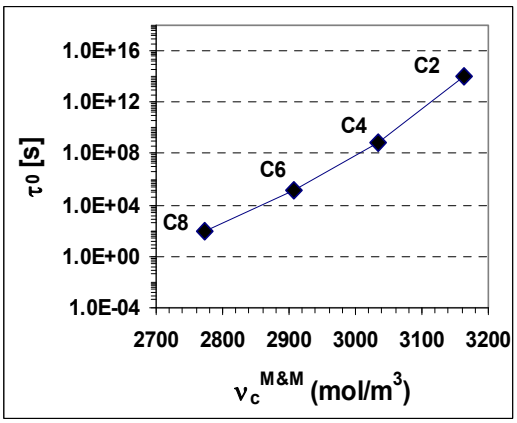

Figure 4.32. The relaxation time constant (τ_0) at T_{ref}=100°C versus the predicted crosslink density (ν_C) for Model system III.

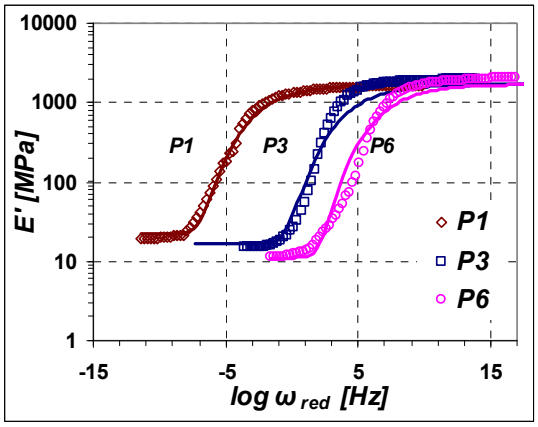

Figure 4.33. The experimental master curves (Symbols) at T_{ref}=100 °C in comparison to the globally fitted master curves (full lines) for Model system IV.

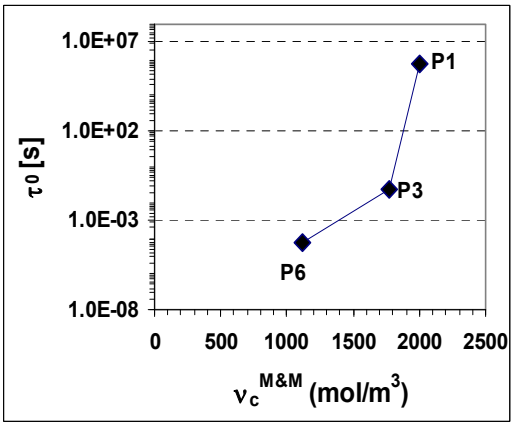

Figure 4.34. The relaxation time constant (τ_0) at T_{ref}=100 °C versus the predicted crosslink density (ν_C) for Model system IV.

4.12. Overall Analysis

For the Model I and Model II systems, the crosslink density controls the T_g as well as the PWHH of the tan δ curve. Also the master curves of the Model systems I & II shifted to the lower frequency scale with increasing crosslink density.

For the Model III system, the increase in the flexible (aliphatic) bonds within a crosslinked network causes a decrease in both the T_g as well as the PWHH of the tan δ curve. This is mainly because the increase in the aliphatic bonds causes a plasticization effect within the network. The process of decreasing the frictional force between the chains in the crosslinked network is called plasticization. It can be concluded that the effect of crosslink density on the PWHH of the tan δ curve decreases with the introduction of flexible bonds. The increase in the flexibility shifted the master curves of the Model system III towards a higher frequency scale.

For the Model IV system, the introduction of flexibility through pendant chains causes a decrease in the T_g due to internal plasticization within the network. Also, the PWHH increases with the increase in the pendant chain length in Model IV system. Also the increase in the flexibility shifted the master curves of the Model system III towards a higher frequency scale.

The glassy modulus (E_g) in all the four model systems is independent of the flexibility and the crosslink density.

The rubbery modulus (E_r) in all the four model systems is independent of the flexibility of the network. Moreover, the rubbery modulus (E_r) is dependent on the crosslink density.

The relaxation time constant (τ_0) increased with the increase in the crosslink density for all the four model systems.

CHAPTER – V

Physical Properties

Chapter 5

Physical properties

5.1. Introduction

The engineering properties of polymers such as *Modulus, T_g, Coefficient of thermal expansion (CTE), Coefficient of moisture absorption (CME)* are often known as physical properties. The physical properties depend on the fundamental properties such as crosslink density, chain flexibility, free volume, polarity etc. The fundamental properties can also be called scaling parameters since the final engineering properties can be scaled with respect to them. Hence exploiting the fundamental properties helps us in understanding and also being able to achieve desired physical properties. Moreover, the *fundamental properties* can be varied by changing the *initial properties* such as functionality, chain length, aromatic nature, mixing ratio and conversion of the resin-hardener mixture. Hence a systematic approach in varying the independent variables gives the chance to understand the changes in the *fundamental properties*. From *Chapter III & IV* it can be understood that the viscoelastic behavior of the hardened epoxy materials changed by the alteration in the *fundamental properties* i.e., crosslink density and flexibility. In this *Chapter* the remaining properties such as *CTE, CME, density* etc. are discussed. A schematic view of the relation between initial properties and final physical properties was shown in *Figure 1.10* introducing the above fundamental properties. The *Figure 1.10* is simplified to *Figure 5.1*.

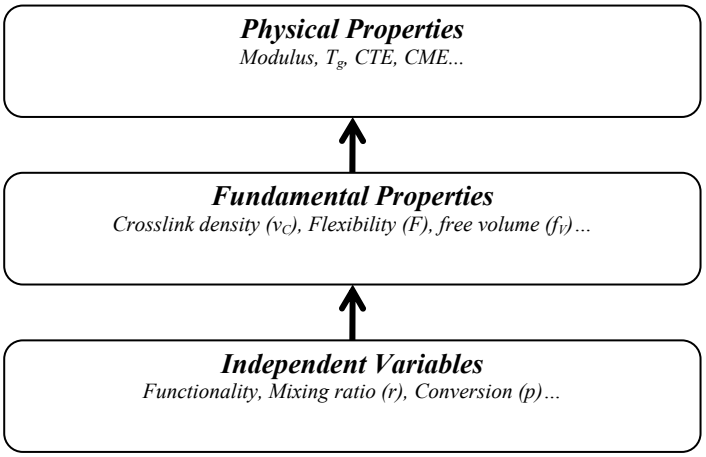

Figure.5.1. Schematic representation of relation between the physical properties, fundamental properties and Independent variables.

5.2. Determination of Fractional free Volume (f_V):

The properties of polymers such as T_g, percentage of moisture absorption (see *Section 5.4.4*), *CTE*, and density depend on the free volume present inside the polymer network [Won et al., 1991]. The *free volume fraction (f_V)* is a fundamental property that controls the mobility of the polymer chains [Gupta et al., 1991]. Free volume is the unoccupied or empty volume present within the network structure. Therefore an increase in the free volume causes an increase in the free space within the network and thereby the mobility of the chain segments increase (i.e., faster relaxation). In addition, the increase in free volume also increases the moisture absorption, saturated moisture content (M_s) and diffusion. In principle, the free volume cannot be directly measured, but several approximate methods exist. Three approximations are discussed in the following Section**.**

5.2.1. f_V below Tg: Empty Volume

The free volume fraction ($f_{V(D)}$) at room temperature can be determined from the measured specific volume, V_M , and the calculated specific empty volume (V_E) using the *Equation 5.1* [Gupta et al., 1991; Gupta and Brahatheeswaran, (1991)]**.**

$$f_{V(D)} = V_E / V_M \qquad \textbf{(5.0)}$$

Here, $V_M = 1/\rho^{Meas}$ and ρ^{Meas} is the measured density. The specific empty volume is the difference between the measured specific volume and the calculated volume occupied by all atoms i.e., specific Van der Waals volume (V_w/M_p)**.**

$$V_E = V_M - \frac{V_W}{M_p} \qquad \textbf{(5.1)}$$

Here, M_p is the molar weight of the structural unit.

The Van der Waals's volume (V_W) in *Equation 5.2* can be calculated using *Equation 5.2*

$$V_W = N_A \sum_i \Delta V_i \qquad \textbf{(5.2)}$$

$$\Delta V_i = \frac{4}{3}\pi R^3 - \sum_i \frac{1}{3}\pi h_i^2 (3R - h_i) \qquad \textbf{(5.3)}$$

$$h_i = R - \frac{R^2 + d_i^2 - R_i^2}{2d_i} \qquad \textbf{(5.4)}$$

where, N_A - Avagadro number (=6.023×10^{23} mol^{-1})

ΔV_i - Incremental volume

$\sum_i \Delta V_i$ - Intrinsic volume

The intrinsic volume represents the total volume increments of the atoms and atomic groups in the crosslinked unit [Slonimskii et.al, 1970]. Here R, R_i, d_i & h_i are the radius, radii of the adjacent valence-bonded atoms, bond length and height of segment respectively**.**

Atom	**R, A^0**	**Atom**	**R, A^0**
C	1.8	N	1.57
H	1.17	O	1.36

Table.5.1. Atomic radii of different atoms.

Bond	**d_i, A^0**	**Bond**	**d_i, A^0**
C-C	1.54;1.48*	C-H	1.08
C=C	1.40	C-O	1.50; 1.36*
C=C	1.34*	C-N	1.37; 1.40*

Table.5.2. Bond lengths of different bonds.

*****The first value is the length of the bond with an aliphatic carbon and the second value is for the aromatic carbon**.**

The atomic radii and bond lengths of atoms used for calculating the volume increments (ΔV_i) are shown in *Tables 5.1 & 5.2*. The calculated Van der Waals volume using *Equation 5.2* for a polymer of simple chemical structure can be shown by the example for polyethylene as shown below. The intrinsic volume ($\sum_i \Delta V_i$) of the repeating unit of polyethylene is made up of two volume increments (ΔV_i) of the CH_2 group:

$$\sum_i \Delta V_i = 2\times17.1 = 34.2 A^{0^3} = 34.2\times10^{-24} cm^3$$

Applying, *Equation 5.2* for calculating the Van der Waals volume for polyethylene results into:

$\Rightarrow 6.023\times10^{23}\times34.2\times10^{-24} = 20.6\ (cm^3/mol)$

Group	***Volume of unit cm^3/mol***	***Group***	***Volume of unit cm^3/mol***
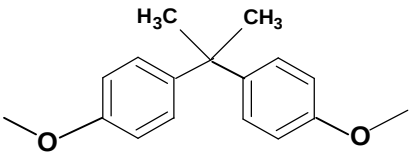	144	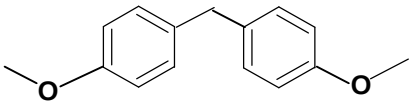	125
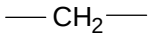	10.3	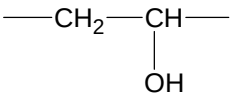	25.1
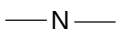	0.54	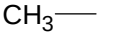	14.15

Table.5.3. Table showing volume values determined using different methods.

The calculated fractional free volume $f_{V(D)}$ for all the model systems are shown in *Table 5.4*. An example of the calculation of the free volume fraction $f_{V(D)}$ for the sample *A4 or C2* is shown below.

Initially the specific volume is calculated by determining the Van der Waals volume. The calculated specific volume is termed as V^{Calc}. Next the measured specific volume (V^{Meas}) is determined from the measured density. The difference between the measured and calculated specific volume is the free volume. The ratio of free volume to the measured specific volume is the free volume fraction ($f_{V(D)}$).

$V_W = 2\times(144+21+50)+1\times(20.6+1.08) = 451.3\ (cm^3/mol)$

Molecular weight of polymer repeating unit: (M)= 2×340.41+1×60=740.8 (g/mol)

ρ^{Calc} = (740.8/451.3) = 1.64 (g/cm^3) $\Rightarrow V^{Calc}=1/\rho^{Calc}=0.609$

ρ^{M} =1.21 (g/cm^3) $\Rightarrow V^{M}=0.826$

$f_{V(D)}=(V^{M}-V^{Calc})/V^{M} = 0.217/0.82= 0.263$

5.2.2. f_V at T_g: Simha Boyer Approach

The fractional free volume can also be calculated using the Simha-Boyer approach [Gupta and Brahatheeswaran, (1991)]. The Simha-Boyer free volume fraction ($f_{V(SB)}$) at T_g is related to the coefficient of thermal expansion and is shown by *Equation 5.5*.

$$f_{V(SB)} = (\alpha_r - \alpha_g)T_g^{Tan\delta} \qquad \textbf{(5.5)}$$

where T_g is in K.

5.2.3. f_V at T_g: WLF Approach

As discussed earlier in *Chapter* IV the WLF parameters (C_1^g & C_2^g) can be determined from the shift factors which are obtained by applying the TTS (Time Temperature Superposition) principle to the modulus data towards the reference temperature (T_g). The WLF parameter C_1^g is related to the f_g (the fractional free volume at T_g), using the following *Equation* [Ferry (1980)].

$$f_{V(WLF)} = \frac{1}{2.303C_1^g} \qquad \textbf{(5.6)}$$

The values of the free volume fraction determined using the WLF parameter C_1^g are shown in *Table 5.4*. From *Table 5.4* it can be seen that the free volume fraction determined using different methods shows a similar trend for all the samples in the four model systems. For the model systems I & II the free volume fraction decreased with the increase in the functionality of amine. Whereas for the model system III, the free volume fraction increased with the increase in chain length from C2 to C8. In the Model IV system the increase in the chain length of the pendant group increases the free volume fraction.

Analysis

The decrease in the free volume fraction with the increase in functionality of amine in model system I and also the increase in the epoxy functionality in model system II is

rather expected. The number of crosslinking points increases with the increase in the functionality of the reacting mixture in model systems I&II and therefore the free volume within the network decreases for model systems I&II. Because the samples in the model system III have equal numbers of crosslinking points with increasing aliphatic methylene units between the crosslinking points, the free volume increases from C2 to C8. Similarly, the increasing pendant chain length from P1 to P6 also increases the free volume in Model system IV**.**

Model System	***Sample Name***	***23 °C***	α_g $[10^{-6}\ k^{-1}]$	α_r $[10^{-6}\ k^{-1}]$	***At T_g***	
		$f_{V(D)}$			$f_{V(SB)}$	$f_{V(WLF)}$
		Eq. *5.2*			***Eq.****5.3*	***Eq.*** *5.4*
I	*A2*	*0.2830*	*62*	*417*	*0.1302*	*0.0334*
	A3	*0.2758*	*65*	*266*	*0.0791*	*0.0161*
	A4	*0.2743*	*72*	*187*	*0.0469*	*0.0150*
II	*E1*	*0.3700*	*20*	*433*	*0.1400*	*0.0395*
	E2.5	*0.3020*	*75*	*380*	*0.1107*	*0.0128*
	E3	*0.2697*	*84*	*251*	*0.0651*	*0.0075*
III	*C2*	*0.2743*	*72*	*187*	*0.0469*	*0.0150*
	C4	*0.2808*	*76*	*199*	*0.0493*	*0.0255*
	C6	*0.2810*	*78*	*217*	*0.0545*	*0.0362*
	C8	*0.2852*	*80*	*230*	*0.0570*	*0.0620*
IV	*P1*	*0.2758*	*65*	*266*	*0.07919*	*0.0161*
	P3	*0.2837*	*61*	*292*	*0.0857*	*0.0289*
	P6	*0.2881*	*32*	*360*	*0.1103*	*0.0434*

Table.5.4. Table showing free volume fraction values determined using different methods and coefficient of thermal expansion in the glassy and rubbery regions (α_g, α_r).

5.3. Polarity

Polarity is a general term for the amount and strength of polar groups in a molecule. The increase in the polarity will increase the internal attraction between the molecular segements (via. hydrogen bridges) and thereby increases the T_g. Furthermore, increasing polarity will increase interaction with external (polar) materials (adhesion)

and increase interaction with water (surface wetting, absorption). A good quantitative measure is needed in this study. It is proposed to take the weight percentage of hydroxyl groups in the cured product as a measure of the polarity. The hydroxyl groups present in the cured product can be calculated using *Equation 5.7*.

For stoichiometric reacting mixtures:

$$n_e E_{fe} + n_a A_{fa} \longrightarrow \text{Cured Product}$$

E_{fe} = *The epoxy reactant containing functionality (f_e)*

A_{fa} = *The amine reactant containing functionality (f_a)*

n_e = *Mols of reacting epoxy group;*

n_a = *Mols of amine group;*

For stiochiometric reacting mixtures: $n_e \times f_e = n_a \times f_a$;

The weight percentage of hydroxyl groups (W_{OH}) in the cure product can now be calculated using *Equation 5.7*.

$$W_{OH} = \frac{M_{OH} n_e f_e p}{M_P} \times 100\% \qquad \textbf{(5.7)}$$

where,

$$M_P = n_e M_E + n_a M_A \qquad \textbf{(5.8)}$$

W_{OH} = *Wt % of hydroxyl group in cured product;*

M_{OH} = *Molecular weight of hydroxyl group (= 17 g/mol);*

M_P = *Total weight of the polymer repeating unit (g/mol);*

p = *Conversion of epoxy groups;*

M_E = *Molecular weight of the reacting epoxy (g/mol);*

M_A = *Molecular weight of the reacting amine (g/mol);*

Note: Equation 5.7 is only applicable to determine the weight percentage of hydroxyl groups present in the cured product for a stoichiometric mixture at different conversion (p) levels.

The values of W_{OH} for other samples are shown in *Table 5.5*. The calculation of W_{OH} for the sample A4 is shown below.

2 moles of DGEBA + 1 mole of EDA react to form a cured product**.**

*n_e=2; n_a=1; f_e=2; f_a=4; p=1; M_P= 2*340+1*60=740*

*Applying Equation 5.9⇒ W_{OH} = (17*2*2*1*100)/740= 9.18 (wt%)*

Model System	***Sample Name***	***$v_C^{M\&M}$ [mol/m^3]***	***W_{OH} wt%***	***D [10^{-12} m^2/s]***	***ρ^{Meas} (g/cm^3)***	***M_S Wt%***	***ε_M wt%***	***CME***
			***Eq.** 5.8*	***Eq.** 5.10*		***Eq.** 5.10*	***Eq.** 5.11*	
I	*A2*	*0*	*7.94*	*9.3*	*1.16*	*2.34*	*1.70*	*0.72*
	A3	*2039*	*8.74*	*6.5*	*1.19*	*1.96*	*2.02*	*1.03*
	A4	*3270*	*9.18*	*4.5*	*1.2*	*2.5*	*3.83*	*1.53*
II	*E1*	*0*	*8.50*	*26*	*1.15*	*3.6*	*2.30*	*0.63*
	E2.5	*1024*	*8.55*	*17*	*1.19*	*4.03*	*3.40*	*0.84*
	E3	*2057*	*8.61*	*10*	*1.20*	*3.365*	*4.50*	*1.33*
III	*C2*	*3270*	*9.18*	*4.5*	*1.2*	*2.50*	*3.83*	*1.53*
	C4	*3097*	*8.85*	*7.6*	*1.185*	*2.62*	*2.93*	*1.11*
	C6	*2966*	*8.54*	*7*	*1.176*	*2.19*	*2.54*	*1.16*
	C8	*2827*	*8.25*	*8.7*	*1.1625*	*1.99*	*2.19*	*1.10*
IV	*P1*	*2039*	*8.74*	*6.5*	*1.19*	*1.95*	*2.02*	*1.03*
	P3	*1767*	*8.25*[#]	*5.8*	*1.18*	*2.08*	*1.52*	*0.73*
	P6	*1115*	*7.48*[#]	*12*	*1.16*	*2.09*	*1.32*	*0.63*

Table.5.5. Table showing the calculated crosslink density ($v_C^{M\&M}$), the hydroxyl concentration (W_{OH}), the diffusion coefficient (D), the density of a dry sample (ρ^{Meas}), the saturated moisture content (M_S), the % moisture expansion (ε_M) and the coefficient of moisture expansion (CME) of the samples in four model systems. Measurement details are discussed in Chapter V.

[#] *Calculated with conversion (p) = 0.99 for P3 and p=0.96 for P6.*

In order to compare the results of the four model systems with the literature values the Dermitzaki (2008) model system is chosen. The experimental results of Dermitzaki are shown in *Table 5.6*. The model system chosen by Dermitzaki is similar to the model system III in our studies. Dermitzaki's model system III contains epoxy resin which has two glydicyl groups attached to a single aromatic ring as shown by *Figure 5.2*. While the epoxy chosen for the model system III (Effect of Chain length) contains two glydicyl groups with a Bisphenol unit. In both cases the aliphatic curing agent selected are identical i.e., *EDA, BMDA, HMDA (n= 2, 4, 6 & n is the number of methylene units)*.

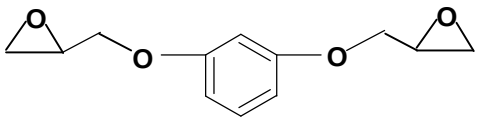

Figure.5.2. 1,3-Bis(2,3-epoxypropyl)-benzene

Material	ρ *(g/cm^3)*	α_g *[10^{-6} K^{-1}]*	α_r *[10^{-6} K^{-1}]*	T_g *[°C]*	$f_{V(SB)}$	M_S	M^{0H} *[WT%]*	*Flexibility [g/mol]*	$\nu_C^{M\&M}$
$C2^D$	1.16	52	174	110	0.0467	4.78	18.88	15.78	6444
$C4^D$	1.14	50	175	98	0.0464	4.8	17.52	16.44	5876
$C6^D$	1.12	55	183	89	0.0463	3.97	16.34	16.81	5384

Table.5.6. The experimental data as well as the calculated data of scaling parameters, flexibility, polarity and crosslink density for Dermitzaki's polymers [Dermitzaki, 2008].

The above data will be included for comparison with our data and will be discussed in the following section**.**

5.4. Results and Analysis

5.4.1. Analysis of the Coefficient of glassy thermal expansion (α_g)

At first we will evaluate if the glassy CTE scales with the crosslink density. Therefore, α_g is plotted against the predicted crosslink density ($\nu_C^{M\&M}$) in *Figure 5.3*.

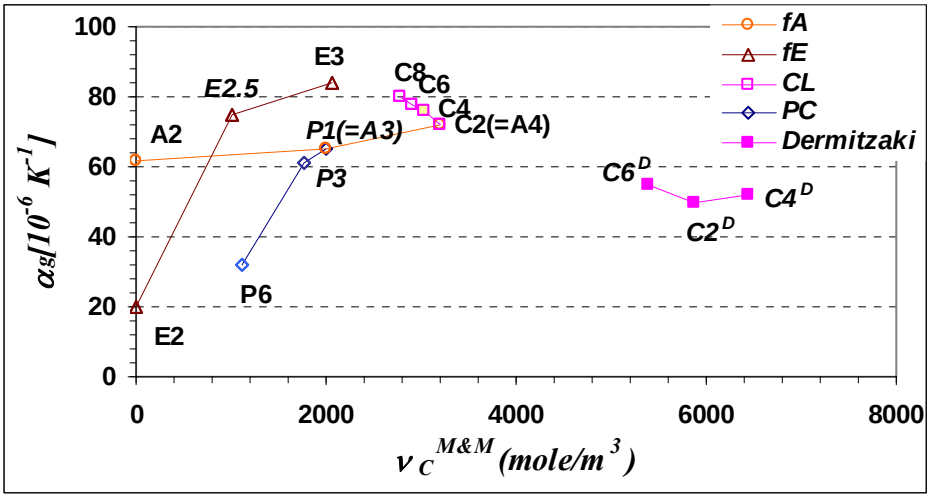

Figure.5.3. Plot of the coefficient of thermal expansion in the glassy region (α_g) versus the calculated crosslink density ($\nu_C^{M\&M}$). The unfilled and filled symbols correspond to the four model systems (f_A, f_E, CL, PC) and the Dermitzaki model system.

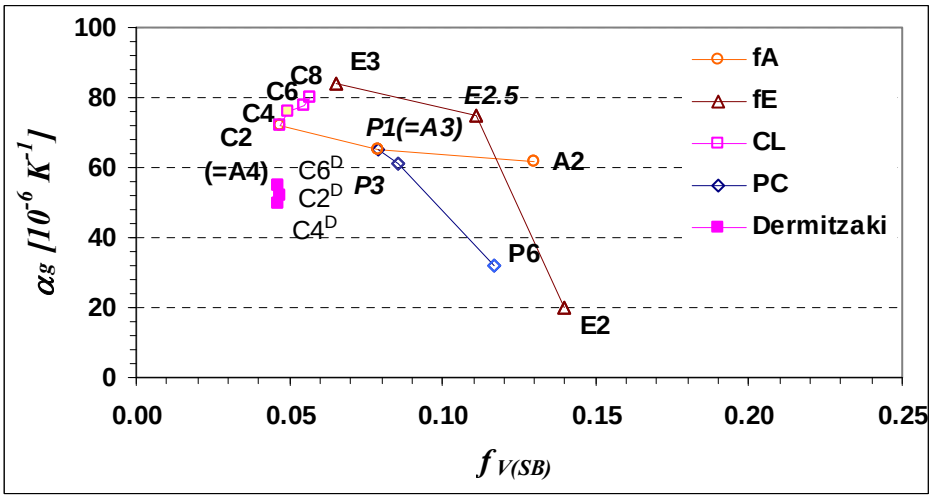

Figure.5.4. Plot of the coefficient of thermal expansion in the glassy region (α_g) versus the free volume fraction ($f_{V(SB)}$). Unfilled and filled symbols correspond to the α_g of the four model systems (f_A, f_E, CL, PC) and Dermitzaki's model system.

The plot of the coefficient of thermal expansion in the glassy region (α_g) versus the calculated crosslink density is shown in *Figure 5.3*. It can be seen that the α_g increases with the increase in the $\nu_C^{M\&M}$ within each model system except for the model III system i.e., the effect of chain length. The increase in the α_g with respect to the crosslink density is also being observed by Ogata (1993) and his coworkers. From *Figure 5.3* it can be observed that the deviation of behavior of α_g of the model III

system, which is shown by square boxes in *Figure 5.3* suggest that α_g depends not only on the crosslink density but also on other parameters. Also from *Figure. 5.3,* it follows that resins E3 and P1 have an identical crosslink density ($\nu_C^{M\&M}$). Therefore it can be concluded that α_g does not scale with the crosslink density. A recapitulation of *Chapter III* and *Chapter IV* indicates that the crosslink density mainly affects properties such as T_g and the rubbery modulus. Studies by Ogata (1993) suggested that the phenomenon of the increase in the α_g can be better understood if α_g is analysed with respect to the free volume.

Figure 5.4 shows the plot of α_g versus the free volume ($f_{V(SB)}$) and it can be seen that α_g decreases with the increase in the free volume fraction for model systems I, II & IV, while α_g increases with increase in free volume fraction ($f_{V(SB)}$) for model system III. In general as the free volume increases in the glassy region it is expected that the molecular chains have more space to move freely and thereby α_g should increase. The expected trend is seen in the model system III (unfilled square boxes in the *Figure 5.4).* The increase in α_g with the increase in the chain length is also observed by Dermitzaki (filled squares in *Figure 5.4)*. The model system III showed an opposite trend compared to the remaining model systems. It is clear that contradictory results are obtained when α_g is analysed either with respect to the crosslink density or the free volume fraction ($f_{V(SB)}$).

From *Figure 5.4* it can be inferred that flexibility (*F*) has probably an effect on α_g. So, α_g is plotted against the flexibility (*F*) as shown by *Figure 5.5*. It can be observed from *Figure 5.5* that with the increasing flexibility the α_g decreases for the model systems I, II &IV. For the model system III the α_g increases with the increase in flexibility and similar trend can be observed for Dermitzaki's model system (shown as filled symbols in *Figure 5.5)*. The deviation behavior of α_g of model system III from the remaining model systems suggest that the introduction of flexibility on the back bone of the crosslinked network increases the thermal expansion in the glassy region. While the introduction of flexibility via pendant chain (*P1, P3, P6*) decreases the thermal expansion in glassy region. Moreover, the higher α_g values for model system III (compared to Dermitzaki's model system) is due to a higher flexibility. From *Figure 5.5* it can be observed that the α_g of different model systems did not scale up with respect to the flexibility (*F*). Therefore from *Figure 5.5* it can be concluded that

the flexibility alone cannot explain the trend in α_g for all the model systems.Therefore a combination of free volume and polarity is tried in the analysis of α_g. *Figure 5.6* shows the plot of α_g versus $W_{OH} * f_{V(SB)}^{2/3}$.

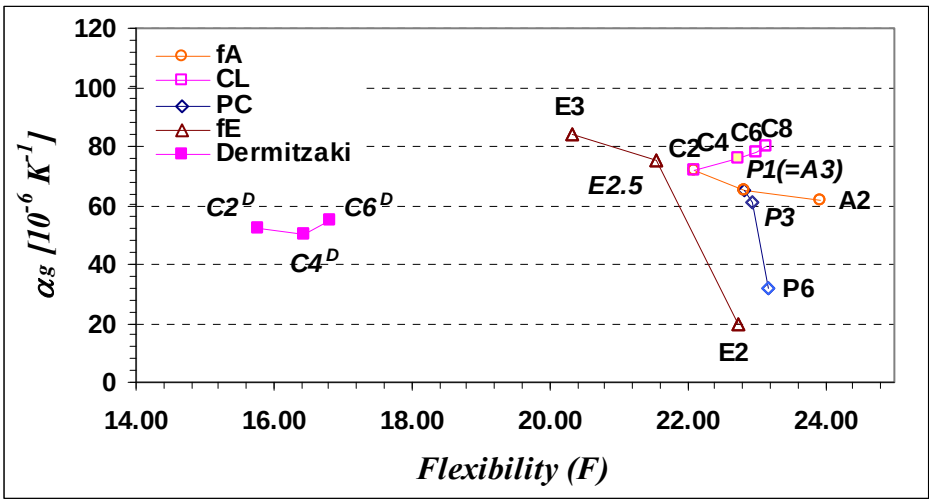

Figure.5.5. Plot of the coefficient of thermal expansion in the glassy region (α_g) versus the Flexibility (F). The open and filled symbols correspond to the α_g values for the four model systems and Dermitzaki's model.

Figure 5.6 shows that the α_g decreases with the increase in the term $W_{OH} * f_{V(SB)}^{2/3}$. The α_g data of the present four model systems and also of Dermitzaki's model scales up with respect to $W_{OH} * f_{V(SB)}^{2/3.}$ Also from *Figure 5.6* it can be clearly observed that the highest value of α_g is shown by the sample *E*3, which belongs to model system II (f_E) and the lowest values are from Dermitzaki's model. Since the model system II contains triphenyl rings i.e., triaromatic and model system I, III, IV (symbols f_A, *CL, PC* in *figure. 5.6*) contain diaromatic and Dermitzaki's system contains mono aromatic ring structures in the network. Therefore it can be concluded that the α_g values depend on the aromatic nature (or aromaticity). The increase in the aromaticity increases the stiffness of the network and hence it can be concluded that

$\alpha_{g(Triaromatic)} > \alpha_{g(diaromatic)} > \alpha_{g(monoaromatic)}$

According to our knowledge this is an interesting result because Ogata and other researchers [Tcharkhtchi et al., 2000] found that with the increase in the crosslink density the α_g increased but they did not have a good explanation for it. They only claimed that α_g is influenced by the chain stiffness and by topological effects. More

importantly they did not find a scaling parameter to understand the changes in the values of α_g.

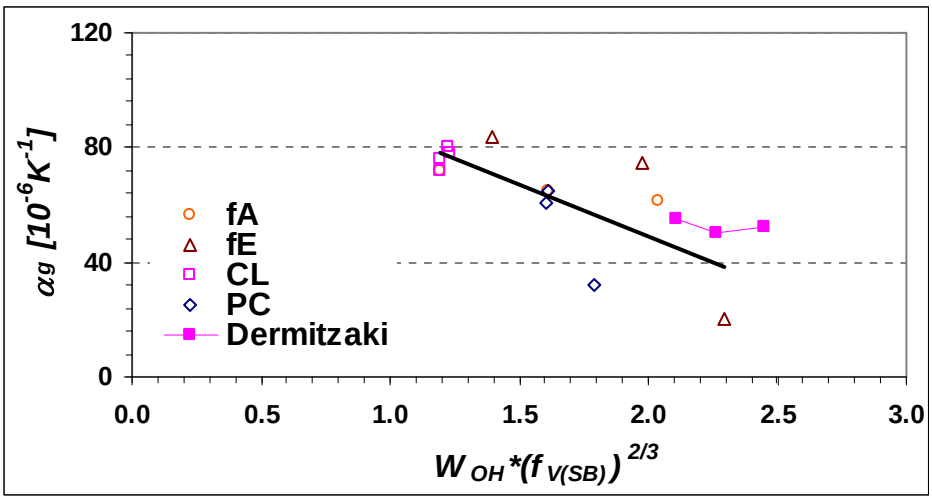

Figure.5.6. Coefficient of thermal expansion in the glassy region (α_g) versus ($W_{OH}*f_{V(SB)}^{2/3}$). Unfilled symbols indicate the experimental values and the thick line indicates their linear fit.

Explanation

The trend $\alpha_{g(Triaromatic)} > \alpha_{g(diaromatic)} > \alpha_{g(monoaromatic)}$ can be explained as follows:

It is well known that an increase in the crosslink density or aromaticity increases the chain stiffness [Nielsen, (1969), Ueberreiter and Kanig, (1950), Tobolsky et al., (1964)]. Therefore it is expected that the increase in the chain stiffness will decrease the expansion and thereby the value of α_g should decrease. It is very important to know that in highly crosslinked systems and also in lowly crosslinked systems containing high aromaticity (aromatic groups) the network structure is under stress due to the bending of the bonds. In the case of crosslinked networks containing aliphatic (flexible) bonds the stress is less. So, when the temperature is increased the release of the stress is more for the highly crosslinked networks in comparison to that of the lowly crosslinked networks. Similarly the stress release in crosslinked networks containing higher aromaticity is more in comparison to low aromaticity. The release of stress with the increase in temperature is seen in the form of a change in the length in the sample during the temperature scan in *TMA*. In otherwords the coefficient of thermal expansion in the glassy region for a highly crosslinked network is more in comparison to a lowly crosslinked network. Also, a network containing aromatic groups will have more thermal expansion in the glassy state in comparison to the

network containing aliphatic groups. Interestingly, the α_g values for the four model systems showed that the effect of aromaticity on α_g is more in comparison to the effect of the crosslink density. Since, it can be observed from *Table 5.5* that the value of the α_g is higher for the sample E3 in comparison to the samples of the remaining model systems (including Dermitzaki's model system). Moreover, the values of α_g in Ogata's (1993) work showed that the network containing a higher aromaticity showed higher α_g values. Whereas lower values of α_g are observed for networks containing aliphatic groups.

If the above explanation is true then the next interesting question would be the anomalous behavior of α_g i.e., increasing values of α_g with a slight decrease in crosslink density for the model system III and also in Dermitzaki's model system (see *Figure 5.3*). In the case of model system III the crosslink density values for all the samples C2, C4, C6, C8 have similar crosslink density values but the free volume fraction ($f_{V(SB)}$) present within the network increases in the order C8> C6> C4> C2 (see *Table 5.4*). The increase in the free volume leads to the increase in the values of α_g. Since, it can be understood logically that the higher the free volume is the more would be the thermal expansion. The above explanation is also valid for Dermitzaki's model system. Also the comparison of the values of α_g of the model system III and Dermitzaki's model system (see *Tables 5.4 & 5.6)* is needed for the better understanding of chemistry on α_g. Since both have a similar network structure but vary in their crosslink densities. It is quite evident that the values of α_g in model system III are relatively higher in comparison to the values of Demitzaki's model system. The higher values of α_g for the model system III is due to higher values of the free volume fraction in comparison to the model system of Dermitzaki. Moreover the higher values of the free volume in the model system III is due to the bisphenol A unit (diaromatic unit) of the epoxy resin whereas the Dermitzaki's model system contains a monoaromatic unit. Also since the crosslink density is relatively high in Dermitzaki's model system, Dermitzaki could not observe much variation in the free volume (see $f_{V(SB)}$ values in *Table 5.6*). In conclusion the contribution of free volume is very important in the model systems containing similar crosslink densities**.**

Ogata's (1993) model systems as well as the Dermitzaki model systems contained crosslink density values which are around and above 5000 mol/m^3. Moreover, Ogata found good scaling of α_g with respect to the crosslink density. Whereas the crosslink

density values of all the samples in the present four model systems are below 3500 mol/m^3. So, in order to scale α_g of networks containing different crosslink densities the polarity and the free volume values are introduced as $M^{OH} * f_{V(SB)}{}^{2/3}$. It can be seen from *Figure. 5.7* that the values of α_g scaled well. The contribution of aromaticity is taken into consideration using the term polarity (M^{OH}). Finally, it can be concluded from *Figure 5.7* that α_g is dependent on the free volume fraction $f_{V(SB)}$, the polarity (M^{OH}) as well as the aromaticity**.**

5.4.2. Rubbery thermal expansion (α_r)

Figure 5.7 shows the plot of coefficient of thermal expansion in the rubbery region *(α_r)* for all the model systems versus the calculated crosslink density ($v_C{}^{M\&M}$). It can be seen in this case that there is a clear relation between the thermal expansion and the crosslink density. The α_r decreases with the increase in the calculated crosslink density. The linear decrease in the thermal expansion in the rubbery region with the increase in crosslink density is also observed by other researchers [*Ogata, 1993 & Dermitzaki, 2008*]. The α_r values of Dermitzaki's model systems are also shown in *Figure 5.7* for comparison with the model system III results**.**

Analysis

The term α_r is a measure of the thermal expansion of the network structure in the rubbery state. From *Chapter III & IV* it is mostly observed that above T_g, the viscoelastic properties are controlled by either the crosslink density or the flexibility. Therefore α_r is analysed initially with respect to the crosslink density.

As already was discussed in *Chapter III,* the increase in the crosslink density increases the number of crosslinking points and therefore the volume of the network structure decreases. The decrease in the network volume hinders the molecular chains from expansion. Hence a network structure which contains a higher crosslink density requires a higher temperature to undergo expansion. In otherwords the increase in crosslink density will decrease the thermal expansion. It can be clearly observed from *Figure 5.7* that Dermitzaki's results showed lower α_r values in comparison to the model system III, due to a higher crosslink density ($v_C{}^{M\&M}$).

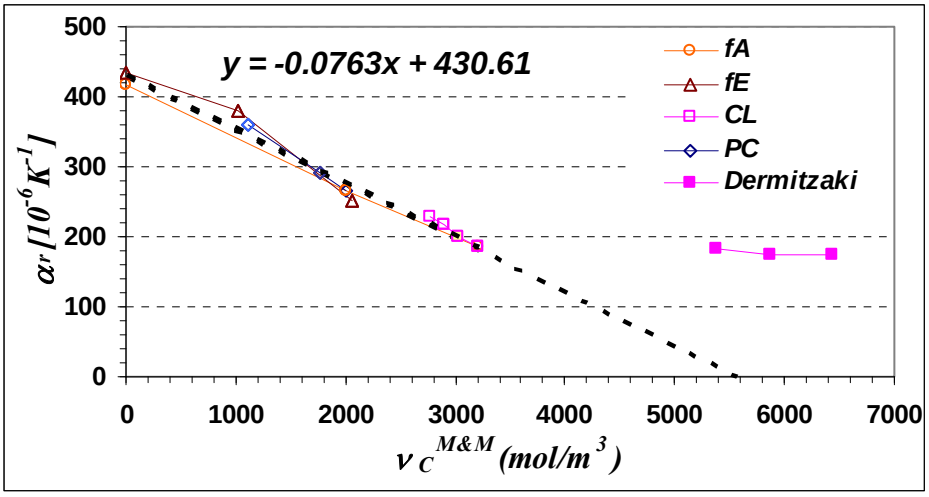

Figure.5.7. Plot of the coefficient of thermal expansion in the rubbery region (α_r) versus the calculated crosslink density ($\nu_C^{M\&M}$). The unfilled and filled symbols are α_r values of the four model systems and Dermitzaki's systems. The dotted straight line indicates the linear fit for the four model systems.

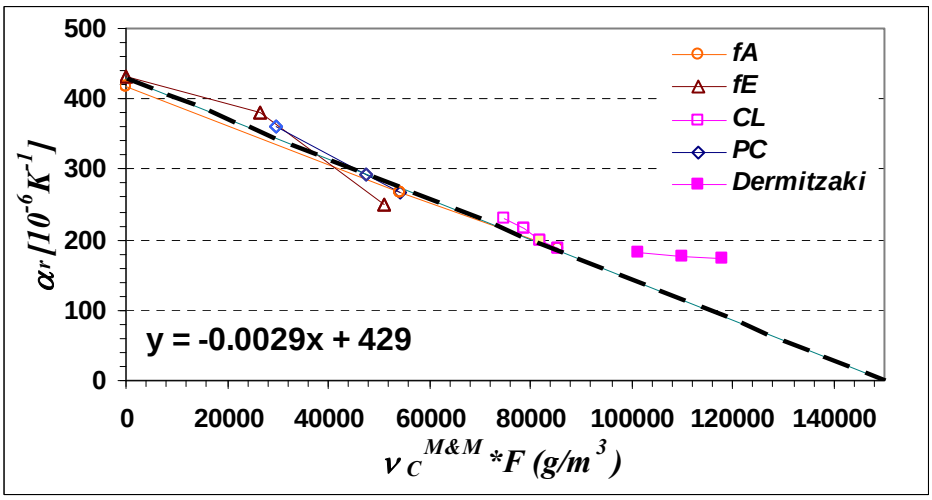

Figure.5.8. Plot of the coefficient of thermal expansion in the rubbery region (α_r) versus the term ($F^*\nu_C^{M\&M}$). The dotted line is the linear fit of α_r.

Note: Alternatively the term ($\nu_C^{M\&M} * f_{V(SB)}$) can also be used to scale α_r.

Also from *Figure 5.7* it can be see that α_r scaled up and also decreased linearly with respect to the crosslink density for all the present four model systems. But, the α_r values determined by Dermitzaki did not scale up with the four model systems. It means that probably the aromaticity (or the flexibility) is also important for the α_r.

So, in order to scale the α_r values of model systems having a varying a crosslink density the flexibility parameter F is used. It can be seen from *Figure 5.8* that the α_r for varying crosslink densities can be scaled up with the term $(\nu_C^{M\&M} * F)$. Moreover from *Figure 5.8* it can be concluded that the flexibility and crosslink density are two scaling parameters which influence the coefficient of thermal expansion $(\alpha_{r)}$ in the rubbery region of the different model systems**.**

5.4.3. Interpretation of density measurements

Figure 5.9 shows a plot of the measured density at room temperature versus the free volume fraction $(f_{V(SB)})$. It can be clearly understood from the *Figure 5.9* that the density decreases with the increase in the fractional free volume $f_{V(SB)}$ for all the samples within each model system**.**

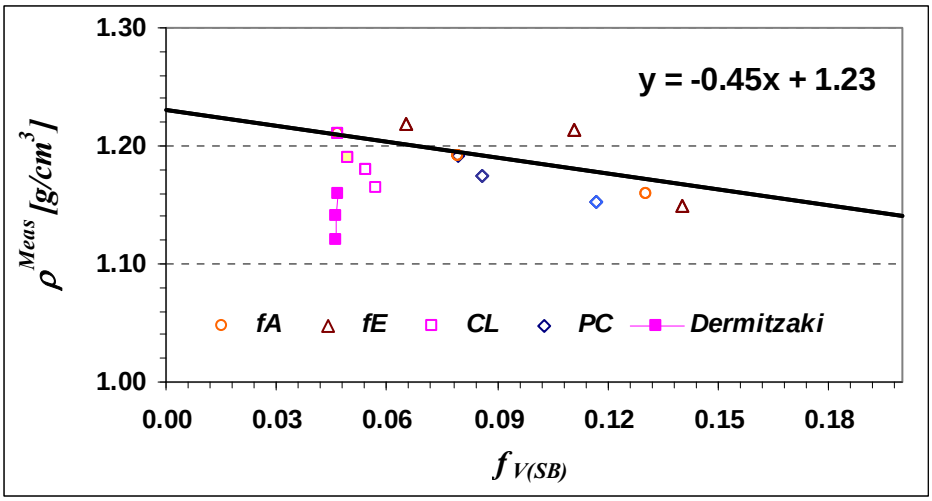

Figure.5.9. Measured density at room temperature versus the free volume fraction determined using the Simha Boyer approach. The open symbols are experimental density values and the full line indicates its linear fit.

The increase in the free volume increases the volume of the network structure and thereby the density decreases. Also from *Figure 5.9* it can be observed that the density of the samples of model systems I, II, III and IV scale up with respect to $(f_{V(SB)})^{2/3}$. Dermitzaki's results are depicted in the *Figure 5.9* for comparision of the present model system density results. The measured density values of Dermitzaki have shown a decreasing trend with increasing chain length (see *Table 5.6)*. The free volume fraction $f_{V(SB)}$ for Dermitzaki's model systems did not show much variation as it can be seen from *Figure 5.9* that the three points align one above the other. The

highest density is observed for C2 and the lowest for C6 in Dermitzaki's result (*see Table 5.6*). Moreover from *Figure 5.9* it can be understood that the measured density results of Dermitzaki did not scale up with the present four model systems with respect to $(f_{V(SB)})^{2/3}$. In order to scale up densities of samples having varying crosslink density the polarity parameter M^{OH} is introduced and is shown in *Figure 5.10*. It can be seen that the measured crosslink density of both the present and Dermitzaki's model system scaled up with respect to $(M^{0H}*f_{V(SB)}{}^{2/3})$. This means that the density of cured epoxies depends on the parameters free volume and polarity.

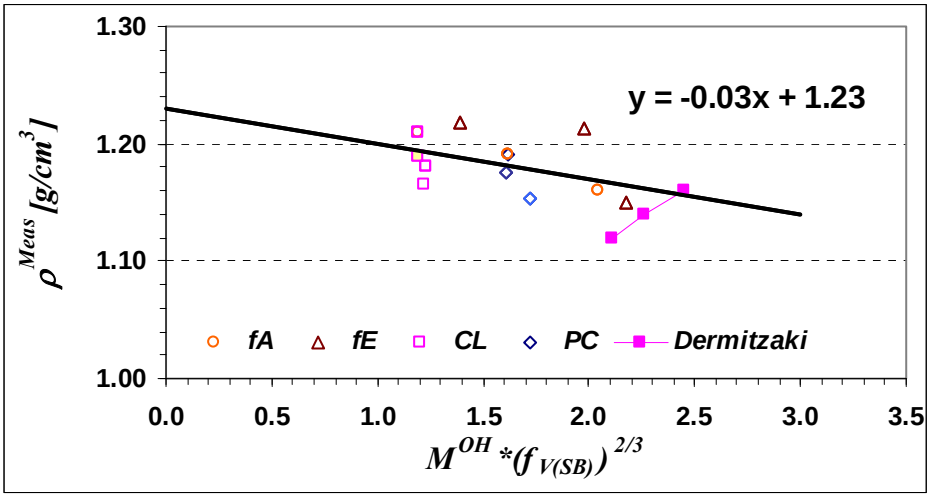

Figure.5.10. Measured density at room temperature versus the term $(W_{OH}*f_{V(SB)}{}^{2/3})$. *The open symbols are experimental density values of the four model systems and filled symbols are of Dermitzaki's system. The full line indicates their linear fit.*

5.4.4. Moisture absorption studies

Epoxies comprise a class of polymeric materials that are widely used in structural applications, such as airframe applications, and also in microelectronics industry as the workhorse encapsulant and as underfill in the mounting of chip assemblies to the printed circuit board. In most applications the epoxy-based component has the potential of being exposed to moisture conditions or a humid environment. It can lead to problems because most epoxies absorb moisture. Absorbed water has deleterious effects on the physical properties of epoxies and can, therefore, greatly compromise the performance of an epoxy-based component. To sufficiently address this problem, the moisture absorption studies are conducted by conditioning the samples in a humidity oven. The moisture absorbed samples are characterized for their viscoelasticity, moisture expansion and the amount of moisture uptake.

Procedure

Initially the samples are pre-conditioned at *150 °C* for 2 hours and then stored in a dessicator containing silica gel such that the samples are free from absorbed moisture. The initial mass of the samples is measured at room temperature and then the samples are conditioned at *85 °C* and *85%* relative humidity for one week. The mass of the samples is measured at regular time intervals to find the amount of moisture absorbed in the sample. The amount of moisture absorbed in the samples of all the model systems is plotted with respect to time. The percentage of moisture in the samples is described by fitting the measured data using a Fickian fit (*Equation 5.10) [Pascault et al., 2002]***.**

$$\frac{M_t}{M_s} = 1 - \sum_{n=0}^{\infty} 1 - \frac{8}{B_n^2} \exp[-B_n^2 \frac{Dt}{h^2}]; \qquad \textbf{(5.9)}$$

$$B_n = (2n+1)\pi$$

where,

M_t - Mass in grams of water absorbed at time t,

M_s - Mass in grams absorbed by the polymeric material at equilibrium

D - Coefficient of diffusivity [10^{-12}m^2/s]

h - Thickness (mm)

t - Time (hours)

For short times $t < \frac{h^2}{D}$ the *Equation 5.9* reduces to *Equation 5.10*.

$$\frac{M_t}{M_s} = \frac{4}{\sqrt{\pi} h} \sqrt{Dt} \qquad \textbf{(5.10)}$$

Equation 5.10 is used to determine the diffusivity (D). The percentage of moisture absorbed in the samples with respect to time for the four model systems *I, II, III & IV* are shown by *Figures 5.11, 5.12, 5.13 & 5.14.* It can be seen that the percentages of moisture absorption for all the samples in the four models systems increase with time. The symbols in the *Figures 5.11, 5.12, 5.13 & 5.14* indicate the experimental results and the thick line indicates its Fickian's fit. It is obvious from the figures that the experimental data is described well using a Fickian fit**.**

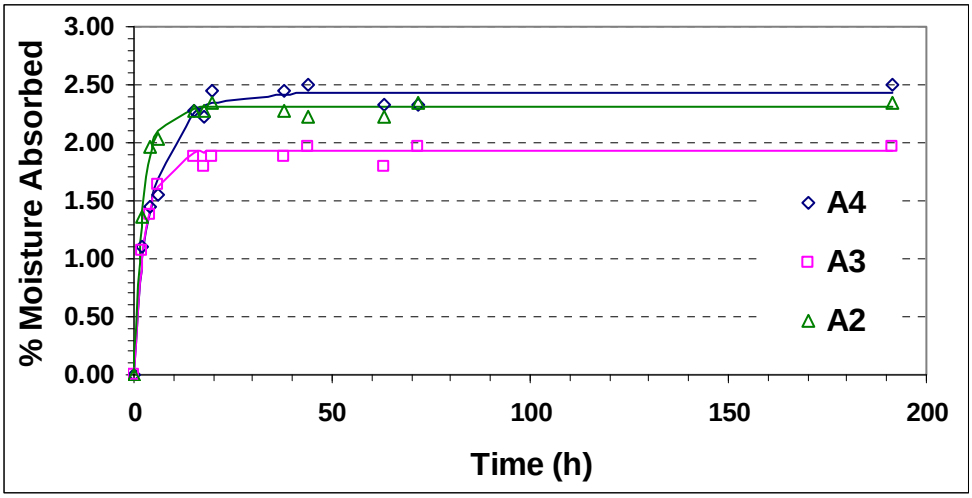

Figure.5.11. % Moisture absorption versus time for the samples in Model I system. Symbols are experimental values and the full lines represent the Fickians fits.

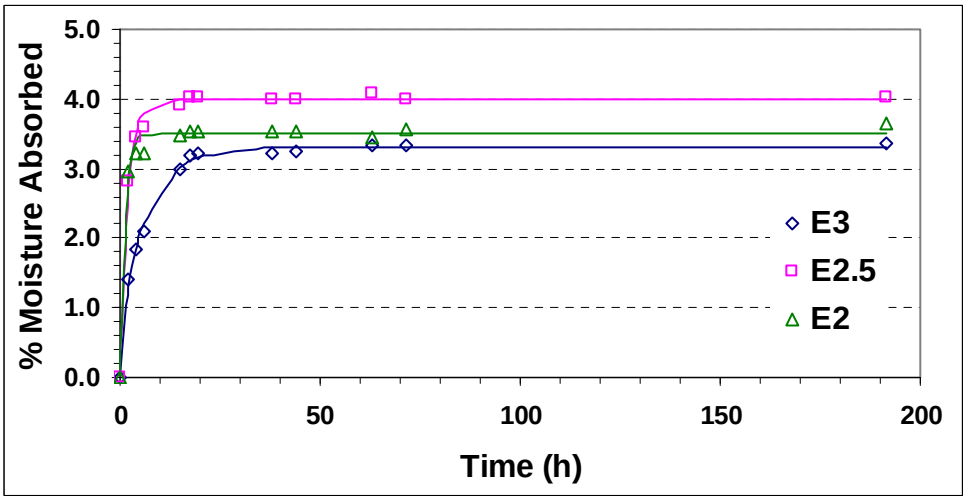

Figure.5.12. % Moisture absorption versus time for the samples in Model II system. Symbols are experimental values and the full lines represent the Fickians fits.

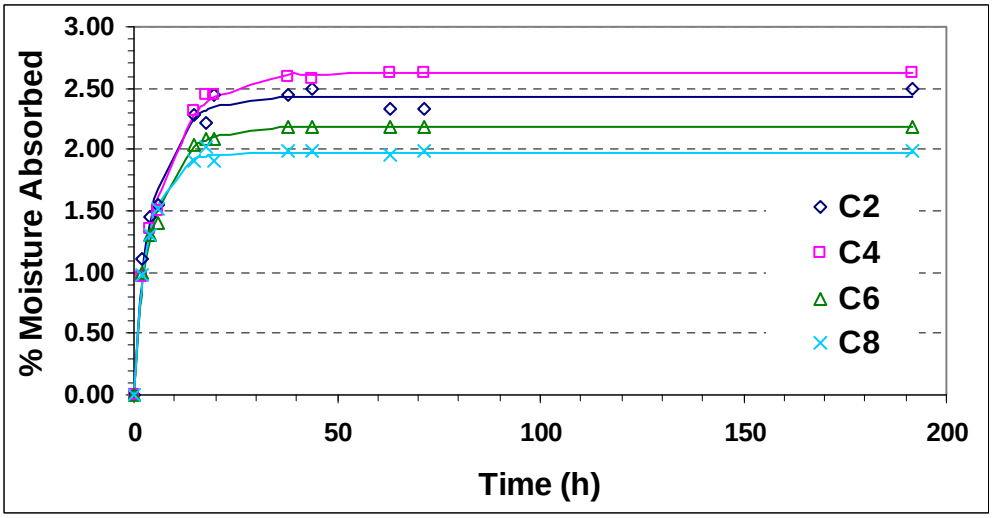

Figure.5.13. % Moisture absorption versus time for the samples in Model III system. Symbols are experimental values and the full lines represent the Fickians fits.

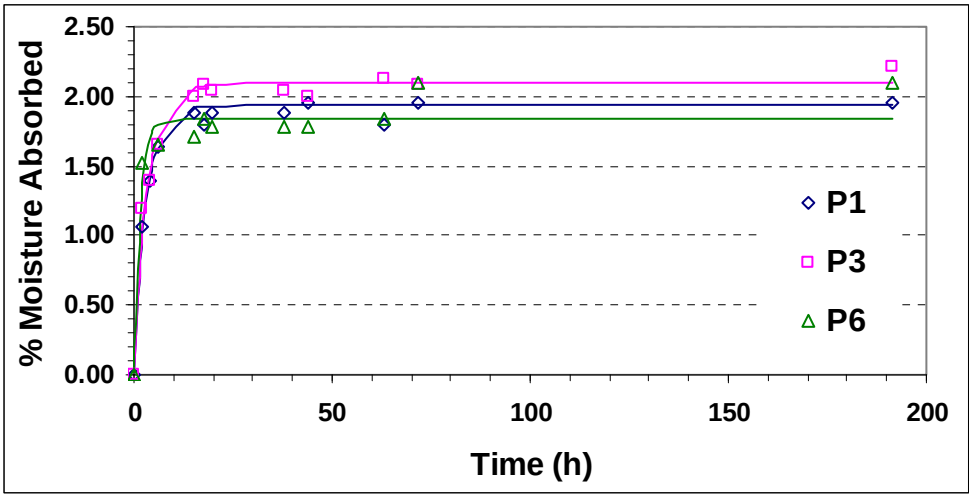

Figure.5.14. % Moisture absorption versus time for the samples in Model III system. Symbols are experimental values and the full lines represent the Fickian fits.

Also from *Figure 5.15a* it can be seen that with the increase in crosslink density the diffusion coefficient *(D)* decreases for all the model systems (including Dermitzaki's). This is expected since the increase in crosslink density will decrease the free volume. Also from *Figure 5.15a* it can be observed that the diffusion coefficient *(D)* data of all the model systems does not scale up with respect to the crosslink density ($\nu_C^{M\&M}$). For example the two linear systems (i.e., *A2* and *E2)* have zero crosslink density and yet widely differ in their diffusion coefficient values**.**

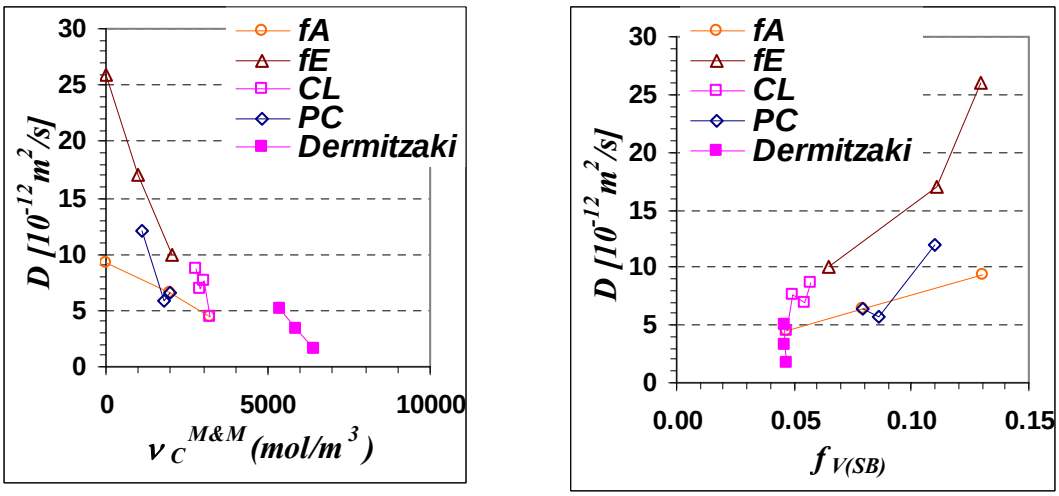

a. *b.*

Figure.5.15. a. Diffusion coefficient (D) versus the crosslink density ($\nu_C^{M\&M}$).
b. Diffusion coefficient (D) versus the free volume fraction ($f_{V(SB)}$).

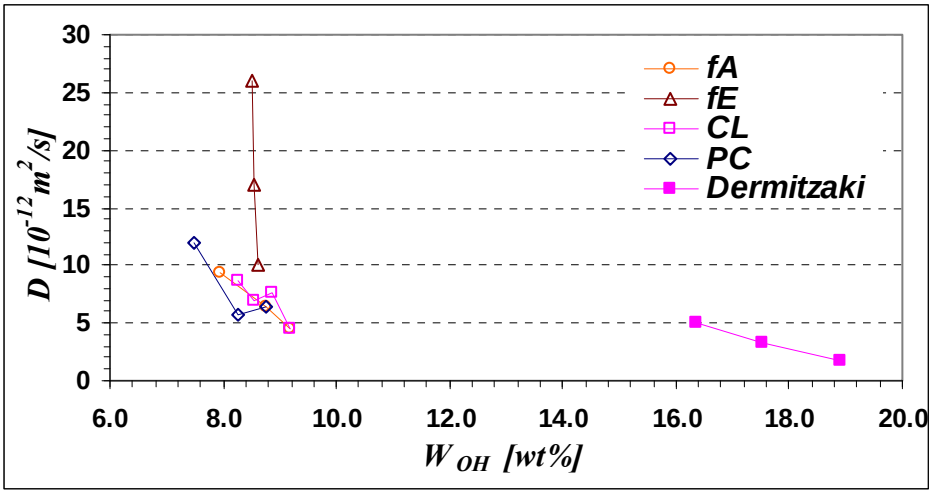

Figure.5.16. Diffusion versus polarity (W_{OH}).

Figure 5.15b shows the plot of the diffusivity versus the free volume fraction ($f_{V(SB)}$). It can be seen that the diffusivity increases with the increase in the free volume fraction. Although the increasing trend in diffusion is already expected, it can be seen from *Figure 5.15b* that the free volume fraction ($f_{V(SB)}$) is a better scaling parameter in comparison to crosslink density. However, the diffusion data of the different model systems do not scale well with respect to free volume fraction ($f_{V(SB)}$) too**.**

But, when the diffusion coefficient (D) is plotted against the polarity (W_{OH}) it is observed that the diffusion coefficient decreases with the increase in W_{OH} although the scatter is still very large. Moreover the diffusion coefficient (D) scales for the four model systems but not for Dermitzaki's model system. The decreasing trend with increasing polarity (W_{OH}) is because in the highly crosslinked system the percentage of hydroxyl groups is larger and therefore more intermolecular hydrogen bonding is present. Due to the intermolecular hydrogen bonding the diffusion of the water molecules into the crosslinked network is difficult for the higher crosslinked systems. And thereby the diffusion coefficient decreases with the increase in the percentage of hydroxyl groups. In conclusion a good overall scaling cannot be determined.

Figure 5.17 shows the maximum moisture absorbed (M_S) by the sample versus the calculated crosslink density. It can be observed that a systematic trend in the M_S is not observed for all the model systems. Model II (f_E) and model IV (PC) shows a decrease in M_S with an increase in crosslink density whereas model system I and III showed an increase in M_S with increasing crosslink density. It is expected that the increase in the crosslink density should decrease the free volume and therefore the percentage of

moisture absorption should decrease as the crosslink density increases. But the expected trend is not observed. This can be explained as follows

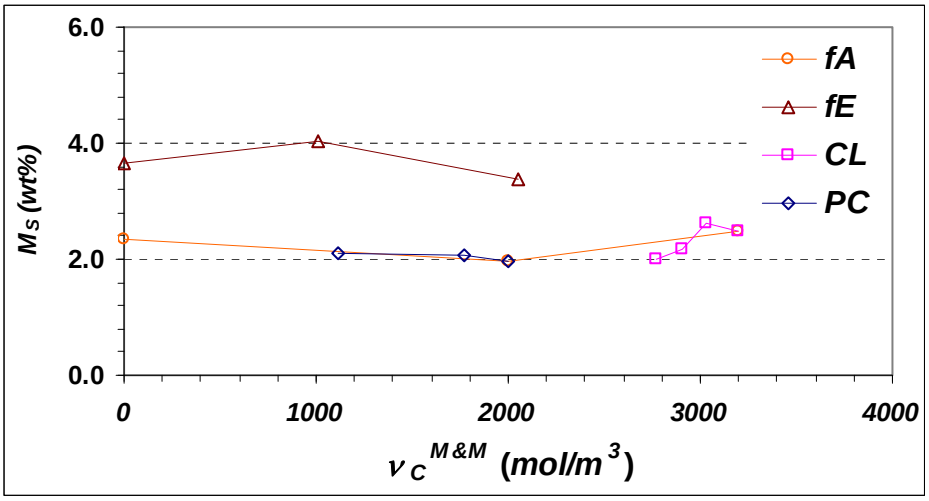

Figure.5.17. The percentage of moisture being absorbed versus the calculated crosslink density.

Explanation

The percentage of moisture absorbed by the polymeric sample depends on the following parameters as shown below

i. The temperature as well as the % RH (percentage relative humidity)
ii. Polymer polarity, determining the polymer-moisture affinity
iii. State (glassy/ rubbery)

The cured epoxy sample consists of both hydrophobic units (e.g., aromatic, methylene) as well as hydrophilic units (hydroxyl, unreacted epoxy). The activation energy needed for the transport processes of water molecules into the cured epoxy resin depends on the temperature. This is because the water molecules have to overcome the energy barriers set up by the interaction potential from intermolecular forces of hydroxyl groups of the cured epoxy resin. Other factors are the unoccupied molecular volume of the epoxy resin and the polymer-water affinity due to the hydrophilic centres (or polarity). This is related to the presence of hydrogen-bonding sites along the polymer chains, which create attractive forces between the polymer and the water molecules.

Although the moisture absorption tests for all the samples are done at constant temperature and humidity, the samples are not always in the same state (i.e., glassy,

rubbery or inbetween). For example, samples like C2 are in the glassy region and for the C8 the testing is in the glass transition region. Therefore a systematic trend in diffusivity and C^{Sat} values cannot be expected. Interestingly, Ogata and others found that in the glassy region the diffusion coefficient and permeability increase. Furthermore, the high value in the polarity of the sample C2 in comparison to other samples in model III support the idea that when the polarity increases the total amount of moisture uptake increases. Also, Dermitzaki found a similar behavior when the moisture absorption test is conducted at *85 °C /85%* relative humidity**.**

5.4.5. Coefficient of Moisture expansion (CME)

The samples which absorb moisture expand. The coefficient of moisture expansion is an important moisture related parameter. In literature not much systematic studies on the relation between the *CME* and the network structure can be found. Here we present a first attempt and calculate the *CME* from the density changes**.**

$$CME = \frac{\varepsilon_M}{M_S} \qquad \textbf{(5.11)}$$

where,

$$\varepsilon_M = \left(\frac{V_M - V_D}{V_D}\right) \times 100\% = \left(\frac{\frac{m_m}{\rho_M} - \frac{m_d}{\rho_D}}{\frac{m_d}{\rho_D}}\right) \times 100\% \qquad \textbf{(5.12)}$$

Note: 100%= 1

ε_M	-	*Percentage of moisture expansion*
M_S	-	*The weight percentage of moisture absorbed in the sample (Table 5.5)*
V_M	-	*The volume of the moisture absorbed sample [cm^3]*
V_D	-	*The volume of the dry sample [cm^3]*
m_m	-	*Weight of the moisture absorbed sample [g]*
m_d	-	*Weight of dry sample [g]*
ρ_M	-	*The density of the moisture absorbed sample (Table 5.5) [g/cm^3]*
ρ_D	-	*The density of the dry sample (Table 5.5) [g/cm^3]*

Initally the *CME* data is plotted against the polarity (W_{OH}). It is found that the *CME* values within each model system increase with the increase in the polarity (W_{OH}) but W_{OH} did not scale the *CME* data quite well. In order to scale the *CME* values of all the samples in the four model systems the free volume fraction determined using Simha Boyer ($f_{V(SB)}$) was included. The plot of *CME* values with respect to (W_{OH} /$f_{V(SB)}$) can be seen from *Figure 5.18.*

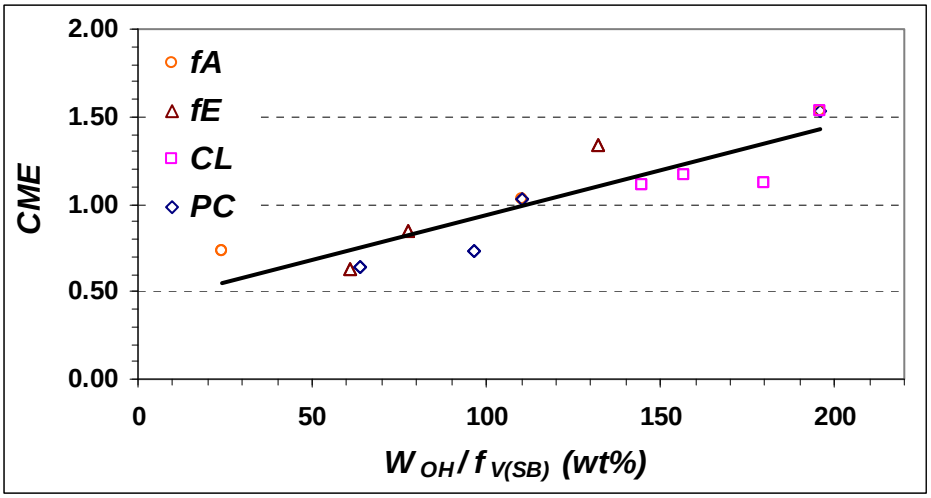

Figure.5.18. Coefficient of moisture expansion versus the ratio ($W_{OH}/f_{V(SB)}$).

It can be seen from *Figure 5.18* that the *CME* values scaled up with respect to (W_{OH} /$f_{V(SB)}$). Hence it can be concluded that the coefficient of moisture expansion depends on both the weight percentage of hydroxyl groups as well as the fractional free volume present in the network structure.

5.5. Effect of absorbed moisture on the viscoelastic behavior

In order to understand the effect of moisture that is absorbed by the sample on its viscoelastic behavior samples from all the model systems that were preconditioned at 85 °C /85 RH for 7 days are characterized for their viscoelastic response in *DMA*. The temperature scan of 1 °C /min is used for the viscoelastic charecterization.

It is known that during the temperature scan the absorbed water will partly evaporate such that the viscoelasticity may change during a measurement. Therefore it can be expected that closeby and above 100 °C the property of wet samples should reduce to the property of the dry ones.

5.5.1. Model I (Effect of Amine functionality)

Initially the moisture absorbed samples that were preconditioned at 85°C /85 RH for 7 days are scanned in *DMA*. The data is shown as unfilled symbols in *Figures 5.19, 5.20 & 5.21*. After that the moisture absorbed sample has undergone a first scan until 175°C the sample is once again scanned. The second scan is the viscoelastic response of the dry sample and is shown by filled symbols in *Figures 5.19, 5.20 & 5.21*.

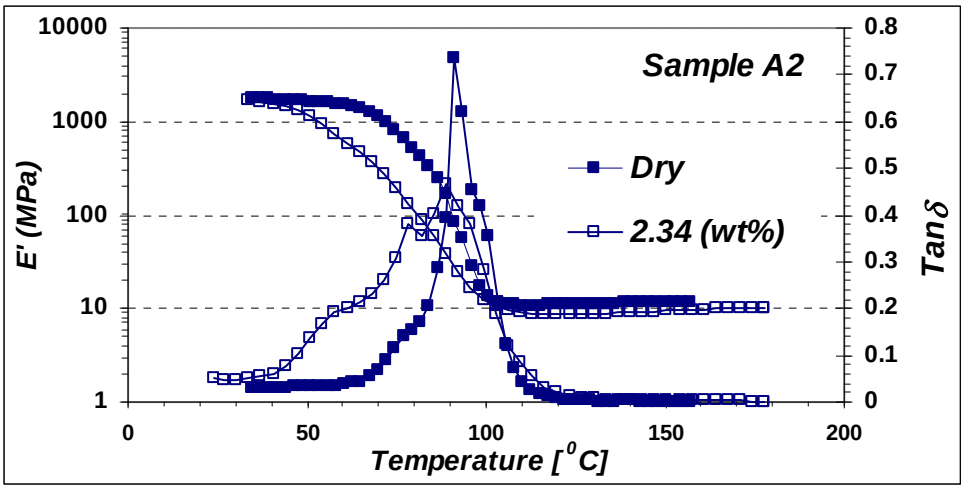

Figure.5.19. 1 Hz data of the storage modulus and tan *δ of the sample (A2). The filled and unfilled symbols correspond to the dry and moisture absorbed samples.*

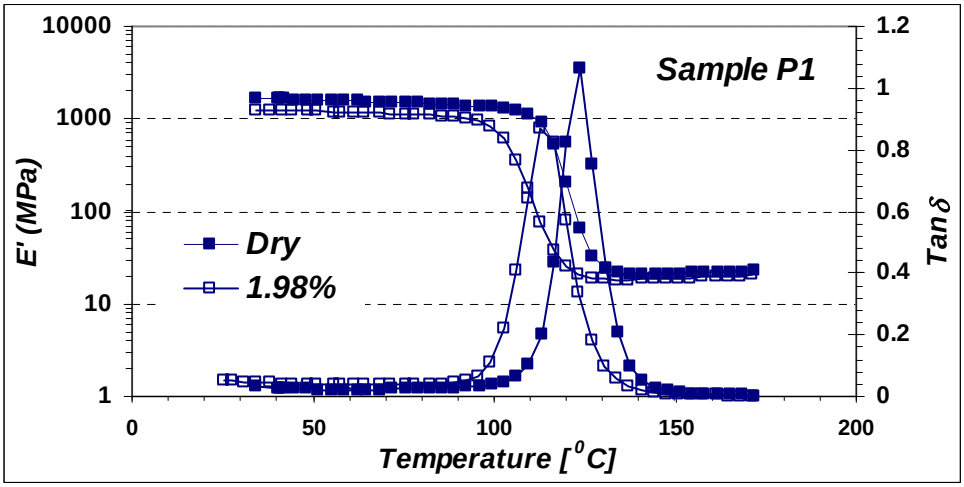

Figure.5.20. 1 Hz data of the storage modulus and tan *δ of the sample P1(=A3). The filled and unfilled symbols correspond to the dry and moisture absorbed samples.*

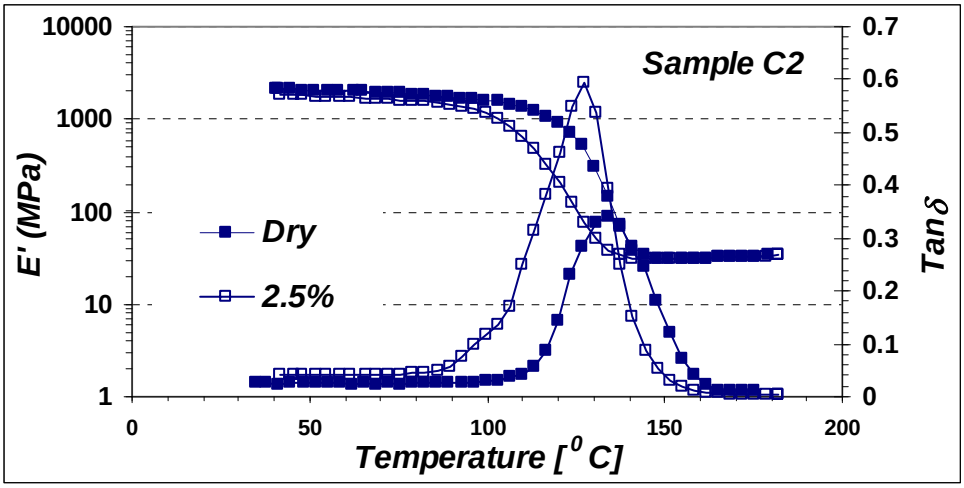

Figure.5.21. 1 Hz data of the storage modulus and tan *δ of the sample A4 (=C2). The filled and unfilled symbols correspond to the dry and moisture absorbed samples.*

The 1 Hz frequency data for the moisture absorbed and the dry sample is analyzed for the viscoelastic response. *Figure 5.19* shows double tan δ peaks at 55 °C and 90 °C for the wet sample of A2. The tan δ peak at 55 °C is probably the T_g of the wet sample of A2 but due the continous evaporation of absorbed moisture in the *DMA* scan the T_g again increases to the T_g of the dry sample (~90 °C) and is therefore seen as second tan δ peak at 90 °C.

Analysis

E_g* and *E_r

The values of the glassy modulus at T_g*-60 °C* and rubbery modulus at T_g*+60 °C* data for the wet as well as the dry samples are shown in the *Table 5.7*. The glassy modulus (E_g) for moisture absorbed (or) wet samples decreased by 2%, 15% and 12% in comparision to the dry sample, for the samples A2, A3, A4. The fact that the rubbery modulus apparently remains constant for both the dry and wet samples of A2, A3 and A4 must be attributed to the evaporation effect: at the temperature of the rubbery state all the absorbed water is evaporated and the dry modulus is retained**.**

Sample Name	M_S *85°C /85 RH*	E_g *(MPa)*		E_r *(MPa)*		T_g *[°C]*		ΔT_g *[°C]*	*PWHH [°C]*		*ΔPWHH [°C]*
		Wet	*Dry*	*Wet*	*Dry*	*Wet*	*Dry*		*Wet*	*Dry*	
A2	*2.34*	*1730*	*1783*	*9*	*11*	*88*	*91*	*3*	*35*	*11.6*	*23.4*
A3 (or) P1	*1.99*	*1520*	*1808*	*20*	*22*	*112.9*	*123.5*	*10.6*	*16*	*15*	*1*
A4 (or) C2	*2.50*	*1668*	*1898*	*34*	*34*	*127*	*134*	*7*	*27*	*29*	*-2*

Table.5.7. DMA data of moisture absorbed (wet) and dry samples of Model system I.

ΔT_g – *The difference in T_g between dry and moisture absorbed samples*

ΔPWHH – *The difference in PWHH between dry and wet samples*

Tan δ

Considering *Figures 5.19, 5.20 & 5.21,* three distinct changes can be observed between the tan δ peak of 1 Hz data for the dry and the moisture absorbed samples

a) The temperature at the peak maximum of the 1 Hz tan δ curve (ie., T_g) is lower for moisture absorbed samples in comparison to the dry samples.
b) The height of the tan δ curve is lower for moisture absorbed samples in comparison to dry samples (except for sample A4).
c) Also the width of the tan δ peak at half height (PWHH) for the moisture absorbed samples is more in comparison to that of the dry samples.

The ΔT_g *(*difference in the T_g between the moisture absorbed and dry samples) increases from A2 to A3 and decreases from A3 to A4. The difference in the tan δ peak width between the moisture absorbed and dry samples i.e., ΔPWHH shows a decrease from A2 to A4.

Note: The peak broadening due to the evaporation may shift the T_g towards the dry value (overestimate T_g^{wet}). Hence, for better results the *DMA* experiments should be performed at higher heat rate or even better under a controlled humidity**.**

Explanation:

The hydrogen bonds between the water molecules and the polar hydroxyl groups of the network will disrupt the interchain hydrogen bonding. The chains will therefore start to slide at lower temperature which is observed as a reduction in T_g [Moy and Karasz, 1980]. The distinct features that are observed in the tan δ curve between the moisture absorbed and dry samples which are discussed earlier indicate that a plasticization effect is seen and the effect of plasticization depends on the percentage of moisture absorbed**.**

Plasticization

The viscoelastic response of the moisture absorbed samples shows a decrease in the glass transition temperature (T_g) and an increase in the width of the tan δ peak in comparison to dry samples is often referred to as a plasticizing effect of water on the polymer [Lee, 1993]. Moreover the peak width at half height (ΔPWHH) does not show much effect with respect to the percentage of moisture absorbed (M_S) for the samples A3 and A4 (see *Table 5.7*). This is due to evaporation; the apparent peak broadening is possible as discussed earlier. Also the height of the tan δ curve for the sample A4 is higher for moisture absorbed samples in comparison to the dry samples. The comparison of height of the tan δ curve would lead to erroneous results since during the *DMA* scan there is a possibility that the data points at the max peak height of the tan δ curve could be omitted (i.e., not recorded). Hence the PWHH is chosen for the comparison of the results of different samples**.**

5.5.2. Model III (Effect of Chain length):

The effect of absorbed moisture in the samples for model III on the viscoelasticity is shown by *Figures 5.22, 5.23, 5.24 & 5.25*. It can be observed from *Figures 5.22 to 5.25* that the T_g of the wet samples (shown by unfilled symbols) is always lower than the T_g of dry samples (filled symbols**).**

E_g and E_r

From *Figures 5.22 to 5.25* and *Table 5.8* it can be seen that there is a decrease in glassy modulus of 12%, 7%, 13%, and 11% respectively for moisture absorbed samples in comparison to the dry samples. The rubbery modulus i.e., E_r appears to remain constant for both the dry and the moisture absorbed samples due to the evaporation of water as discussed earlier**.**

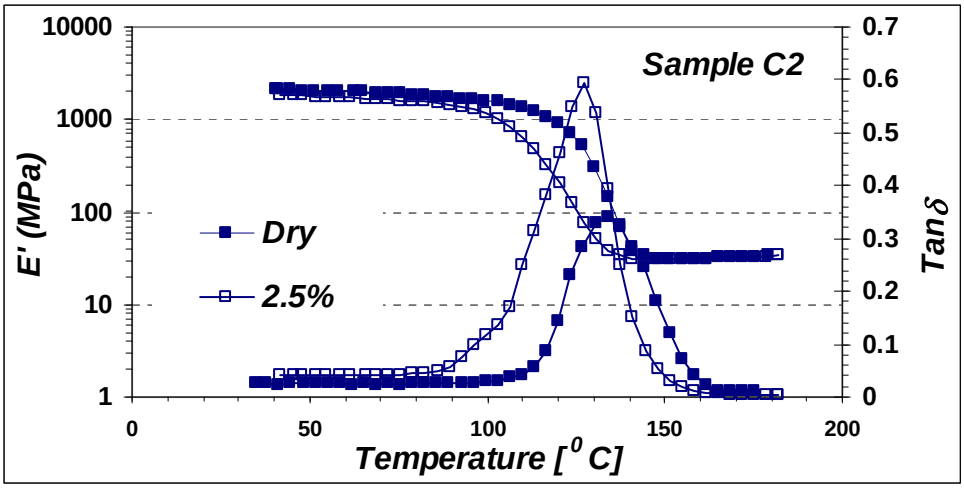

Figure.5.22. 1 Hz data of the storage modulus and tan *δ for the sample C2. The filled and unfilled symbols correspond to the dry and moisture absorbed samples.*

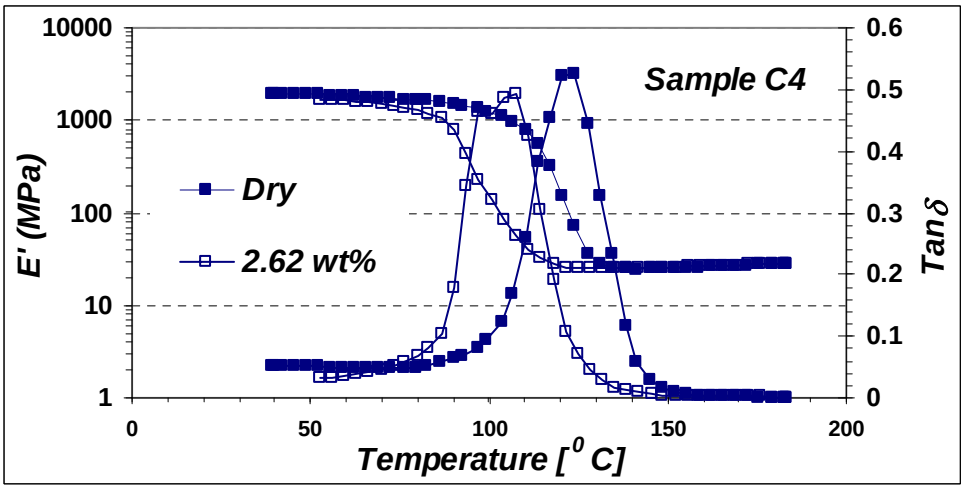

Figure.5.23. 1 Hz data of the storage modulus and tan *δ for the sample C4. The filled and unfilled symbols correspond to the dry and moisture absorbed samples.*

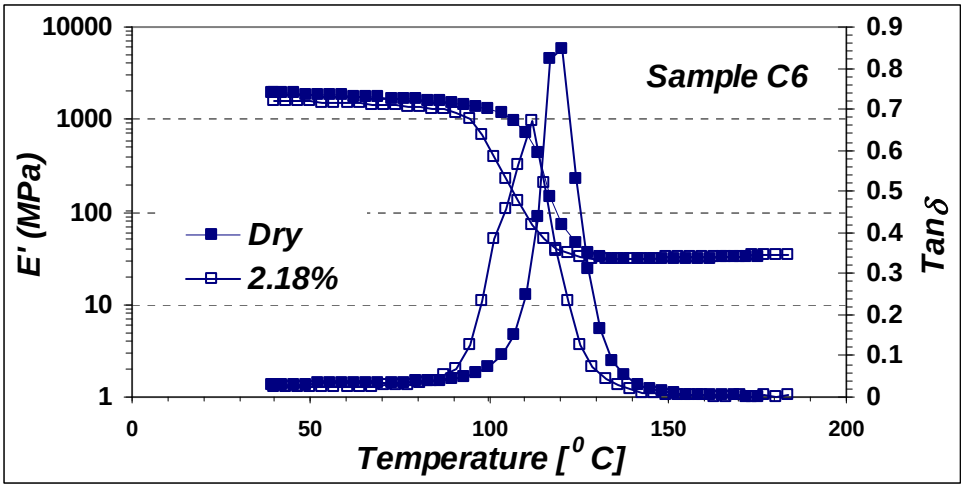

Figure.5.24. 1 Hz data of the storage modulus and tan *δ for the sample C6. The filled and unfilled symbols correspond to the dry and moisture absorbed samples.*

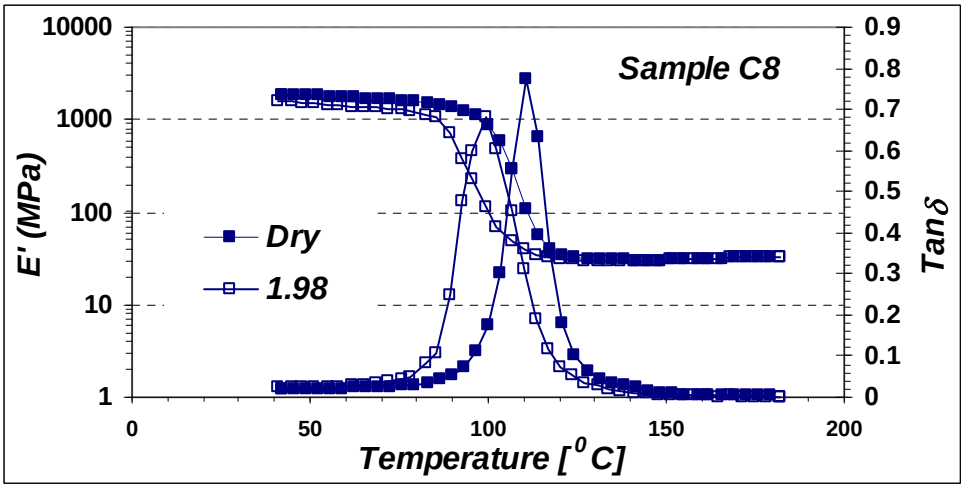

Figure.5.25. 1 Hz data of the storage modulus and tan *δ for the sample C8. The filled and unfilled symbols correspond to the dry and moisture absorbed samples.*

Sample Name	***M_S 85°C / 85%RH***	***E_g (MPa)***		***E_r (MPa)***		***$T_g^{\tan\delta}$ [°C]***		***ΔT_g [°C]***	***PWHH [°C]***		***ΔPWHH [°C]***
		Wet	***Dry***	***Wet***	***Dry***	***Wet***	***Dry***		***Wet***	***Dry***	
C2	*2.50*	*1668*	*1898*	*34*	*34*	*127*	*134*	*7*	*27*	*29*	*-2*
C4	*2.62*	*1753*	*1891*	*27*	*27*	*107*	*124*	*17*	*26*	*16.5*	*9.5*
C6	*2.18*	*1540*	*1770*	*34*	*34*	*112*	*121*	*9*	*20*	*14*	*6*
C8	*1.98*	*1592*	*1789*	*31*	*32*	*100*	*110*	*10*	*20*	*15*	*5*

Table.5.8. DMA data of moisture absorbed and dry samples of Model system III.

Tan δ

Three distinct changes between the tan δ peak of 1 Hz data for the dry and moisture absorbed samples can be observed for all the *Figures* from *5.22 to 5.25*. The temperature at the peak maximum of the tan δ curve is lower for moisture absorbed samples in comparison to the dry samples (except for sample C2). The height of the tan δ curve is lower for moisture absorbed samples in comparison to the dry samples. Also the width of the tan δ peak is more for the moisture absorbed sample in comparison to the dry sample.

It can be observed from *Figure 5.22* to *Figure 5.25* that a plasticization effect is apparently present and the amount of plasticization depends on the amount of the moisture absorbed by the samples. Moreover, the sample *C4* has the highest percentage of moisture absorption out of all the samples in model III. Therefore the sample *C4* has the highest plasticization effect which is seen by the maximum of ΔT_g and $\Delta PWHH$ in *Table 5.8*.

5.5.3. Model IV (Effect of pendant chain)

The effect of absorbed moisture in the samples for the model IV on the viscoelasticity is shown by *Figures 5.26 & 5.27*.

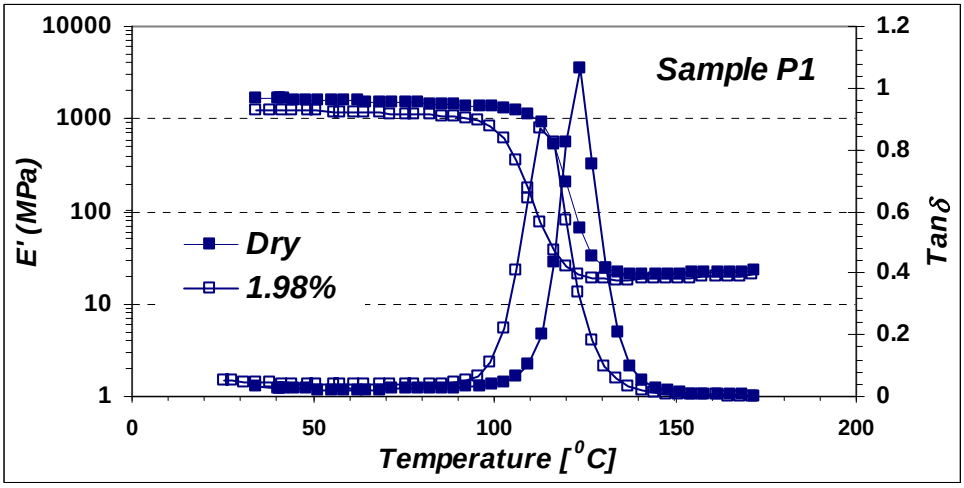

Figure.5.26. 1 Hz data of the storage modulus and tan δ *for the sample P1. The filled and unfilled symbols correspond to the dry and moisture absorbed samples.*

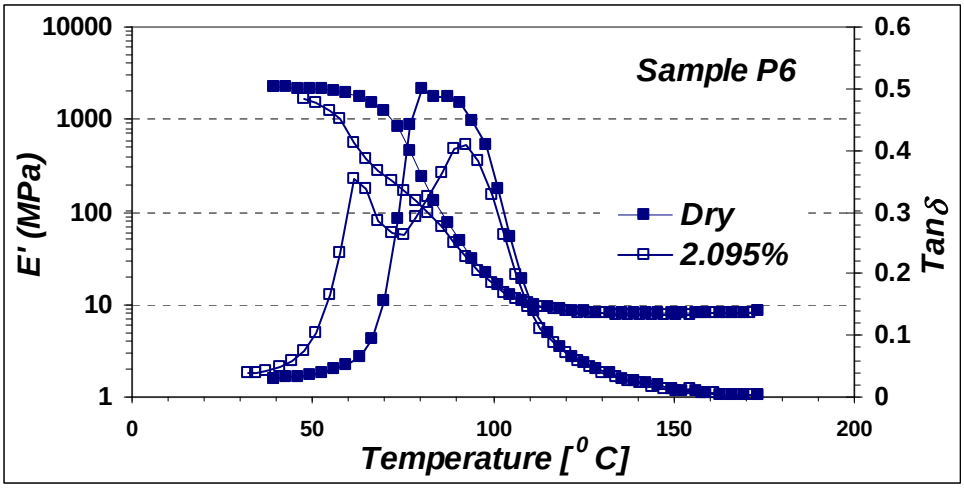

Figure.5.27. 1 Hz data of the storage modulus and tan *δ for the sample P6. The filled and unfilled symbols correspond to the dry and moisture absorbed samples.*

Sample Name	***M_S***	***E_g (MPa)***		***E_r (MPa)***		***$T_g^{\tan\delta}$ [°C]***		***ΔT_g***	***PWHH [°C]***		***Δ PWHH [°C]***
	85 °C / 85%RH	***Wet***	***Dry***	***Wet***	***Dry***	***Wet***	***Dry***	***[°C]***	***Wet***	***Dry***	
P1	*1.98*	*1520*	*1808*	*20*	*22*	*113*	*123.5*	*10.6*	*17*	*14*	*3*
P6	*2.09*	*2070*	*2303*	*8*	*8.5*	*61* *91*	*82*	*21*	*52*	*37*	*15*

Table.5.9. DMA data of moisture absorbed and dry samples of Model system IV.

E_g and E_r

From *Figure 5.26 & 5.27* it can be seen that there is a decrease of 15% and 10% in the glassy modulus for the *P1* and the *P6* sample respectively. The rubbery modulus i.e., E_r remained constant for both the dry and moisture absorbed sample**.**

Tan *δ*

It can be observed from *Figures 5.26 to 5.27* that a plasticization effect is observed and the amount of plasticization depends on the amount of moisture absorbed by the sample. The sample *P1* shows a lower plasticizing effect in comparison to the *P6* sample. In the *P6* sample, only 96% of epoxy groups have reacted and hence due to the incomplete reaction in *P6* the numbers of crosslinking points are reduced. The epoxy groups in sample *P1* are fully reacted and so the number of crosslinking points is more in comparison to *P6*. The decrease in the number of crosslinking points will

therefore increase the free volume and the percentage of moisture absorbed in *P6* is larger in comparison to sample *P1*. Therefore the higher percentage of moisture absorbed by the sample *P6* shows a larger plasticizing effect in comparison to the sample *P1*.

Also the tan δ peak from *Figures 5.26* for the moisture absorbed sample of *P6* two tan δ peaks can be observed. The first peak is observed at around *60 °C* and the second peak at *100 °C*. This is mainly because during a temperature scan first the wet T_g of 60 °C is detected (1st peak). Due to continous evaporation the T_g again increases to the dry value (~100 °C) which is detected as a 2nd peak. The 2nd peak is thus an apparent effect and will not be observed if the evaporation is prevented. Note that in other cases where the T_g's are closer, the evaporation effect will result in an apparent peak broadening. This may have occurred in *Figure 5.27***.**

5.6. Overall analysis

a. The coefficient of thermal expansion in the glassy region (α_g) is dependent on the free volume, the polarity and the aromaticity of the network structure
b. The coefficient of thermal expansion in the rubbery region (α_g) scales with the crosslink density. Moreover the inclusion of a flexibility parameter can be used to understand cases of varying crosslink densities
c. The density of the cured polymeric sample depends on the free volume of the network. Polarity scales with the density of samples having varying crosslink densities
d. The diffusion coefficient (D) depends on the free volume and the polarity of the network structure. The flexibility parameter scales with the diffusion coefficient of cured samples having a varying crosslink density.
e. The coefficient of moisture expansion *(CME)* increased with the increase in polarity (W_{OH}). The ratio $(W_{OH} / f_{V(SB)})$ scales with the *CME* of cured samples having a varying crosslink density.
f. Effects of moisture on the glassy modulus (E_g) and the width at half height of the damping (tan δ) curve is observed for the cured sample.
g. The effect of moisture on the rubbery modulus (E_r) could not be observed due to the evaporation effects.

h. The relaxation behavior is dependent on the crosslinking density of the cured resin.
i. Cured resins having a higher crosslink density have a transition region at a lower frequency or at a longer time, so that the relaxation occurs over a wide time scale
j. A higher crosslink density is characterized by smaller relaxation strength (difference in elastic modulus between glassy and rubbery states).
k. The flexibility (aliphatic nature) plays an important role in controlling the engineering properties such as the coefficient of thermal expansion in the glassy state and near the glass transition region.
l. The coefficient of linear thermal expansion in the glassy state (α_g) is dependent on the ratio ($f_{V(D)} / F$)
m. α_g is independent of the crosslink density
n. As the crosslink density increases in the cured resins, T_g rises, the relaxation time is lengthened, and the coefficient of linear thermal expansion becomes smaller in the rubbery region.
o. As the crosslink density increases in the cured resins, the coefficient of thermal expansion in the glassy region, the water absorption, the diffusion coefficient, and the permeability become larger
p. The physical properties of polymers are dependent on the independent variables via fundamental properties
q. Usually when the concentration of epoxy groups is equal to or lower than the concentration of NH groups, side reactions like homopolymerisation do not take place.

CHAPTER – VI

Conclusions

Chapter 6

Conclusions

6.1. Introduction

The aim of this research work is to understand the effect of varying the *compositional properties* of reacting mixtures (epoxy and amine) on the *physical properties* of their cured epoxy-amine product. Therefore, four model systems are selected with varying *compositional properties*. The *physical properties* are measured and the relations between *compositional properties* and *physical properties* are investigated.

In the four model systems discussed below the epoxies and amines are reacted stoichiometrically.

6.2. Model system I (Effect of Aliphatic Amine functionality)

A two functional epoxy ($f_E = 2$) was reacted with aliphatic amines of functionality $f_A = 2$ to $f_A = 4$. With increasing amine functionality:

Network properties

- The calculated crosslink density ($v_C^{M\&M}$) increased from 1104 mol/m^3 to 3270 mol/m^3 [see *table 3.3*].
- 4% decrease in the flexibility (F) [see *table 3.3*].
- 64% decrease in the free volume fraction ($f_{v(SB)}$) [see *table 5.4*].
- 15% increase in the polarity (W_{OH}) [see *table 3.5*].

Physical properties

- The E_g remains constant (~1800 *MPa*).
- The E_r increased from 9 *MPa* to 34 *MPa*
- $T_g^{\tan\delta}$ increased from 93 °*C* to 135 °*C* [see *table 3.2*].
- The peak width at half height *(PWHH)* of the tan δ curve for the dry samples increased by 17 °*C* [see *table 5.7*].
- The relaxation time constant (τ_0) increased from 2.5×10^{-3} [s] to 10^{14} [s] [see *table 4.2*].
- 16% increase in the α_g and 55% decrease in the α_r [see *table 5.4*].
- The density (ρ^{Meas}) increased from 1.16 g/cm^3 to 1.20 g/cm^3 [see *table 5.*5].

- The coefficient of moisture expansion (*CME*) increased from 0.72 to 1.53 [see *table 5*.5].

6.3. Model system II (Effect of Aromatic Epoxy functionality)

Mixtures of f_E= 2 and f_E= 3 functional aromatic epoxies were reacted with a 2 functional amine (f_A= *2*). With the increasing average epoxy functionality:

Network properties

- $v_C^{M\&M}$ increased from 0 mol/m^3 to 2194 mol/m^3.
- ~10% decrease in the flexibility
- 53% decrease in the free volume fraction
- 1 % increase in the polarity

Physical properties

- The E_g remains constant (~1800 *MPa*).
- The E_r increased from 0 *MPa* to 25 *MPa*
- $T_g^{\tan\delta}$ increased from 64 °*C* to 117 °*C*.
- Systematic trends are not observed in the *PWHH* of the tan δ curve.
- The relaxation time constant (τ_0) increased 2.6×10^{-6} [s] to $6.45\times10^{+3}$ [s].
- The α_g increased from 20×10^{-6} K^{-1} to 84×10^{-6} K^{-1} whereas α_r decreased from 433×10^{-6} K^{-1} to 251×10^{-6} K^{-1}.
- The density (ρ^{Meas}) increased from 1.15 g/cm^3 to 1.20 g/cm^3.
- The *CME* increased from 0.63 to 1.33.

6.4. Model system III (Effect of Chain Flexibility)

A two functional epoxy was reacted with 4 functional aliphatic amines. With increasing aliphatic chain length of the amine:

Network properties

- Slight decrease in the $v_C^{M\&M}$ i.e., from 3270 mol/m^3 to 2827 mol/m^3.
- 5% increase in the flexibility.
- 21% increase in the free volume fraction.
- 10% decrease in the polarity.

Physical properties

- The E_g remains constant (~1800 *MPa*).
- The E_r decreased from 35 *MPa* to 29 *MPa*.

- $T_g^{\tan\delta}$ decreased from 135 °*C* to 108 °*C*.
- ~15 °*C* decrease in the *PWHH (see table 5.8)*.
- The relaxation time constant (τ_0) decreased form 10^{14} [s] to 84 [s].
- 11% increase in the α_g increased and 22% increase in the α_r.
- The density (ρ^{Meas}) decreased from 1.20 g/cm^3 to 1.162 g/cm^3.
- The *CME* decreased from 1.53 to 1.10.

6.5. Model system IV (Effect of Pendant Chain length)

A two functional epoxy was reacted with 4 functional aliphatic amines. With increasing aliphatic pendant chain length of the amine:

Network properties

- The $v_C^{M\&M}$ decreased from 2039 to 1095 mol/m^3.
- ~ 40% increase in the flexibility.
- ~ 40% increase in the free volume fraction.
- ~ 15% decrease in the polarity.

Physical properties

- The E_g remains constant (~1800 *MPa*).
- The E_r decreased from 20 *MPa* to 10 *MPa*.
- The $T_g^{\tan\delta}$ decreased by 39 °*C i.e.*, from 121 to 82 °*C*.
- The *PWHH* of the tan δ curve increased by 12 °*C*.
- The relaxation time constant (τ_0) decreased from $6.0\times10^{+5}$ [s] to 5.7×10^{-5} [s].
- 50% decrease in the α_g and 35% increase in the α_r.
- The density (ρ^{Meas}) decreased from 1.19 g/cm^3 to 1.16 g/cm^3.
- The *CME* decreased from 1.03 to 0.63.

6.6. Modeling of the physical properties

The modeling of the T_g for all the samples of the four model systems is done using DiMarzio's model (see *Figure 3.24).* The prediction of the viscoelasticity for all the samples is done using KWW-fit function (see *Figures 4.27, 4.29, 4.31* and *4.33*). It was possible to scale the *physical properties* using the network properties (see *Chapter V*). The modeling of the kinetics of the moisture absorbed in the cured epoxy samples for the four model systems is done using a Fickian fit function (see *Figures*

5.11 to 5.14). The effect of moisture on the viscoelastic behavior of the 100% cured epoxy samples was studied (see *Chapter V*).

Note: All the values shown below are the % maximum increase or % minimum decrease in the different physical properties due to moisture.

For the model system I:

- ~15% decrease in the E_g [see *table 5.7*].
- ~18% decrease in E_r.
- ~11 °*C* decrease in ΔT_g.
- ~24 °*C* increase in $\Delta PWHH$.

For the model system III:

- ~12% decrease in the E_g [see *table 5.7*].
- E_r remained constant.
- ~17 °*C* decrease in ΔT_g.
- ~10 °*C* increase in $\Delta PWHH$.

For the model system IV:

- ~15% decrease in the E_g [see *table 5.7*].
- E_r remained constant.
- ~21 °*C* decrease in ΔT_g.
- ~15 °*C* increase in $\Delta PWHH$.

References:

Aharoni, S.M., 1998, “Increased glass transition temperature in motionally constrained semicrystalline polymers”, Polymers for Advanced technologies, Vol. 9, pp: 169-201.

Babayevsky, P.G. and Gilham, J.K., 1973, “Dynamic mechanical analysis of epoxy/aromatic reactions”, Journal of Applied Polymer Science, Vol. 17, pp: 2067.

Banks, L. and Ellis, B., 1982, “The glass transition temperatures of highly crosslinked networks: Cured epoxy resins”, Polymer, Vol. 23, pp: 1466.

Bakker, C.J.de., John, N.A,St., and George, G.A., “Simultaneous differential scanning calorimetry and near-infrared analysis of the curing of tetraglycidyldiaminodiphenylmethane with diaminodiphenylsuphone”, Polymer, Vol. 34, pp: 716-724.

Barbeau, P., Gerard, J.F., Magny, B., Pascault, J.P., Vigier, G, 1999, “Morphological analysis of photocured polyurethane acrylate networks. Correlation with viscoelastic properties”, J.Polym.Sci.B, Vol. 37, pp: 919-937.

Baselga, J., Prolongo, S.G., Mikes, F., Cabanelas, J.C., 2003, “Diffusion control on the cure kinetics of DGEBA with ethylenediamines”, Journal of Materials Processing Technology, 143-144, pp: 546-550.

Bauchière, D., Halary, J.L., Monnerie, L. and Schirrer, R., 2000, “Relationships between thermally induced residual stresses and architecture of epoxy-amine model networks”, Journal of Applied Polymer. Science, Vol. 75, pp: 638-650.

Bell, J.P., 1970, “Mechanical properties of a glassy epoxide polymer. Effect of molecular weight between crosslinks”, Journal of Applied Polymer Science, Vol. 14, pp: 1901-1906.

Bellenger, V., Verdu, J., Francillette, J., Hoarau, P. and Morel, E., 1987, “Infrared study of hydrogen bonding in amine-crosslinked epoxies”, Polymer, Vol. 28, pp: 1079-1086.

Bellenger, V., Verdu, J., Morel, E., 1987, “Effect of structure on glass transition temperature of amine crosslinked epoxies”, Journal of polymer science: Part B: Polymer Physics, Vol. 25, pp: 1219-1234.

Bershtein, V.A., Yegorov, V.M., 1985, “General mechanism of the β transition in polymers”, Polymer science USSR, Vol. 27, 2743-2757.

Bershtein, V.A., Yergorov, V.M., Yemel’yanov, Yu, A., 1985, “Relations between

the main relaxation transitions in polymers and the length of segments and the character and degree of cooperation in molecular motion in the vicinity of T_g", Polymer science USSR, Vol. 27, 2575-2764.

Bicerano, J., 2002, Prediction of polymer properties, 3rd edition, New York: Dekker, pp: 369.

Bidstrup, S.A., and Macosko, C.W., 1990, "Chemorheology relations for epoxy-amine crosslinking", Journal of polymer science Part B Polymer physics, Vol, 28, pp: 691-709.

Billaud, C., Vandeuren, M., Legras, R., and Carlier, V., 2002, "Quantitative analysis of epoxy resin cure reaction: A study by Near-infrared spectroscopy", Applied Spectroscopy, Vol. 56 , pp:1413-1421.

Billmeyer, F.W., 1984, Textbook of Polymer Science, 3rd edition, New York: Wiley-Interscience.

Boyer, R.F., 1963, Rubber Chem.Tech. Vol. 28, pp: 1303.

Catalani, A., and Bonicelli, M.G., 2005, "Kinetics of the curing reaction of diglycidyl ether of bisphenol A with a modified polyamine", Themochimica Acta, 438, pp: 126-129.

Charlesworth, J.M., 1988, "Effect of crosslink density on the molecular relaxations in diepoxide-diamine network polymers, Part1. The glassy region", Polymer Engineering and Science, Vol. 28, pp: 221.

Chompff, A. J. and Newman, S., 1971, Polymer Networks: Structure and Mechanical Properties; ACS symposium on highly cross-linked polymer networks, Chicago, New York: Plenum, p.145

Cook, W.D., 1978, "An analysis of the effect of crosslinking on the T_g of polyester and other networks", European Polymer Journal, Vol. 14, pp: 715.

Couchman, P.R. 1984, "Composition–dependent glass transition: Relations between temperature, pressure and composition", Polymer Engineering and Science, Vol. 24, pp: 135-143.

Cukierman, S., Halary, J.L and Monnerie, L., 1991, "Dynamic mechanical response of model epoxy networks in the glassy state", Polymer Engineering and Science, Vol. 31, pp: 1476-1482.

Cukierman, S., Halary, J.L., Monnerie, L., 1991, "Molecular analysis of the viscoelastic properties of epoxy networks as deduced from the study of model systems", Journal of Non-crystalline Solids, Vol. 131-133, pp: 898-905.

Curro, J.G., Pearson, D.S., Helfand, E., 1985, "Viscoelaticity of randomly cross-linked polymer networks. Relaxation of dangling chains", Macromolecules, Vol. 18, pp: 1157-1162.

Crawford, E. and Lesser, A.J., 1997, "The role of Network Architecture on the Glass Transition Temperature of Epoxy Resins", Journal of Applied Polymer Science, 66, pp: 387-395.

Crawford, E. and Lesser, A.J., 1998, "The Effect of Network Architecture on the Thermal and Mechanical Behavior of Epoxy Resins"", Journal of Polymer Science: Part B: Polymer Physics, Vol. 36, 1371-1382.

DiBenedetto, A.T., 1987, "Prediction of the glass transition temperature of polymers: A model based on the principle of corresponding states", Journal of Polymer Science: Part B: Polymer Physics, Vol. 25, pp: 1949-1969.

DiMarzio, E.A., 1964, Journal of Research of the National Institute of Standards and Technology, 68A, pp: 611.

Drum, M.F., Dodge, C.W.H and Nielsen, L.E., 1956, "Industrial and Engineering Chemistry Research, Vol. 48, pp: 76.

Ellis, B., 1993, Chemistry and Technology of Epoxy Resins, Ellis, B. ed., Chapman and Hall, Bury St Edmunds.

Fedderly, J.J., Lee, G.F., Lee, J.D., *Hartmann*, B., 2000, "Network structure dependence of volume and glass transition temperature", Journal of Rheology", Vol. 44, 4, pp: 961- 972.

Flory, P.J, 1953, Principles of Polymer Chemistry, Cornell University Press, Ithaca, NY, pp: 347

Flory, J.P., 1979, "Molecular theory of rubber elasticity", Polymer, Vol. 20, pp: 1317-1320.

Fox, T.G., and Flory, P.J., 1950, "Second-order transition temperature and related properties of polystyrene", Journal of applied physics, Vol. 21, pp. 581-591.

Fox, T.G. and Loshaek, S., 1955, "Influence of molecular weight and degree of crosslinking on the specific volume and glass transition temperature of polymers", Journal of Polymer Science, Vol. 15, pp: 371.

Galy, J., 1985, Thése d'Etat, Université Claude Bernard, Lyon.

Galy, J., Sabra, A and Pascault, J.P., 1986, "Characterization of epoxy thermosetting systems by differential scanning calorimetry", Polymer Engineering and Science. Vol. 26, pp: 1514-1523.

Gérard, J.F., Galy, J., Pascault, J.P., Cukierman, S. and Halary, J.L., 1991, "Viscoelastic response of model epoxy networks in the glass transition region", Polymer Engineering and Science, Vol. 31, pp: 615.

George, G. A., Cole-Clarke, P.A., St. John, N. A. and Friend, G., 1991, "Real time monitoring of the cure reaction of a TGDDM/DDS epoxy resin using fiber optic FT-IR", Journal of Applied Polymer Science, Vol. 42, pp: 643-657

Gibbs, J.H. and DiMarzio, E.A., 1958, "Nature of the glass transition and the glassy state", The Journal of Chemical physics, Vol. 28, pp: 373-383.

Gonis, J., Simon, G.P. and Cook, W.G., 1997, "Cure properties of epoxies with varying chain length as studied by DSC", Vol. 72, pp: 1479-1488.

Gupta, V.B., Drzal, J.T., Lee, L.Y.C., and Rich, M.J., 1985, "Temperature-Dependence of some mechanical properties of a cured epoxy resin system", Polymer Engineering and Science, 25, pp: 812-823.

Gupta, V.B. and Brahatheeswaran, 1991, "Molecular packing and free volume in crosslinked epoxy networks", Polymer, Vol. 32, pp: 1875-1884.

Halary, J.L., Cukierman, S. and Monnerie, L., 1989, Bull. Soc. Chim. Belg, 98, 623

Halary, J.L., Cukierman, S. and Monnerie, L., 1992, Annales des Composites, I-2, pp: 103-112.

Halary, J.L., Bauchière, D., Lee, P.L. and Monnerie L., 1997, Polimery 42, 86.

Halary, J.L., 2000, "Structure-property relationsips in epoxy-amine networks of well-controlled architecture", High Performance Polymers Vol. 12, pp: 141-153.

Hale, A., Macosko, C.W., Bair, H., 1991, "Glass transition temperature as a function of conversion in thermosetting polymers", Macromolecules, Vol. 24, pp: 2610-2621.

Halley, P.J and Mackay, M., 1996, "Chemorheology of Thermosets-An overview" Polymer Engineering and Sceicne, Vol. 36, pp: 593-609.

Heinze, H.D., Schmieder, K., Schnell, G and Wolf, K.A., 1962, Rubber Chemistry and Technology, Vol. 35, pp: 776.

Heux, L., Lauprêtre, F., Halary, J.L and Monnerie, L., 1998, "Dynamic mechanical and ^{13}C n.m.r, analyses of the effects of antiplasticization on the β secondary relaxation of aryl-aliphatic epoxy resins", Polymer, Vol. 39, pp: 1269.

Heux, L., Halary, J.L., Lauprêtre, F. and Monnerie, L., 1997, "Dynamic mechanical and ^{13}C n.m.r inverstigations of molecular motions involved in the β relaxation of epoxy networks based on DGEBA and aliphatic amines", Polymer, Vol. 38, pp:

1767-1778.

Hill, L.W., 1997, “Calculation of crosslink density in short chain networks”, Progress in Organic Coatings, Vol. 31, pp: 235-243.

John, N.A and George, G.A., 1992 “Cure kinetics and mechanism of a tetraglycidyl-4,4’-diaminopheylmethane/diaminodipheyl sulphone epoxy resin using near i.r. spectroscopy”, Polymer, Vol. 33, pp: 2679-2688.

John D.Ferry., 1980, Viscoelastic Properties of Polymers, 3rd edition, New York, Wiley, pp.271.

Kanig, G., 1967, Journal of polymer science, Vol. 16, pp: 1957.

Kannurpatti, AR., Anderson, K.J., Anseth, J.W., Bowman, C.N., 1997, “Use of living radical polymerizations to study the structural evolution and properties of highly crosslinked polymer networks”, Journal of Polymer Science, Part B, Polymer Physics, Vol. 35, pp: 2297-307.

Kannurpatti, AR., Anseth, J.W., Bowman, C.N., 1998, “A study of the evolution of mechanical properties and structural heterogeneity of polymer networks formed by photopolymerizations of multifunctional methacrylates”, Polymer, Vol. 39, pp: 2507-13.

Kenyon, A.S and Nielsen, L.E., 1969, “Characterization of network structure of epoxy resins by dynamic mechanical and liquid swelling tests”, Journal of Macromolecular Science, Part A, Vol. 3, 275-295.

Kim, K.S. and Hahn, H.T., 1989, “Residual stress development during processing of graphite/epoxy composites”, Composites Science and Technology, Vol. 36, pp: 121.

Langley, N.R. and Polmanteer, K.E., 1974, “Isothermal crosslinking studies on polyquinoxalines by dynamic mechanical methods”, Journal of Polymer Science, Part A, Vol. 12, pp: 1023-1039.

Lee, G., and *Hartmann*, B., 1983, “Glass transition temperature predictions in some epoxy polymers”, Journal of applied polymer science, Vol. 28, pp: 823-830.

Lee, C.J., 1989, J. Macromol. Sci.- Rev. Macromol. Chem. Phys., C29, pp: 431-560.

Lee, M.C., Peppas, N.A., 1993, “Water transport in graphite/epoxy composites”, Journal of applied polymer science, Vol. 47, pp: 1349.

Mason, P., 1964, “Thermal expansion and viscoelasticity of rubber in relation to crosslinking and molecular packing”, Polymer, Vol. 5, pp: 625-635.

Manson, J.E. and Lange, J., 1996, “Build-up of structure and viscoelastic properties in epoxy and acrylate resins cured below ultimate glass transition temperature”, Vol.

37, pp: 5859-5868.

Martin, G.M., and Mandelkern, L., 1959, J.Res.Nat.Bur.Std, Vol. 62, pp: 141.

Masaki shimbo et al, 1985, "Internal stress of epoxide resin modified with spiro ortho-ester type resin" Journal of Material Science, Vol. 20, pp: 2965-2972.

Matejka, L., Chabanne, P., Tighzert, L. and Pascault, J.P., "Cationic polymerization of diglycidyl ether of bisphenol a", Vol. 32, pp: 1447-1458.

Merritt, M.E., Goetz, J.M., Whitney, D., Chang, C.P.P., Heux, L., Halary, J.L. and Schaefer, J., 1998, "Location of the Antiplasticizer in Cross-Linked Epoxy Resins by ^{2}H, ^{15}N, and ^{13}C REDOR NMR", Macromolecules, Vol. 31, pp: 1214-1220.

Mijovic, J., Andjelic, S. and Yee, C.F.W., 1995, "A study of reaction kinetics by near infrared spectroscopy 2. Comparison with dielectric spectroscopy of model multifunctional fepxy/amine systems", Macromolecules, Vol. 28, pp: 2979-2806.

Miller, D.R., and Macosko, C.W., 1976, "A new derivation of post gel properties of network polymers", Macromolecules, Vol. 9, pp: 206-211.

Miller, D.R., and Macosko, C.W., 1978, "Average property relations for nonlinear polymerization with unequal reactivity", Macromolecules, Vol. 11, pp: 656-662.

Miller, D.R., and Macosko, C.W., 1980, "Substitution effects in property relations for stepwise polyfunctional polymerization", Macromolecules, Vol. 13, pp: 1063-1069.

Miller, D.R., and Macosko, C.W., 1988, "Network parameters for crosslinking of chains with length and site distribution", Journal of Polymer Science, Part B: Polymer Physics, Vol. 26, pp: 1-54.

Mostovoy, S. and Ripling, 1966, "Fracture toughness of an epoxy system", Journal of applied polymer science, Vol. 10, pp: 1351-1371.

Moy, P., and Karasz, F.E., 1980, "Epoxy-water interactions", Polymer Engineering and Science, Vol. 20, pp: 315-319.

Morgan, R.J. and Mones, E.T., 1987, "The cure reactions, network structure, and mechanical response of diaminodiphenyl sulfone-cured tetraglycidyl 4,4' diaminodiphenyl methane epoxies", Journal of Applied Polymer Science, Vol. 33, pp: 999-1020.

Nakka, J.S.., Kathi, J. and Tammishetti, S., 2005, "Thermoplastic modification of monomeric and partially polymerized Bisphenol A diglycidyl ester", Europian Polymer Journal, Vol. 41, Issue.12, pp: 2963-2972.

Nakka, J.S, Jansen, K.M.B., Ernst, L.J. and Jager, W.F, 2008, "Effect of the epoxy

resin chemistry on the viscoelasticity of its cured product", Journal of Applied Polymer Science, Vol. 108, Issue 3, pp: 1414-1420.

Ogata, M., Kinjo, N and Kawata, T., 1993, "Effects of crosslinking on physical properties of phenol-formaldehyde novolav cured epoxy resins", Journal of Applied Polymer Science, Vol. 48, pp: 583-601.

Neki, K. and Geil, P.H., 1973, "Morphology-property studies of amorphous polycarbonate", Journal of Macromolecular Science, Part B:Physics,Vol. 8, 295-341.

Nicolas Amouroux and Liliane Léger, 2003, "Effect of dangling chains on adhesion hysteresis of silicone elastomers, probed by JKR test", Vol. 19, pp: 1396-1401.

Nielsen, L.E., 1969, J. Macromol.Sci.Rev. Macromol.Chem, C3 (1), pp: 69.

Nielsen, L.E, 1994, Mechanical properties of polymers and composites, second ed., revised and expanded, pp: 141.

O'Brien, D.J., Mather, P.T., White, S.R., 2001, "Viscoelastic Poperties of an Epoxy resin during cure", Journal of Composite Materials, 35, pp: 883-904.

Pascault, Jean-Pierre, Henry Sautereau, Jacques Verdu, Roberto J.J. Williams, 2002, *Thermosetting Polymers*, New York: Dekker, pp: 340, 428.

Rietsh, E., Daveloose, D., and Froelich, D., 1976, "Glass transition temperature of ideal polymer networks", Polymer, 17, pp: 859-863.

Sabra, A., Lam, T.M., Pascault, J.P., Grenier-Loustalot, M.F. and Grenier, P., 1987, "Characterization and behavior of epoxy-based diaminodiphenylsulphone networks", Polymer, Vol. 28, pp: 1030-1036.

Scanlan, J., 1960, "The effect of network flaws on the elastic properties of vulcanizates", Journal of Polymer Science, 43, pp: 501-508.

Scott, T.F., Cook, W.D. and Forsythe, J.S., 2008, "Effect of the degree of cure on the viscoelastic properties of vinyl ester resins", European Polymer Journal, Vol. 44, pp: 3200-3212.

Sear, J.K. and Darby, J.R., 1982, The Technology of Plasticizers, Wiley, New York.

Selby, K. and Miller, L.E., 1975, "Fracture toughness and mechanical behaviour of an epoxy resin", Journal of Material Science, Vol. 10, pp: 12-24.

Shibayam, K., 1975, "Temperature dependence of the physical properties of crosslinked polymers", Progress in organic coatings, Vol. 3, pp: 245-260.

Shibayama, K. and Suzuki, Y., 1965, "Effect of crosslinking density on the viscoelastic properties of unsaturated polyesters", Journal of Polymer Science., Vol.

3, pp: 2637-2651.

Simha, R. and Boyer, R.F., 1962, “On a general relation involving the glass temperature and coefficients of expansion of polymers”, Journal of chemical Physics, Vol. 37, pp: 1003-1007.

Simon, S.L., Mckenna, G.B., and Sindt, O., 1999, “Modeling the evolution of the Dynamic Mechanical Properties of a Commercial Epoxy during Cure”, Vol.76, pp: 495-508.

Simon, L. and Meng, Y., 2005, “Relation between mobility factor and diffusion factor for thermoset cure”, Thermochemica Acta, 437, pp: 179-189.

Simpson, J.O., and Bidstrup, S.A., 1995, “Rheological and dielectric changes during epoxy-amine cure”, Journal of polymer science part B Polymer physics, Vol. 33, pp: 55-62.

Slonimskii, G.L., Askadskii, A. and Kitaigorodskii, A.L., 1970, “The packing of polymer molecules”, Vysokomol.soyed.A12: No. 3, pp. 494-512.

Stevens, G.C., 1981, “Cure kinetics of a low epoxy/hydroxyl group-ratio bisphenol a epoxy resin-anhydride system by infrared absorption spectroscopy”, Journal Applied Polymer Science, Vol. 26, 4259-4278.

Stuart, B., 2004, “Infrared spectroscopy: Fundamentals and Applications”, John Wiley & Sons, Ltd.

Stutz, H., Illers, K.H. and Metes, J., 1990, “A generalized theory for the glass transition temperature of crosslinked and uncrosslinked polymers”, Journal of Polymer Science: Part B: Polymer Physics, Vol. 28, pp: 1483.

St. John, N.A. and George, G.A., 1992, “Cure kinetics and mechanisms of a tetraglycidyl-4,4’-diaminodiphenylmethane/diaminodiphenylsulphone epoxy resin using near i.r.spectroscopy”, Polymer, Vol. 33, pp: 2679-2688.

Suzuki, K., Miyano, Y., and Kunio, T., “Change of viscoelastic properties of epoxy resin in the curing process”, Journal of Applied Polymer Science, Vol. 21, pp: 3367-3379.

Tcharkhtchi, A., Gouin, E., Verdu, J., 2000, “Thermal expansion of epoxide-amine networks in the glassy state”, Journal of Polymer Science: Part B: Polymer Physics, Vol. 38, pp: 537-543.

Ueberreiter, K. and Kanig, G., 1950, Journal of Chemical Physics, Vol. 18, pp: 399.

Vakil, U.M. and Martin, G.C., 1992, “Crosslinked epoxies: Network structure characterization and physical –mechanical properties”, Journal of Applied Polymer

Science, Vol. 46, pp: 2089.

Varley, R.J et al., "Toughening of trifunctional epoxy system; 1.Near infrared spectroscopy study of homopolymer cure", Polymer, Vol. 36, pp: 1347-1355.

Van Krevelen, D.W and Hoftyzer, P.J., 1976, "Properties of Polymers: Their Estimation and correlation with chemical structure", 2 nd ed., Elsevier, Amsterdam.

Vladimirov, L.V and Oleinik, E.F., 1980, "Epoxy-aromatic amine networks in the glassy state structure and properties", Advances in Polymer Science, Vol. 80, pp: 49-99.

Vladimirov, L.V and Oleinik, E.F., 1988, "FT-IR studies of thermal history effects on molecular Structure of epoxy resins", Microchimica Acta, Vol. 94, pp: 329-333.

Wang, X. and Gillham, J.K., 1990, "Competitive primary/epoxy and secondary amine/epoxy reactions. Effect on the isothermal TTT cure diagram", Polymeric materials science and engineering, Proceedings of the ACS division of polymeric materials science and engineering, Vol. 63, 505-510.

White, S.R., and Mather, P.T., 1992, "A comparison of ultrasonic and thermal cure monitoring of an epoxy", Resin. Compos. Polym., Vol. 4, pp:403-422.

White, S.R. and Hahn, H.T., 1992, "Process modeling of Composite materials: Residual stress development during cure. Part II. Experimental validation", Vol. 26, pp: 2423-2452.

Wingard, C.D and Beatty, C.L., 1990, "Crosslinking of an epoxy with a mixed amine as a function of stoichiometry" I.Cure kinectics via dynamic mechanical spectroscopy", Journal of Applied Polymer Science, Vol. 40, pp: 198l-2005.

Wisanrakkit, G. and Gillham, J.K., 1988, "Effect of crosslink density on molecular relaxations in diepoxide-diamine network polymers, Part2. The rubbery plateau region", Polymer Engineering and Science, Vol. 28, pp: 230.

Wisanrakkit, G. and Gillham, J.K., 1990, "The glass transition temperature (T_g) as an index of chemical conversion for a high -T_g amine/epoxy system: Chemical and diffusion-controlled reaction kinetics", Journal of Applied Polymer Science, Vol. 41, pp: 2885-2929.

Won, Y.G., Galy, J. and Pascault, J.P., 1991, "Volumetric properties of epoxy networks cured by cycloaliphatic mono- and diamines", Vol. 32, pp: 79-83.

Yamini, S. and Young, R.J., 1980, "The mechanical properties of epoxy resins- Part 1 Mechanisms of plastic deformation", Journal of Material Science, Vol. 15, pp: 1814-1822.

Young, J.S., Kannurpatti, A.R., Bowman, C.N., 1998, “Effect of comonomer concentration and functionality on photo polymerization rates, mechanical properties and heterogeneity of the polymer”, Macromolecular Chemistry Physics, Vol. 199, pp: 1043.

List of publications & Conference

1. Nakka, J.S., Jansen, K.M.B, Ernst, L.J, Jager, W.F, 2008, "Effect of the epoxy resin chemistry on Viscoelasticity of its cured product", Journal of applied polymer science, Volume 108, pp: 1142-1420.

2. Nakka, J.S., Ernst, L.J, Jansen, K.M.B, 2008, "Effect of Chain Flexibility in the Network Structure on the Viscoelasticity of Thermosets", 30th Australasian Polymer Symposium (30 Nov-4Dec).

3. Nakka, J.S., 2008, "Effect of resin chemistry on the viscoelasticity", Polymer Processing Society (PPS-24) [June 15-19], Salerno, Italy.

4. Nakka, J.S., Jansen, K.M.B, Ernst, L.J, Jager, W.F, 2007 "Effect Of Adhesive Resin Chemistry On The Viscoelasticity Of Its Cured Product", MCMAT Conference, ASME Applied mechanics and materials conference, June 3-7, University of Texas, Austin. (MCMAT2007-30021).

5. Nakka, J.S., 2008, "Effect of resin chemistry on the viscoelasticity", Polymer Processing Society (PPS-24) [June 15-19], Salerno, Italy.

6. Tomasz Falat, Jan Felba, Arthur Wymslowski, K.M.B. Jansen, Nakka, J.S., 2006, "Viscoelastic Characterization of Polymer Matrix of Thermally Conductive Adhesives", Electronics Systemintergration Technology Conference, Dresden, Germany, pp: 773-781.

7. K.M.B. Jansen, Nakka, J.S., L.J. Ernst, 2009, "Tailoring of epoxy properties", Thermosets 2009 Conference, Berlin, 30 Oct-2 Nov 2009.

ACKNOWLEDGEMENTS

This thesis is dedicated to my beloved wife G. Florence Diana and lovely daughter N.Annie Michella.

Firstly, I would like to thank God, for giving me good life, family and health. I thank and praise the god for showing me new people, places, cultures, climates and many more.

A great number of people contributed to the outcome of this thesis. Particular thanks are owed to the following.

I am deeply indebted to my promoter Prof. Leo Ernst for offering me the opportunity to pursue a PhD position in his group. I always enjoyed his stimulating discussions and valuable suggestions which he pointed out during the technical discussions. My special thanks to him for the thorough reading of my manuscript. He spared no pains in going through this work in spite of his busy schedule. I am grateful for his unfailing support and esteemed guidance in the preparation of the report.

I am immensely thankful to my toegevogd promoter Dr.ir.K.M.B Jansen for his great scientific support and daily supervision. He always gave me innovative ideas, suggestions and showed me the different ways to approach a problem and solve it. I also thank him for giving me the freedom to develop innovative ideas. It is a great pleasure working with him. I have great respect for his concern that he showed me during my PhD study.

I thank Dr.ir.W.F.Jager from the chemical engineering department of TUDelft for his valuable ideas and also assisting me in conducting the characterization studies.

I sincerely thank the industrial partners i.e., NXP, TNO for their financial as well as technical support in this PhD research work. My special thanks to Dr. Amar Mavinkurve and Ir. J.H.J Jansen from NXP, Ir. J.A.C.M. Pijnenburg form TNO for their valuable suggestions and ideas during the quarterly meeting.

Thanks to Dr. Ing Yvette Roman from STW for organizing regular meetings and assisting me in getting thorough feed back from the industrial partners.

Thanks to all the members of Precision and Microsystems Engineering (*PME*) department for their encouraging meetings and mind refreshing parties. Thanks to the administrative staff: Corinne du Burck, Birgit Rademakers, Inge van Marion, Marli Guffens, Marianne Stolker, Jan Booij, Olga van Paassen and Jordi Kerkum for arranging everything for me in this group.

Thanks to Jos van Driel, Harry Jansen, Patrick van Holst and Rob Luttjeboer for their competent and prompt technical support at the university in Delft.

I gratefully acknowledge the help rendered by my colleagues Lingen Wang, Jan de Vreugd, Xiaosong, An Xiao, Manoj Saraswat, Heru Utomo Beate, Michiel van Soestbergen, Jodi Kooijman, Tomasz Falat, Navin Balini and Mahdi Sadeghinia who over years have contributed and supported me during this PhD work.

My special thanks to all the church members from the Evangelisch-Lutherse Gemeente, Oude Delft, Delft. I and my family felt like home in this new country because of their love, concern and hospitality. Thanks to Pastor Rev. Taco Smit, his wife Boel and their family members for their spiritual concern and care. Thanks to Prof. dr. J. Arbocz and Mrs. Margot Arbocz for taking care of me and my family. Mr and Mrs. Arbocz have always boosted me with lots of energy and love. Thanks to families: Dr. Herman Meijer and Mrs. Bep Meijer MD, Ir. Reinoud Koolhaas and Mrs. Janny Koolhaas, Ing. Nick Schmidt and Mrs. Martha Schmidt, Mr. Maarten van Woerden and Mrs. Gerda van Woerden, Mr. Dick Van Loenen and Mrs. Marianne van Woerden, Mr. Gerard van Leeuwen and Mrs. Corrie van Leeuwen, Mr. Addie and Mrs. Deborah Flohr. I sincerely thank each one of the lurtheran church members for their great love, help, support and encouragement.

Thanks to the unconditional love and support of both the families of mine and my wife's. Thanks to my parents father Peterson and mother Dorathy for encouraging me to pursue PhD study. Thanks to my brothers John Suneel, John Swaroop & Samson Suhason for their support. Thanks to my mother-in-law Cardelia and my wife's sisters Sirisha, Indira and their families. Lastly, I have to thank my wife and my little daughter who have put-up without complaint during my preoccupation with research work. I am particularly grateful to my wife Florence Diana who has willfully shouldered much of the responsibility of the family during my work on the thesis and allowed me more time.

My debt is greatest to all the scholars and critics who have helped me with suggestions, feedback and piloting during the development of this thesis. Thank you one and all.

PROFILE

John Suman Nakka

John Suman Nakka was born on July 2nd, 1978 in Visakhapatnam, Andhra Pradesh, India. He did Masters in Organic chemistry in 2000 from Andhra University, Andhra Pradesh, India. Also he has done Masters in polymer engineering in 2002 from Cochin University, Kerala, India. From 2003 to 2005 he worked as researcher on the project entitled "*High performance polymers*" in Indian Institute of Chemical technology, Hyderabad, India. In 2005 he started his Ph.D in Delft University of Technology.